VNIVERSITAT
ⅮE VALÈNCIA

PhD Program in Biomedicine and Biotechnology

INTERNATIONAL PhD THESIS

Application of endometrial extracellular matrix hydrogels developed from decellularized uterus in reproductive medicine.

Author:

Sara López Martínez

Bachelor's Degree in Biotechnology

Master's Degree in the Biotechnology of Assisted Human Reproduction

Supervised by:

Dr. Irene Cervelló Alcaraz

Dr. Hortensia Ferrero Cháfer

Valencia, May 2021

Dra. Irene Cervelló Alcaraz, Doctora en Biología, Investigadora principal del área de Células Madre y Bioingeniería en Fundación IVI (FIVI) y Coordinadora del laboratorio de FIVI.

CERTIFICA:

Que el trabajo de investigación titulado: "**Application of endometrial extracellular matrix hydrogels developed from decellularized uterus in reproductive medicine.**" ha sido realizado íntegramente por Sara López Martínez bajo mi dirección. Dicha memoria está concluida y reúne todos los requisitos para su presentación y defensa como TESIS DOCTORAL ante un tribunal.

Y para que así conste a los efectos oportunos, firmo la presente certificación en Valencia a 26 de mayo de 2021.

Fdo. Dra. Irene Cervelló Alcaraz

Dra. Hortensia Ferrero Cháfer, Doctora en Biomedicina y Biotecnología, Investigadora principal del área de Diagnóstico y Tratamiento de Enfermedades Uterinas en Fundación IVI.

CERTIFICA:

Que el trabajo de investigación titulado: "**Application of endometrial extracellular matrix hydrogels developed from decellularized uterus in reproductive medicine.**" ha sido realizado íntegramente por Sara López Martínez bajo mi dirección. Dicha memoria está concluida y reúne todos los requisitos para su presentación y defensa como TESIS DOCTORAL ante un tribunal.

Y para que así conste a los efectos oportunos, firmo la presente certificación en Valencia a 26 de mayo de 2021.

Fdo. Dra. Hortensia Ferrero Cháfer

ACKNOWLEDGEMENTS

No recuerdo exactamente en qué momento de mi vida descubrí mi vocación, tal vez tras ver alguna cinta de "Érase una vez el Cuerpo Humano". Primero quise ser veterinaria, pasando por médica y finalmente biotecnóloga, pero desde niña siempre he tenido muy claro que lo que me gustaba era la ciencia aplicada a la medicina. Cuando empecé este camino nunca pensé que llegaría un momento en el que me sentaría a escribir los agradecimientos de mi tesis doctoral. Y desde luego, no pensé en lo difícil que me resultaría hacerlo.

Aquí termina una etapa que comenzó con muchísima ilusión y que lo largo del camino me ha generado momentos de mucho estrés e inseguridad, pero también de motivación (sobre todo cuando miraba al microscopio y ese experimento que daba por perdido resultaba positivo, ¡Eureka!). En fin, ese continuo amor-odio por la ciencia. Durante este tiempo, he aprendido a equivocarme sin hundirme y a sentirme orgullosa de los pequeños aciertos. En definitiva, a crecer como profesional y persona. Pero nada de esto hubiese sido posible sin el apoyo de gente maravillosa, unos han estado ahí desde siempre y otros se han hecho indispensables en cuestión de meses. Estas páginas son para vosotros.

En primer lugar, agradecer a mis directoras de tesis. A Irene, por guiarme en la realización de esta tesis doctoral y por todo tu apoyo durante estos años. Gracias por brindarme la oportunidad de ser parte de tu grupo de investigación, y tras esto por tu confianza y tus consejos, sin los cuales no podría haber llegado hasta este momento. También, me gustaría agradecer a mi directora Horten por recibirme como doctoranda y por toda su ayuda.

A todo el equipo de apoyo a fundación IVI. En especial a Marcos, por ayudarme con los trámites administrativos. A Leo, por enseñarme a no tener cientos de subcarpetas y rescatar todos mis archivos de las profundidades del disco duro. Y al servicio de estadística, bioinformática y educación, los que siguen y los que emprendieron nuevos caminos; Patri Sebastián, Alejandros, Víctor, Guille, y en especial a Alfredo por nuestros ratos de análisis estadístico.

Al personal del animalario de Facultad de Medicina y Odontología de Universidad de Valencia, en especial a Ana y Eva, por toda la ayuda prestada.

A mis amigas Mireia, Rebeca y Clara, gracias por ser mi familia valenciana. A Samantha por ser la mejor profesora de inglés. Y a mis amigos Amanda y Migue, siempre cerca a pesar de la distancia.

A mis padres, por hacerme fuerte y alentarme a perseguir mis sueños, a mis hermanos Ernesto, Rubén y Noelia por crecer conmigo, a mis tías y a mi abuelo (seguro el más orgulloso). A la futura médica Ana. Y por supuesto a mi otra familia, Miguel, Inma e Inma junior, gracias por dejarme ser una más.

Finalmente, quería dedicar esta tesis a ti, Alejandro. Gracias por cada momento de mi vida que he tenido la suerte de contar contigo. Gracias por no dejar que me hundiese en los malos momentos y hacer los buenos increíbles. Y, sobre todo, gracias por seguirme si hiciese falta hasta el fin del mundo.

"La medicina es como una lenta obra de albañilería, somos afortunados si en el plazo de una vida podemos poner un solo ladrillo." (El médico, Noah Gordon)

RESUMEN

INTRODUCCIÓN

Útero, endometrio y patologías endometriales que afectan a la fertilidad.

El aparato reproductor femenino es un conjunto de órganos encargados de la concepción, el embarazo y el parto del recién nacido. Los principales órganos implicados son los ovarios, las trompas de Falopio u oviductos, el útero y el cérvix. El **útero** es el órgano de mayor dimensión del aparato reproductor femenino y juega un papel fundamental en la implantación embrionaria, la gestación y la expulsión final del recién nacido. El útero es una estructura hueca que comienza en los oviductos y termina en el cérvix. La anatomía de este varía entre las distintas especies de mamíferos pudiendo ser una única cavidad (como la encontrada en primates), un útero bicorne (típico de los artiodáctilos como el cerdo), o dos cuernos uterinos independientes (usualmente encontrado en lagomorfos y roedores). En humanos la anatomía del útero es simple y posee forma de pera invertida donde subyace una cavidad triangular. La pared del útero está compuesta por tres capas principales: una membrana que recubre la superficie externa llamada perimetrio, una capa intermedia de músculo liso llamada miometrio y una mucosa que reviste la cavidad uterina denominada **endometrio**. Esta última capa, el endometrio, desempeña un papel crucial en la implantación del embrión y comienzo del embarazo.

El endometrio es un tejido altamente regenerativo que se somete a grandes cambios durante el ciclo hormonal y que es capaz de renovarse de forma continuada sin pérdida de función. El ciclo hormonal consiste en una serie de cambios regulares que de forma natural ocurren en el sistema reproductor femenino. El ciclo se encuentra gobernado por las hormonas producidas en la glándula hipofisiaria y en el ovario y puede ser clasificado

RESUMEN

en dos: el ciclo menstrual, encontrado principalmente en primates, y el ciclo estral típico del resto de mamíferos. El **ciclo menstrual** humano tiene una duración total de unos 28 días y consiste en tres fases, proliferativa, secretora y menstrual, durante las cuales el endometrio crece, se diferencia para permitir la implantación embrionaria y se destruye para nuevamente ser reparado e iniciar un nuevo ciclo. Por otra parte, el **ciclo estral** no implica menstruación y se compone de cuatro fases, proestro, estro, metaestro y diestro, durante las cuales el endometrio crece, se diferencia para permitir la implantación y se reabsorbe para comenzar de nuevo.

El endometrio está formado por un compartimento epitelial y otro estromal mantenido por un nicho endógeno de células madre, una gran vasculatura y una población de células inmunes residentes. El compartimento epitelial está compuesto por el epitelio luminal que reviste la cavidad uterina y glándulas, ambos formados por células epiteliales endometriales (EECs, del inglés Endometrial Epithelial Cells). Por su parte, el compartimento estromal contiene células estromales endometriales (ESCs, del inglés Endometrial Stromal Cells). El endometrio también puede ser dividido en dos capas: la capa funcional, que es descartada durante la menstruación, y la capa basal, la cual es preservada a lo largo de la vida y actúa como suministro de células madre endometriales para la regeneración de la capa funcional. Hasta la fecha, distintos tipos de células madre endometriales han sido identificadas como residentes en el endometrio, entre ellas, células madre mesenquimales, endoteliales y progenitores epiteliales. Estas células madre fueron reconocidas mediante diferentes marcadores y técnicas, como la capacidad de expulsar colorantes vitales (Side Population).

El endometrio puede verse afectado por patologías que desencadenan un crecimiento endometrial deficiente, eventos fibróticos o destrucción endometrial. Estos eventos afectan a su vez a la implantación embrionaria y conducen a infertilidad. Este el caso de

la Atrofia Endometrial (EA, del inglés Endometrial Atrophy), enfermedad provocada por una deficiencia en el crecimiento endometrial que impide la anidación del embrión, o el Síndrome de Asherman (AS, del inglés Asherman Syndrome), una patología adquirida tras intervenciones como la dilatación y el legrado agresivo, que conlleva a una continua destrucción endometrial y presencia de adherencias en la cavidad uterina.

La matriz extracelular.

La **matriz extracelular** (del inglés extracelular matrix, ECM) es un complejo macromolecular en el que las células de todos los tejidos del cuerpo residen. Se trata de una compleja mezcla de proteínas fibrosas tales como colágeno, elastina, fibronectina, lamininas, glucosaminoglicanos (GAGs) y proteoglicanos, pero también de otras proteínas afiliadas, factores secretados y reguladores. La ECM tiene dos roles principales: el físico, actuando como un sustrato para la adhesión celular y la estructura del tejido, y el biológico, proveyendo señales vitales para la función de las células que contiene y para la correcta homeostasis del tejido en su conjunto. Una parte de la señalización producida por la ECM es mecánica y se ejerce a través de su topología, porosidad, viscoelasticidad o rigidez. En concreto, la rigidez está íntimamente relacionada con el crecimiento y diferenciación celular y puede variar por cambios en la composición de la ECM (p. ej. de colágeno). La otra parte es bioquímica e implica el secuestro, almacenamiento y liberación selectiva de moléculas bioactivas (p.ej. factores de crecimiento), controlando de esta forma su funcionabilidad.

Una característica importante de la ECM es la **especificidad de tejido**. La ECM de cada tejido, incluido el endometrio, posee una composición específica que brinda el microambiente ideal para las células que allí se encuentran e influye en la actividad tisular. La ECM es también un ambiente dinámico en continúo remodelado por las propias

células que alberga. Así pues, el diálogo entre célula y ECM es bidireccional y conduce a un constante ciclo de causa-efecto que influye a ambas, tanto en condiciones de salud como de enfermedad.

La ingeniería tisular en medicina reproductiva.

La ECM no solo modula la homeostasis de los tejidos, sino que también ejerce un rol fundamental en la regeneración de estos, lo que abre la ventana a su uso en medicina regenerativa. La **medicina regenerativa** es el campo de la medicina que busca reparar órganos no funcionales a la vez que reducir el uso de la inmunosupresión. Dentro de esta, la **ingeniería tisular** o **bioingeniería** se basa en el uso de biomateriales para el desarrollo de tejidos y órganos funcionales. Los materiales aplicados en bioingeniería son de índole muy diversa, desde sintéticos (como polímeros artificiales) a pertenecientes a la ECM natural, como componentes purificados (como colágeno) o ECM sintetizada en cultivo celular *in vitro* (como el extracto de membrana basal secretada por sarcoma de ratón, conocido como Matrigel). Sin embargo, estos biomateriales carecen de la complejidad de los órganos naturales, lo que hace difícil la recreación del microentorno nativo.

En las últimas décadas, el auge de los tejidos descelularizados (DC) ha hecho posible la obtención de biomateriales directamente derivados de tejidos y órganos, siendo en la actualidad los biomateriales con mayor cercanía al tejido original. La **descelularización** es el proceso por el cual las células, y con ella los epítopos antigénicos asociados, son eliminados de un tejido u órgano, teniendo como resultado la creación de un molde acelular compuesto por ECM específica del tejido de origen. La descelularización puede ser aplicada en órganos fraccionados o completos mediante la aplicación de métodos físicos, químicos o enzimáticos. La técnica más usada es la aplicación de detergentes como el Tritón X-100 o el dodecilsulfato sódico (SDS). En el caso de la descelularización

de órgano completo, las soluciones decidualizantes son perfundidas a través del propio sistema vascular del órgano, el cual las suministra a través de las arterias a todas las localizaciones del órgano y produce la destrucción celular. Tras esto los restos celulares son eliminados a través de las venas. La descelularización es un proceso complejo que requiere de un delicado balance entre eliminación de componentes celulares y conservación de la ECM. Al igual que el resto de los biomateriales trasplantables, los tejidos DC causan una respuesta inmune positiva o negativa que es determinante en el proceso de regeneración y en la que intervienen células como los macrófagos.

La descelularización ha sido aplicada con éxito en una amplia gama de órganos, entre ellos el útero. Hasta la fecha, la descelularización de piezas uterinas ha sido reportada en varias especies incluida la humana, mientras que la descelularización de órgano completo se ha desarrollado en úteros de pequeño tamaño como rata, conejo y recientemente en úteros de mayor tamaño como el de oveja o cerdo. Estos úteros DC han sido usados en cultivo celular *in vitro*, con el propósito de lograr la recelularización y estudiar el comportamiento celular, pero también como parches trasplantables en modelos preclínicos *in vivo* que perseguían la recelularización con células autólogas del hospedador y la recuperación de la función reproductora. Estos últimos estudios han reportado resultados prometedores como la incipiente recelularización y cierto soporte del embarazo. A pesar de los avances, la completa recelularización del útero DC continúa siendo un desafío para la ingeniería tisular de órganos reproductivos.

Hidrogeles de matriz extracelular específica de tejido.

Un hidrogel es una red tridimensional (3D) de polímeros hidrofílicos con un alto contenido en agua. Recientemente, los avances en ingeniería tisular han permitido el diseño de **hidrogeles de ECM específicos de tejido** a partir de órganos DC. Estos

hidrogeles conservan la complejidad bioquímica y ciertas características físico-mecánicas del tejido DC del que proceden mientras que mejoran ciertos aspectos, como la incapacidad de moldearse o la necesidad intervenciones quirúrgicas agresivas para su uso en propósitos médicos.

La formación un hidrogel de ECM específica de tejido es un proceso de autoensamblaje de los polímeros pertenecientes a fibras de ECM (principalmente colágeno). El procesado de un tejido DC hasta hidrogel implica cuatro etapas: (I) molienda y liofilización para la obtención de un polvo anhidro, (II) digestión enzimática para la obtención de una solución con fibras de ECM desintegradas, (III) neutralización de la actividad enzimática y (IV) aumento de la temperatura a 37ºC, con la consiguiente repolimerización de las fibras y la gelificación de la solución. En la actualidad, los hidrogeles tejido-específicos son una herramienta prometedora para el cultivo 3D *in vitro* y la regeneración tisular *in vivo* en muchas áreas de la medicina.

La aplicación de hidrogeles de matriz extracelular específica de tejido en cultivo tridimensional *in vitro*.

El cultivo de células en monocapa es la técnica estándar del cultivo *in vitro* y ha generado importantes avances en biomedicina debido a su fácil manejo y reproducibilidad. Sin embargo, la información obtenida de un cultivo celular en monocapa está limitada a sus condiciones bidimensionales, siendo incapaz de capturar la complejidad anatómica y bioquímica del tejido de origen. La creación de **cultivos 3D** *in vitro* supone el desarrollo de ambientes más próximos a la realidad *in vivo* para el estudio de los procesos biológicos y el ensayo de medicamentos. Los hidrogeles son el soporte más usado para el establecimiento de cultivos 3D. En particular, los materiales más comunes son

componentes purificados como colágeno y matrices derivadas de células, como el Matrigel.

En las investigaciones relacionadas con el endometrio, una cantidad importante de estudios han desarrollado modelos 3D con hidrogeles con el objetivo de recrear la fisiología endometrial y responder a preguntas sobre la interrelación útero/embrión y diferentes patogénesis. Estos modelos 3D incluyen sistemas de cocultivo celular y organoides endometriales. Los sistemas de cocultivo son una mezcla de diferentes tipos celulares, principalmente EECs y ESCs, que persiguen la recreación de la estructura endometrial. Mientras, los organoides endometriales son la técnica más vanguardista y consisten en células epiteliales autoorganizadas capaces de recapitular las características de las glándulas uterinas *in vivo*. La sustitución de las matrices comerciales por hidrogeles específicos de tejido podría marcar un antes y un después en los sistemas de cultivo 3D, y su aplicación está siendo testada en diversos tejidos como hígado, corazón o el sistema nervioso. Hasta la fecha, se ha demostrado la viabilidad de diversas líneas celulares, células primarias y células madre en hidrogeles tejido-específicos, reportándose en algunos casos un comportamiento más cercano al natural. No obstante, estas investigaciones no habían sido aplicadas al endometrio hasta la presente tesis.

La aplicación de hidrogeles de matriz extracelular específica de tejido en medicina regenerativa.

Los hidrogeles de ECM específicos de tejido poseen una serie de características atractivas para la medicina regenerativa. En particular, su inyectabilidad, maleabilidad, la infiltración celular, degradabilidad y bioactividad tejido-específica. En concreto, la posibilidad de ser inyectados en forma líquida y gelificar *in situ* espontáneamente gracias a la temperatura corporal fisiológica es particularmente llamativa, ya que permite el

diseño de terapias menos invasivas. Hasta la fecha, se han realizado estudios preclínicos con hidrogeles tejido-específicos en diversos órganos con el fin de probar su eficacia contra enfermedades típicas de sus tejidos de origen. Algunos ejemplos con son los hidrogeles de músculo esquelético, menisco, grasa, nervios, córnea, hígado, hueso o corazón. Los hidrogeles de ECM cardíaca para el tratamiento del infarto de miocardio son los más avanzados y están siendo evaluados en la actualidad en ensayos clínicos en humanos. Sin embargo, si nos centramos en el tratamiento de patologías endometriales con predisposición a infertilidad, los estudios actuales están clásicamente enfocados al uso de células madre o factores bioactivos con el fin de regenerar el endometrio patológico. Recientemente, la bioingeniería se ha abierto paso con estudios preclínicos que incluyen polímeros sintéticos y componentes de ECM purificados como ácido hialurónico o colágeno. Sin embargo, los hidrogeles específicos de tejido permanecían, hasta la presente tesis, como asignatura pendiente en la medicina regenerativa endometrial.

OBJETIVOS

El objetivo principal de este estudio es desarrollar hidrogeles de matriz extracelular endometrial derivados de útero porcino y estudiar su aplicabilidad en sistemas de cultivo 3D *in vitro* con células humanas y en modelos murinos *in vivo*.

Objetivos específicos

- Diseñar hidrogeles de matriz extracelular endometrial a partir de útero porcino descelularizado:

- Establecer un protocolo para el desarrollo de hidrogeles de matriz extracelular endometrial a partir de útero porcino.

- Estudiar las características físicas y bioquímicas de hidrogeles de matriz extracelular endometrial.

- Aplicar estos hidrogeles de matriz extracelular endometrial como plataforma de cultivo tridimensional *in vitro*:

  - Analizar su biocompatibilidad *in vitro* con células endometriales humanas procedentes de líneas de células madre y cultivo primario.

  - Estudiar su idoneidad para dar soporte al cocultivo tridimensional de células endometriales humanas a largo plazo.

  - Testar su idoneidad como sustituto al Matrigel para el cultivo de organoides endometriales humanos.

- Aplicar estos hidrogeles de matriz extracelular endometrial como tratamiento regenerativo de patologías reproductivas *in vivo*:

  - Evaluar su biocompatibilidad *in vivo* en un modelo murino subcutáneo.

  - Evaluar su potencial para promover la regeneración endometrial y la restauración de la fertilidad en un modelo murino de daño endometrial.

METODOLOGÍA

Diseño de hidrogeles de matriz extracelular a partir de úteros descelularizados porcinos.

Descelularización de útero porcino y purificación de la matriz extracelular endometrial.

RESUMEN

Todos órganos fueron obtenidos de cerdas donadas por Mercavalencia (Valencia, España) acorde con la norma ISO 9001 y sometidos a descelularización de órgano completo. Para ello, la arteria uterina de los cuernos fue conectada a una bomba peristáltica y se realizaron dos ciclos de perfusión de SDS 0,1% (18 horas), agua destilada (30 minutos), Tritón X-100 1% (30 minutos), y solución salina (PBS) (5 horas). El endometrio fue entonces aislado mediante la microdisección. Posteriormente, se realizaron una serie de lavados con PBS y DNasa I y se monitorizó el SDS remanente con Stains-All. La eficiencia de la descelularización se comprobó mediante análisis histológico de células (hematoxilina y eosina, H&E), núcleos (DAPI), epítopo alpha(α)-gal y colágeno (tinción tricrómica de Masson, MT).

Creación de hidrogeles de matriz extracelular endometrial.

El tejido endometrial DC fue molido, liofilizado y digerido con pepsina 0,1% en HCl 0,01M durante 48 h. La solución de ECM endometrial (EndoECM) resultante fue neutralizada con 10% de NaOH 0,1 M, 11,11% PBS 10X y PBS 1X. La estabilidad y esterilidad de EndoECM fue comprobada en cultivo *in vitro*. Este proceso se repitió con tejido miometrial DC y endometrial no descelularizado para la creación de soluciones de matriz extracelular miometrial (MyoECM) y endometrio no descelularizado (No-DC Endo).

Caracterización de los hidrogeles de matriz extracelular endometrial.

El contenido en ADN, proteína total, colágeno, GAGs y elastina fue monitorizado durante la generación de EndoECM. Tras esto, se analizó la cinética de gelificación de los hidrogeles por turbidimetría, el estudio de su ultraestructura por microscopía electrónica de barrido (SEM) y el análisis proteómico por cromatografía líquida acoplada a

espectrometría de masas (LC-MS/MS). EndoECM fue analizado en comparación a MyoECM y No-DC Endo en SEM y LC-MS/MS.

Hidrogeles de matriz extracelular endometrial como plataforma para cultivo tridimensional *in vitro*.

Los estudios aquí mencionados fueron aprobados por el Comité de Ética Humana de Fundación IVI (1706-FIVI-053-IC). En ellos, se emplearon EECs y ESCs procedentes de biopsias endometriales humanas y de líneas de células madre endometriales preestablecidas de epitelio (ICE6) y estroma (ICE7).

<u>Compatibilidad *in vitro* de la matriz extracelular endometrial porcina con células madre y primarias endometriales humanas.</u>

Células EECs, ESCs, ICE6 y ICE7 se cultivaron mediante tres metodologías diferentes: sobre un revestimiento (2D), sobre un hidrogel (2.5D) y encapsuladas dentro de un hidrogel (3D). Para 2D, revestimientos de EndoECM, colágeno, Matrigel o PBS (control no revestido) fueron testados. Para 2.5D y 3D se utilizaron hidrogeles de colágeno (3 mg/mL), Matrigel (3 mg/mL) o EndoECM (3, 6 y 8 mg/mL). La proliferación celular fue comparada a las 72 h por el ensayo de tetrazolio.

<u>Cocultivo tridimensional a largo plazo de células endometriales humanas.</u>

Se construyeron sistemas de cocultivo 3D con EndoECM y células epiteliales y estromales endometriales procedentes de líneas de células madre ICE (ICE6 y ICE7) o de biopsias primarias (EECs y ESCs). Para ello, primero se creó un hidrogel de EndoECM con células estromales embebidas y después la fracción epitelial se sembró sobre la superficie en el mismo día (método A) o 3 días después (método B). Tras 10 días *in vitro*, la morfología (MT), viabilidad (calceína/yoduro de propidio o TUNEL), proliferación

RESUMEN

(marcador Ki67) y expresión de los marcadores E-cadherina y Vimentina de las construcciones fueron analizadas.

<u>Estudio preliminar de la matriz extracelular endometrial como sustituto de Matrigel en el sistema de cultivo de organoides endometriales.</u>

Glándulas endometriales humanas fueron aisladas y cultivadas en Matrigel para establecer una línea de organoides. Se analizó la expresión de citoqueratina y vimentina y la estabilidad cromosómica por microarray de hibridación genómica. Organoides en pases tempranos (pase 1, 2 y 5) fueron transferidos a gotas de EndoECM 8 mg/mL o Matrigel y su viabilidad se analizó tras 2 y 5 días.

Hidrogeles de matriz extracelular endometrial como tratamiento regenerativo para patologías reproductivas *in vivo*.

Los procedimientos con animales se realizaron en las instalaciones de la Unidad Central de Investigación de Medicina de la Universidad de Valencia de acuerdo con la Directiva 2010/63/UE y el Comité de Ética para el Bienestar Animal (A1510673251016/A-1550574856754). En todos los estudios se utilizó la cepa inmunocompetente C57BL/6.

<u>Estudio preliminar de la compatibilidad *in vivo* de los hidrogeles de matriz extracelular endometrial en un modelo subcutáneo murino.</u>

Se inyectaron 200 µl de EndoECM 8 mg/mL o de Endo No-DC (control de rechazo inmune) en el espacio subcutáneo dorsal de ratonas. Tras 2, 7 y 14 días, se evaluó histológicamente la infiltración y morfología celular (MT) y los macrófagos CD68+.

<u>Estudio de regeneración endometrial y restauración de la fertilidad en un modelo murino de daño endometrial.</u>

Se indujo una lesión endometrial por inyección de etanol 70% en el cuerno uterino derecho, dejando el izquierdo como control sin daño. Tras cuatro días, tres tratamientos fueron introducidos en el cuerno dañado: solución salina (control sin tratamiento), EndoECM o EndoECM suplementado con factores de crecimiento (EndoECM+GF), concretamente, factor de crecimiento fibroblástico básico (bFGF), factor de crecimiento derivado de plaquetas-bb (PDGFbb) y factor de crecimiento similar a la insulina-1 (IGF-1). Los hidrogeles fueron marcados con biotina para su rastreo. 14 días postratamiento, una parte de las ratonas fueron sacrificadas para el análisis de la regeneración endometrial por grosor endometrial, número de glándulas, la proliferación celular (Ki67) y la deposición de colágeno (MT y retrotranscripción cuantitativa, RT-PCR, de *Col1a1*). El resto de las ratonas (con uno o ambos cuernos dañados y tratados) fueron apareadas para la evaluación de la fertilidad 10 días después de la presencia de tapón vaginal. El ciclo estral fue monitorizado por frotis vaginal durante todo el experimento.

RESULTADOS

Diseño de hidrogeles de matriz extracelular a partir de úteros descelularizados porcinos.

Descelularización de útero porcino y purificación de la matriz extracelular endometrial.

La eficacia de la descelularización fue verificada por la eliminación de las células y del epítopo α-gal así como por la preservación del colágeno. La cuantificación de SDS tras seis lavados post-disección mostró una reducción significativa del 78,6% del SDS residual de la descelularización hasta alcanzar 33,9±12,4 µg de SDS/g de tejido húmedo.

Producción y caracterización de los hidrogeles de matriz extracelular endometrial.

RESUMEN

La monitorización del contenido en ADN durante la elaboración del EndoECM mostró una reducción del 92,4% (polvo liofilizado) tras la descelularización con ausencia de bandas tras electroforesis. También se reveló una eliminación del 80% de la fracción proteica mientras se obtuvo un enriquecimiento del 148% en colágeno y la preservación del 18% en elastina y GAGs. La posterior digestión provocó el aumento del contenido proteico total (42% respecto al liofilizado), una reducción del colágeno (61,3%) y la pérdida de la elastina, mientras que el contenido en GAGs no se vio afectado.

EndoECM formó hidrogeles espontáneamente tras incubación a 37ºC y permaneció estable y estéril en cultivo *in vitro*. La cinética de gelificación reprodujo una curva sigmoidal con parámetros dependientes de la concentración. Los hidrogeles de EndoECM presentaron una ultraestructura fibrilar homogénea y entrelazada al azar mientras que Endo-DC formó hidrogeles con una estructura alterada por restos celulares. El análisis proteómico mostró que EndoECM y MyoECM estaban compuestos en más de un 90% por ECM frente al 41,4% de ECM de No-DC Endo. Esta ECM estaba formada en un 83% por colágenos. Por su parte, las moléculas potencialmente inmunorreactivas disminuyeron drásticamente con respecto a No-DC Endo. EndoECM y MyoECM presentaron diferencias en la composición, indicando especificidad de tejido.

Hidrogeles de matriz extracelular endometrial como plataforma para cultivo tridimensional *in vitro*.

<u>Compatibilidad *in vitro* de la matriz extracelular endometrial porcina con células madre y primarias endometriales humanas.</u>

EndoECM no indujo inhibición del crecimiento celular en las configuraciones 2D, 2.5D y 3D, mostrando biocompatibilidad. Respecto a 2D, no hubo diferencias entre EndoECM y el resto de los revestimientos. En 2.5D se observó un aumento significativo de la

proliferación de ICE6 y ICE7 en EndoECM en comparación con colágeno y Matrigel, mientras que la proliferación de ICE6, ICE7 y ESCs aumentó con la concentración. En 3D, se observó un aumento significativo de la proliferación de ICE6, ICE7 y ESCs en EndoECM respecto al colágeno y de ICE6 y ICE7 respecto a Matrigel, mientras que la proliferación de ESCs disminuyó con la concentración.

Cocultivo tridimensional a largo plazo de células endometriales.

Los cultivos 3D experimentaron un aumento de densidad y una reducción del volumen formando una estructura compacta que se mantuvo hasta el día 10. Cuando la concentración celular inicial fue alta (método A), la degradación fue más agresiva. Tras 10 días, la viabilidad celular fue del 90% tanto en ICE6-7 como EECs-ESCs, con un 33% de células proliferativas en ICE6-7 y un 60% en EECs-ESCs. Ambas construcciones presentaron células estromales positivas para el marcador vimentina en conformación 3D y células epiteliales positivas para E-cadherina sobre la superficie, aunque sin polarización apico-basal.

Estudio preliminar de la matriz extracelular endometrial como sustituto de Matrigel en el sistema de cultivo de organoides endometriales.

Las glándulas endometriales humanas fueron capaces de autoorganizarse para desarrollar organoides y de reensamblarse en cada pase, aumentando su tamaño y número durante su cultivo en Matrigel (condiciones standard). Los organoides fueron positivos para citoqueratina y negativos para vimentina confirmando su origen epitelial; y además estables cromosómicamente hasta pase 12. Tras 2 días en cultivo con EndoECM, los organoides mostraron una expansión comprometida junto con un halo de degradación del EndoECM circundante. Esta degradación culminó con la digestión total del EndoECM en día 5 y la fusión de los organoides entre sí.

RESUMEN

Hidrogeles de matriz extracelular endometrial como tratamiento regenerativo para patologías reproductivas *in vivo*.

<u>Estudio preliminar de la compatibilidad *in vivo* de los hidrogeles de matriz extracelular endometrial en un modelo subcutáneo murino.</u>

Tras 48 h, los hidrogeles aparecieron gelificados en el tejido subcutáneo. EndoECM presentó una la infiltración celular 4 veces menor que No-DC Endo (1599±402 y 6243±244 células en EndoECM y No-DC Endo, respectivamente), mientras que la infiltración de macrófagos CD68 positivos fue significativamente mayor (72,0±15,0% y 19,2±7,77%). Después de 14 días, se observó una disminución del volumen de EndoECM acompañada de un cambio de la morfología celular desde tipo inflamatoria hacia fibroblástica, mientras la infiltración de macrófagos CD68 positivos se mantuvo.

<u>Estudio de regeneración endometrial y restauración de la fertilidad en un modelo murino de daño endometrial.</u>

El tratamiento con etanol indujo una importante lesión endometrial que no afectó a la ciclicidad estral. Los hidrogeles inyectados desaparecieron del lumen uterino tras 14 días mientras que se detectó colágeno biotinizado en el interior del 62,5% de los tejidos uterinos tratados. El análisis de regeneración endometrial mostró una mejora ascendente desde el grupo salino a EndoECM+GF con un aumento del grosor endometrial (0,91±0,44, 1,05±0,43, 1,18±0,27 en salino, EndoECM and EndoECM+GF, datos de cuernos dañados/tratados normalizados respecto los no dañados), aumento de la concentración glandular (0,84±0,13, 1,18±0,20, 1,34±0,65), reducción de la deposición de colágeno en términos de expresión de *Col1a1* (2,74±1,26, 0,71±1,25 and -1,20±0,91) y aumento de la proliferación celular (0,89±0,32, 1,18±0,35 and 1,69±0,47). Las dos últimas con mejora significativa en EndoECM+GF. El daño endometrial por etanol causó

una reducción significativa de la fertilidad (17% de embarazo en salino respecto al 80% en cuernos control sin daño) no mejorada con EndoECM (8%). En cambio, EndoECM+GF mostró una fertilidad incrementada (45%) sin diferencias significativas en comparación con los cuernos control sin tratamiento.

DISCUSIÓN

La infertilidad afecta al 15% de las parejas españolas en edad reproductiva y existen cerca de un millón de parejas que necesita asistencia reproductiva para poder concebir. El endometrio es el tejido uterino encargado de la implantación embrionaria y puede ser la causa de la infertilidad cuando se ve afectado de forma irreversible por patologías como la EA y el AS, las cuales continúan sin solución médica hoy en día. En la actualidad, la lucha contra la infertilidad por factor endometrial ha tomado rumbo hacia nuevas tecnologías como son la terapia celular y la ingeniería de tejidos. Dentro del campo de la ingeniería de tejidos, los hidrogeles de ECM procedentes de tejidos DC han demostrado tener un alto potencial como plataforma para el cultivo 3D *in vitro* y para la regeneración tisular *in vivo* en distintas áreas de la medicina.

El primer objetivo de esta tesis fue el desarrollo de hidrogeles de ECM específicos de endometrio. Las razones por las que se utilizó el cerdo como fuente de tejido endometrial fueron su alta disponibilidad sumado a la presunción de biocompatibilidad de los tejidos DC y a la alta conservación de la ECM entre especies de mamíferos. Tras la descelularización, los análisis de contenido celular y ADN fueron satisfactorios, si bien existe una falta de criterios oficiales que definan una buena descelularización. Para evaluar más a fondo la potencial inmunoreactividad, estudiamos la principal causa de rechazo de xenotrasplantes de cerdo en humanos, el epítopo α-gal, y demostramos su

RESUMEN

eliminación en nuestro endometrio DC. Otro aspecto crítico para la biocompatibilidad fue evadir la toxicidad por cúmulo de detergentes residuales proveniente del proceso de descelularización. Para ello, monitorizamos la eliminación del SDS y alcanzamos concentraciones no nocivas *in vitro* tras seis lavados. Tras el procesamiento del endometrio DC, creamos hidrogeles de EndoECM porcina con una cinética de gelificación y ultraestructura típica de hidrogeles específicos de tejido previamente descritos en otros órganos y tejidos. La comparación del perfil proteómico de EndoECM con MyoECM demostró su tejido-especificidad mientras que la comparación con No-DC Endo fue clave para corroborar de forma teórica su hipoinmunogenicidad y preservación de la ECM endometrial.

El segundo objetivo fue el uso de EndoECM como plataforma para sistemas de cultivo 3D *in vitro*. El primer experimento consistió en comprobar la compatibilidad *in vitro* de EndoECM mediante el cultivo de células primarias y madre endometriales de procedencia humana en condiciones bi- y tridimensionales, así como la comparación de su proliferación con dos matrices estándar, colágeno y Matrigel. Tras confirmar la citocompatibilidad, encontramos un aumento significativo de la proliferación celular en EndoECM en sistemas 2,5D y 3D, sobre todo en las líneas de células madre endometriales, lo que sugiere un efecto beneficioso de EndoECM en estos sistemas de cultivo. Esta mejora puede atribuirse a la señalización bioquímica o mecánica, ya que es conocido que las características específicas del sustrato afectan a la diferenciación y proliferación de las células madre. A continuación, nos propusimos diseñar la estructura clásica del endometrio humano cocultivando células humanas endometriales en EndoECM. No usamos suplementación hormonal para examinar el efecto inherente de la matriz. Nuestros hallazgos mostraron que tanto los sistemas 3D con células madre como con células primarias permanecieron viables a largo plazo y fueron rápidamente

remodeladas de forma similar a otras matrices basadas en colágeno. Sin embargo, los constructos endometriales presentaron una baja expresión de E-cadherina y no había polarización apico-basal, probablemente debido a la falta de estimulación hormonal. El siguiente paso fue el uso de hidrogeles EndoECM como soporte para el cultivo de organoides endometriales con el objetivo de conseguir un microambiente más natural que el proporciona actualmente el Matrigel. Para ello, establecimos una línea de organoides a partir de endometrio humano que mostró las características típicas previamente reportadas. Sin embargo, cuando se sustituyó el Matrigel por EndoECM, este fue objeto de una degradación agresiva y los organoides se fusionaron entre sí, lo que sugiere la invalidez de EndoECM en formulación pura para el cultivo de organoides endometriales. No obstante, estos resultados abren la ventana a nuevas investigaciones como el uso de compuestos estabilizantes para evitar la degradación de EndoECM o el uso de este como suplemento de medios de cultivo.

El tercer y último objetivo fue la aplicación de EndoECM como tratamiento regenerativo *in vivo* para patologías endometriales en un modelo murino. Como primera toma de contacto, realizamos un estudio preliminar de biocompatibilidad *in vivo* en un modelo subcutáneo inmunocompetente. Esta prueba nos permitió verificar la inyectabilidad y la gelificación espontánea *in vivo* de EndoECM al mismo tiempo que evaluar la respuesta general al mismo y determinar sus efectos tóxicos a corto plazo. Una vez analizado, EndoECM fue testado como tratamiento regenerativo de daño endometrial. Para crear un modelo de lesión endometrial en ratonas, los cuernos uterinos fueron intervenidos con etanol, el cual produjo una lesión notable y una reducción de la fertilidad mientras que la función ovárica no fue afectada. Tras dos semanas postratamiento con hidrogeles, estos desaparecieron del lumen y fueron detectados en los tejidos uterinos, lo que sugiere su absorción. Tras analizar la regeneración tisular del endometrio, encontramos que el

tratamiento con EndoECM inducía una tendencia a la mejora del grosor endometrial, la concentración glandular, la deposición de colágeno y la proliferación celular con respecto al control con solución salina. Esta tendencia era acrecentada con EndoECM+GF, alcanzando un aumento significativo de la proliferación endometrial y una disminución de la expresión de colágeno que podría conllevar a la reducción de la fibrosis tisular. Cuando evaluamos la fertilidad, detectamos que el tratamiento con EndoECM no contrarrestó la lesión producida por etanol, sin embargo, sí que observamos el ascenso de las gestaciones con EndoECM+GF. Estos resultados sugieren que la suplementación con IGF-1, bFGF y PDGFbb podría aumentar el efecto terapéutico de EndoECM y promover la regeneración endometrial y la restauración de la fertilidad en un modelo murino con lesión endometrial. Dada la capacidad las fibras ECM para secuestrar y controlar la actividad de biomoléculas, EndoECM podría emplearse como vehículo para tratamientos basados en factores de crecimiento purificados como los incluidos en este estudio, u otras combinaciones prometedoras (p. ej. plasma rico en plaquetas), que podría conducir a un efecto sinérgico y ser una solución para tratar patologías endometriales como la EA y la AS.

La presente tesis abre una puerta hacia el uso de EndoECM *in vitro* y futuras aplicaciones *in vivo* en medicina reproductiva para tratar patologías endometriales.

CONCLUSIONES

De esta tesis se pueden extraerse las siguientes conclusiones:

1. La descelularización de útero completo y procesamiento del tejido endometrial permite la generación de hidrogeles de matriz extracelular endometrial de origen porcino, exhibiendo los rasgos propios de hidrogeles de matriz extracelular específicos de tejido.

2. Los hidrogeles de matriz extracelular endometrial son mezclas purificadas de componentes bioactivos y estructurales pertenecientes a la matriz extracelular del endometrio natural con baja presencia de moléculas potencialmente inmunorreactivas.

3. Los hidrogeles de matriz extracelular porcina o no humana son compatibles con células endometriales humanas *in vitro*, permitiendo el crecimiento celular y mejorando la proliferación de líneas de células madre en comparación con las matrices estándar de colágeno y Matrigel en sistemas de cultivo tridimensional.

4. Los cocultivos tridimensionales de células endometriales en hidrogeles de matriz extracelular endometrial son viables y proliferativos a largo plazo, mostrando la naturaleza modelable y degradable típica de las matrices basadas en colágeno.

5. Los hidrogeles de matriz extracelular endometrial presentan, en términos generales, una respuesta inmunitaria temprana disminuida en comparación con hidrogeles no descelularizados cuando son aplicados *in vivo* en un modelo subcutáneo murino.

6. Los hidrogeles de matriz extracelular endometrial promueven la regeneración del endometrio dañado (no estadísticamente significativo) pero no solventan la pérdida de fertilidad producida por etanol en modelos murinos.

7. La suplementación de hidrogeles de matriz extracelular endometrial con factor de crecimiento fibroblástico básico (FGFb), factor de crecimiento derivado de plaquetas-BB (PDGF-bb) y factor de crecimiento similar a la insulina-1 (IGF-1) mejora la regeneración endometrial y la fertilidad en un modelo murino de daño endometrial (no estadísticamente significativo).

CONTENTS

CONTENTS

LIST OF FIGURES

LIST OF TABLES

ABBREVIATIONS

A

ACN	acetonitrile
AS	Asherman's syndrome
α	alpha

B

BM-MSCs	bone-marrow mesenquimal stem cells
BSA	bovine serum albumin
β	beta

C

CD	cluster of differentiation
cDNA	complementary DNA
cm	centimeter
CO_2	carbon dioxide
ºC	degree(s) Celsius

D

DAB	3, 3′ diaminobenzidine tetrahydrochloride
DAPI	6-diamidino-2-phenylindole
DC	decellularized
DMEM	Dulbecco's modified Eagle's medium
DMEM/F-12	Dulbecco's modified Eagle's medium: nutrient Mixture F-12
DMSO	dimethyl sulfoxide

E

E10.5	embryonic day 10.5
EA	endometrial Atrophy
ECM	extracellular matrix
EECs	endometrial epithelial cells
EGF	epidermal growth factor
EndoECM	endometrial extracellular matrix
EndoECM+GF	endoECM plus growth factors
ESCs	endometrial stromal cells
mg	milligram

F

FA	formic acid
FBS	fetal bovine serum
FCS	fetal calf serum
FGF(b)	(basic) fibroblast growth factor
FSH	follicle-stimulating hormone

G

g	gram
G	gauge
GAGs	glycosaminoglycans
Gapdh	glyceraldehyde-3-phosphate dehydrogenase gene

H

h	hour(s)
H&E	hematoxylin and eosin
HBSS	hank's balanced salt solution
HCl	hydrochloric acid
HGF	hepatocyte growth factor

I

IGF	insulin-like growth factor
T_1	time to complete gelation
$T_{1/2}$	time to half gelation
T_{Lag}	lag time

L

LC-MS/MS	liquid chromatography and tandem mass spectrometry

M

µg	microgram
µL	microliter
µm	micrometer
m/z	mass-to-charge ratio
R-Spondin	roof plate-specific spondin

min	minute(s)		**RT**	room temperature
mL	milliliter		**RT-qPCR**	real-time quantitative polymerase chain reaction
mM	millimolar			
mm	millimeter			
MMPs	matrix metalloproteinases		**$\underline{S}$**	
MSCs	mesenchymal stem cells		*S*	gelation rate
MT	Masson's trichrome		**SCSIE**	servicio central de soporte a la investigación experimental
MTS	3-(4,5-dimethylthiazol-2-yl)-5-(3-carboxymethoxyphenyl)-2-(4-sulfophenyl)-2h-tetrazolium		**SD**	standard deviation
			SDS	sodium dodecyl sulfate
MyoECM	myometrial extracellular matrix		**SEM**	scanning electron microscopy
			SP	side population
$\underline{N}$			**SSCs**	somatic stem cells
NaOH	sodium hydroxide			
ng	nanogram		**$\underline{T}$**	
nM	nanomolar		*Col1a1*	collagen type I α-1 chain gene
nm	nanometer		**T_1**	time to complete gelation
No-DC	non-decellularized		**$T_{1/2}$**	time to half gelation
No-DC Endo	non-decellularized endometrial matrix		**TFA**	trifluoroacetic acid
NoTT	no treatment		**T_{Lag}**	lag time
			TUNEL	terminal deoxynucleotidyl transferase-mediated dUTP nick-end labelling
$\underline{O}$				
O_2	oxygen		**$\underline{V}$**	
			v	volume
$\underline{P}$				
PBS	phosphate-buffered saline		**$\underline{W}$**	
PDGFbb	platelet-derived growth factor-bb		**w**	weight
PFA	paraformaldehyde			
PGs	proteoglycans		**$\underline{Others}$**	
P*n*	passage number *n*		**2D**	two-dimensional
p	p value		**3D**	three-dimensional
			% cov	percentage of individual coverage
$\underline{R}$				
rpm	revolutions per minute			
RPMI	Roswell Park Memorial Institute medium			

I. INTRODUCTION

I.   INTRODUCTION

1. The female reproductive system: Anatomy and physiology

The female reproductive system consists of a set of internal reproductive organs and external genitalia (Jones and Lopez 2014; Guzmán-López and Guzmán-López 2014). The internal reproductive organs include the ovaries, fallopian tubes, uterus and cervix, which play key roles in ovulation, embryo transport and implantation, fetus development and birth. On the other hand, the external genitalia are accessory structures used during sexual intercourse, and include the vagina, vulva, and perineum.

The uterus is the largest multifunctional organ in the female reproductive system. Its functions include sperm transport and storage, communication with the ovary, embryo implantation, pregnancy recognition, placenta formation, gestation, and eventual expulsion of offspring at birth. In general, the uterus is a hollow structure which begins in the oviducts and terminates at the cervix, but this organ may present with a simplex, bicornate or duplex form depending on the mammalian species (Hayssen 2017) *(Figure 1)*. Simplex uteri, found in humans, primates and nine-banded armadillos, are characterized by a single cavity or lumen. On the contrary, duplex uteri, found in a variety of taxa including lagomorphs and some rodents, are characterized by bilateral uterine horns whose individual cervixes meet at the vagina, but whose lumens remain separate. Meanwhile, bicornuate uteri, found in mice and artiodactyls such as pigs, shrews, perissodactyls, cetaceans, carnivorans and some bats, also have two uterine horns but their lumens come together at a single cervical opening to the vagina.
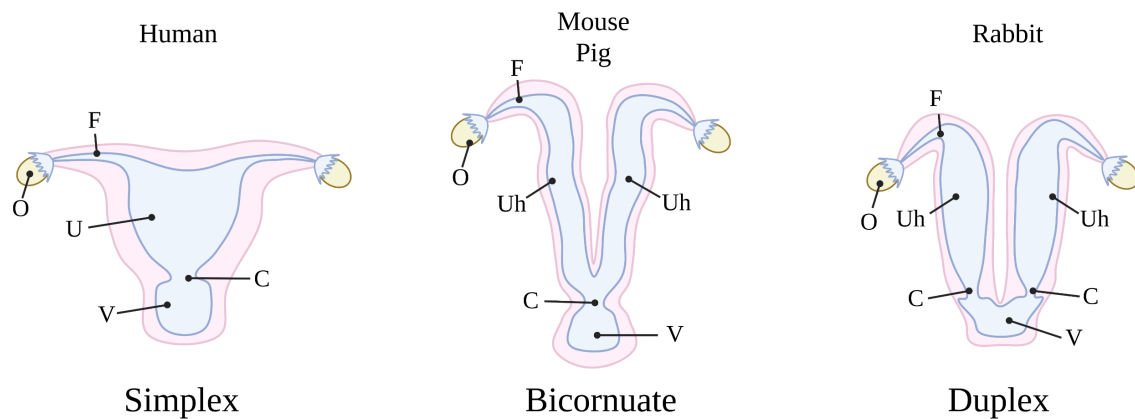
Figure 1. Comparison of the three major uterine anatomies found in mammals. *Simplex shape of the human uterus with a unique uterine cavity and cervix. Bicornuate shape of the pig uterus with the uterus partially divided into two uterine horns but that meet a single cervix. Duplex shape of the mouse uterus with two separated uterine horns and cervices. O: ovary; F: Fallopian tube; U: uterus; Uh: uterine horn; C: cervix; V: vagina. Created with BioRender.com.*

The human uterus is of simplex form, with an inverted pear silhouette and a triangular-shaped cavity *(Figure 1)*. It normally measures 7.5-centimeter (cm) in length, 5 cm in width and is 1.75 cm thick (however these proportions may increase in multiparous women). The uterus can be divided in three zones: the uterine fundus (upper domed-shaped region), the body of the uterus, and the uterine isthmus (narrow region between the corpus and the cervix) *(Figure 2)*. Broad, uterosacral and round ligaments support the uterus within the pelvic cavity. Blood supply is principally sustained by the uterine artery which branches off directly from the internal iliac artery while venous drainage occurs through tributaries that lead to the internal iliac vein.
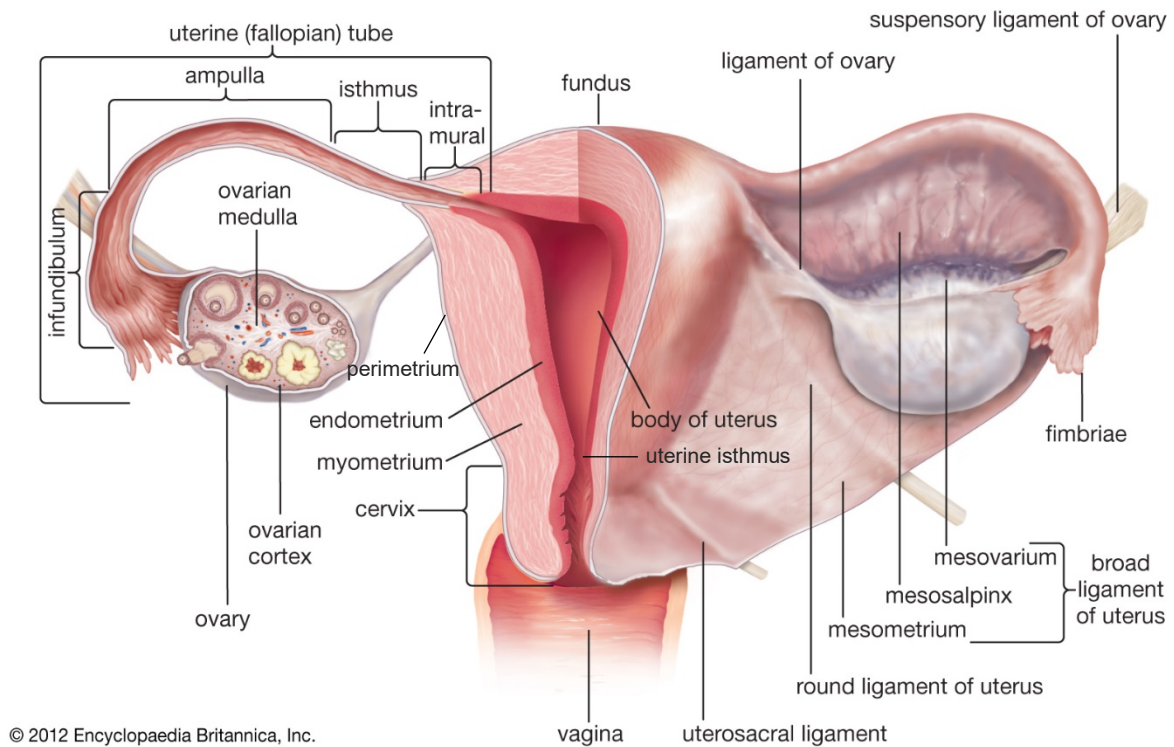
Figure 2. Anatomy of the human female reproductive tract. By courtesy of Encyclopædia Britannica, Inc., copyright 2009; used with permission.

The wall of the uterine fundus and corpus consist of three principal layers *(Figure 2)*: the perimetrium, which is the thin outermost layer covering the external surface; the myometrium, which is the thick middle layer of smooth muscle capable of supporting growing fetus(es) during pregnancy and producing very strong contractions required for birth; and finally the endometrium, the innermost, mucus-producing and more complex layer of the uterus that will be explained in detail in the following section. Notably, the myometrium itself also has an inner and outer layer of longitudinally oriented fibrillar bundles and a middle layer which is highly vascularized.

The cervix connects the vagina to the uterus and produces mucus with different consistency depending on the stage of the menstrual cycle, which aids or impedes the entry of spermatozoa toward the uterus. Moreover, the uterus is linked to the ovaries through the fallopian tubes, also known as the oviducts. The fallopian tubes are bilateral

structures approximately 10 cm long, consisting of four parts: the oviductal infundibulum (containing the fimbriae), ampulla, isthmus and the intramural oviduct. At ovulation, the ovulated oocyte (commonly named eggs or ovum) is caught by the infundibulum and transported along the tube towards the ampulla, where fertilization may take place if the oocyte encounters sperm. The resulting zygote (fertilized oocyte) begins the first stages of embryonic divisions as it travels through the oviduct towards the uterus (Jones and Lopez 2014; Guzmán López and Guzmán López 2014; Pritchard JA, MacDonald PC, and Gant 1986).

The ovaries, or female gonads, are white to yellowish oval-shaped structures located in the upper pelvic cavity, on either side of the uterus. They have an irregular surface as a consequence of the continuous scars produced by ovulation. The ovary is responsible for the production of two crucial components for reproduction: (I) mature oocytes (oogenesis), and (II) sexual hormones (steroidogenesis). Oogenesis begins in the ovaries at 16-20 weeks of fetal development, and these primordial oocytes remain in a quiescent state until puberty (Albamonte *et al.* 2008; Hartshorne *et al.* 2009). Every month after puberty, a pool of oocytes is recruited and activated to grow to the ovulatory stage (by a process known as folliculogenesis) until depletion (at menopause). As a result of folliculogenesis and steroidogenesis remaining active from puberty to menopause, women can produce about 400 mature oocytes during their reproductive life (Mauch and Schoenwolf 2001).

2. The endometrium

2.1. Endocrine regulation of endometrial remodeling

The endometrium is the mucus membrane lining the lumen of the uterus, and its principal functions are to prepare for and receive the embryo at implantation, maintain pregnancy if implantation occurs, and menstruate in the absence of pregnancy (Critchley *et al.* 2020). The endometrium is a highly dynamic multicellular tissue influenced by the estrogen and progesterone produced by the ovary that regenerates through scar-free remodeling during each menstrual cycle.

The human menstrual cycle consists of three phases: proliferative, secretory and menstrual, with a total duration of 28 days *(Figure 3)*. In response to follicle-stimulating hormone (FSH) produced by the anterior pituitary gland during the proliferative phase (the first 9 days after menstruation), ovarian follicles grow and in turn produce estradiol that induces proliferation of the steroid-responsive endometrial cells, and ultimately thickens the endometrium for potential implantation. On day 14, a spike in luteinizing hormone (LH; also produced by the anterior pituitary), triggers ovulation of a mature oocyte from the ovary. The secretory phase begins after ovulation and is marked by the ovulatory site transforming into a progesterone-secreting corpus luteum. In turn, the progesterone induces differentiation of the endometrium, resulting in remarkable changes (i.e., glandular secretion, stromal decidualization) that open the "window of implantation", the time period when the endometrium is receptive to embryo implantation. If embryo implantation does not occur, the progesterone withdrawal initiates the menstrual phase, where the endometrial lining is broken down and shed. Finally, a new increase in estradiol levels, produced by another pool of growing ovarian follicles, begins a new cycle. Notably, in each cycle the endometrium is rapidly repaired

without residual scarring or loss of function, with processes such as inflammation, angiogenesis, tissue remodeling, and formation of new tissue (Critchley *et al.* 2020).
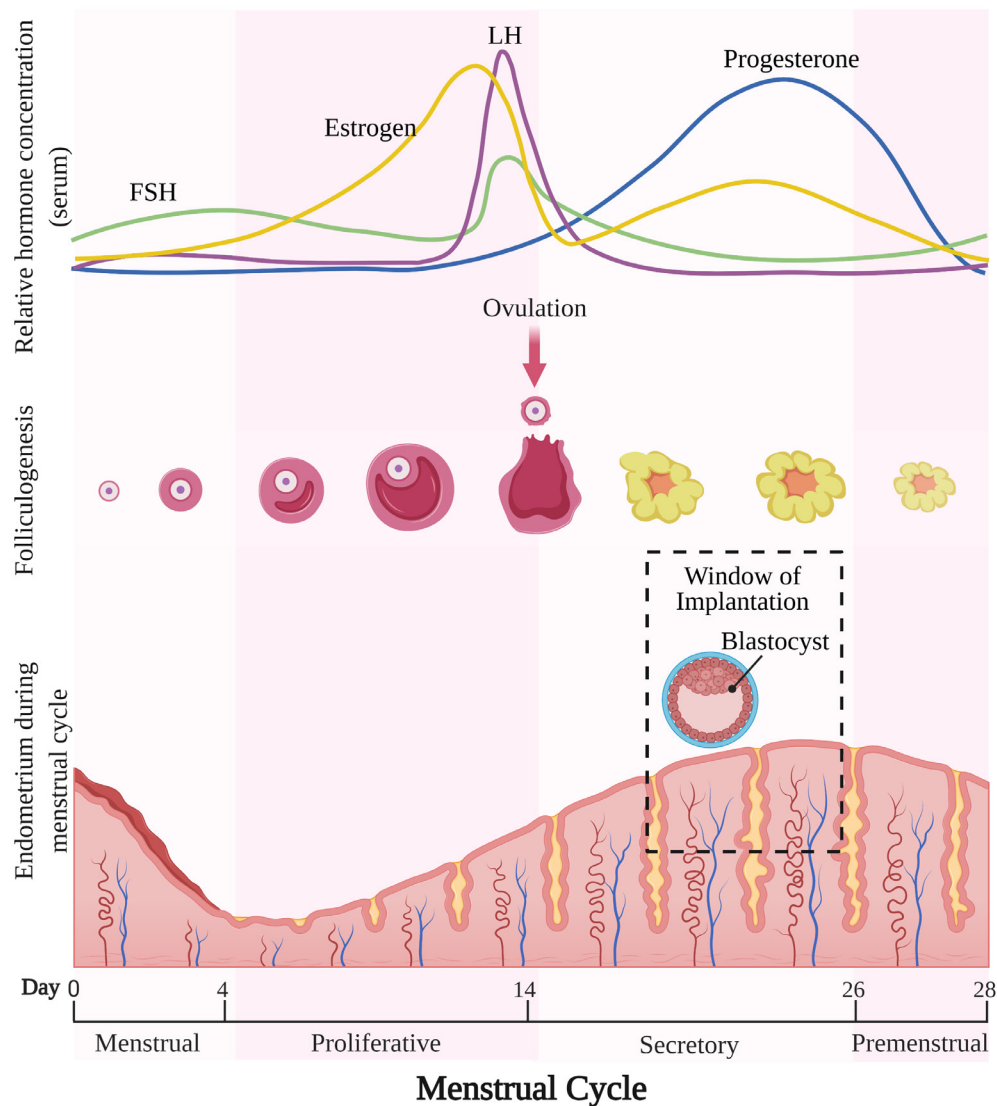
Figure 3. The human menstrual cycle. *Diagram showing the relative concentration of serum FSH, LH, estrogen and progesterone hormones, stages of follicle growth during folliculogenesis and state of the endometrium during the human menstrual cycle. Adapted from "The Estrus Cycle of Mice", by BioRender.com (2021). Retrieved from https://app.biorender.com/biorender-templates.*

It is important to highlight that in other mammals, the cycle does not involve menstruation. In fact, menstruation is restricted to higher primates, some bats, and elephant shrew (Emera, Romero, and Wagner 2012). This other type of cyclicity is referred to as the estrous cycle and consists of four hormone-dependent stages: proestrus,

estrus, metestrus and diestrus. Proestrus is the pre-receptive period during which pre-ovulatory development takes place in the ovary, with consequent secretion of estrogens and endometrial growth. The following estrous phase is a brief interval during which ovulation occurs, external genitalia are more pronounced (e.g., swollen vulva and large vaginal opening) and females are receptive to mating. The subsequent metestrus and diestrus phases correspond to the human early and late luteal phase, respectively, during which the endometrium is reabsorbed. In mice, the estrous cycle lasts a total of 4.3 days of cycle and is divided as follows: 32.4 h of proestrus, 20.7 h of estrus, 21.8 h of metestrus and 21.8 h of diestrus (Bronson, Dagg, and Snell 1966) *(Figure 4)*.
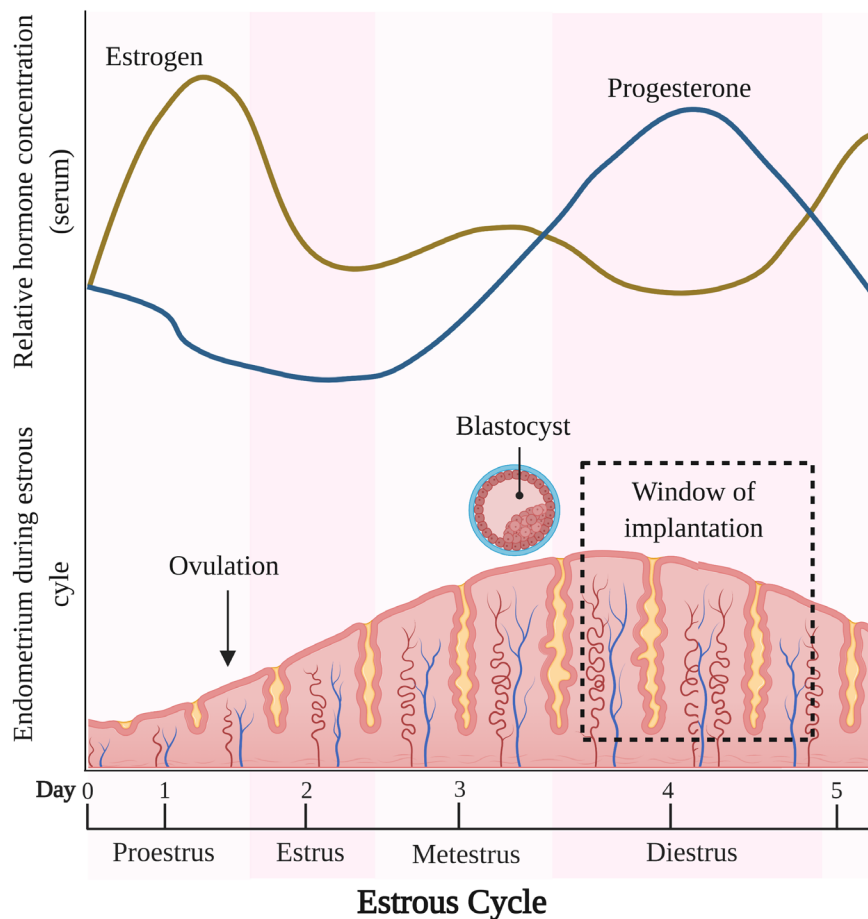
Figure 4. The murine estrous cycle. *Diagram showing the relative concentration of estrogen and progesterone hormones in serum, state of the follicle during folliculogenesis and state of the endometrium during the murine estrous cycle. Adapted from "The Estrus Cycle of Mice", by BioRender.com (2021). Retrieved from https://app.biorender.com/biorender-templates.*

2.2. Structure and composition of the endometrium

The endometrium consists of epithelial and stromal compartments supported by an endogenous niche of stem cells, a generous vasculature and a population of immune-resident cells (Carrascosa, Horcajadas, and Moreno-Moya 2018). The epithelial compartment can be divided into luminal epithelium and endometrial epithelial glands, both composed of endometrial epithelial cells (EECs), while the stromal compartment contains endometrial stromal cells (ESCs). The endometrium can also be divided in two layers, the stratum functionalis (functional layer) and the stratum basalis (basal layer). The functional layer of the endometrium is the portion that undergoes the most changes and is shed during menstruation. Meanwhile, the underlying basal layers remain in place to act as an endometrial supply for the regeneration of a new functional layer in the next menstrual cycle.

The basal layer is preserved throughout the female's life (Simón *et al.* 2009). Accumulative evidence since 1978 suggests that the basal layer is a reservoir of a population of endogenous endometrial somatic stem cells (SSCs) (Prianishnikov 1978). The presence of the SSCs has recently been confirmed using approaches focused on the concept of stemness - self-renewal and cell differentiation. The techniques to confirm self-renewal of cells are clonogenicity and long-term culturing capabilities, while capacity to differentiate is assessed through multilineage differentiation and reconstruction of new tissue (Santamaria *et al.* 2018). Other common approaches include the search of already-known stem cell markers and the "side population" (SP) method. The SP method is based on the adult stem cell´s ability to efflux fluorescent vital dyes (such as Hoechst 33342) with the help of special ATP-binding cassette transporters. Endometrial stem cells from differentiated cells (who lack these transporters and

therefore are unable to fluoresce) can easily be identified and isolated by flow cytometry (Cervelló *et al.* 2010; 2011; Miyazaki *et al.* 2012). To date, three different types of SSCs have been described in the endometrium: mesenchymal stem cells (MSCs), epithelial progenitor cells, and endothelial cells *(Figure 5)*.
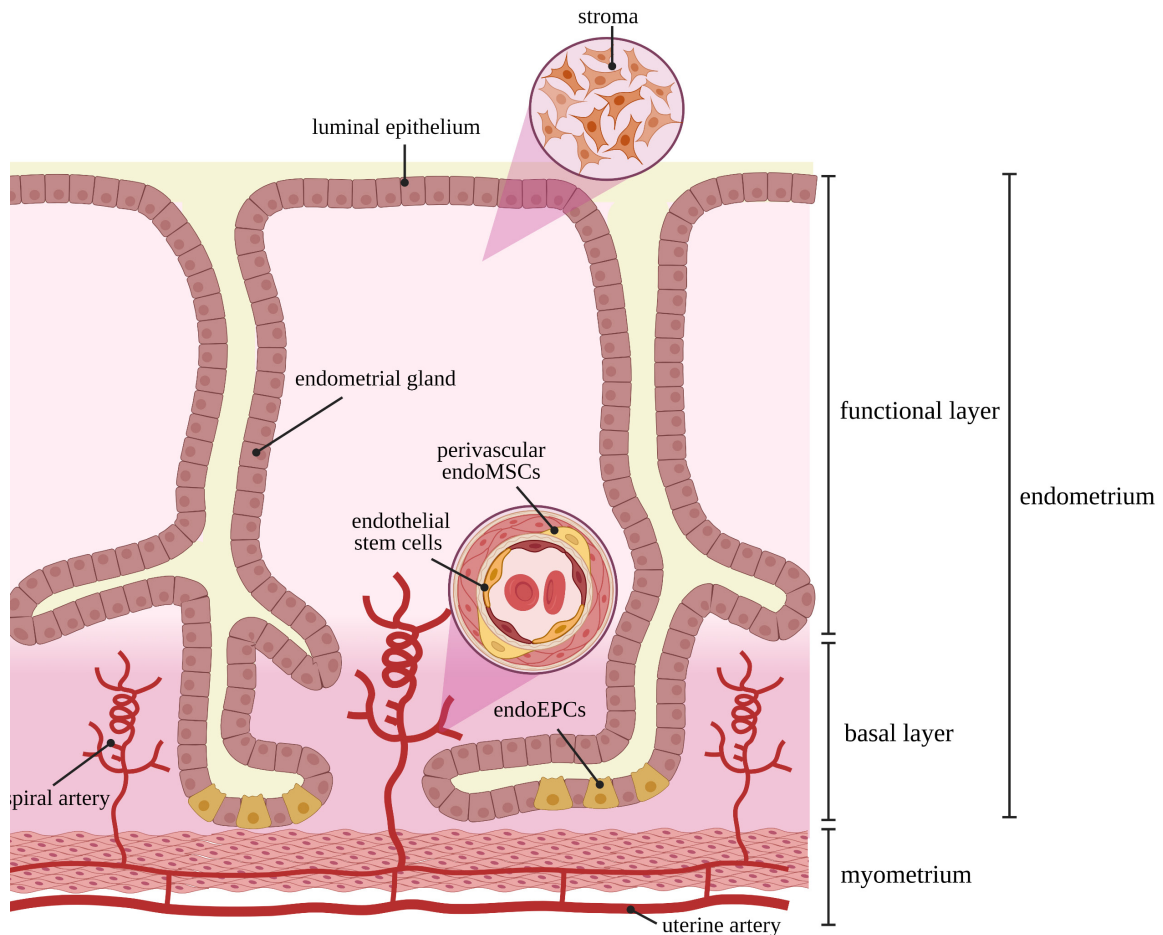
Figure 5. Morphology of the endometrium. Diagram illustrates the functional and basal endometrial layers. Endometrial glands contain endometrial epithelial progenitor cells (endoEPCs) while the spiral arteries originating from the uterine artery are a source of perivascular endometrial MSCs (endoMSCs) and endothelial stem cells. Picture created with BioRender.com.

Endometrial MSCs have been identified as perivascular cells located adjacent to the endothelial cells lining the microvessels (Crisan *et al.* 2008; Masuda *et al.* 2012; Schwab and Gargett 2007). On the other hand, the endometrial epithelial progenitor cells are postulated to be a subpopulation of cells located in the base of the glands found in the

basalis layer (Gargett, Schwab, and Deane 2016; Valentijn *et al.* 2013; Nguyen *et al.* 2017). Endothelial stem cells expressing the classical cluster of differentiation (CD) markers CD31$^+$/CD34$^+$ have also been postulated to be part of the endometrial stem cell niche (Tsuji *et al.* 2008). In theory, the dysfunction of any type of these endometrial SSCs could be the underlying cause of endometrial pathologies.

2.3. Endometrial pathologies affecting fertility: Endometrial atrophy and Asherman's syndrome

The World Health Organization describes infertility as ¨a disease of the reproductive system defined by the failure to achieve a clinical pregnancy after 12 months or more of regular unprotected sexual intercourse¨ (Zegers-Hochschild *et al.* 2009). Nowadays, 8–12% of reproductive-aged couples worldwide suffer from infertility (Vander Borght and Wyns 2018). The achievement of a successful pregnancy depends on two crucial factors: the presence of a healthy embryo and a functional uterus. Uterine factor infertility may affect up to 1 in 500 reproductive-aged women (Hur *et al.* 2019), Endometrial disorders, such as endometrial atrophy (EA) and Asherman's syndrome (AS), with underlying problems arising from insufficient endometrial growth, fibrotic events or endometrial destruction can affect the receptivity of the endometrium and can ultimately result in sterility.

Adequate thickness of the endometrium is a fundamental basis for accomplishing a successful pregnancy. Endometrial atrophy is a congenital or iatrogenic pathology characterized by aberrant or deficient endometrial growth *(Figure 6)*. Women who suffer from EA present an atrophic and usually thin endometrium (below 7 millimeter (mm)), which cannot reach the threshold to support embryo implantation (Lebovitz & Raoul Orvieto, Informa, and Ltd 2014).
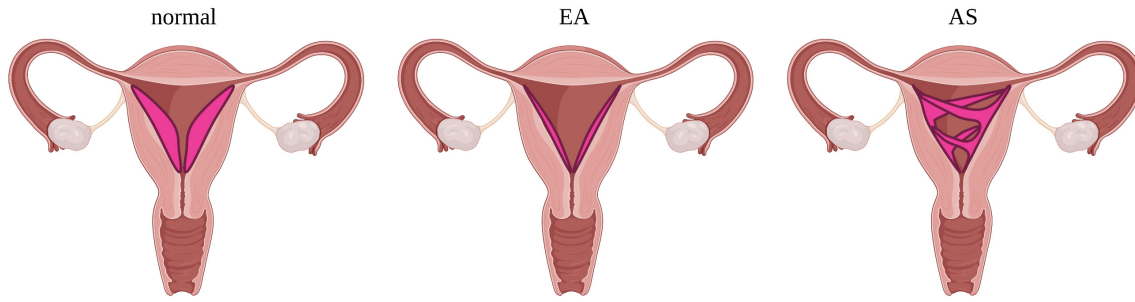
Figure 6. Normal endometrium, endometrial atrophy and Asherman's syndrome. *Pictures showing a secretory endometrium presenting a normal endometrial thickness, a thin/atrophic uterus characteristic of endometrial atrophy (EA) and endometrial adhesions produced by Asherman´s syndrome (AS). The endometrium is indicated in pink. Created with BioRender.com.*

In contrast, AS is an acquired pathology characterized by the destruction of the endometrium and presence of adhesions within the uterine cavity *(**Figure 6)*. Asherman´s syndrome can be provoked by a postpartum hemorrhage, myomectomy, septum resection and more likely, endometrial infection after dilatation and aggressive curettage after abortion or miscarriage (90% of cases) (Hur *et al.* 2019). To date, there are no effective therapies for the loss of endometrial function, included EA or AS. Some studies have reported effective cell therapy (Morelli, Rameshwar, and Goldsmith 2013; Zhao *et al.* 2014a; Zhao *et al.* 2015; Cervelló *et al.* 2015; Gil-Sanchis *et al.* 2015; Santamaria *et al.* 2016), but important barriers, such as the low retention of cells in the damaged areas (Cervelló *et al.* 2015; Zhao *et al.* 2014a; Zhao *et al.* 2015; Gil-Sanchis *et al.* 2015; Xiao *et al.* 2019), probably because of lack of resources for the cells in the damaged tissue (Singelyn *et al.* 2012), has hampered its clinical implementation.

3. The importance of the extracellular matrix

The extracellular matrix (ECM) is a non-cellular macromolecular network in which cells from all tissue and organs reside. The ECM provides a milieu of vital importance for various cell functions and behaviors, in both healthy and ill conditions (Evangelatov and Pankov 2013; Theocharis *et al.* 2016). The importance of ECM is so critical that, with a few exceptions, cells must be bound to the ECM to survive; loss of this bond results in cell death (Schultz and Wysocki 2009).

The ECM is principally a complex mixture of fibrous-forming proteins (such as collagens, elastin, fibronectin, laminins, glycoproteins, glycosaminoglycans (GAGs) and proteoglycans (PGs)), which are highly acidic hydrated molecules that when associated with each other, build a complex three-dimensional (3D) scaffold. These fibrous macromolecules comprise the core of the matrisome*,* which is defined as the ensemble of ECM and ECM-associated proteins (Naba *et al.* 2012). In mammals, the core matrisome comprises approximately 300 proteins classified into collagens, ECM glycoproteins and PGs (Hynes and Naba 2012; Naba *et al.* 2016). Apart from this core, the matrisome contains many ECM regulators (i.e., matrix-degrading enzymes, and inhibitors of these proteases), ECM-affiliated proteins (i.e., lectins, annexins, mucins) and secreted factors (i.e., ECM-binding growth factors, chemokines and cytokines) *(Figure 7)*. All of the aforementioned ECM-associated proteins collaborate to assemble and remodel extracellular matrices as well as bind to cells through ECM receptors (Hynes and Naba 2012; Theocharis *et al.* 2016).
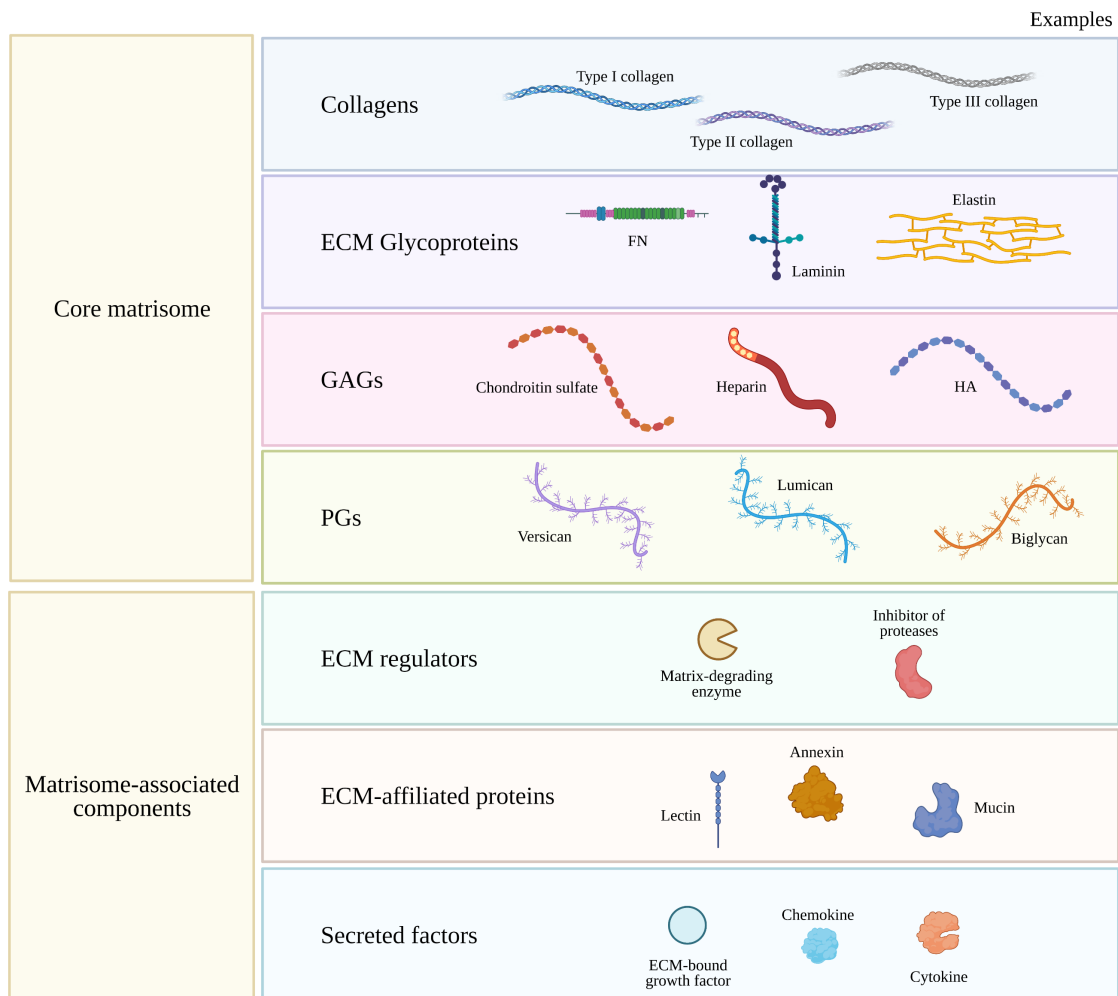
Figure 7. Classification of extracellular matrix components. *List of main ECM components by the matrisome data base (MatrisomeDB 2.0) and several examples. ECM: extracellular matrix; GAGs: glycosaminoglycans, PGs: proteoglycans; FN: Fibronectin; HA: hyaluronic acid; MMPs: Matrix metalloproteinases. Created with BioRender.com.*

In general, the ECMs can be categorized into two types: interstitial and pericellular matrices. The interstitial matrices surround cells, whereas the pericellular matrices are in close contact with them *(Figure 8)*. An example of a pericellular matrix is the basement membrane, found at the interface between parenchyma and connective tissue, which provides an anchoring sheet-like layer for parenchymal cells.
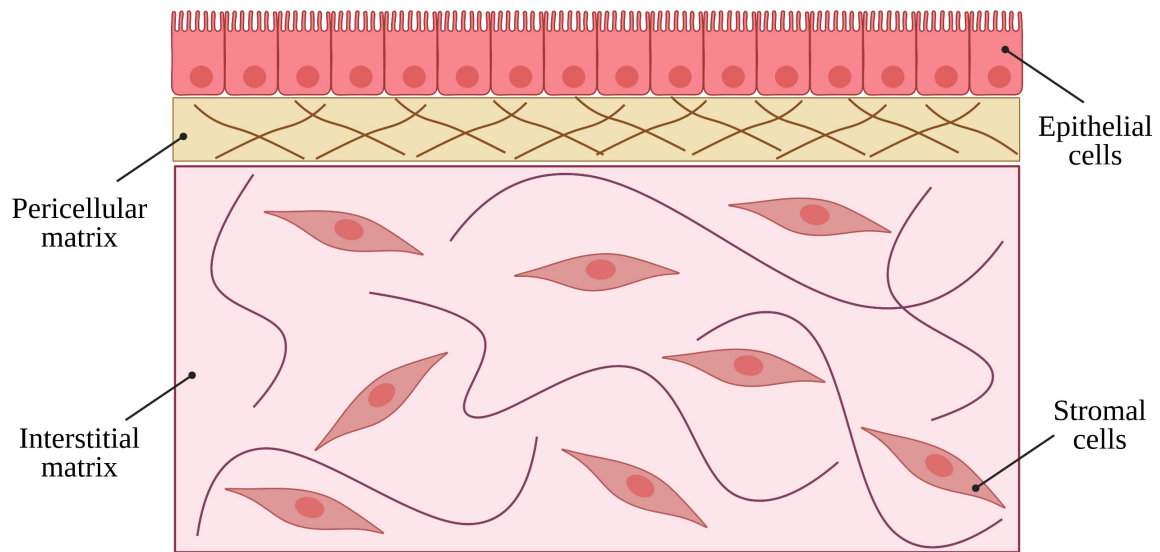
Figure 8. Pericellular and interstitial matrices distribution in the endometrial layer. The pericellular matrix attaches to EECs and interstitial matrix embedding ESCs. Created with BioRender.com.

3.1. Composition of the core extracellular matrisome

3.1.1. *Collagens*

Collagen is the most abundant fibrous protein (30% of the proteins in humans) within the interstitial ECMs in all animals, but it is also located in the basement membranes. Collagens are mainly synthesized and secreted by fibroblasts and can be classified into several categories depending on their structure. Among them, fibrillar collagens (Collagen types I, II, III, V, XI, XXIV and XXVII) have the function of adding tensile strength to tissues, transmit signals to cells, and affect important cellular functions (such as cell migration, angiogenesis, tissue development and repair). Other types of collagens such as beaded-filament-forming collagens (i.e., collagen type VI) interact with ECM proteins (i.e., PGs) in basement membranes. Among the 28 different collagen types known, Collagen type I is the most abundant in tissues and forms perfect heterotrimeric

16

triple helices. Collagen biosynthesis and structure is markedly changed during ECM remodeling in several pathologies, including tumorigenesis (Theocharis *et al.* 2016).

3.1.2. *Extracellular matrix glycoproteins*

Elastin and elastin-associated proteins

Elastin forms long fibers that allow blood vessels, muscle and skin to stretch. Elastin fibers contain fibrillins that form microfibrils, which perform structural roles in elastin fiber assembly. Fibrillins contain heparin and growth factor-binding domains that may directly send signals to cells (Theocharis *et al.* 2016).

Fibronectin

Fibronectin is a multifunctional glycoprotein which acts as a biological adhesive that mediates cell-to-cell adhesion and cell-to-ECM interactions (Schultz and Wysocki 2009). Fibronectin forms supramolecular fibers with lengths of tens of micrometers, which are created during the dynamic remodeling phases of tissue formation or repair. Fibronectin fibers have fibrin-, collagen- and heparin-binding domains and bind to cells via integrin receptors.

Laminins

Laminins are large heterotrimeric glycoproteins that are assembled along with collagen type IV and other molecules in basement membrane matrices. The influence of laminin is vital for cell adhesion, migration, differentiation or survival of the tissues. Laminin participates in the organization of ECM and cell adhesion, by interacting with other laminin and ECM molecules as well as tissue-resident cells, respectively. They are up-regulated in wounded epithelia, to provide a substrate for epithelial cell movement and

recolonization. The distribution of laminin isoforms is tissue-specific, suggesting its involvement in specific tissue functions (Theocharis *et al.* 2016).

3.1.3. *Glycosaminoglycans and Proteoglycans*

Glycosaminoglycans are long and highly negatively charged polymers that contain repeating disaccharides. In fact, each GAG chain is a unique mosaic of disaccharides of variable length and structure. Members of this extremely heterogeneous family fall into six categories: chondroitin sulfate, dermatan sulfate, heparan sulfate, heparin, keratan sulfate and hyaluronic acid. Several GAGs can covalently attach to a core protein to form a PG *(Figure 7)*. Remarkably, PGs are capable of absorbing up to 1,000 times their volume in water (Schultz and Wysocki 2009).

Playing important structural and functional roles, GAGs and PGs are abundant in the ECM. They interact with numerous growth factors, cytokines, chemokines, cell surface receptors and other ECM molecules *(Figure 9)*, as well as participate in pivotal cell functions such as cell signaling, proliferation, migration, differentiation and apoptosis. Proteoglycans are also important in ECM organization, contributing to the formation of the ECM scaffold and the embedding of the cells within it. The GAGs and PGs are remarkably modified during ECM remodeling in all pathologies.
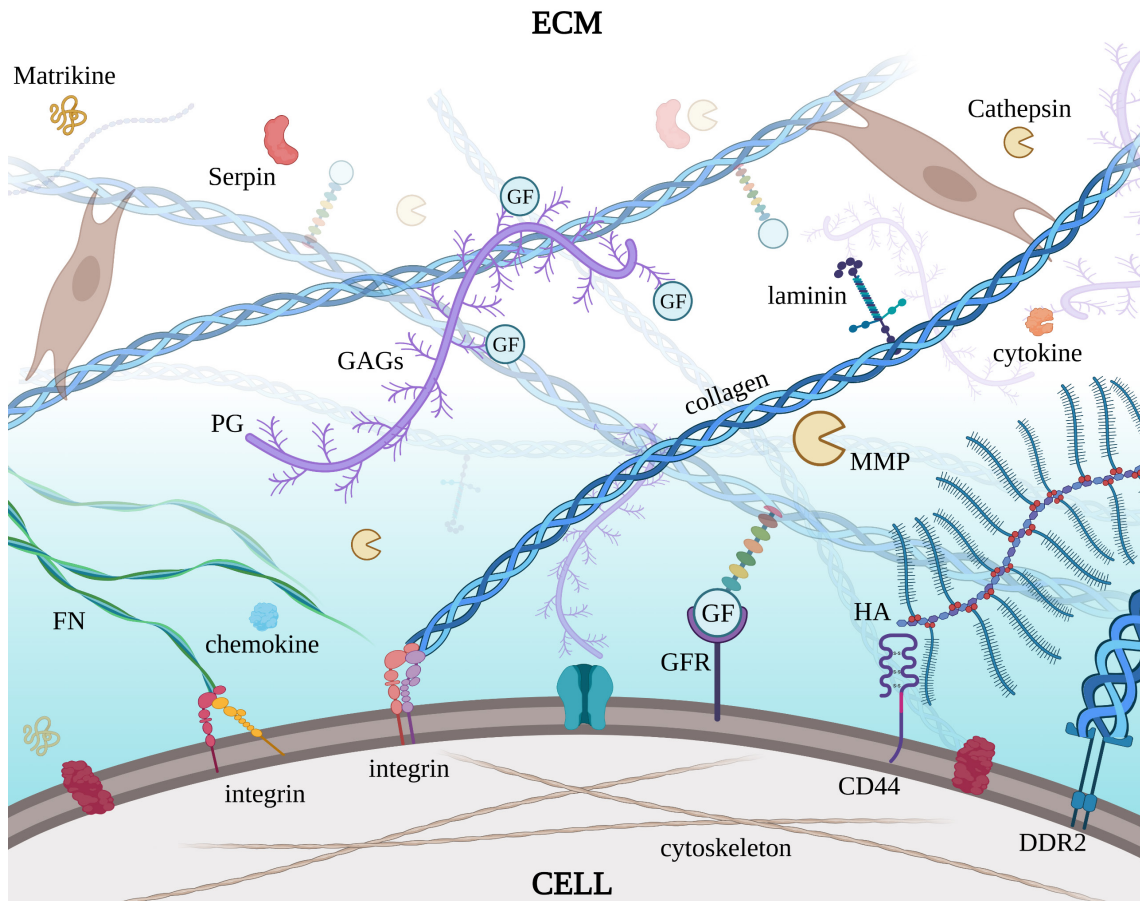
Figure 9. Molecular interactions in the extracellular matrix. *Illustration of molecules that constitute the extracellular matrix (ECM), as well as their interactions with each other and/or cell surface receptors. Glycosaminoglycans (GAGs) join to form proteoglycan (PGs) molecules. In turn, PGs bind to collagen fibers, laminin and ECM-binding growth factors (GF). Fibronectin (FN), collagen, hyaluronic acid (HA) fibers and GF molecules, bind to their respective cell surface receptors. Matrix-degrading enzymes (matrix metalloproteinase (MMP) and cathepsin) and inhibitors of proteases (Serpin) regulating the ECM. Free matrikines, chemokines and cytokines. GFR: Growth factor receptor; DDR-2: Discoidin domain receptor-2. Created with BioRender.com.*

3.2. Physical and biological functions of the extracellular matrix

As discussed in previous sections, the ECM not only provides the scaffold in which cells are embedded but also regulates many biological processes including cell growth, migration, differentiation, survival, homeostasis, and morphogenesis. The ECM has two main roles: (1) acting as a physical substrate for cell adhesion and structure; and (2)

providing appropriate biomechanical and biochemical stimulation to maintain tissue homeostasis (Saldin *et al.* 2017; Rozario and DeSimone 2010; Theocharis *et al.* 2016).

3.2.1. ***Biomechanical cues in the extracellular matrix regulate cell behavior***

Cell surface receptors relay signals from the ECM into cells to regulate diverse cellular functions. These ECM receptors include families of transmembrane integrins, discoidin domain receptors, the hyaluronic acid receptor CD44, and membrane PGs *(Figure 9)*. In particular, by binding with collagen molecules capable of sensing ECM, integrins and discoidin domain receptors provide sensory input via mechanotransduction (Theocharis *et al.* 2016).

Extracellular matrix stiffness, viscoelasticity, porosity and topology are important physical features that can mediate cell behavior (Chaudhuri *et al.* 2020). To date, most studies have focused on stiffness, which is defined as the resistance to deformation. In the ECM, stiffness is modulated by the concentration and cross-linking degree of the ECM fibers. In particular, increases in collagen deposition stiffens the ECM. Furthermore, substrate stiffness can regulate cell growth and viability, as well as resistance to apoptosis. The ideal stiffness of an ECM differs for each tissue and alterations of the latter may provoke illness (Wells 2008; Wang *et al.* 2020a). Moreover, mechanical properties of the ECM have been demonstrated to regulate cellular stemness, differentiation and lineage commitment. A great example of the important role stiffness plays in the stem cell niche is the differentiation of precursor cells into adipocytes or osteoblasts in fat tissue and bone, respectively (Zhao *et al.* 2014b). Additionally, several studies have correlated high stiffness with cell differentiation and low stiffness with stemness (Wells 2008; Gerardo *et al.* 2019).

3.2.2. *Biochemical cues in the extracellular matrix regulate cell behavior*

The ECM also serves as a reservoir for bioactive proteins that work in conjunction with the whole cellular milieu to determine cellular phenotype and behavior. As such, the ECM can sequester, store and release certain growth factors *(Figure 9)*. ECM-bound growth factors provide multiple cell signals that not only control survival, proliferation, differentiation, shape, polarity and motility, but also production and degradation of the ECM itself (Hynes and Naba 2012; Schultz and Wysocki 2009).

The sequestration and release of growth factors by the ECM has two principal effects: (1) protect their degradation, prolonging growth factor action, and (2) concentrate or dilute their activity. Sometimes, cells must adhere to the ECM in order to respond to a specific growth factor signal. For example, in order to act as a mitogen, basic fibroblast growth factor (bFGF) must be bound to heparan sulfate chains of PG so it can bind to its receptor on fibroblasts and endothelial cells during wound healing (Schultz and Wysocki 2009).

Free peptides liberated upon degradation of the ECM proteins, also known as matrikines *(Figure 9)*, also have influence over cellular activities such as migration, chemotaxis and mitogenesis, and are involved in wound healing, angiogenesis or immune responses (Wells, Gaggar, and Blalock 2015). Some examples of matrikines are the (1) peptide Val-Gly-Val-Ala-Pro-Gly derived from elastin, which is involved in chemotaxis, neovascularization and matrix remodeling, and (2) tri-peptide proline‑glycine‑proline derived from collagen, which is involved in neutrophil chemotaxis and inflammation.

3.3. Tissue-specificity and dynamic reciprocity of the extracellular matrix

The ECMs are tissue-specific, consisting of a large variety of biomolecules whose precise composition and particular structures vary from tissue to tissue. The ECM of each tissue offers a unique niche for the cells embedded within it. In particular, the tissue-specific ECM in the endometrium plays a fundamental role (Kaloglu and Onarlioglu 2010; Carrascosa, Horcajadas, and Moreno-Moya 2018).

All cell types of the body synthesize and secrete ECM molecules under the control of multiple signals (i.e., growth factors, cytokines and mechanical signals), actively participating in the formation of their tissue-specific ECM. However, it is important to note, they also produce matrix-degrading enzymes to destroy it. This degradation is a key feature of leukocyte influx, angiogenesis and tissue remodeling (Schultz and Wysocki 2009). There are three principal types of matrix-degrading enzymes: metalloproteinases, plasminogen and cathepsin proteases *(Figure 9)*. Matrix metalloproteinases (MMPs) are the largest class of proteases and their activity can be blocked by MMPs inhibitors. Meanwhile, the plasminogen proteolytic enzymatic cascade is associated with the turnover of the matrix and cell migration, can be irreversibly inhibited by the serpin family. Lastly, cathepsins are a large family of proteases involved in processes ranging from intracellular protein degradation to ECM cleavage, and they are tightly regulated by endogenous cellular inhibitors, such as cystatins (Theocharis *et al.* 2016).

Continuous cell-mediated ECM remodeling makes the ECM a highly dynamic environment. In turn, the variation in the composition and structure of the ECM affects its biomechanical properties, and consequently, the signals that modulate cell behavior and response to the ECM (Lu *et al.* 2011). This cause-effect cycle of the constant cell-

ECM communication is referred to as dynamic reciprocity *(Figure* 10*)* (Schultz and Wysocki 2009).
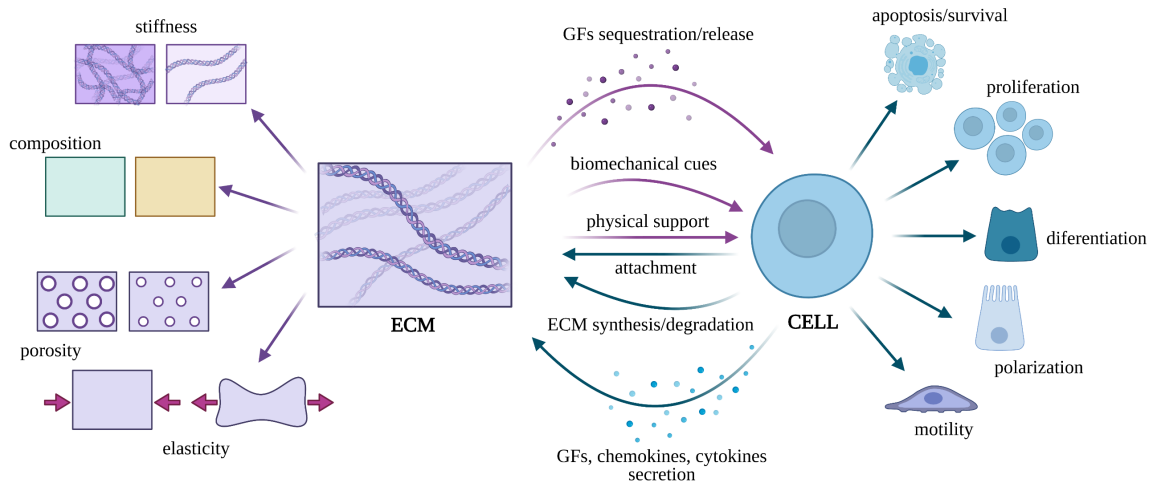
Figure 10. Dynamic reciprocity of the extracellular matrix. *The extracellular matrix (ECM) provides physical support to cells and interacts with them through biomechanical and biochemical cues such as growth factor sequestration and release. Cells attach to ECM, degrade and synthetize new ECM as well as secrete biomolecules such as growth factors, chemokines and cytokines that influence the behavior of surrounding cells. GFs: growth factors. Created with BioRender.com.*

4. Tissue engineering in reproductive medicine

As discussed in the previous sections, the ECM not only modulates cell function but also plays a remarkable role in wound healing, paving the way for an opportunity toward its use in regenerative medicine, a field which aims to repair and/or regenerate poorly functioning organs. One of the main goals of regenerative medicine is to eliminate the need for immunosuppression in transplanted patients, to reduce complications and toxicities, ultimately improving their quality of life (Edgar *et al.* 2020).

Regenerative medicine has two main branches: cell therapy and tissue engineering. In cell therapy, cells are transplanted to replace unfunctional cells or to repair damaged tissue. While tissue engineering, also known as bioengineering, uses biomaterials (that can also

be combined with cells and biologically active molecules) for the development of functional tissues and organs. A broad range of biomaterials are used within the field of tissue engineering, ranging from synthetic to naturally derived scaffolds *(Figure 11)* (Evangelatov and Pankov 2013).
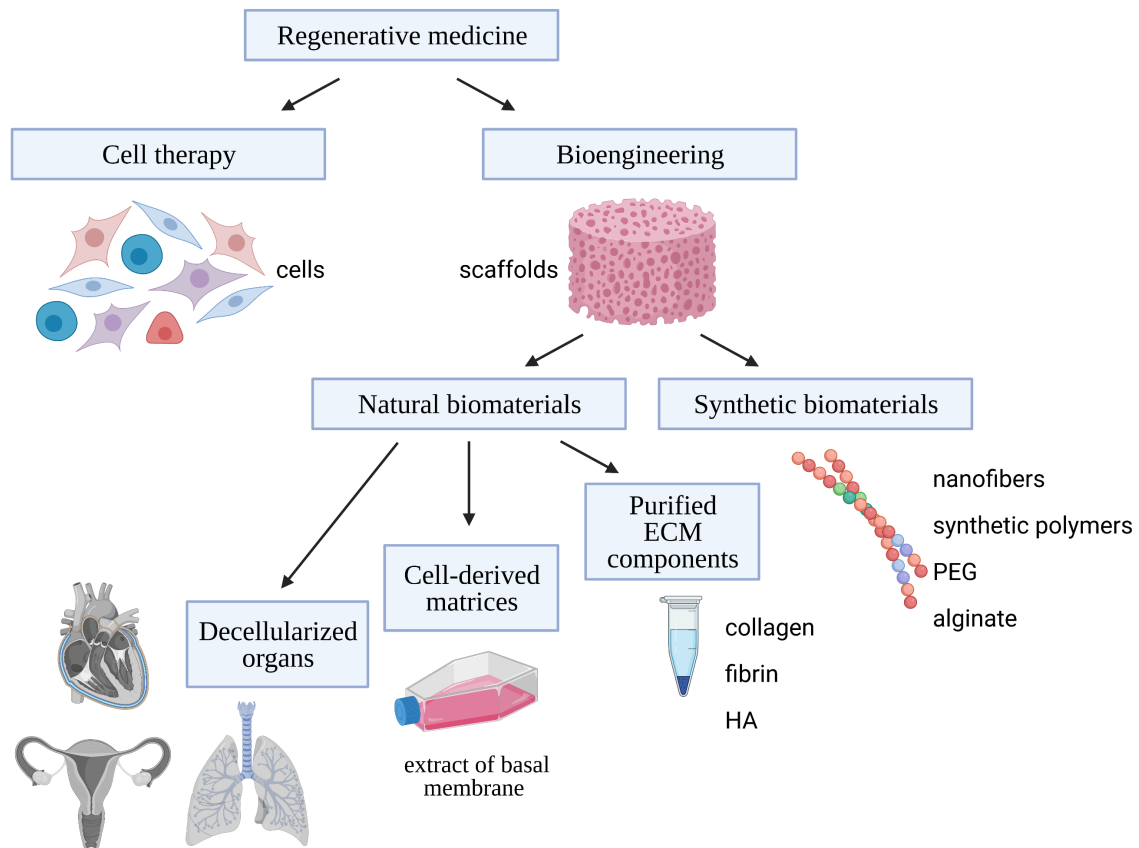
Figure 11. The two branches of regenerative medicine: cell therapy and bioengineering. Regenerative medicine is split into two disciplines: one based on the use of cells (cell therapy) and the other on the use of scaffolds (tissue engineering or bioengineering). The scaffolds used in bioengineering can be from synthetic or natural origins. Likewise, natural biomaterials can be divided into purified ECM components, cell-derived matrices and decellularized organs. PEG: polyethylene glycol; HA: hyaluronic acid. Created with BioRender.com.

Synthetic scaffolds are ECM-mimetic materials consisting of synthetic nanofibers, polymers or molecules that do not belong to the natural mammalian ECM, such as polyethylene glycol, alginate or agarose. On the other hand, natural scaffolds consist of

components naturally synthetized by ECM and they can be classified into purified ECM components, cell-derived matrices and decellularized (DC) tissues or organs (Xing *et al.* 2020). Artificial scaffolds used in bioengineering must: (1) provide basic ECM requirements, such as nutrients and waste diffusion, (2) allow cell adhesion, proliferation, migration and differentiation, and (3) have some degree of biodegradability to allow an alternative substitution by native ECM synthetized by resident cells.

Bioengineered scaffolds have pros and cons depend on their source *(Table I)*. Synthetic scaffolds have the advantage of an editable chemical composition (allowing the modification of their physicochemical features) and, together with purified ECM components, can have a well-defined composition, low batch-to-batch variability, and the possibility of being produced on a large-scale. However, the lack of biochemical complexity and the huge difference in composition compared to a natural tissue, raises challenges to recreate the native milieu. In particular, cells embedded in synthetic scaffolds are continuously activated to remodel their surroundings, which is unnatural (Grinnell 2003; Hoshiba *et al.* 2016).

Cell-derived matrices result from the *in vitro* production of ECM by cell lines and consist of a complex mixture of natural fibrous and bioactive ECM proteins, that partially solve the deficiencies of synthetic and purified ECM components. A well-known example is Matrigel, a basal membrane extract secreted by Engelbreth-Holm-Swarm mouse sarcomas (Kleinman *et al.* 1982; 1986; Vukicevic *et al.* 1992). Nonetheless, these cell-derived matrices still do not acquire the full biochemical complexity, native organization and mechanical properties of the ECMs due to the lack of tissue-specificity. Additionally, it is important to note that although they are considered highly-valuable materials for 3D *in vitro* culture, cell-derived matrices are not suitable for clinical application *in vivo* because they derive from tumorigenic cell lines (Saldin *et al.* 2017).

Table I. Characteristics of the different scaffolds used in bioengineering.

	Synthetic Scaffold	Natural Scaffold		
		Purified ECM component	Cell-derived matrices	Decellularized tissue/organ
Three-dimensionality	+++	+++	+++	+++
Editable physical and chemical features	+++	-	-	-
Defined composition	+++	++	-	-
Low Batch-to-bath variability	+++	+	-	-
Large-scale production	+++	++	+	-
Absence of residual cell material	+++	++	+	+
Native mechanical properties	-	+	++	+++
Native organization	-	+	+	+++
Native bioactivity	-	+	++	+++
Native biochemical complexity	-	-	+	+++
Tissue-specificity	-	-	-	+++
Overall similarity to native tissue/organ	-	+	++	+++

-: not applicable; +: light compliance; ++: moderate compliance; +++: high compliance.

Over the last decades, decellularization has emerged as a new bioengineering technique, and makes it possible to obtain tissue-specific ECM scaffolds directly from tissues and organs. These DC tissues are stripped of cellular material (eliminating possible incompatibility issues) but retain the maximum biochemical and mechanical properties of the original tissue, resulting in a scaffold with the closest proximity to the native milieu.

4.1. Decellularized scaffolds

Decellularization is the process by which cells (and therefore the antigenic epitopes associated to the cell membrane and intracellular components) are removed from a tissue or organ while the structure (including the microstructure of the vascular system) of the native tissue is conserved. Consequently, this DC tissue or organ is transformed into an acellular scaffold consisting of tissue-specific ECM *(Figure 12)*. To date, decellularization has been successfully applied to a large variety of organs, including complex tissues such as the heart (Ott *et al.* 2008) or the liver (Uygun *et al.* 2010).
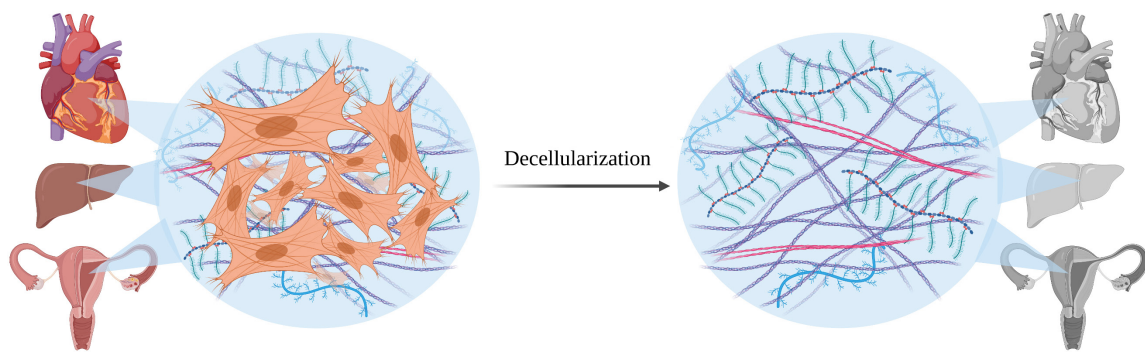
Figure 12. Concept of decellularization. Decellularization removes cells while maintaining the native ECM in any organ or tissue. Created with BioRender.com.

Decellularization can be achieved in fragmented or whole organs, using either physical, enzymatic or chemical methods, however most decellularization protocols include a combination of these methods *(Table II)*. The chemical technique is the most commonly used among DC protocols and applies detergents such as Triton X-100 and sodium dodecyl sulfate (SDS) (Badylak, Taylor, and Uygun 2011). In the case of whole organ decellularization, decidualizing solutions are perfused through the organ's vascular system, which delivers the solutions through the arteries to all locations of the organ. Affected cells are lysed and destructed and this waste is removed through the veins.

Optimizing the decellularization protocol is crucial, since it is a complex process, and most DC scaffolds retain certain amounts of residual DNA, cytoplasmatic and nuclear components. The degree of cell component removal together with the preservation of functional ECM biomolecules will have an influence on the functional outcome of the resulting scaffold. That being said, a weak decellularization protocol can result in biocompatibility problems in the scaffold receptors, while an aggressive protocol may result in the loss of bioactive ECM molecules and lack of the DC scaffold functionality (Soto-Gutierrez *et al.* 2011; Brown *et al.* 2009; Xing *et al.* 2020).

Table II. Methods used for decellularization.

Decellularization Methods		
Physical	**Enzymatic**	**Chemical**
Freezing-thawing	Exonucleases	Non-ionic detergents (i.e., Triton X-100)
Mechanical agitation Sonification	Endonucleases	
Radiation	Other proteases (i.e., trypsin)	Ionic detergents (i.e., SDS, SDC)
High hydrostatic pressure		Zwitterionic detergents (CHAPS)
		Hypotonic/hypertonic solutions (i.e., EDTA, EGTA)

SDC: Sodium deoxycholate; CHAPS: 3-[(3-cholamidopropyl)dimethylammonio]-1-propanesulfonate. EDTA: Ethylenediamine tetraacetic acid; EGTA: Ethylene glycol tetraacetic acid.

An implanted biomaterial causes an intensive cascade of interactions with the host tissue, including an immune response which is the key determinant of biocompatibility and functional outcome. Specifically, macrophages play key phagocytic roles that regulate tissue repair and regeneration. During the first days to weeks after implantation of a biomaterial, an initial inflammatory response, led by infiltrating neutrophiles and M1 type

macrophages, begins to degrade the scaffold, releasing matrikines. In the subsequent weeks (or months), M2 type macrophages invade the matrix and initiate remodeling of new tissue (Meyer 2019). Far from previously accepted belief that macrophage infiltration in wound healing leads to adverse events (such as necrosis and scar tissue), these beneficial cells modulate unique interactions with the ECM that promote wound healing (Scanameo and Ziats 2019).

4.2.   Uterus decellularization

A milestone for the first application of bioengineering in reproductive medicine was the clinical pilot study carried out by Dr. Atala's group, in which bioscaffolds were used to reconstruct vaginas in patients of Mayer-Rokitansky-Küster-Hauser syndrome (Raya-Rivera *et al.* 2014). Since then, other reproductive organs, especially the uterus, have been successfully decellularized. To date, decellularization of diced uterine tissue has been reported in rats (Young and Goloman 2013; Santoso *et al.* 2014; Hiraoka *et al.* 2016), rabbits (Yao *et al.* 2020) and humans (Young and Goloman 2013; Olalekan *et al.* 2017) while whole uterus decellularization has been achieved in rats (Miyazaki and Maruyama 2014; Hellström *et al.* 2014 ; Hellström *et al.* 2016; Miki *et al.* 2019; Li *et al.* 2020), rabbits (Campo *et al.* 2019), pigs (Campo *et al.* 2017) and sheep (Daryabari *et al.* 2019; Tiemann *et al.* 2020) *(Figure 13)*. Notably, these DC uterine tissues have been used for *in vitro* culture and recellularization as well as for *in vivo* applications.
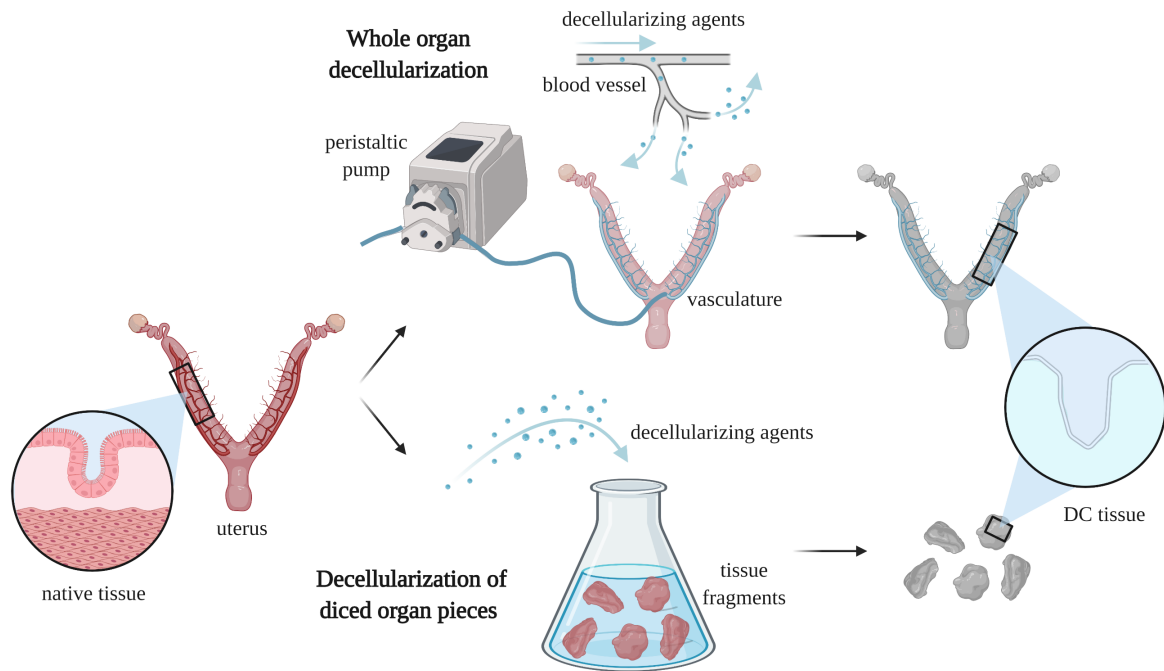
Figure 13. Organ decellularization approaches: uterus decellularization. Decellularization of an organ can be performed by immersing diced organ pieces in decellularizing solutions or by perfusing these decellularizing solutions through the organ´s intact vasculature using a peristaltic pump (whole organ decellularization). Created with BioRender.com.

In 2013, the first attempt of uterine decellularization sought to develop myometrial patches for transplantation. In this case, DC scaffolds from rat and human myometrium were decellularized using ethanol and trypsin, then cultured with myocytes *in vitro* for 51 days. Interestingly, cultured myocytes were able to contract spontaneously (Young and Goloman 2013).

A year later, whole organ decellularization of rat uteri was achieved by perfusing SDS and Triton X-100 detergents through the uterine artery (Miyazaki and Maruyama 2014; Hellström *et al.* 2014) *(Figure 14)*. Miyazaki *et al.,* used these whole DC uteri to perform three different studies. First, the eutopic transplant of the whole DC uterus *in vivo* to a hysterectomized rat, which confirmed conservation of the intact vasculature. Second, the *in vitro* recellularization of whole DC uterus, with uterine cells and bone-marrow MSCs,

where the organ remained viable for six days. And third, the transplantation of recellularized uterine patches into several rat uteri *in vivo* to study the formation of new uterine tissue and its function. In this last experiment, although endometrial cells inside the graft showed decidualization, the grafts failed to achieve placentation during pregnancy (Miyazaki and Maruyama 2014). Hereinafter, rat uterus DC and subsequent transplantation of uterine patches was replicated by several groups, with (Hellström *et al.* 2016; Li *et al.* 2020) or without (Santoso *et al.* 2014; Hiraoka *et al.* 2016; Miki *et al.* 2019) previous *in vitro* recellularization, achieving spontaneous tissular regeneration of the uterine layers from endogenous cells and some pregnancy support.
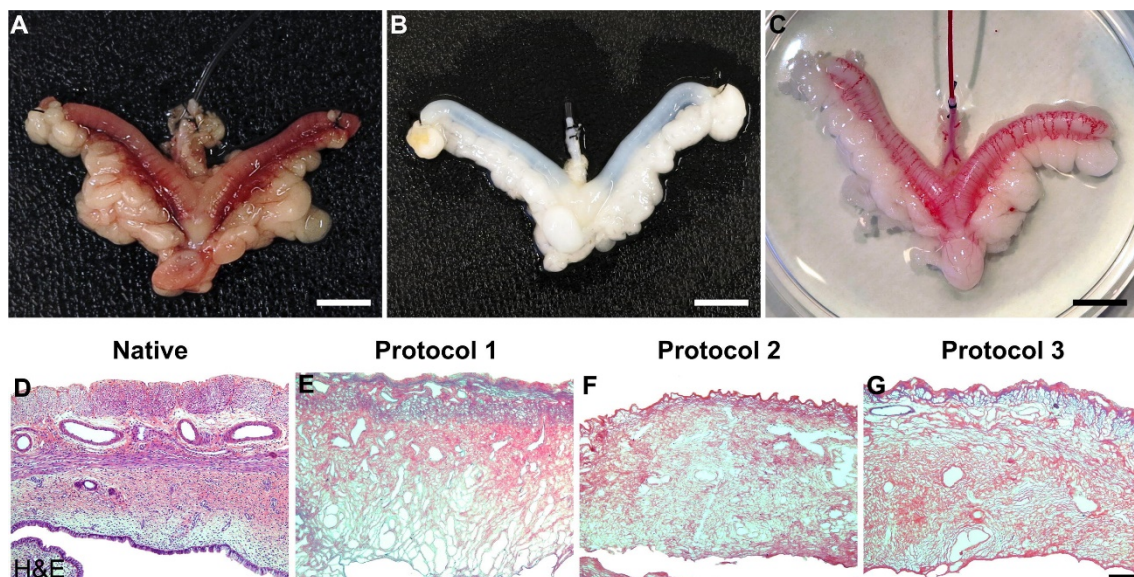
Figure 14. Whole rat uterus decellularization. *A) Native rat uterus. B) Decellularized rat uterus resembling the native uterus in size and shape. C) Analysis of the integrity of decellularized uterine blood vessel conduits by perfusing a dye through the vascular system. D) H&E staining showing the achitecture of native tissue. E-G) H&E staining showing substantial removal of cells by decellularization protocols 1-3. Sections are oriented with the perimetrium at the top and lumen at the bottom (D–G). Scale bars: 1 cm (A–C) or 100 µm (D–G). H&E: Haematoxylin and eosin. Reprinted from (Hellström et al. 2014) with permission from Acta Biomaterialia.*

It was not until 2016 that whole organ decellularization of large uterine organs was performed by our group (Campo *et al.* 2017). Uterine horns were decellularized using

0.1% SDS and 1% Triton X-100, and then uterine discs were recellularized *in vitro,* using ICE6-7 endometrial stem cell lines (with epithelial and stromal origins) obtained through the SP method (Cervelló *et al.* 2010; 2011). Whole uterus decellularization was also studied in sheep, who have a human-sized uterus. A study by Daryabari *et al. (2019)* determined that a decellularization protocol based on 0.25-0.5% SDS perfusion and preservation in 10% formalin is optimal for efficient cell removal and ECM preservation, as well as corroborated *in vivo* biocompatibility and recellularization (Daryabari *et al.* 2019). In accordance, Tiemann *et al.(2020),* presented three different protocols for whole sheep uteri decellularization, 0.5% SDS (Protocol 1), 2% SDC (Protocol 2) or 2% SDC and 1% Triton X-100 (Protocol 3), which showed a good decellularization and supported *in vitro* culture of ovine fetal stem cells for 2 weeks*,* allowing their proliferation as well as the preservation of their undifferentiated phenotype (Tiemann *et al.* 2020). Finally, with the purpose of making an *in vitro* 3D endometrial model that could be repopulated with primary endometrial cells, biopsied human endometrium has been partially decellularized using Triton X-100 and SDC (Olalekan *et al.* 2017). The primary endometrial cells within the (recellularized) scaffolds proliferated, remained viable and hormone responsive *(Table III)*.

Table III. Compilation of published articles on uterus decellularization to date.

Species	Sample for decellularization	Decellularization protocol(s)	Recellularization process	Seeded cells *in vitro*	Year of publication	Reference
Human and rat	Uterine fragments	70% Ethanol and 0.25 g/dL Trypsin	*In vitro*	Myometrial cells	2013	(Young and Goloman 2013)
Rat	Whole uterus	0.01-0.1% SDS and 1% Triton X-100	*In vitro*	EECs, ESCs and MSCs	2014	(Miyazaki and Maruyama 2014)
Rat	Uterine fragments	HHP, 1%SDS or 1-3% Triton X-100 (different protocols)	*In vivo*	-	2014	(Santoso *et al.* 2014)
Rat	Whole uterus	4% DMSO and 1% Triton X-100 or 2% SDC (different protocols)	-	-	2014	(Hellström *et al.* 2014)
Rat	Uterine fragments	1% SDS and 0.2 mg/mL DNase I	*In vivo*	-	2016	(Hiraoka *et al.* 2016)
Rat	Whole uterus	4% DMSO and 1% Triton X-100 or 2% SDC (different protocols)	*In vivo*	Endometrial and myometrial cells, BM-MSCs	2016	(Hellström *et al.* 2016)
Pig	Whole uterus	Freezing-thawing, 0.1% SDS and 1% Triton X-100	*In vitro*	Endometrial SSCs	2016	(Campo *et al.* 2017)
Human	Uterine fragments	0.25% Triton X-100 and 0.25% SDC	*In vitro*	EECs and ESCs	2017	(Olalekan *et al.* 2017)
Rat	Whole uterus	0.01%-1% SDS and 1% Triton X-100	*In vivo*	-	2019	(Miki *et al.* 2019)
Rabbit	Whole uterus	0.1% SDS and 1% Triton and 2 mg/mL DNase I	-	-	2019	(Campo *et al.* 2019)
Sheep	Whole uterus	1% SDS and 1% Triton X-100, 4% DMSO and 1% Triton X-100 or 0.25-5% SDS and 10% neutral buffered formalin (different protocols)	*In vivo*	-	2019	(Daryabari *et al.* 2019)
Sheep	Whole uterus	0.5% SDS, 2% SDC or 2% SDC and 1% Triton X-100	*In vitro*	Fetal stem cells	2020	(Tiemann *et al.* 2020)
Rabbit	Uterine fragments	1% Triton, 1% SDS	*In vitro*	Umbilical vein endothelial cells	2020	(Yao *et al.* 2020)
Rat	Whole uterus	0.1% SDS, 1-0.001% Triton X-100	*In vitro*	MSCs	2020	(Li *et al.* 2020)

SDS: sodium dodecyl sulfate; DMSO: dimethyl sulfoxide; HHP: high Hydrostatic Pressure; SDC: Sodium deoxycholate; EECs: endometrial epithelial cells; ESCs: endometrial stromal cells; SSCs: somatic stem cells; MSCs: mesenquimal stem cells; BM-MSCs: Bone-marrow MSCs; g/dL: gram per deciliter; mg/mL: milligram per milliliter.

In summary, the last decade has stablished the bases for uterus decellularization. Decellularized uteri have been used for *in vitro* 3D culture of different cell types, with the main goal of studying cell behavior and achieving uterus recellularization in this novel biomaterial. Moreover, DC uteri have been used for transplantation of uterine patches *in vivo* (with or without previous *in vitro* recellularization) to generate DC uterine scaffolds. Nevertheless, despite the promising results of transplanting these uterine patches *in vivo*, the full recellularization of uterine DC tissues is still a challenge in reproductive bioengineering.

5. Tissue-specific extracellular matrix hydrogels: A new tissue engineering tool for three-dimensional *in vitro* research and regenerative medicine

A hydrogel is a 3D network of hydrophilic polymers, with large water retention, which maintains its structure with physicochemical cross-linking of individual polymer chains. Hydrogels possess a degree of flexibility very similar to natural tissue due to their water content (Bahram, Mohseni, and Moghtader 2016). New advances in bioengineering have allowed the design of tissue-specific ECM hydrogels from DC tissues, which have shown to be a valuable tool for *in vitro* 3D culture and regenerative medicine. Tissue-specific ECM hydrogels conserve the biochemical complexity of their DC tissue source (by including growth factors, chemokines and other important biomolecules), maintaining their bioactive (Londono and Badylak 2015), mechanical and physical properties.

The first tissue-specific ECM hydrogel designed was a porcine urinary bladder matrix, which was developed by the group of Dr. Badylak from the University of Pittsburgh in

2008 (Freytes *et al.* 2008). Since then, tissue-specific ECM hydrogels have been developed for several tissues/organs including the heart, artery, esophagus, intestine, liver, pancreas, lung, teeth, tendon, cartilage, bone, muscle, brain and kidney (Saldin *et al.* 2017). The reproductive system remained unexplored, until our group´s recent advances allowed the creation of tissue-specific ECM hydrogels from the fallopian tubes (Francés-Herrero *et al.* 2021), myometrium (López-Martínez *et al.* 2021) and endometrium (Campo *et al.* 2019; López-Martínez *et al.* 2021).

5.1. Creation of a tissue-specific extracellular matrix hydrogel from a decellularized scaffold

Tissue-specific ECM hydrogels are formed through a (mainly collagen) polymer-based self-assembly process regulated by GAGs, PGs and other ECM proteins. The polymerization kinetics and final 3D organization is influenced by native biochemical composition of the source tissue (Saldin *et al.* 2017). Hydrogel formation from a DC tissue involves four key steps: milling/lyophilization, enzymatic digestion, neutralization and gelation *(Figure 15)*. Basically, DC tissue is milled and lyophilized to produce a fine anhydride powder of tissue-specific ECM. Then, the fibers comprising the ECM powder are broken up into peptide monomers by enzymatic digestion. This enzymatic digestion is usually carried out using pepsin, an enzyme derived from porcine gastric juice, which can solubilize up to 99% of acid-insoluble collagen when acting in its naturally acidic environment (Saldin *et al.* 2017). After about 48 hours (h) of enzymatic digestion, pepsin activity is blocked by neutralization to physiological pH and salt concentration. Finally, a rise in temperature to 37 degrees Celsius (ºC) induces the spontaneous repolymerization of the intramolecular bonds of ECM monomers, forming a homogeneous hydrogel in an entropy-driven process dominated by collagen kinetics.
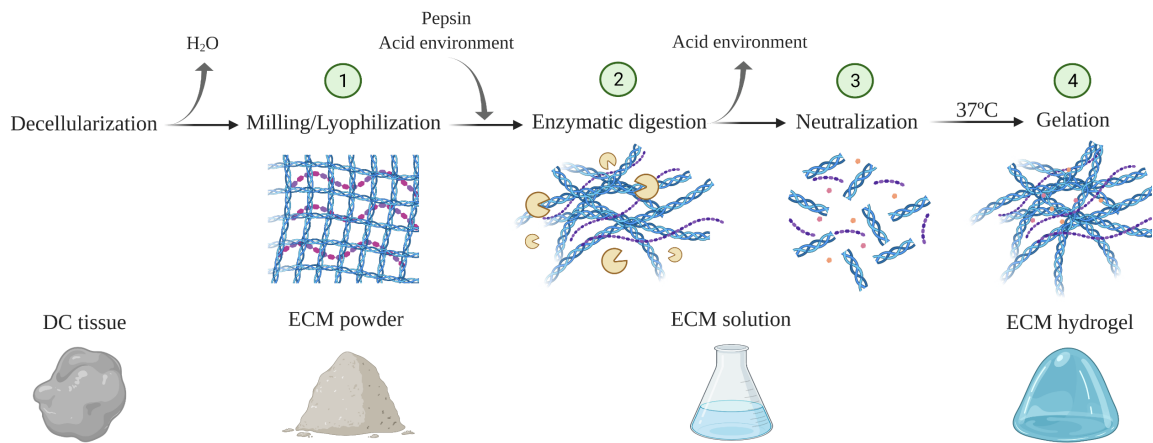
Figure 15. Creation of a tissue-specific ECM hydrogel from a decellularized scaffold. *1) Milling and lyophilization maintains extracellular matrix (ECM) structure in the ECM powder. 2) Enzymatic digestion breaks down the polymers and creates an ECM solution. 3) Neutralization of enzymatic activity. 4) Incubation at 37ºC induces gelation and repolymerization, resulting in an ECM hydrogel. H₂O: water. Created with BioRender.com.*

Enzymatic digestion of ECM hydrogels could potentially disintegrate the fibrous ECM proteins, and destroy their functionality, without any apparent improvement over DC scaffolds. However, previous studies confirm that the final proteome in hydrogels not only maintains collagen and GAG content, but also preserves a remarkable percentage of bioactive proteins (including growth factors) (Pouliot *et al.* 2016; Saldin *et al.* 2017). Moreover, the release of matrikines by the enzymatic break down of fibrous proteins may increase the bioactive potential of tissue-specific ECM hydrogels.

5.2. *In vitro* application of tissue-specific extracellular matrix hydrogels: Three-dimensional *in vitro* culture of endometrial cells

Standard monolayer *in vitro* culture of cells has generated important advances in endometrial research providing simple and high throughput assays for biomedical research purposes. However, the information obtained through a monolayer of cells cultured on a synthetic hard plastic surface is limited, principally because the unnatural

two-dimensional (2D) culture conditions are unable to capture the anatomical and biochemical complexities of the native tissues and may be misleading. To mimic the complexity of a natural organ/tissue in a dish, more sophisticated 3D *in vitro* models have been developed. The main advantage of 3D versus 2D culture is that it allows cells to interact with each other and the surrounding matrix in all directions, creating a microenvironment more similar to *in situ* physiological conditions. Other advantages of 3D cultures are their variable stiffness, freedom from apical-basal polarity, allowing cells to maintain a natural 3D conformation, mimicking soluble gradients present *in vivo*, permitting cell migration in 3D, and co-culturing different cells in a physiological microenvironment *(Figure 16)*. Altogether, 3D culture offers a more accurate milieu to study various biological processes and drug interactions *ex vivo*.
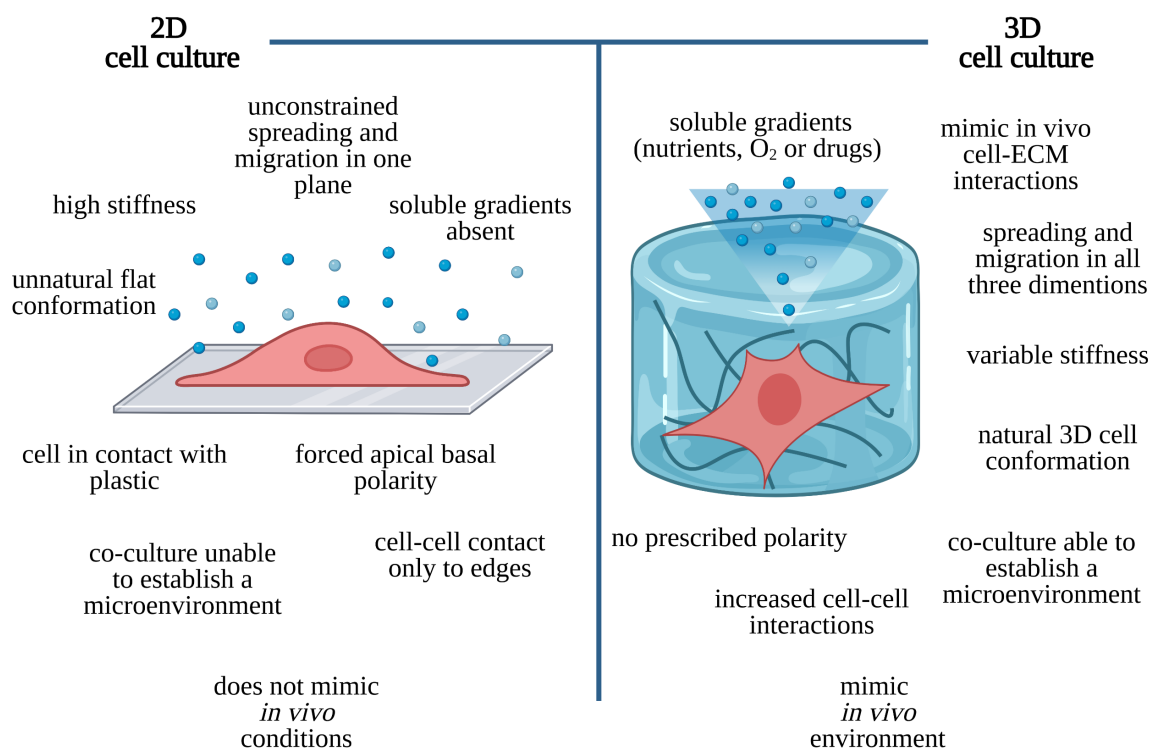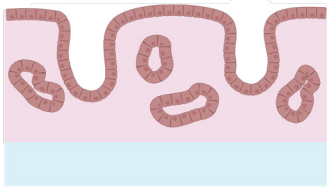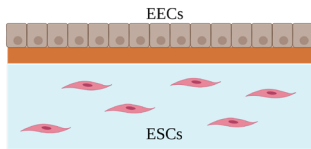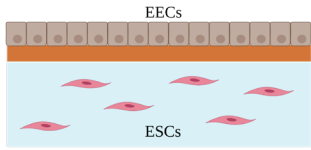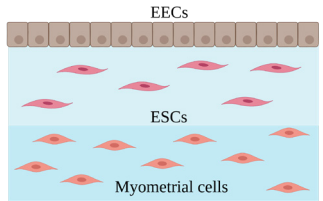
Figure 16. Two-dimensional versus three-dimensional in vitro cell culture. Advantages of 3D cell culture over the conventional 2D monolayer culture. Created with BioRender.com.

Hydrogels are the most relevant tissue-like matrices used to support the development of 3D *in vitro* models, since they are akin to the ECM in many ways (Zhao *et al.* 2020). Over the last decades, 3D *in vitro* models have been developed using hydrogels from purified ECM molecules and cell-derived ECM matrices (such as collagen I and Matrigel). Specifically, numerous 3D *in vitro* endometrial models have been developed to investigate uterine/embryo cross-talk and pathogenesis in a more accurate representation the natural physiology. These 3D models include cell-laden biomimetic constructs, and more recently, endometrial organoids *(Table IV)*.
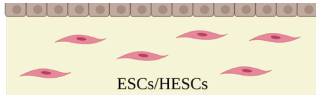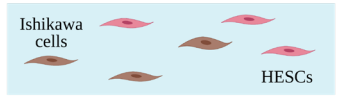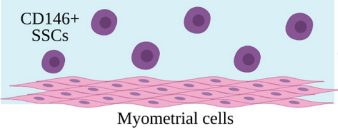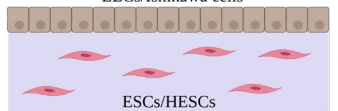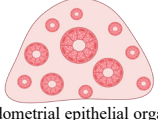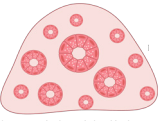
Cell-laden biomimetic constructs have consisted of a mixture of different cell types (principally EECs and ESCs) co-cultured with hydrogels, with the purpose of creating a more complete endometrial model *in vitro* (Cook *et al.* 2017; Meng *et al.* 2009; Wang *et al.* 2012; 2013; Lü *et al.* 2009; Bentin-Ley *et al.* 2000).

In contrast, organoids are self-organized 3D culture systems which include stem and differentiated cells and resemble the tissue of origin. They are cultured in Matrigel drops supplemented with a complex culture medium, which includes various growth and signaling factors. Organoids have been derived from many tissue sources including gut (Sato *et al.* 2011), liver (Huch *et al.* 2015), pancreas (Huch *et al.* 2013), prostate (Karthaus *et al.* 2014), fallopian tube (Kessler *et al.* 2015) and more recently, endometrial glands (Turco *et al.* 2017; Boretto *et al.* 2017). Endometrial organoids can reproduce features of uterine glands *in vivo,* such as the responsiveness to hormones or secretion of "uterine milk", and as such, can be applied in the study of reproductive pathologies (Wiwatpanit *et al.* 2020; Boretto *et al.* 2019).

Table IV. Compilation of three-dimensional in vitro endometrial models: cell-laden biomimetic constructs and endometrial epithelial organoids.

Purpose	3D Culture type	Components of the culture system	Seeded cells	Cell species	Culture medium	Culture conditions	Days *in vitro*	Scheme	Reference
Study of implantation	Cell-laden biomimetic constructs	Collagen	Explant from endometrial functional layer	Human	RPMI-1640	37ºC Unspecified O_2 and CO_2	1	Explant / Collagen	(Landgren *et al.* 1996)
Establish an endometrium-like 3D culture and study of implantation	Cell-laden biomimetic constructs	Matrigel Collagen	Primary ESCs Primary EECs	Human	Alpha Medium supplemented with 0.2% Amniomax, 0.2% glutamine, 5% FCS, 0.5% BSA	37ºC 5% CO_2 Unspecified O_2%	7	EECs / Matrigel / Collagen / ESCs	(Bentin-Ley *et al.* 2000)
Study of endometrial receptivity	Cell-laden biomimetic constructs	Matrigel Collagen	Primary ESCs Primary EECs	Human	Alpha Medium supplemented with 0.2% Amniomax, 0.2% glutamine, 5% FCS, 0.5% BSA	37ºC 5% CO_2 Unspecified O_2%	10	EECs / Matrigel / Collagen / ESCs	(Meng *et al.* 2009)
Create a full uterine tissue *in vitro* and study of implantation	Cell-laden biomimetic constructs	Collagen/Matrigel	Primary myometrial cells Primary ESCs Primary EECs	New Zealand rabbit	DMEM/F-12 supplemented with 10% FBS	37ºC 5% CO_2 Unspecified	14	EECs / Collagen/Matrigel / ESCs / Collagen/Matrigel / Myometrial cells	(Lü *et al.* 2009)

Purpose	3D Culture type	Components of the culture system	Seeded cells	Cell species	Culture medium	Culture conditions	Days *in vitro*	Scheme	Reference
Establish an endometrium-like 3D culture and study of implantation	Cell-laden biomimetic constructs	Fibrin Agarose	Primary ESCs or HESCs Primary EECs or HEC-1A	Human	DMEM/F-12 or DMEM supplemented with 100mM sodium pyruvate	37ºC 5% CO_2 Unspecified O_2%	7	Agarose/Fibrin; ESCs/HESCs	(Wang *et al.* 2012)
Establish an endometrium-like 3D culture and study of Interleukin-6 and metalloproteinase activity	Cell-laden biomimetic constructs	Collagen/Matrigel	HESCs Ishikawa endometrial adenocarcinoma cells	Human	DMEM/F-12 supplemented with HEPES, L-glutamine, sodium pyruvate, amino acids, 10% FBS. A more complex medium with estrogen was included after day 2.	Unspecified	5	Ishikawa cells; Collagen/Matrigel; HESCs	(Schutte *et al.* 2015)
Establish an endometrium-like 3D culture and study of differentiation	Cell-laden biomimetic constructs	Collagen /Matrigel	CD146+ endometrial SSCs Myometrial cells	Human	DMEM/F-12 supplemented with 10% FBS	Unspecified	10	CD146+ SSCs; Collagen/Matrigel; Myometrial cells	(Fayazi, Salehnia, and Ziaei 2017)
Establish an endometrium-like 3D culture	Cell-laden biomimetic constructs	PEG	Primary ESCs or Ishikawa endometrial adenocarcinoma cells Primary EECs or tHESCs	Human	DMEM/F-12 supplemented with 1% FBS, 2% Supplement and Williams Medium supplemented with 4% Supplement, 100 nM hydrocortisone. Decidualizing hormones (MPA, cAMP) added later.	37ºC 5% CO_2 Unspecified O_2%	14	EECs/Ishikawa cells; PEG; ESCs/HESCs	(Cook *et al.* 2017)
Establish endometrial epithelial organoid cell lines	Organoids	Matrigel	Primary EECs	Human	DMEM/F-12 supplemented with a cocktail of growth and signaling factors	37ºC 5% CO_2	7-10 days for passage	Matrigel; Endometrial epithelial organoids	(Turco *et al.* 2017)
Establish endometrial epithelial organoid cell lines	Organoids	Matrigel	Primary EECs	Human Mouse	DMEM/F-12 supplemented with a cocktail of growth and signaling factors	37ºC 5% CO_2	7-10 days for passage	Matrigel; Endometrial epithelial organoids	(Boretto *et al.* 2017)

3D: three-dimensional; DMEM/F12: Dulbecco's modified Eagle's medium nutrient mixture f-12; RPMI: Roswell Park Memorial Institute medium; FBS: fetal bovine serum; FCS: fetal Calf Serum; BSA: Bovine serum albumin; EECs: endometrial epithelial cells; ESCs: endometrial stromal cells; SSCs: somatic stem cells; HEC-1A: human endometrial adenocarcinoma Cell Line; HESCs: immortalized human endometrial stromal cells Line. MPA: medroxyprogesterone 17-acetate; cAMP: 8-bromoadenosine 3',5'-cyclic monophosphate; HEPES: 4-(2-hydroxyethyl)-1-piperazineethanesulfonic acid; tHESCs: TERT-immortalized human endometrial stromal cells; PEG: polyethylene glycol; PolyHIPEs: emulsion-templated porous polymers. EGF: epidermal growth factor; FGF-10: fibroblast growth factor-10; HGF: hepatocyte growth factor. CO_2; dioxide carbon; O_2; oxygen.

Substituting standard commercial hydrogels for tissue-specific ECM hydrogels may improve the accuracy of 3D culture systems. In fact, the latter have been applied in 3D *in vitro* culture in many biomedicine subspecialties, such as dermic (Wolf *et al.* 2012), hepatic (Skardal *et al.* 2012), cardiac (Nehrenheim *et al.* 2019) and nervous system (Medberry *et al.* 2013). To date, the viability of cells cultured on the surface of ECM hydrogels *in vitro* has been consistently demonstrated for cell lines, primary cells and stem cells (Saldin *et al.* 2017). Moreover, tissue-specific ECM hydrogels produce the best results (in terms of cell function/behavior) when cultured with cells originating from the same tissue, as compared to with cells that do not match the tissue of origin *(Figure 17)*. For example, ECM hydrogels from spinal cord tissues are more likely to facilitate optimal stem cell behavior for constructive spinal cord regeneration (Viswanath *et al.* 2017).
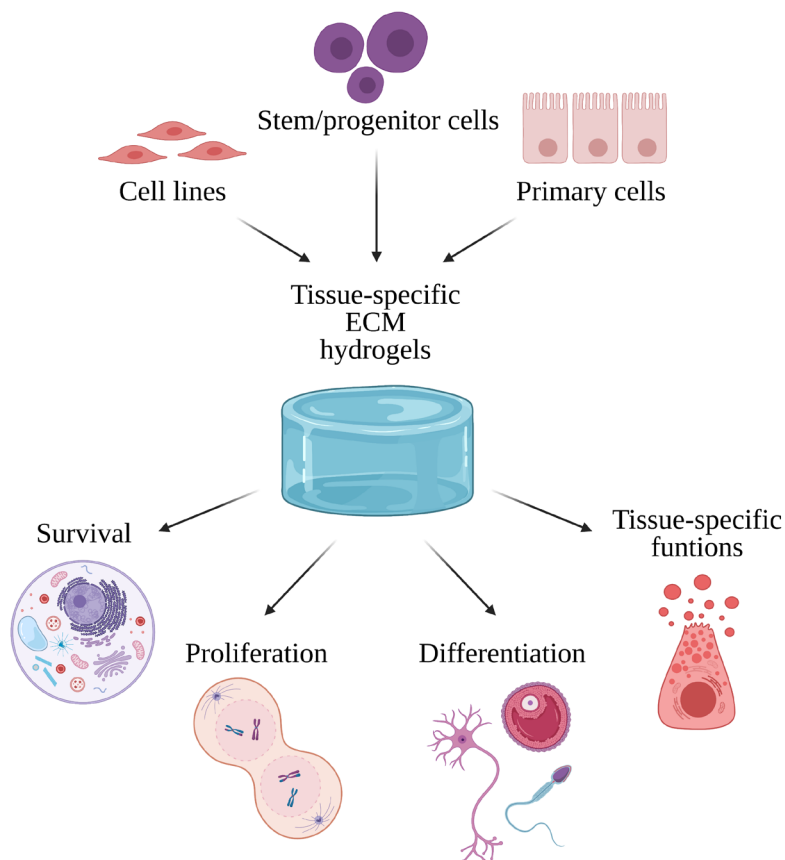
Figure 17. Cellular responses to tissue-specific ECM hydrogels under three-dimensional in vitro culture currently under investigation. *The expected cell responses include the improvement of cell survival, proliferation, tissue-specific functions and differentiation towards tissue-specific lineages. ECM: extracellular matrix.*

41

5.3. *In vivo* application of tissue-specific extracellular matrix hydrogels: Regenerative medicine for endometrial pathologies

Use of tissue-specific ECM hydrogels is still largely experimental but is showing great promise for regenerative medicine. Despite the remarkable progress that tissue-specific DC scaffolds have led in the field of bioengineering, they are limited by the inability to mold and require invasive surgical interventions to be used for medical purposes. In this sense, tissue-specific ECM hydrogels derived from DC tissues are more advantageous than DC scaffolds because of their malleability, injectability, improved cell infiltration and degradability *(Figure 18)*. Specifically, ECM hydrogels can easily be injected in liquid form, and undergo spontaneous gelation *in vivo* with the 37ºC physiological body temperature. This feature alone facilitates the design of less invasive therapies, as compared to those including DC biomaterials.

To date, *in vivo* preclinical studies have been performed on a wide range of tissue-specific ECM hydrogels to test their efficacy in diverse illnesses typically suffered by their tissues of origin. For example, skeletal muscle ECM hydrogels have been developed to treat peripheral arteries, promoting a pro-regenerative environment which improves blood perfusion in hindlimb ischemia models (Ungerleider *et al.* 2016; Hernandez *et al.* 2020). Likewise, meniscus ECM hydrogels have been applied to meniscal injury, improving the retention of stem cells in damaged areas, as well as enhancing meniscus healing and chondroprotection (Yuan *et al.* 2017; Zhong *et al.* 2020). While adipose ECM hydrogels have also stimulated host-derived adipogenesis and angiogenesis in subcutaneous adipose deficits (Kim, Choi, and Cho 2017; Young, Bajaj, and Christman 2014). Other tissue-specific ECM hydrogels such as nerve (Lin *et al.* 2018), cornea (Wang *et al.* 2020b), liver

(Hussein *et al.* 2020), bone (Emami *et al.* 2020) and intervertebral discs (Peng *et al.* 2021) have also been explored with promising outcomes *(Table V)*.
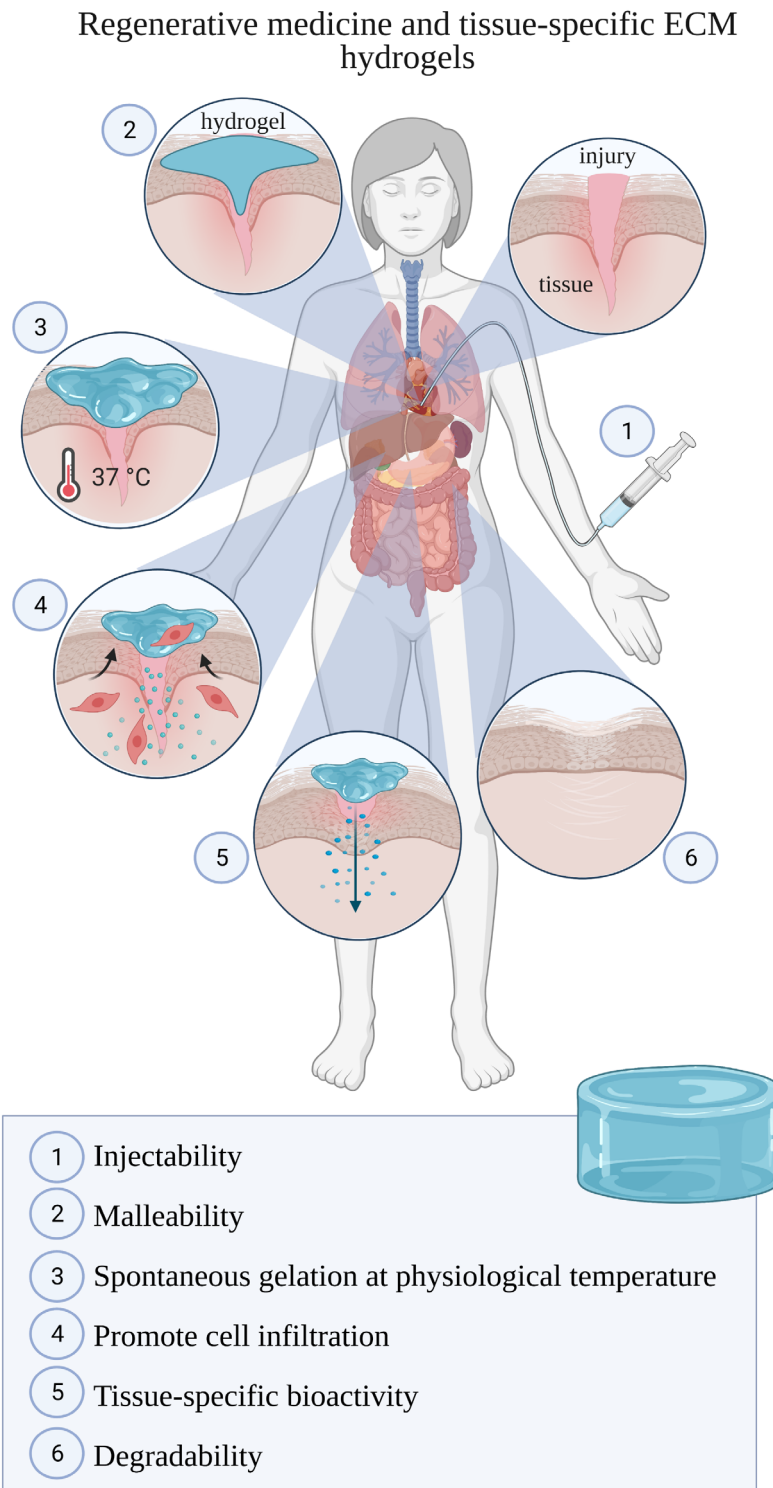
Figure 18. Application and function of tissue-specific extracellular matrix hydrogels in regenerative medicine. Created with BioRender.com.

In spite of these interesting findings, cardiology has advanced the furthest, since cardiac ECM hydrogels demonstrated to have positive effects over the myocardial infarction. In 2012, Singelyn *et al.* demonstrated that the injection of porcine cardiac ECM hydrogels (without any additives) within infarcted myocardium of rats increased endogenous cardiomyocytes in the affected area and maintained cardiac function without inducing arrhythmias. The same group also validated the feasibility of transendocardial catheter delivery of these cardiac ECM hydrogels in pigs (Singelyn *et al.* 2012). In 2017, Efraim *et al.,* continued with this line of research demonstrating the significant improvement of infarcted rat hearts when they were treated with porcine cardiac ECM hydrogels cross-linked with genipin alone or with different amounts of chitosan. Here, hydrogels were applied for both acute and chronic myocardial infarction and they not only provided the mechanical support needed to stop deterioration and preserve heart functions, but also alleviated the damage caused by myocardial infarction, even after the formation of a mature scar tissue (Efraim *et al.* 2017).

Today, porcine-derived myocardial ECM hydrogel, with the commercial name of VentriGel, is currently in clinical trials. This hydrogel has been designed to go through a cardiac injection catheter towards the heart to treat post-myocardial infarction by enriching the myocardial-specific extracellular microenvironment and facilitating endogenous cell infiltration and repair. VentriGel finished its phase I clinical trial in June 2019, where its safety and feasibility were evaluated in subjects with 25 to 45% left ventricular ejection fraction, secondary to myocardial infarction (ClinicalTrials. gov Identifier: NCT02305602).

Table V. Summary of preclinical studies using tissue-specific extracellular matrix hydrogels for tissue repair and regenerative medicine in vivo.

Tissue-specific ECM hydrogel	Additives	Target organ/tissue	Therapeutic application	Animal model	Results	Reference
Porcine cardiac ECM hydrogel	None	Heart	Myocardial infarction	Rat and pig	Increased endogenous cardiomyocytes in the infarcted area and maintained cardiac function without inducing arrhythmias.	(Singelyn *et al.* 2012)
Human adipose ECM hydrogel	Adipose-derived stem cells or transglutaminase	Fat	Reconstruction of adipose tissue defects	Mouse	Stimulated neovascularization. Facilitated new adipose regeneration.	(Young, Bajaj, and Christman 2014)
Porcine skeletal muscle ECM hydrogels and Human umbilical cord-ECM hydrogel	None	Limb	Peripheral artery disease	Rat	Improved tissue perfusion by both hydrogel types. Skeletal muscle ECM hydrogels mimicked healthy tissue morphology better than placenta ECM hydrogels.	(Ungerleider *et al.* 2016)
Porcine cardiac ECM hydrogel	Genipin w/wo chitosan	Heart	Myocardial infarction	Rat	Improved heart dimensions and cardiac function of acutely or chronically infarcted hearts.	(Efraim *et al.* 2017)
Human placenta ECM hydrogel	None	Heart	Myocardial infarction	Rat	Reduced infarct size, retained more viable myocardium and maintained electrophysiological contraction profile of acute infarcted hearts.	(Francis *et al.* 2017)
Bovine meniscus ECM hydrogel	Human MSCs	Meniscus	Meniscal injury	Rat	Acted as a good vehicle for human MSCs retention in the damaged area, contributing to the protection against osteoarthritis development.	(Yuan *et al.* 2017)
Human adipose ECM hydrogel	Methylcellulose	Fat	Reconstruction of adipose tissue defects	Mouse	Facilitated the infiltration of endogenous adipose-derived stem cells and macrophages. Enhanced host-derived adipogenesis and angiogenesis.	(Kim, Choi, and Cho 2017)
Porcine nerve ECM hydrogel	poly(lactic-acid)-co-poly(trimethylene-carbonate)	Nerve	Peripheral nerve degeneration	Rat	Promoted the activation of M2 macrophages. Promoted nerve regeneration, myelination, and functional recovery.	(Lin *et al.* 2018)
Porcine skeletal ECM matrix hydrogels	None	Limb	Peripheral artery disease	Rat	Improved tissue perfusion.	(Hernandez *et al.* 2020)
Porcine meniscus ECM hydrogel	Rat BM-MSCs	Meniscus	Meniscal injury	Rat	Acted as a good vehicle for the delivery of rat BM-MSCs and enhanced meniscus healing and chondroprotection. Showed superiority with respect to collagen in the prevention of joint space narrowing and osteoarthritis development.	(Zhong *et al.* 2020)
Porcine cornea ECM hydrogel	CMC and N-hydroxysuccinimide	Cornea	Focal corneal defects	Rabbit	Restored the thickness of the corneal epithelium and stroma without significant inflammation or scar formation.	(Wang *et al.* 2020b)
Mouse hepatic ECM hydrogel	None	Liver	Liver fibrosis	Mouse	Enhanced the reduction of fibrosis and recovery to a nearly normal structure.	(Hussein *et al.* 2020)
Sheep bone ECM hydrogel	Hydroxyapatite w/wo osteoblast-derived extracellular vesicles	Bone	Bone defect repairing	Rabbit	Increased the bone area, the number of bone-specific cells and the angiogenesis.	(Emami *et al.* 2020)
Bovine nucleus pulposus ECM hydrogel and annulus fibrosus ECM hydrogel	None	Intervertebral discs	Intervertebral disc degeneration	Rat	Promoted tissue regeneration in nucleus pulposus degeneration and annulus fibrosus defect.	(Peng *et al.* 2021)

ECM: extracellular matrix; w/wo: with/without; BM-MSCs: bone-marrow mesenquimal stem cells; CMC: N-cyclohexyl-N'-(2-morpholinethyl) carbodiimide metho-p-toluenesulfonate.

Interestingly, ECM hydrogels derived from DC umbilical cord (Ungerleider *et al.* 2016) or placenta (Francis *et al.* 2017) have also been tested for non-tissue-specific applications with good results. Nonetheless, tissue-specificity still shows its supremacy over young tissue sources (Ungerleider *et al.* 2016).

As previously mentioned, serious damage of the endometrium in women of reproductive age is often accompanied by uterine scar formation and the loss of functional endometrium, predisposing the patient to infertility or miscarriage. In the search for therapies that could be used to heal these types of injuries, many preclinical models have been developed using stem cells (Alawadhi *et al.* 2014; Kilic *et al.* 2014; Gil-Sanchis *et al.* 2015; Gan *et al.* 2017; Domnina *et al.* 2018; Gao *et al.* 2019; Jun *et al.* 2019; Ouyang *et al.* 2020; Zhang *et al.* 2016; de Miguel–Gómez *et al.* 2019), stem cells with collagen scaffolds (Xin *et al.* 2019; Ding *et al.* 2014), cytokines (Ersoy *et al.* 2017) or platelet-rich plasma (Jang *et al.* 2017; de Miguel–Gómez *et al.* 2020). Recently research has also expanded toward the use of synthetic polymers (Xu *et al.* 2017; Yang *et al.* 2017; Zhang *et al.* 2020; Lin *et al.* 2021) and natural hydrogels from purified ECM components, such as hyaluronic acid hydrogels (Kim *et al.* 2019c). Nonetheless, tissue-specific hydrogels have not yet been approved for use in regenerative medicine focused on the endometrium.

II. HYPOTHESIS

II. HYPOTHESIS

Endometrial extracellular matrix hydrogel derived from decellularized porcine endometrium could be a promising and compatible biomaterial, with tissue-specific activity, that mimicks the endometrial microenvironment and provides functionality, biocompatibility and potential bioactivity in *in vitro* and *in vivo* models.

Endometrial extracellular matrix hydrogels contain unique components of the extracellular matrix from the endometrium, which are different from those found in other tissues, and influence the behavior of tissue-specific cells and may improve the current 3D *in vitro* culture approaches. Moreover, endometrial extracellular matrix hydrogels could minimize immune rejection *in vivo,* and therefore can be used as biocompatible xenogeneic treatments to enhance endometrial tissue repair, altogether providing a regenerative treatment for endometrial pathologies.

III. OBJECTIVES

III. OBJECTIVES

The main objective of this study was to develop endometrial extracellular matrix hydrogels derived from porcine uterus, and to study their applicability in 3D *in vitro* human cell culture systems and in *in vivo* murine models. The specific objectives are to:

1. Design endometrial extracellular matrix hydrogels from decellularized porcine uterus:

- Establish a protocol for the development of endometrial extracellular matrix hydrogels from porcine uterine tissue.

- Characterize physical and biochemical features.

2. Evaluate the use of endometrial extracellular matrix hydrogels as a platform for 3D culture *in vitro:*

- Analyze cytocompatibility with human endometrial stem cell lines and endometrial primary cells *in vitro*.

- Value suitability for supporting 3D co-culture of human endometrial cells long-term.

- Evaluate if they can substitute Matrigel in human endometrial organoids culture.

3. Assess the use of endometrial extracellular matrix hydrogels as a regenerative treatment for reproductive pathologies *in vivo:*

- Evaluate biocompatibility *in vivo*, by subcutaneous injection in a murine model.

- Assess potential to promote endometrial regeneration and fertility restoration in a murine model of endometrial damage.

IV. EXPERIMENTAL DESIGN
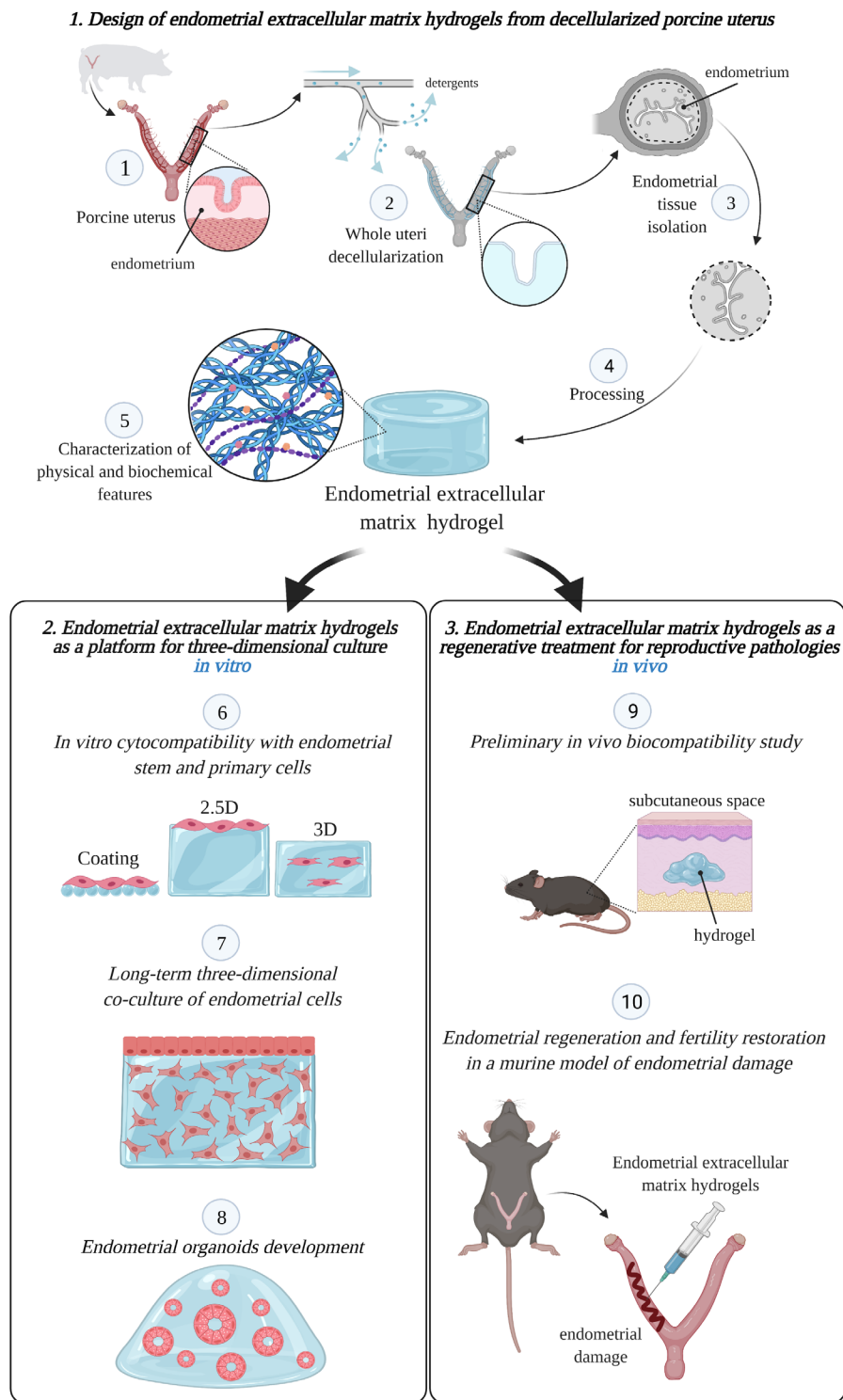
Figure 19. Experimental design. *Diagram of the experimental design showing the three specific objectives: (1) Design of endometrial extracellular matrix hydrogels from decellularized porcine uterus (steps 1-5), (2) Endometrial extracellular matrix hydrogels as a platform for three-dimensional culture in vitro (steps 6-8) and (3) Endometrial extracellular matrix hydrogels as a regenerative treatment for reproductive pathologies in vivo (steps 9,10).*

V. MATERIAL & METHODS

V. MATERIAL & METHODS

1. Design of endometrial extracellular matrix hydrogels from decellularized porcine uterus

1.1. Porcine uterus decellularization and endometrial-specific extracellular matrix purification

All the organs used for this study were obtained from pigs (approximately 220 kilograms) donated by Mercavalencia slaughterhouse (Valencia, Spain) according to ISO 9001 quality management. Pigs were sacrificed by carbon dioxide (CO_2) exposure (which results in a gradual loss of consciousness) together with exsanguination through the jugular vein. Entire reproductive tracts were collected and preserved on ice during transport to the IVI Foundation laboratory, where they were thoroughly washed to eliminate contaminants from other organs. Uteri were selected based on their appearance, size, and vascular system preservation. The superior part of vagina, ducts, mesometrium and ovaries were kept intact during decellularization to conserve the vasculature.

1.1.1. *Whole organ decellularization*

Entire female porcine reproductive tracts with intact vasculature were subjected to whole organ decellularization following a previously stablished 48-h protocol (Campo *et al.* 2017). Basically, porcine uterine horns were cannulated using 20-G cannulas (BD, ApositosNavarro, S.L.) and adequate perfusion was verified by the output of blood from the uterine vein after manual infusion of phosphate-buffered saline (PBS, pH 7.4, Sigma-Aldrich). Afterwards, horns were coupled to L/S 16 tubing (Masterflex, Fisher Scientific) and attached to a peristaltic pump (Cole-Parmer Instruments, Fisher Scientific).

An initial perfusion of PBS (1 h) removed the remaining blood. Decellularization was carried out with two cycles of the following steps: perfusion with 0.1% SDS for 18 h, distilled water for 30 min, 1% Triton X-100 for 30 min, and PBS for 5 h. A total of five horns were decellularized: three of them from uteri with a single cannulated horn and two from uteri with both horns cannulated. Decellularized horns were cut and frozen at -80ºC for posterior endometrial isolation.

1.1.2. *Endometrial isolation*

Frozen DC horns stored at -80ºC were cut transversally into 1 mm thick ring-shaped discs, washed with and maintained in ice-cold PBS during the isolation process. Taking the inner circular myometrial layer as a reference, the luminal endometrial fraction was isolated via microdissection under a stereomicroscope (SMZ800, Nikon)*(Figure 20A)* (Campo *et al.* 2019). This inner circular myometrial layer appears as a dense line in both non-decellularized (No-DC) and DC horns *(Figure 20B-C)*. The remaining myometrial fraction was kept, to use as a control, when verifying the selective isolation of pure endometrium and the presence of tissue-specific components during proteomic analysis. Similarly, endometrial tissue from No-DC uterine horns (n=5) was also isolated via microdissection as a control for subsequent analyses. Isolated tissues were stored at -80ºC.
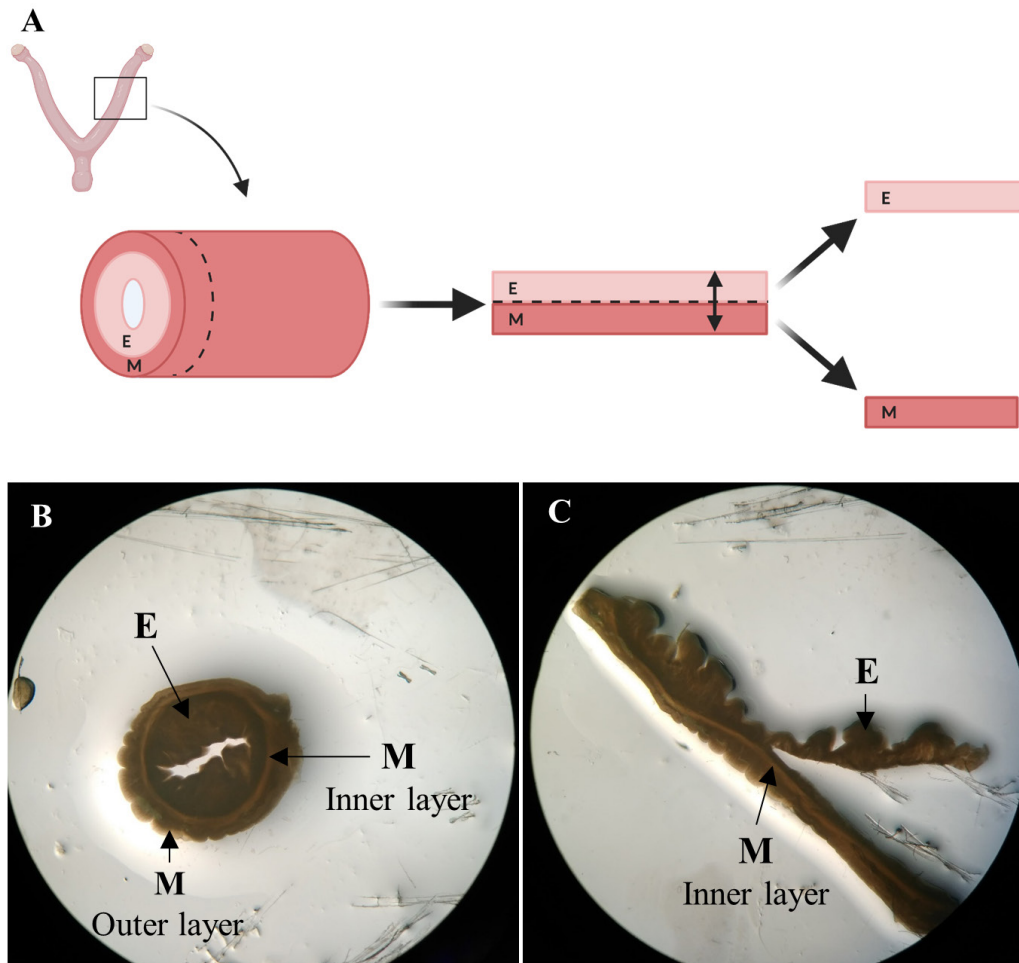
Figure 20. Endometrial layer isolation by microdissection. *A) Diagram showing manual endometrial isolation. Porcine horns were cut into ring-shaped discs, opened, and cut at the luminal side of the inner circular myometrial layer to isolate the endometrium. Image created with BioRender.com. B) Ring-shaped sections from control uterus showing uterine layers under a stereomicroscope. C) Open disc from control uterus during microdissection under a stereomicroscope. E: endometrium, M: myometrium.*

1.1.3. *Detergent removal and residual DNA digestion. Sodium dodecyl sulfate quantification assay*

To ensure the removal of residual DNA and detergents, DC endometrial tissue was treated with DNase and the remaining SDS was subsequently quantified. Endometrial and myometrial tissue stocks from uterus decellularization were thawed, weighed, and washed in cold PBS (10 milliliter (mL)/gram (g) tissue) for 30 minutes (min) at 200-250 revolutions per minute (rpm). Then, tissues were incubated for 1 h in 5 microgram

(µg)/mL Dnase I solution (D5025, Sigma-Aldrich) at room temperature (RT) and washed again. Aliquots from these washing medias were stored to detect residual SDS in the DC endometrial tissue.

Residual SDS in the washing media after endometrial isolation (n=8 DC horn pieces) and subsequent washes (pool of total isolated endometrial tissue) was quantified by measuring the absorbance of SDS reacting with a Stains-All dye (Sigma-Aldrich) (Rupprecht *et al.* 2015). A calibration curve of 7 standards (0,01-0,1 milligram (mg) SDS/mL) was made with serial dilution in PBS. Stains-All was dissolved in N, N-dimethylformamide to 2.0 mg/mL and then diluted a 1:20 working solution in ultrapure distilled water. For the assay, 10 microliters (µL) of all standards and samples were pipetted in a 96-well plate containing 140 µL PBS (0.1X). Afterwards, 50 µL of the Stains-All working solution (1:20) was added and absorbance was immediately measured at 453 nanometer (nm) using a microplate reader (Spectra Max 190, BioNova Científica, S.L.). Residual SDS concentration was calculated by adjusting the calibration curve to a lineal fit. The total amount of SDS was calculated from the initial volume and normalized to the individual weight of the DC endometrial tissues used in each wash. Samples were evaluated in triplicate.

1.1.4. *Determining decellularization efficiency and alpha-gal expression*

DC and native endometrial tissues were fixed in 4% paraformaldehyde (PFA), embedded in paraffin, and sectioned (to 4 micrometers, µm) with a microtome to assess adequacy of decellularization using histological analyses. Representative tissue sections were deparaffinized using xylene and rehydrated by decreasing concentrations of ethanol and finally distilled water. The absence of cellular components and nuclei was confirmed by Hematoxylin and Eosin (H&E) staining and a counterstaining mounting media containing

6-diamidino-2-phenylindole (DAPI, Thermo Fisher Scientific). Collagen preservation was also evaluated by Masson's Trichrome (MT) staining following the manufacturer's protocol.

Lastly, samples were immunoassayed for the presence of alpha(α)-gal epitope expression on cells, glycolipids and glycoproteins. Heat-mediated antigen retrieval was performed in deparaffinized sections using 10 milimolar (mM) citrate buffer pH 6.0, supplemented with 0.05% Tween (TWEEN® 20, P1379, Sigma-Aldrich) for 20 min in a 95 °C water bath. Then, sections were permeabilized using PBS (1X) supplemented with 0.05% Tween, blocked with 5% bovine serum albumin (BSA) for 1 h at RT and incubated with α-gal epitope monoclonal antibody (M86, ALX-801-090-1, Enzo Life Sciences, 1:5 dilution) in 1% BSA overnight at 4ºC. Immunostaining was revealed with 3, 3′ diaminobenzidine tetrahydrochloride (DAB) (DAB Substrate Kit, Sigma-Aldrich) in bright-field microscopy according to the manufacturer's instructions. Finally, sections were counterstained with hematoxylin, dehydrated and coverslipped. Alpha-gal expression was verified by visualization at microscope (10X, 40X magnification).

1.2. Creation of endometrial extracellular matrix hydrogel

Isolated DC endometrial tissue stock was flash-frozen in a mortar with liquid nitrogen, milled manually, and lyophilized (Lyoquest-85, Telstar, Valencia's Polytechnic University) over 96 h at 20 Pascals. The resulting endometrial lyophilized powder was digested and neutralized using a modified protocol (Brown, Buckenmeyer, and Prest 2017). One percent (weight (w)/volume (v)) lyophilized powder was suspended in 0.01 M hydrochloric acid (HCl, H1758, Sigma-Aldrich) with 0.1% pepsin (P7000, Sigma-Aldrich) and digested for 48 h with agitation. On ice, the solution was neutralized with 10% (v/v) 0.1 M sodium hydroxide (NaOH, S8045, Sigma-Aldrich), 11.11% (v/v) 10X

PBS (P5493, Sigma-Aldrich), and finally 1X PBS to reach the desired concentration. The resulting endometrial extracellular matrix (EndoECM) solution was stored at -80 ºC. To test stability and sterility, EndoECM hydrogels were maintained in Dulbecco's Modified Eagle's Medium (DMEM) Nutrient Mixture F-12 (DMEM/F-12; Sigma-Aldrich) containing 10% fetal bovine serum (FBS) and 0.1% streptomycin/penicillin for 7 days under standard *in vitro* culture conditions (37ºC, 5% CO_2).

This process was repeated with isolated DC myometrial and No-DC endometrial tissue stocks, to create myometrial extracellular matrix (MyoECM) and No-DC endometrial matrix (No-DC Endo), which were then used as controls for subsequent proteomic analyses.

1.3. Characterization of endometrial extracellular matrix hydrogels

Endometrial ECM samples were collected at different stages of hydrogel creation (wet tissue, lyophilized powder and hydrogel) in order to characterize the efficacy of critical steps governing the creation of the EndoECM hydrogel.

1.3.1. *DNA quantification and fragmentation analysis*

DNA was extracted from 23-25 mg wet tissue and 15 mg lyophilized powder using a DNeasy Blood & Tissue kit (#69504, Qiagen) as per manufacturer's instructions. DNA concentration was then measured using the Qubit™ dsDNA HS Assay Kit (Q32851, Thermo Fisher Scientific) and normalized to the initial weight of each sample. DNA fragmentation was determined using gel electrophoresis, where 10 µL of each extracted DNA sample was loaded onto a 1% agarose gel stained with GelRed® nucleic acid gel stain (#41003, Biotium) for a total runtime of 40-50 min at 100 V. A 1 kb plus DNA ladder (#10787018, Invitrogen) was used for comparison.

1.3.2. *Total protein, collagen, glycosaminoglycans, and elastin quantifications*

The total protein fraction was extracted from 100 mg wet tissue, 10 mg lyophilized powder, and 35 µL 8 mg/mL EndoECM using 100-400 µL of a modified Laemli buffer (0.125M Tris HCl, 4% SDS, 0.0001% beta(β)-mercaptoethanol; Gibco™ 2-Mercaptoethanol 1000X 55mM in DPBS, #21985023, Fisher Scientific) for 48 h at 37$^\text{o}$ C and 300 rpm. Protein concentration was determined with the Pierce$^\text{TM}$ BCA protein assay kit (#23225, Thermo Fisher Scientific) following the standard protocols provided by the manufacturer.

Collagen, elastin, and GAGs were extracted from 23-25 mg wet tissue, 3-6 mg lyophilized powder, and 70-250 µL 8 mg/mL EndoECM. Collagen, elastin, and GAGs were respectively quantified using Sircol™ insoluble collagen assay, Fastin™ elastin assay and Blyscan™ glycosaminoglycan assay (Bicolor, Life Sciences Assays), following the standard protocols provided by the manufacturer.

All quantifications were normalized to the initial weight of each corresponding sample.

1.3.3. *Turbidimetric-kinetic gelation assay of endometrial extracellular matrix hydrogel*

The gelation kinetics of EndoECM (n=3) was evaluated by turbidimetry. Absorbance at 405 nm for 100 µL of 3, 6, and 8 mg/mL EndoECM was measured every minute in a microplate reader (SpectraMAX 190, Molecular Devices) at 37°C. Absorbance was normalized with the following formula as described by Freytes *et al.* (Freytes *et al.* 2008):

$$NA = \frac{A - A_0}{A_{max} - A_0}$$

Where *NA* is the normalized absorbance, *A*: absorbance at given time, A_0: initial absorbance and *Amax*: maximum absorbance.

Kinetic parameters (lag time, time to half gelation, time to complete gelation and gelation rate) from the different concentrations were compared (Freytes *et al.* 2008). The lag time (T_{Lag}) was defined as the intercept of the linear region of the gelation curve with 0% absorbance, the time to half gelation ($T_{1/2}$) as the time to 50% absorbance, the time to complete gelation (T_1) as the time to 100% absorbance, and the gelation rate (*S*) as the slope of the linear region of the gelation curve. Data were statistically analyzed with respect to the minimum concentration of 3 mg/mL.

1.3.4. *Scanning electron microscopy of tissue-specific hydrogels*

The ultrastructure of 3, 6, and 8 mg/mL EndoECM, 8 mg/mL MyoECM, and 8 mg/mL No-DC Endo hydrogels was evaluated using scanning electron microscopy (SEM). Sample processing was performed in the proteomics facility of the Servicio Central de Soporte a la Investigación Experimental (SCSIE) at the University of Valencia. Hydrogels were fixed in 2.5% glutaraldehyde in PBS (Sigma-Aldrich, grade II, 25%) for 24 h, washed in PBS, and maintained in PBS at 4ºC. Hydrogels were then treated with 2% osmium tetroxide for 2h, dehydrated in a graded series of ethanol (30, 50, 70, 90, 100%) for 30 min per wash, kept in 100% ethanol overnight at 4°C, and washed thrice in 100% ethanol for 30 min. Hydrogels were then dehydrated using an Autosamdri® 814 Critical Point Dryer (Tousimis) with liquid CO_2 at high pressure (1200 pound-force per square inch) and a maximum heating temperature of 40ºC. Dried samples were coated with gold-palladium for 2 min using a SC7640 Sputter Coater (Quorum technologies) and imaged with a SEM FEG Hitachi S-4800 (SCSIE University of Valencia, Spain). To

analyze fiber diameter, four measurements per three fields at 30.000X resolution per sample were measured using ImageJ software (Schindelin *et al.* 2012).

1.3.5. *Proteomic analysis*

The proteome of EndoECM was analyzed and compared with MyoECM, and No-DC Endo using liquid chromatography and tandem mass spectrometry (LC-MS/MS). Fifty micrograms of EndoECM, MyoECM, and No-DC Endo (8 mg/mL) were loaded and resolved in a 1D SDS-PAGE gel. Every sample lane was sliced into seven fragments. Gel slides were digested using 200 nanogram (ng) sequencing grade trypsin (Promega) at 37ºC, as described elsewhere (Shevchenko *et al.* 1996). Trypsin digestion was stopped with 10% trifluoroacetic acid (TFA) and the supernatant was removed. The library gel slides were dehydrated with pure acetonitrile (ACN) and the new peptide solutions were combined with their corresponding supernatant. The peptide mixtures were dried in a speed vacuum and resuspended in 2% ACN and 0.1% TFA. The final volume ranged between 6 and 25 µL.

For LC-MS/MS, 5 µL of each sample was loaded onto a trap column (NanoLC Column, 3µm C18-CL, 350 µmx0.5mm; Eksigen) and desalted with 0.1% TFA at 2 µL/min for 10 min. Peptides were then loaded onto analytical columns (LC Column, 3 µm C18-CL, 75 umx12cm, Nikkyo) equilibrated in 5% ACN, 0.1% formic acid (FA). Elution was carried out with a linear gradient of 5-40% B in A (where A: 0.1% FA; B: ACN, 0.1% FA) for 60 min, at a flow rate of 300 nanoliters/min. Peptides were analyzed in a mass spectrometer nanoESI qQTOF (5600 TripleTOF, ABSCIEX). Each sample was ionized applying 2.8 kilovolt to the spray emitter. Subsequent analysis was carried out in a data-dependent mode. Survey MS1 scans were acquired from 350–1250 mass-to-charge ratios (m/z) for 250 milliseconds. The quadrupole resolution was set to 'UNIT' for MS2

experiments, which were acquired at 100–1500 m/z for 50 milliseconds in 'high sensitivity' mode. The following switch criteria were used: charge: 2+ to 5+; minimum intensity; 70 counts per second. Up to 50 ions were selected for fragmentation after each survey scan. Dynamic exclusion was set to 15 seconds. The system sensitivity was controlled with 2 femtomole of 6 proteins (LC Packings).

The following proteomic analysis was performed in the SCSIE proteomics facility of University of Valencia. ProteinPilot default parameters were used to generate a peak list directly from 5600 TripleTof wiff files. The Paragon algorithm (Shilov *et al.* 2007) of ProteinPilot (ProteinPilot v5.0. search engine, ABSciex) was used to search the UniprotMammals database (version 03-2018) with the following parameters: Trypsin specificity, (iodoacetamide) cys-alkylation, taxonomy not restricted, and the search effort was set to through. The proteins were grouped using the Pro group algorithm. Protein grouping was considered to be guided by spectra because the formation of protein groups was guided entirely by observed peptides only (which originated from the experimentally acquired spectra). Unobserved regions of the protein sequence were not considered for data analysis. Proteins showing an unused score >1.3 were identified with confidence ≥95%. Mass spectrometry information of all the fragments was combined for protein identification using the UniprotMammals database.

Filtered output files for each peptide were grouped according to the protein from which they were derived, and their percentage of individual coverage (% cov) was indicative of protein abundance in relative quantification analysis. Common contaminants were excluded following the exclusion criteria of Hodge *et al.,* (Hodge *et al.* 2013) and according to their expression in target tissue according to The Human Protein Atlas database (http://www.proteinatlas.org) (Uhlen *et al.* 2015). Lists of peptides found in the aforementioned proteomic analysis of EndoECM, MyoECM and No-DC Endo can be

found in Appendix A *(Supplementary Table I, Supplementary Table II, Supplementary Table III)*. ECM proteins were identified according to their cellular or extracellular origin as well as presence in the MatrisomeDB 2.0. data base (The Matrisome Project, http://matrisomeproject.mit.edu/proteins/). Gene ontology analysis (for cellular component and molecular function) of the detected proteins was performed using the PANTHER classification system (Mi *et al.* 2018) and refined according to ECM-related processes.

1.4. Statistical analysis

Data were analyzed using RStudio® software version 3.6.3 (RStudio Team 2020) and presented as mean ± standard deviation (SD). All statistical analyses were performed using a linear regression model to account for total variability (non-parametric analysis). In this case, the value for each group's variable was estimated by its average difference with respected to a reference group. The *P* value was obtained from contrast hypotheses of the linear model, indicating with 95% confidence that the difference between the groups is not zero, and different without having to use multiple comparison tests. In all cases, a p value (p) <0.05 was considered statistically significant.

2. Endometrial extracellular matrix hydrogels as platforms for three-dimensional culture *in vitro*

2.1. Ethical statements and cell collection

The studies presented in this section were approved by the Human Ethics Committee at the IVI Foundation (1706-FIVI-053-IC, Valencia, Spain). For these studies, fresh

endometrial biopsies were collected from healthy oocyte donors (who underwent controlled ovarian stimulation) on the day of oocyte retrieval.

In vitro cytocompatibility and long-term 3D co-culture studies were carried out with epithelial and stroma cells from human endometrial stem cell lines and primary human endometrial cells. For primary cell isolation, fresh endometrial tissues were mechanically minced into small pieces (<1 mm). To separate ESCs from EECs, minced tissue was digested with collagenase (0.1% collagenase type IA; Sigma-Aldrich) in DMEM/F-12 at 4ºC overnight. To separate cells based on size (gravity sedimentation), sample tubes were place in vertical position. The supernatant (ESCs) was collected and filtered with 50-mm cell filters (Celltrics, GmbH) while the pellet (glandular and luminal EECs) was washed three times for 10 min with 5 mL of DMEM. The resulting supernatants (with ESCs) from these rinses were also recovered every time. The EECs pellets was digested with 300 µL TrypLE™ Select Enzyme to obtain single EECs, filtered with 50-mm cell filters and neutralized with DMEM. Finally, ESCs and EEC solutions were centrifuged at 2,000 rpm for 7 min and resuspended in DMEM (Simón *et al.* 1993; Cervelló *et al.* 2010; 2011). Only fresh or first passage (P1) EECs and ESCs were used for subsequent experiments.

Epithelial (ICE6) and stromal (ICE7) endometrial stem cell lines were obtained using Hoechst methodology and cloning efficiency (Clone ICE6 & Clone ICE7, Richmond, British Columbia, Canada). Characterization, purity, and clonogenicity of these stem cell lines were previously reported by Cervelló *et al.* (Cervelló *et al.* 2010; 2011). Only passages 7-12 of ICE6 and ICE7 were used for subsequent experiments.

2.2. *In vitro* cytocompatibility of endometrial extracellular matrix hydrogels with human endometrial stem and primary cells

2.2.1. *Experimental design*

The ICE6, ICE7, EECs, and ESCs were cultured in different two- and three-dimensional configurations: on top of an EndoECM coating (2D) or hydrogel (2.5D), or encapsulated within the EndoECM hydrogel (3D) (Link *et al.* 2017). Two standard culture matrices, type I collagen (collagen solution from bovine skin, C4243, BioReagent) and Matrigel (Corning® Matrigel® Basement Membrane Matrix, 354234, Corning), were used as controls. The acidic collagen solution was neutralized with 1% (v/v) 1 M NaOH and 11.11% (v/v) 10X PBS following the manufacturer's instructions. Collagen and Matrigel were both diluted in PBS to a concentration of 3 mg/mL. For the coating condition, 96-well culture plates with 20 µL per well of PBS (no treatment, NoTT), collagen, Matrigel or 3 mg/mL EndoECM were incubated overnight at 4°C. Then, the solutions were aspirated, and wells were rinsed with PBS *(Figure 21A)*. Meanwhile, for 2.5D culture, 96-well culture plates with 100 µL of collagen, Matrigel, or 3, 6, or 8 mg/mL EndoECM per well were incubated at 37°C for 30 min for spontaneous hydrogel gelation *(Figure 21B)*. Both conditions were seeded with 15,000 stem cells/cm^2 or 55,000 primary cells/cm^2 in 150 µL of culture media (10% FBS DMEM/F-12 containing 0.1% streptomycin/penicillin).

To grow the cells in a 3D environment, cells were first suspended in ice-cold collagen, Matrigel, or 3, 6, or 8 mg/mL EndoECM (1.0 x 10^6 cells/mL). Then, 16 µL drops of the cell-suspension was added per well and the plate was incubated at 37°C during 30 min for hydrogel gelation before flooding with 150 µL of culture media *(Figure 21C)*.
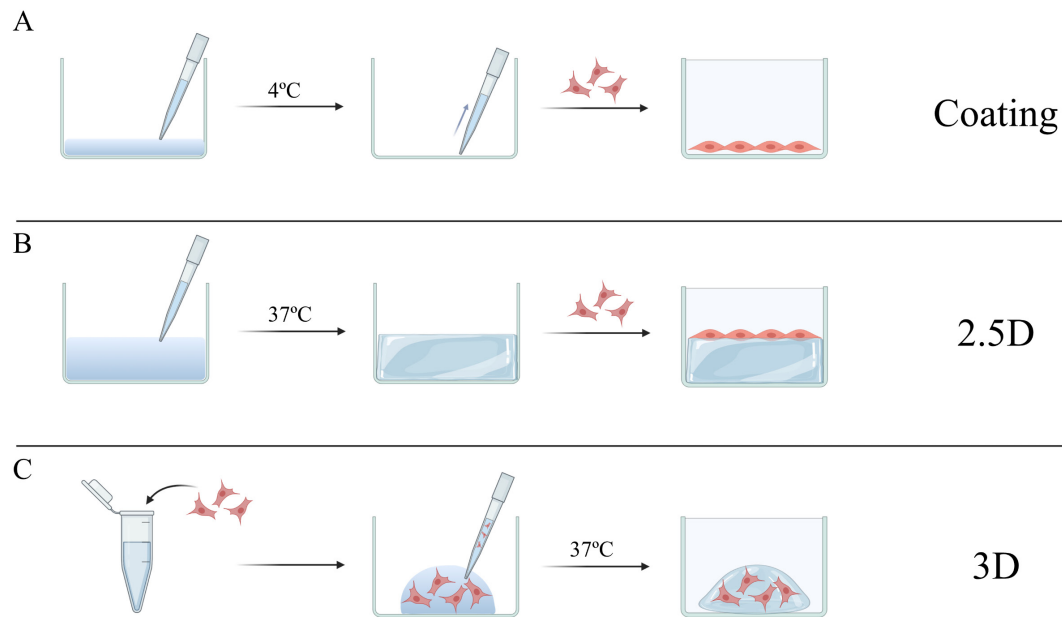
Figure 21. Experimental design of coating, 2.5D and 3D cell culture. *A) Collagen, Matrigel and EndoECM solutions were incubated at 4°C overnight and then aspirated to make a coating where cells were seeded. B) Solutions were incubated at 37°C to form a thick hydrogel and cell were then seeding on the top. C) Solutions were mixed with cells and cell-solution drops were incubated at 37°C to gel. Created with BioRender.com.*

2.2.2. *Tetrazolium assay*

Cell proliferation in 2D and 3D cultures was assessed after 72 h by incubating samples with 3-(4,5-dimethylthiazol-2-yl)-5-(3-carboxymethoxyphenyl)-2-(4-sulfophenyl)-2H-tetrazolium (MTS) reagent (CellTiter 96® Cell Proliferation Assay, Promega) for 2 h at 37°C according to the manufacturer's instructions. Negative controls without cells (blank absorbance values) were included. After incubation, culture media was transferred to a reader plate and absorbance was measured at 490 nm. To determine fold change, data was normalized with respect to NoTT group for the coating condition or the collagen group for 2.5D and 3D conditions. Cell proliferation was compared between the different solutions (collagen, Matrigel, and EndoECM) at the same concentration (3 mg/mL), and different concentrations of EndoECM (3, 6 and 8 mg/mL) in 2.5D and 3D cultures.

2.3. Long-term three-dimensional co-culture of human endometrial cells

2.3.1. *Experimental design*

Three-dimensional co-culture systems were constructed using both stromal and epithelial cells from endometrial stem cell lines (ICE6-7 constructs) and cultured primary biopsies (EEC-ESC constructs). Endometrial stromal cells (P1) or ICE7 stem cells were mixed with EndoECM (0.75-1.0 x 10^6 cells/mL) and 150 µL of the mixture was quickly pipetted into a 6.5 mm insert (0.4 µm Pore, Corning Costar Transwell, Sigma-Aldrich) and allowed to solidify. Subsequently, 10% FBS DMEM/F-12 containing 0.1% penicillin-streptomycin was added, and 200,000-300,000 epithelial cells/cm^2 (EECs (P1) or ICE6) were seeded onto the ESC or ICE7 hydrogel immediately after solidification (Method A) or on day 3 of culture (Method B). Co-cultures were maintained up to 10 days in normoxia (21% oxygen (O_2) in the case of EECs-ESCs constructs) or hypoxia (2% O_2 in the case of ICE6-7 constructs) under standard cell culture conditions. The experimental design is shown in *Figure 22*. This protocol is a modification of a previously described protocol for 3D endometrium-like culture systems (Wang *et al.* 2012).
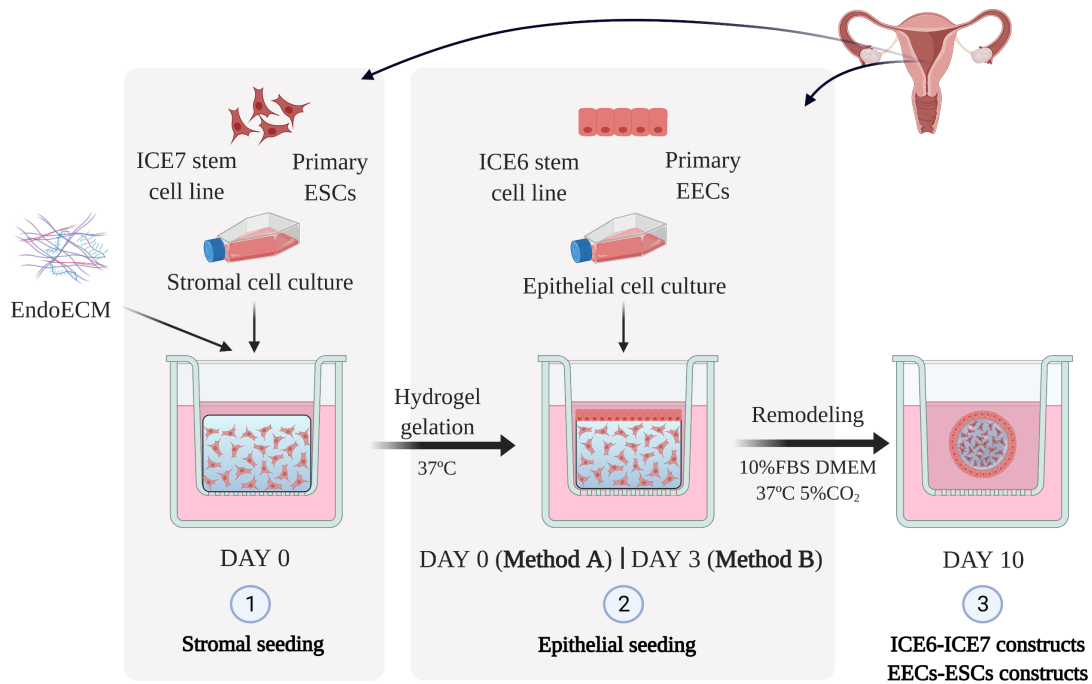
Figure 22. Experimental design of 3D co-culture of endometrial cells. *Endometrial-like co-cultures were constructed with primary cells (EECs or ESCs constructs, epithelial and stromal cells respectively) or stem cell lines (ICE6 or ICE7 constructs) using EndoECM. 1) First, stromal fraction (ESCs or ICE7) was mixed with EndoECM solution and allowed to gel to form a hydrogel with embedded stromal cells. 2) Epithelial fraction (EECs or ICE6) was seeded on the hydrogel surface using two seeding approaches. 3) EECs-ESCs and ICE6-7 constructs were cultured under standard in vitro conditions for 10 days. Created with BioRender.com.*

2.3.2. *Histological analysis*

Constructs were fixed, dehydrated, and embedded in paraffin as previously described in section 1.1.4. Paraffin-embedded sections (5 µm) were deparaffined and construct remodeling was investigated using MT staining. Cell viability was verified using a terminal deoxynucleotidyl transferase-mediated dUTP nick-end labelling (TUNEL) assay (DNA Fragmentation Imaging Kit, Roche) for ICE6-7 constructs or *in vivo* LIVE/DEAD™ cell imaging (Invitrogen™ kit 488/570, Thermo Fisher Scientific) for EECs-ESCs constructs, following the manufacturer's instructions.

For histological and immunohistochemistry/fluorescence analysis, heat-mediated antigen retrieval was performed in 10 mM Citrate Buffer with 0.05% Tween (pH 6.0) for 20 min

in a 95 °C water bath. Sections were permeabilized with 0.05% Tween in PBS, blocked with 3-10% BSA in PBS for 1h at RT and incubated with primary antibodies in 1% BSA overnight at 4ºC.

Cell proliferation was measured by Ki67 expression (Anti-Ki67 polyclonal antibody, ab9260, Sigma-Aldrich, 1:300 dilution). Ki67 is a nuclear protein, with a high net electrical charge that forms a steric and electrostatic charge barrier on the chromosome surface, preventing its collapse into a single chromatin mass, and dispersing individual mitotic chromosomes. Samples were revealed using DAB (DAB Substrate Kit, Sigma-Aldrich) for bright-field microscopy according to the manufacturer's instructions. Sections were then counterstained with hematoxylin. The percentage of cells expressing Ki67 was quantified from three x20 fields of view per sample using Image ProPlus analysis software v6.3 (MediaCybernetics, Rockville, MD, USA) (Francisco, de Moraes, and Dias 2004).

Vimentin (Vimentin monoclonal antibody [V9], ab8069, ABCAM, 1:100 dilution) and E-cadherin (E-Cadherin polyclonal antibody, ab53033, ABCAM, 1:100 dilution), specific markers for stroma and epithelium respectively, were analyzed by immunofluorescence. Slides were incubated with an Alexa-Fluor 488 secondary antibody (A21121, 1:500 dilution) and sections were mounted with mounting media containing DAPI.

2.4. Endometrial extracellular matrix hydrogels and human endometrial organoids development: A proof-of-concept study

2.4.1. *Establishment of an endometrial organoid line*

For the establishment of the endometrial organoid culture, we used a procedure modified from a previous established protocol (Turco *et al.* 2017). A fresh endometrial biopsy was incubated in DMEM (without phenol red) containing 0.1% penicillin-streptomycin for 20 min with gentle agitation to remove blood. The remaining blood clots and mucus were removed manually using scalpel blades and endometrial tissues were minced to 1 mm^2 fragments. The sample was then placed in a 40-mL tube and incubated in a warm collagenase/dispase solution (10% 4 mg/mL collagenase V, 2.5% 50 U/mL dispase II, 10% inactivated Fetal Calf Serum (FCS), 77.5% Roswell Park Memorial Institute medium (RPMI) 1640 medium) at 37ºC, with gently agitation, to disaggregate the stromal fraction. The reaction was halted when free intact glands were detected in the medium under bright-field microscopy (30-40 min), by diluting the enzyme solution 1:3 with RPMI-1640 medium. This media was used cold to prevent the adhesion of the glands to the plastic surfaces in subsequent steps. The sample tube was gently agitated and the remaining undigested tissue was left to precipitate for 2 min. The supernatant was passed through a sterile 100 µm cell sieve (100µm Cell Strainer 431752, Corning) to new 40-mL tubes and then, the cell sieve was washed thrice. The filtered stromal fraction was discarded while the remaining glandular fraction was backwashed from the cell sieve membrane by pipetting over a new 40-mL tube. The glandular fraction was pelleted by centrifugation at 600xg for 5 min and resuspended in 1.5 Eppendorf tubes. Finally, the pellet containing the endometrial glands was resuspended in Advanced DMEM/F-12 (Gibco™ DMEM/F-12 Advanced 12634010, Thermo Fisher Scientific) and incubated on ice for 2 min. Ice-cold Matrigel (with an approximate protein concentration of 10 mg/mL)

was added for a final concentration of 85% Matrigel. For establishing 3D cell culture of the glands, 25 µL ice-cold drops were placed in a 48-well culture plate and incubated at 37ºC for 15 min to promote Matrigel gelation. Finally, 250 µL of organoid-specific expansion medium was added to each well and incubated under standard *in vitro* culture conditions (37ºC and 5% CO_2).

Organoid-specific expansion medium was previously defined by (Turco *et al.* 2017). It was elaborated using: advanced DMEM/F-12, 100 µg/mL Primocin™ (Antimicrobial agent for primary cells, ant-pm-1, Invitrogen), 1X nitrogen supplement (Gibco™ N-2 Supplement (100X), 17502048, Thermo Fisher Scientific), 1X B-27 supplement (supplement B-27™ (50X), minus vitamin A, 12587010, Thermo Fisher Scientific), 1.25 mM N-Acetyl-L-cysteine (A9165-5G, Thermo Fisher Scientific), 2 mM L-glutamine (G7513, Sigma-Aldrich), 50 ng/mL epidermal growth factor (Animal-Free Recombinant Human EGF, AF-100-15, PeproTech), 100 ng/mL recombinant human noggin (120-10c, PeproTech), 500 ng/mL roof plate-specific spondin-1 (Recombinant Human R-Spondin-1, 120-38, Peprotech), 100 ng/mL fibroblast growth factor-10 (Recombinant Human FGF-10, 100-26, Peprotech), 50 ng/mL hepatocyte growth factor (HGF; Recombinant Human HGF (Insect derived), 100-39, Peprotech), 500 nanomolar (nM) ALK5 Inhibitor IV (A 83-01, 9094360, Biogems), 10 nM nicotinamide (N0636, Sigma-Aldrich).

2.4.2. *Passaging the endometrial organoid cell line*

Organoids were sub-cultured according to the established protocol by (Turco *et al.* 2017). Pipette tips were used to scrape up Matrigel drops containing organoids, without removing the expansion media. In order to minimize the attachment of the glands, every four Matrigel drops were pooled and transferred into each 1.5 mL LoBind microcentrifuge tube (Eppendorf®, Z666505, Sigma-Aldrich). Organoids were

centrifuged at 600xg for 5 min, resuspended in 150 μL cold Advanced DMEM/F-12, and broken down by pipetting 300 times using a P200 pipette. One milliliter of Advanced DMEM/F-12 was then added and organoid fragments were pelleted by centrifugation. Pellets were resuspended in 150 μL cold Advanced DMEM/F-12, and organoids were further broken down by pipetting 80 extra times. Another milliliter of cold Advanced DMEM/F-12 was added, and samples were pelleted one last time before a 2 min incubation on ice and addition of 85% ice-cold Matrigel. Drops of 25 μL were transferred to a 48-well culture plate, which was incubated for gelation prior to the addition of expansion medium.

2.4.3. *Preservation of the endometrial organoid cell line*

To depolymerize the Matrigel without enzymatic digestion, organoids were retrieved from Matrigel drops using 250 μL recovery solution (Corning® Cell Recovery Solution, 354253, Corning) per well, during 60 min on ice. Organoids were pelleted by centrifugation, resuspended, broken down by pipetting 80 times and centrifuged again. Ice-cold organoid pellets were mixed with 1 mL of freezing medium (Gibco™ Recovery™ Cell Culture Freezing Medium, 10% dimethyl sulfoxide (DMSO), Thermo Fisher), transferred to cryovials and first stored in -80ºC and finally in liquid nitrogen for long-term cryopreservation.

Cryovials were thawed by diluting freezing medium with 9 mL of Advanced DMEM/F-12 at 37ºC. Organoids were centrifuged, resuspended with Matrigel and seeded in a 48-well culture plate. Expansion media was supplemented with Y-27632 (Y-27632 - CAS 146986-50-7 – Calbiochem, Sigma-Aldrich) during the first three days of culture.

2.4.4. *Characterization of endometrial organoids*

2.4.4.1.   Histological analysis

The organoids were retrieved from Matrigel drops using 250 μL of recovery solution during 60 min on ice, as previously described. The organoids were pelleted by centrifugation, fixed with 4% PFA for 30 min at RT and washed in PBS. Samples were once again pelleted by centrifugation, embedded in 1% warm agarose and allowed to gel in ice-cold 50 μL cylindrical molds. Organoid-agarose blocks were included in bigger 500 μL molds to prevent the loss of the sample during the inclusion procedure. Constructs were dehydrated and embedded in paraffin. Paraffin-embedded sections (4 μm) were deparaffined and analyzed by H&E staining.

Organoids were analyzed for the presence of epithelial and stromal cell markers to verify their epithelial origin. Heat-mediated antigen retrieval was performed in 10 mM Citrate Buffer with 0.05% Tween (pH 6.0) during 20 min in a 95 °C water bath. Sections were permeabilized with 0.1% Triton X-100 in 1X PBS, blocked with 5% BSA, 5% NGS for 1 h at RT and incubated with primary antibodies overnight at 4ºC. Expression of a specific marker for stroma, Vimentin (Vimentin monoclonal antibody [V9], ab8069, ABCAM, 1:10 dilution), and a specific marker for epithelium, Cytokeratin (Anti-Cytokeratin 18 antibody, ab52948, ABCAM, 1:300 dilution), was analyzed by immunofluorescence. Slides were incubated with an Alexa-Fluor 488 secondary antibody (A21121, 1:500 dilution) and Alexa-Fluor 568 secondary antibody (A21124, 1:500 dilution) and mounted with mounting media containing DAPI.

2.4.4.2.   Genomic hybridization array

To verify that chromosomal stability was not affected in the organoid line, an early and a late passage of the organoid line was analyzed using a genomic hybridization array

(Affymetrix CytoScan 750k Array, Affymetrix Inc., Santa Clara, CA, USA). The Affymetrix CytoScan 750K Array is a cytogenetic microarray designed to provide whole-genome coverage and high performance for detecting chromosomal aberrations. It includes 750,000 markers for copy number analysis, with 200,000 single nucleotide polymorphisms and 550,000 non-polymorphic probes.

Organoids from passage 3 and 12 were thawed by diluting freezing medium with 9 mL of Advanced DMEM/F-12 at 37ºC. Organoids were centrifuged and DNA was extracted from the resulting pellet using the Cells and Tissue DNA Isolation Micro Kit (Norgen, 57300). DNA quantity and quality were analyzed using the Nanodrop ND-1000 Spectrophotometer while integrity was assessed by gel electrophoresis (using a 0.8% agarose gel to verify the presence of a 10-20 kb band). In order to be considered optimal to perform the CytoScan 750k, the DNA samples needed a concentration >50 ng/µl (or have >250 ng DNA in total) with a 260/280 ratio between 1.8-2.1, a 260/230 ratio between 1.8-2.2 and no fragmentation after gel electrophoresis. Resulting data was analyzed using Chromosome Analysis Suite v4.2 software. The weighted Log2 ratio was analyzed using the Whole Genome View tool to check the copy number state of each chromosomic region. The presence of signal above or below 0 in the weighted Log2 ratio was respectively considered an increase or decrease of chromosomes or number of copies inside a specific chromosome.

2.4.5. *Preliminary study of endometrial extracellular matrix as a substitute for Matrigel in endometrial organoid culture system*

Matrigel drops (containing early organoid passages) were pooled and transferred into each 1.5 mL LoBind microcentrifuge tube and retrieved from Matrigel drops as detailed in section 2.4.2. Organoid pellets were incubated on ice for 2 min and mixed with ice-

cold Matrigel or 8 mg/mL EndoECM. Drops of 25 µL were placed in a 48-well culture plate (approximately 8 drops per condition) and incubated 15 min for gelation prior to the addition of 250 µL expansion medium (per well). Organoid development and morphology were visualized with an inverted microscope after 2 and 5 days. This study was repeated in triplicate for each passage. The experimental design is shown in *Figure 23*.
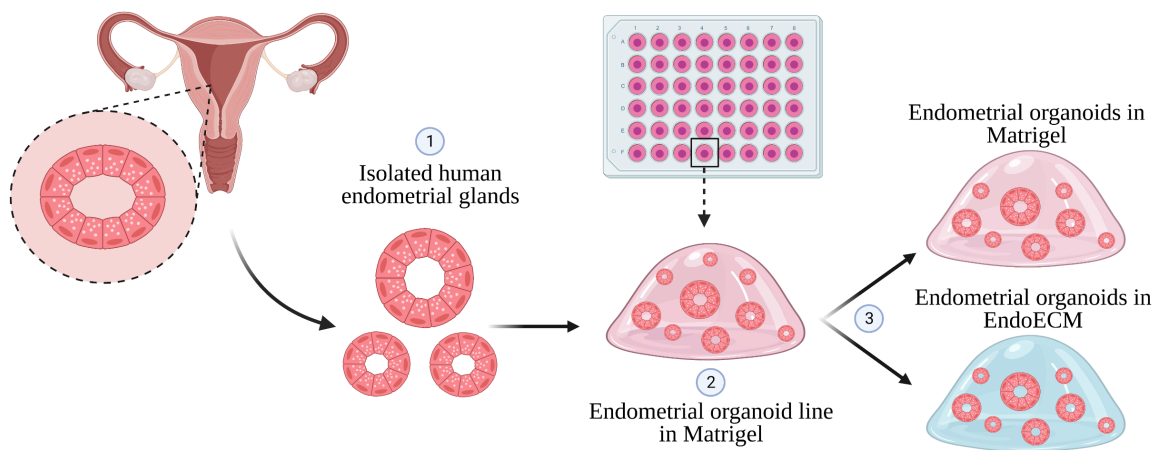
Figure 23. Endometrial extracellular matrix hydrogel as a substitute for Matrigel in endometrial organoid culture. Experimental design showing that the endometrial glands were 1) isolated from fresh endometrial biopsy, 2) cultured in Matrigel drops (in 48-well culture plates) to establish an endometrial organoid line in 3D culture, and subsequently 3) early-passage organoids were cultured in EndoECM or Matrigel drops. Created with BioRender.com.

2.5. Statistical analysis

Data were analyzed using RStudio® software version 3.6.3 (RStudio Team 2020) and presented as mean ± standard deviation (SD). All statistical analyses were performed using a linear regression model to account for total variability (non-parametric analysis) as previously described in section 1.4. In all cases, a p value (p) <0.05 was considered statistically significant.

3. Endometrial extracellular matrix hydrogels as a regenerative treatment for reproductive pathologies *in vivo*

3.1. Ethical statements and C57BL/6 mice

All the animal procedures described in this study were performed in accordance with Directive 2010/63/EU and the Ethics Committee for Animal Welfare of University of Valencia (A1510673251016/A-1550574856754). On account of the presumed biocompatibility of DC materials among different species (a fundamental pillar of the present thesis), and the cytocompatibility of EndoECM hydrogels evaluated in the *in silico* and *in vitro* experiments previously described herein, the immunocompetent murine inbred strain C57BL/6 (C57BL/6NCrl, Charles River Laboratories) was used for all the experiments. The mice were maintained in 12 h light/dark cycles, with unlimited access to food and water, in the animal facilities of the Central Research Unit of the Faculty of Medicine at the University of Valencia.

3.2. Preliminary *in vivo* biocompatibility of endometrial extracellular matrix hydrogels in a subcutaneous murine model

3.2.1. *Experimental design*

For a preliminary testing of *in vivo* biocompatibility, EndoECM hydrogels were injected subcutaneously in immunocompetent female C57BL/6 mice (n=9). Mice were anesthetized with isoflurane (in prone position) and dorsal hair was shaved. Injections of 200 µL of 8 mg/mL EndoECM or No-DC Endo (control group for immune rejection) were administered through a 25-Gauge (G) needle in the dorsal subcutaneous space. Hydrogels remained inside the mice for 2 (n=3 for EndoECM and n=2 for No-DC Endo), 7 (n=1 for EndoECM and n=1 for No-DC Endo), and 14 (n=1 for EndoECM and n=1 for

No-DC Endo) days before mice were euthanized. Skin samples containing hydrogel grafts were harvested for histological analysis.

3.2.2. *Histological analysis*

Samples were fixed in 4% PFA, dehydrated and embedded in paraffin. To quantitatively assess cell infiltration and scaffold morphology, 4 µm sections were deparaffined and stained with MT.

The macrophage response to implanted hydrogels at 2-, 7-, and 14-days post-surgery was analyzed by immunolabeling. Heat-mediated antigen retrieval was performed in 10 mM Citrate Buffer with 0.05% Tween (pH 6.0) for 20 min in a 95 °C water bath. Sections were permeabilized with 0.05% Tween in PBS, blocked with 5% BSA for 1h at RT and incubated with CD68 pan-macrophage marker antibody (CD68 polyclonal antibody, 304 ab125212, ABCAM, 1:100 dilution). Samples were revealed using DAB (DAB Substrate Kit, Sigma-Aldrich) in bright-field microscopy and sections were then counterstained with hematoxylin. Five 20x magnification fields were quantified per sample, using QuPath analysis software v0.2 (Bankhead *et al.*, 2017).

3.3. Endometrial regeneration and fertility restoration in a murine model of endometrial damage

3.3.1. *Experimental design*

Endometrial injury was induced by injecting ethanol in the uterine horns of eight-week-old C57BL/6 female mice (n=37). After four days, mice were randomized using the True Random Number Service tool (Haahr 2021) and treated with one of the following: (a) saline (negative control), (b) biotin-labelled EndoECM or (c) biotin-labelled EndoECM supplemented with growth factors (EndoECM+GF). For the EndoECM+GF condition,

biotin-labelled EndoECM was mixed with 10 ng/mL basic fibroblast growth factor (bFGF, Peprotech), 100 ng/mL platelet-derived growth factor-BB (PDGFbb, Peprotech) and 100 ng/mL insulin-like growth factor-1 (IGF-1, Peprotech). These concentrations were chosen based on a previous published study by (Farnebo *et al.* 2017). The final concentration of EndoECM hydrogels was 6 mg/mL.

Results were evaluated by the analysis of endometrial regeneration (for n=3 saline, n=4 for EndoECM, and n=4 EndoECM+GF mice with a damaged/treated horn and a non-injured horn) and fertility restoration two weeks post-treatment (n=8 saline, n=9 EndoECM, n=9 EndoECM+GF, one or both damaged/treated horns). The estrous cyclicity of mice with unilateral (n=27) and bilateral (n=6) damage/treatment to their horns was monitored and considered in the analyses. The experimental design is showed in *Figure 24*.
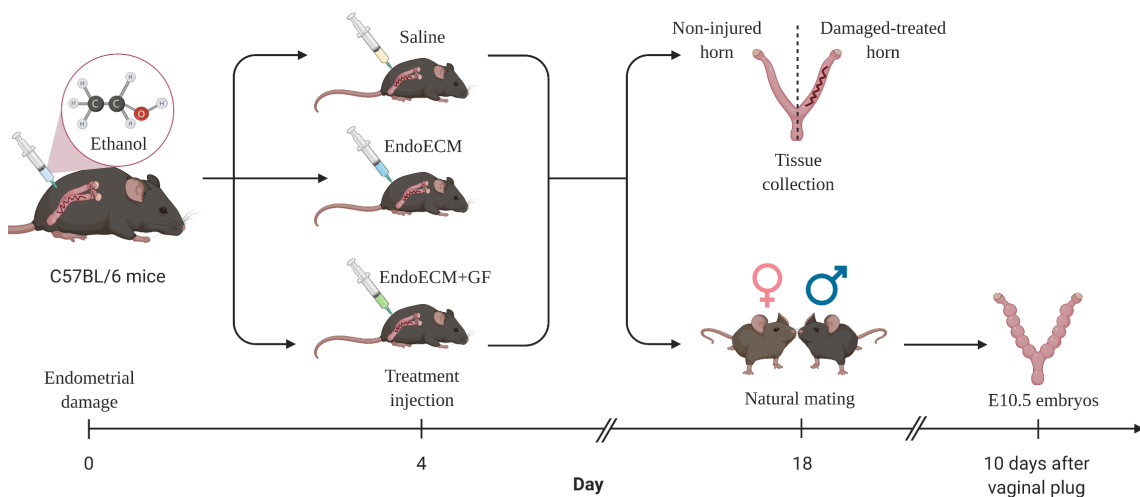
Figure 24. Study timeline for endometrial regeneration and fertility restoration in a murine model of endometrial damage. *Day 0: Endometrial damage was induced in C57BL/6 female mice by injection of ethanol in uterine horns. Day 4: Three different treatments (saline solution, EndoECM and EndoECM+GF). Day 18: two weeks after treatment, mice were either sacrificed for tissue collection or mated to reproduce naturally. Ten days after vaginal plug detection, pregnancy was assessed and embryonic day 10.5 (E10.5) embryos were counted. Created with BioRender.com.*

3.3.2. *Induction of endometrial damage*

Surgical intervention was required to induce endometrial damage. Mice were anesthesized using Isoflurane and administered intraperitoneal analgesics and antibiotics (0.03 mg/mL buprenorphin (Bupaq®), 2.5 mg/mL enrofloxacin (Alsir®), 0.5 mg/mL meloxicam (Metacam®)). A dorsal incision was used to expose the uterine horns and the ends of each horn (proximal to the oviducts and cervix) were clamped with suture thread to protect the ovaries and vagina from damage. To induce damage, 20 µl of 70% ethanol in Hank's Balanced Salt Solution (HBSS, ThermoFisher Scientific) was injected into the uterine horn, using a 25G needle, and incubated 3 min *(Figure 25A)*. Subsequently, the endometrial cavity was washed with HBSS and unclamped. The dorsal incision was sutured closed and mice remained under veterinarian supervision until fully recovered. Post-operative analgesic/antibiotic treatment was administered during the following days as required.
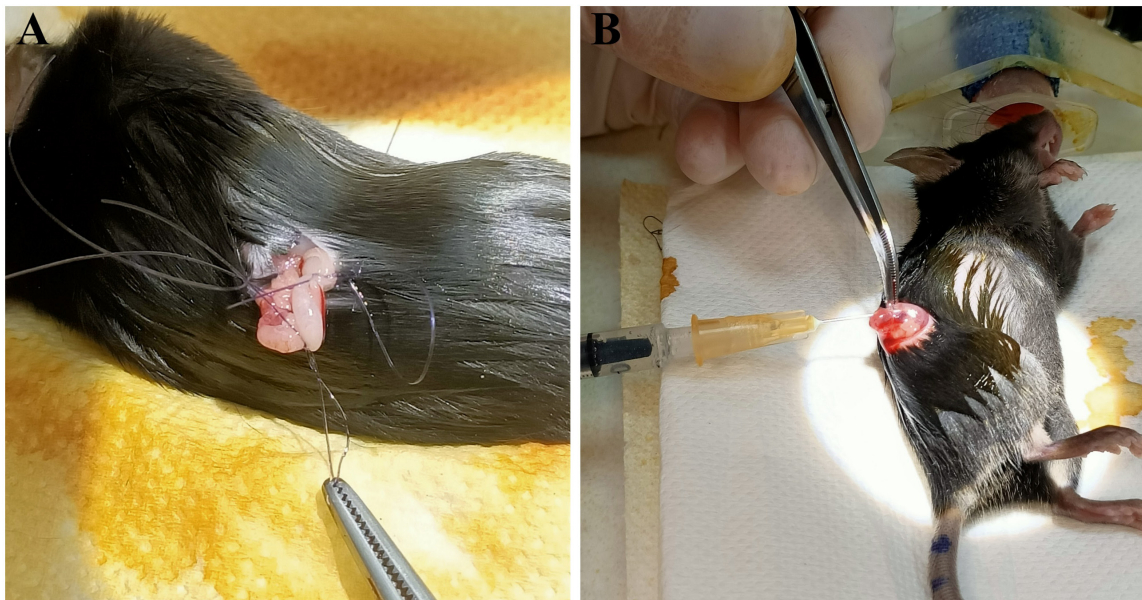
Figure 25. Interventions performed in the murine model of endometrial regeneration and fertility restoration. A) Endometrial damage by ethanol. Uterine horns were clamped at each end with sutures to prevent the damage of the ovary and vagina and 70% ethanol was injected. B) Intra-uterine injection of treatments four days after inducing uterine damage.

3.3.3. *Preparation of injectable biotin-labelled endometrial extracellular matrix hydrogels*

EndoECM hydrogels were diluted up to 6 mg/mL and stained with biotin to facilitate histological tracking. A 10 mM solution of EZ link Sulfo-NHS-Biotin (A39256, Thermo Scientific) was combined with the liquid EndoECM matrix for a final concentration of 20 mol of biotin/mol matrix according to commercial instructions. The mixture was set on ice for 2h before being injected. The feasibility of detection of biotin-labelled EndoECM hydrogels as well as reagent concentration were previously verified in the postmortem C57BL/6 uterus.

3.3.4. *Intra-uterine injection of endometrial extracellular matrix hydrogels*

A second surgery was performed to inject the EndoECM hydrogels. After induction of anesthesia by inhalation of isoflurane and intraperitoneal administration of analgesics, the uterine horn was exposed by dorsal incision once again. A 25G needle was used to inject 20-50 µl of PBS, liquid EndoECM or liquid EndoECM+GF into the damaged horn *(Figure 25B)*. Notably, hydrogel gelation took place spontaneously after injection as a consequence of the physiological body temperature of the animals. Again, the dorsal incision was sutured closed, and mice remained under veterinarian supervision until fully recovered. Post-operative analgesic/antibiotic treatment was administered during the following days as required.

3.3.5. *Estrous cycle evaluation*

The mice's estrous cycles were monitored to confirm ovarian function during the experiment, as well as to know in which stage of the cycle the uteri were harvested for evaluation of endometrial regeneration. The estrous cycle was monitored daily (every

morning between 10 am-12 pm) from the endometrial damage (day 0) to the end of the experiment (day 18) by vaginal cytology. To obtain the vaginal smear, a 100 µl drop of saline (isotonic saline solution with 3.6% glucose, Braun Vetcare, S.A., Spain) was placed in the vagina orifice without penetration. Then, with the aid of a 1-mL syringe, the drop was repeatedly picked up and placed again until the drop turned an opaque white color. The lavage was then spread across a glass slide and allowed to dry. Samples contaminated with urine were discarded. Slides were stained with 0.1% crystal violet staining (Sigma-Aldrich) during 1 min and then washed twice in distilled water (1 min).

Vaginal smears were assessed under a microscope, and the stage of the estrus cycle was determined by the presence and proportion of polymorphonuclear leukocytes, squamous cornified epithelial cells and squamous nucleated epithelial cells of mouse vagina, as follows: Proestrous: presence of epithelial cells with visible nuclei together with a low presence of leukocytes; Estrous: presence of cornified epithelial cells with no visible nuclei and absence of leukocytes; Metestrous: high quantity of leukocytes and few leftovers of cornified epithelial cells; Diestrous: predominance of leukocytes sometimes in association with the nucleated epithelial cells, indicating the beginning of a new cycle *(Figure 26)*.

The presence of non-cornified epithelial cells together with the absence of proestrous/estrous for a long period was classified as absence of cycling (anestrous).

Vaginal cytology of the murine estrous cycle
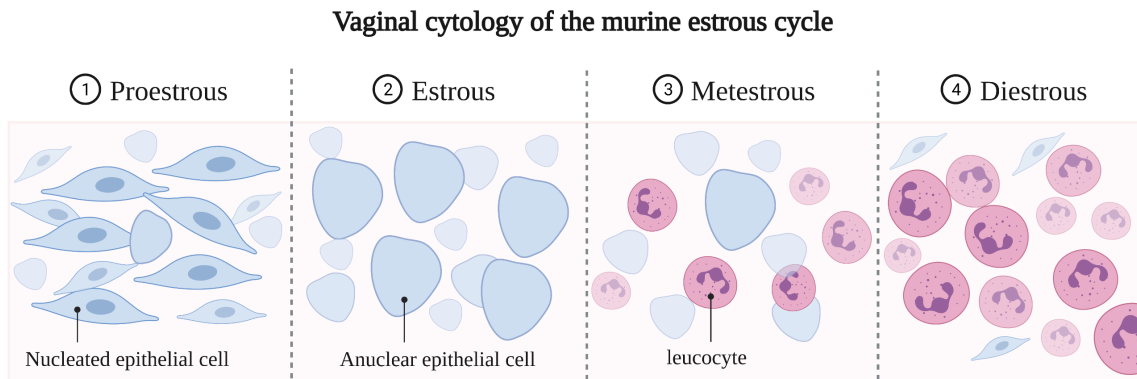
Figure 26. Cytology of the murine estrous cycle. Proestrous: epithelial cells with visible nuclei, low presence of leukocytes and some cornified epithelial cells indicate the proximity of estrus; Estrous: cornified anuclear epithelial cells in high abundance and absence of leukocytes; Metestrous: high quantity of leukocytes still with the presence of cornified epithelial cells; Diestrous: predominance of leukocytes and some nucleated epithelial cells indicating the beginning of a new proestrus phase. Adapted from "The Estrus Cycle of Mice", by BioRender.com (2021). Retrieved from https://app.biorender.com/biorender-templates.

Representative images of the vaginal smears used to classify the stages of the estrous cycle stages of the mice used in this experiment are shown in *Figure 27*.
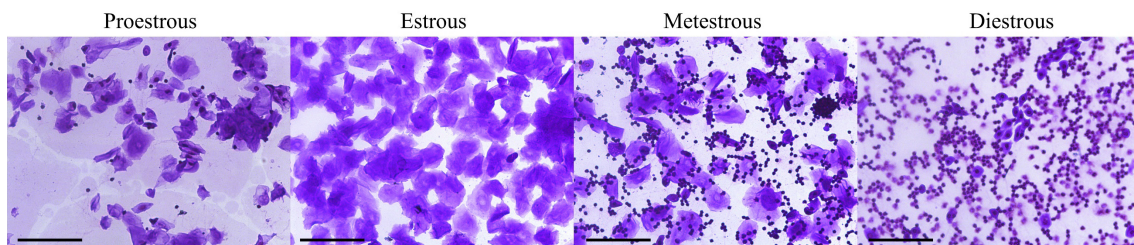
Figure 27. Vaginal cytology for C57BL/6 mice to determine estrous cycle staging after endometrial damage/treatment. Proestrous: epithelial cells with visible nuclei, few leukocytes and some cornified epithelial cells; Estrous: high abundance of cornified epithelial cells and absence of leukocytes; Metestrous: leukocytes and cornified epithelial cells; Diestrous: primarily leukocytes with some nucleated epithelial cells remaining. Scale bars: 100 μm.

The length of the estrous cycle was calculated as the period between two proestrus stages with at least one day of cornified epithelial cells (estrous) and one day of leukocyte predominance (metestrous/diestrous). Furthermore, the number of estrous cycles in 19

days, the proportion of stages and the consecutive days in estrus and diestrus stages were also analyzed.

3.3.6. *Evaluation of endometrial regeneration*

3.3.6.1. Sample processing and histological analyses

The eleven mice previously described in section 3.3.1 were sacrificed two weeks after treatment (n=3 saline, n=4 EndoECM, n=4 EndoECM+GF), and uteri were harvested. A quarter of each uterine horn (from vaginal proximal edge) was cut and stored in RNAlater™ Stabilization Solution (Invitrogen) at -80ºC for subsequent transcriptomic analysis. The remaining three quarters of the uterine horns were fixed with 4% PFA overnight, dehydrated and embedded vertically in paraffin to facilitate 4-μm cross-sectioning for histological analyses. Samples were cut sequentially to evaluate 3-4 cross-sections from two different heights of the uterine horn (excluding approximately 80-160 μm of tissue between both locations).

3.3.6.2. *In utero* tracking of endometrial extracellular matrix hydrogels

The presence of biotin-labelled EndoECM was assessed in the uterine horns using histological analysis. Cross-sections were deparaffined and heat-mediated antigen retrieval was performed in 10 mM Citrate Buffer with 0.05% Tween (pH 6.0) for 20 min in a 95 °C water bath. Sections were permeabilized with 0.05% Tween in PBS, blocked with 5% BSA for 20 min at RT and finally incubated with Alexa Fluor™ 594 Streptavidin Conjugate (Invitrogen, 1:1000 dilution) for 1 h at RT. Samples were washed thrice and mounted with mounting media containing DAPI.

3.3.6.3. Endometrial thickness and of endometrial gland concentration

To assess the quality of the recovered endometrial glands, four cross-sections from different heights of the horn were stained with MT and analyzed using QuPath analysis software v0.2 (Bankhead *et al.*, 2017). To evaluate endometrial thickness, we quantified the whole endometrial area (excluding the uterine lumen and myometrium) in four sections (at 2.5x magnification) per mouse *(Figure 28)*. Meanwhile, to evaluate gland concentration, glands in four random fields (at 20x magnification) from four 4-µm cross-sections (n=16 fields in total) per mouse were counted, and the number of glands per mm^2 of endometrial area was calculated. Notably, the data obtained from the injured/treated right horn in study was normalized with its respective non-injured/non-treated left horn, to prevent biases from estrous cycle stages and intern variability.
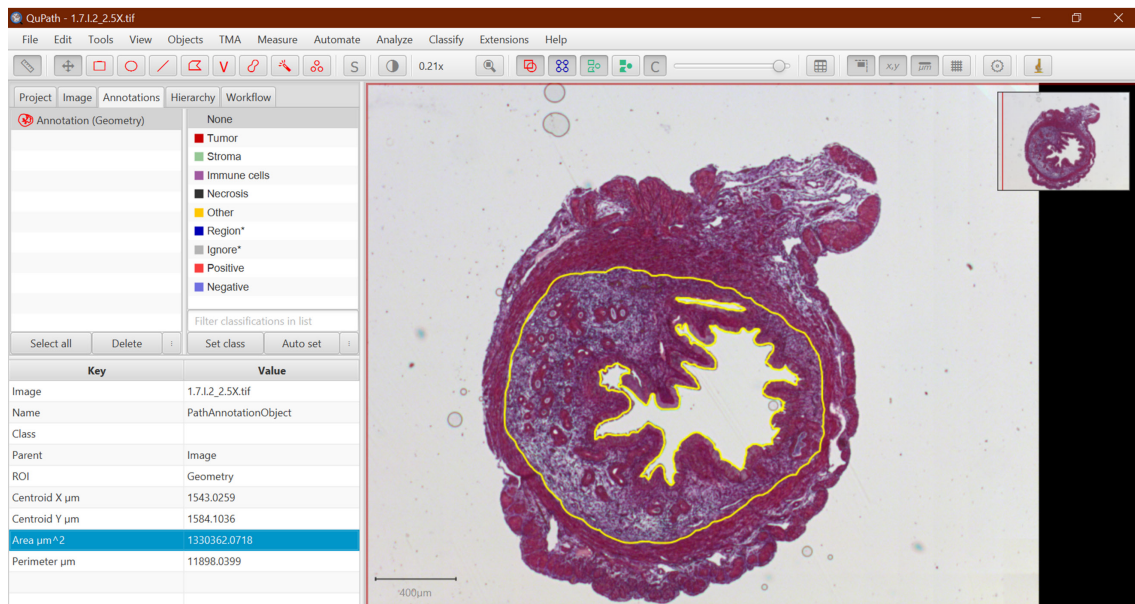
Figure 28. Quantification of the endometrial thickness using QuPath analysis software. *Scale bars were set and total endometrium, excluding myometrium and uterine lumen was outlined (yellow line) to obtain the total endometrial area.*

3.3.6.4. Collagen deposition

Fibrosis was analyzed by quantification of the total collagen area. For each mouse, two cross-sections from different heights of the damaged/treated horn were stained with MT and analyzed using ImageJ software. Briefly, RGB MT-stained images were split into their three principal colors, blue (collagen), red (cell cytoplasm) and black (nuclei), using the Color Deconvolution plugin, selecting the "Masson Trichrome" option. The resulting blue image (containing only the stained collagen from the original image) was chosen and the selection threshold was manually adjusted to quantify all the blue area using the "analyze particles" tool. The percentage of area containing collagen was acquired, and statistical analysis was performed to compare collagen values between groups.

3.3.6.5. Endometrial cell proliferation

Proliferation of endometrial cells was measured using Ki67 immunostaining (Anti-Ki67 polyclonal antibody, ab15580, ABCAM, 1:300 dilution). Samples were revealed using DAB (DAB Substrate Kit, Sigma-Aldrich) in bright-field microscopy according to the manufacturer's instructions and subsequently counterstained with hematoxylin. The percentage of cells expressing Ki67 was quantified from four fields (at 20x magnification) per sample, using QuPath analysis Software.

3.3.6.6. Real-time quantitative polymerase chain reaction

RNA extraction

Total RNA was extracted from all murine uterine horns (n=22) from the regeneration group, using the RNeasy Mini Kit (Qiagen, ref. 74104), according to manufacturer's instructions. Briefly, samples were mechanically disaggregated, and the resulting lysate was mixed with RLT buffer, containing a guanidine salt, which inactivates RNases to

ensure purification of intact RNA. Ethanol was then added to provide appropriate binding conditions for RNA, and the mixture was transferred to a RNeasy MinElute spin column, where the total RNA binds to the membrane while contaminants are efficiently washed away. Finally, total RNA was eluted in 35 μL of RNase-free water and RNA concentration was quantified using a Nanodrop spectrophotometer (Thermo Fisher).

cDNA synthesis: Reverse transcription

Reverse transcription of the total extracted RNA to its complementary DNA (cDNA) was performed using the PrimeScript RT Reagent Kit (Takara, ref. RR037A) according to manufacturer's instructions. Basically, 500 ng of total RNA from each sample was mixed with 2 μL of PrimeScript Buffer, 0.5 μL of PrimeScript Reverse Trasncriptase Enzyme Mix I, and 0.5 μL of Oligo dT Primer (50 μM; for use as reverse transcription primers). The resulting cDNA concentration was quantified using a Nanodrop spectrophotometer (Thermo Scientific).

Quantitative gene expression analysis

Quantitative gene expression of collagen type I α-1 chain (*Col1a1*) was evaluated by real-time quantitative polymerase chain reaction (RT-qPCR). Briefly, cDNA from all samples (n=22) was mixed with RT² SYBR Green qPCR Mastermix (Applied Biosystems), and corresponding forward and reverse primers. Glyceraldehyde-3-phosphate dehydrogenase (*Gapdh*) was used as the housekeeping gene. Specific sequences of the primers (Integrated DNA Technologies) and the specific quantities of RT-qPCR reagents can be found in ***Table VI.***

Table VI. Sequences of primers used in real-time quantitative polymerase chain reaction and the compositon of the reaction mixture.

Gene	Forward primer	Reverse primer	RT-qPCR mix per well
Col1a1	AGATGTGCCACTCTGACT	TCTGACCTGTCTCCATGTT	5 μL RT² SYBR Green qPCR Mastermix 0.5 μL 10 μM Forward primer 0.5 μL 10 μM Reverse primer 4 μL cDNA 50 ng/ μL
Gapdh	TCAAGAAGGTGGTGAAGCAGG	ACCAGGAAATGAGCTTGACAAA	

Col1a1: collagen type I α-1 chain; Gapdh: Glyceraldehyde-3-phosphate dehydrogenase.

RT-qPCR was performed in a StepOnePlus™ Real-Time PCR System (Applied Biosystems) with the following cycling conditions: 50 °C for 20 seconds (initial holding stage cycle); 95 ºC for 20 seconds (to activate the polymerase enzyme, responsible of the DNA replication during the PCR amplification process); 40 cycles of 15 seconds at 95 °C (to denature DNA) followed by one minute at 60 °C (to induce the annealing of the primers and the DNA amplification). The threshold cycle (C_T) was calculated using the StepOnePlus Software.

Quantitative RT-PCR data was analyzed using the ΔΔCT method. All data were normalized computing ΔCT values, to obtaining fold regulation with the following equation: $C_{T\ target\ gene} - C_{T\ Gapdh}$. Finally, statistical analysis was performed for each gene, comparing ΔCT values between groups.

3.3.7. *Evaluation of fertility restoration*

Recovery of uterine function was evaluated after two weeks of treatment, by pregnancy after natural mating. A total of twenty-six female mice (n=8 for PBS, n=9 for EndoECM, n=9 for EndoECM+GF) with unilateral or bilaterally damaged/treated horns were mated

with twelve-week-old C57BL/6 male. Females were housed with males during one week and mating was confirmed by presence of a vaginal plug *(Figure 29)*.

Figure 29. Vaginal plug after mating a ten-week-old C57BL/6 female with a twelve-week-old C57BL/6 male mouse. *Sexual intercourse was confirmed by the presence of a vaginal plug, detected early in the morning, every day during the week of mating. Coagulating and vesicular glands of the male produce secretions which fill and plug the vagina during 8-24 h after sexual intercourse.*

Uteri were harvested 10 days after detecting the vaginal plug (embryonic day 10.5, E10.5) to assess pregnancy rate and count the number of embryonic sacs present.

3.4. Statistical analysis

For the preliminary *in vivo* biocompatibility study, data were analyzed using RStudio® software version 3.6.3 (RStudio Team 2020) and presented as a mean ± SD. All statistical analysis was performed using a linear regression model to account for total variability (non-parametric analysis). For the endometrial regeneration in a murine model of endometrial damage, data were analyzed using GraphPad Prism software version 8.3

(GraphPad Software, La Jolla California USA, www.graphpad.com). For the histological analysis of endometrial regeneration, non-parametric analyses using *Kruskal Wallis test* with Dunn's multiple comparison were carried out. For RT-qPCR analysis, non-parametric *Kruskal Wallis* test with Dunn's multiple comparison analysis was performed for each gene comparing ΔCT values between groups. Non-parametric and paired Willcoxon test was used to compare right horns with their respective left horns in histology and RT-qPCR. For the fertility evaluation, the *Fisher Exact test* was performed to compare pregnancy rates and the *Kruskal Wallis test* with Dunn's multiple comparison to compare the number of embryonic sacs. In all cases, p<0.05 was considered statistically significant.

VI. RESULTS

VI. RESULTS

1. Creating endometrial extracellular matrix hydrogels from decellularized porcine uterus

1.1. Porcine uterus decellularization and endometrial tissue-specific extracellular matrix purification

Whole uterus decellularization was carried out in a total of five uterine horns and the entire endometrial fraction was isolated via microdissection *(Figure 30A)*. Macroscopically, decellularization changed the coloration of uterus from pink *(Figure 30A I)* to white *(Figure 30A II)*. Decellularization efficiency was verified by H&E *(Figure 30B1-2)* and MT staining *(Figure 30B3-4)* and confirmed complete depletion of cellular material. Absence of nucleic DAPI staining further corroborated decellularization *(Figure 30B5-6)*. The blue coloration from MT staining in DC tissues indicated the principal ECM component, collagen, was nevertheless conserved. Immunostaining of the α-gal epitope, a key player in hyperacute rejection of pig xenograft organs in humans (Macher and Galili 2008), showed a high abundance in luminal and glandular epithelium, as well as in blood vessels from No-DC endometrial tissue. In contrast, there was no α-gal detected within DC endometrium *(Figure 30C)*.

Initial quantification of SDS residues from endometrial isolation showed 158 ± 60.1 μg SDS/g in wet tissue. However, after six 30 min washes with ice-cold PBS under agitation, it was reduced to 33.9 ± 12.4 μg SDS/g wet tissue, corresponding to a statistically significant reduction of 78.6% ($p<0.001$) *(Figure 30D)*.
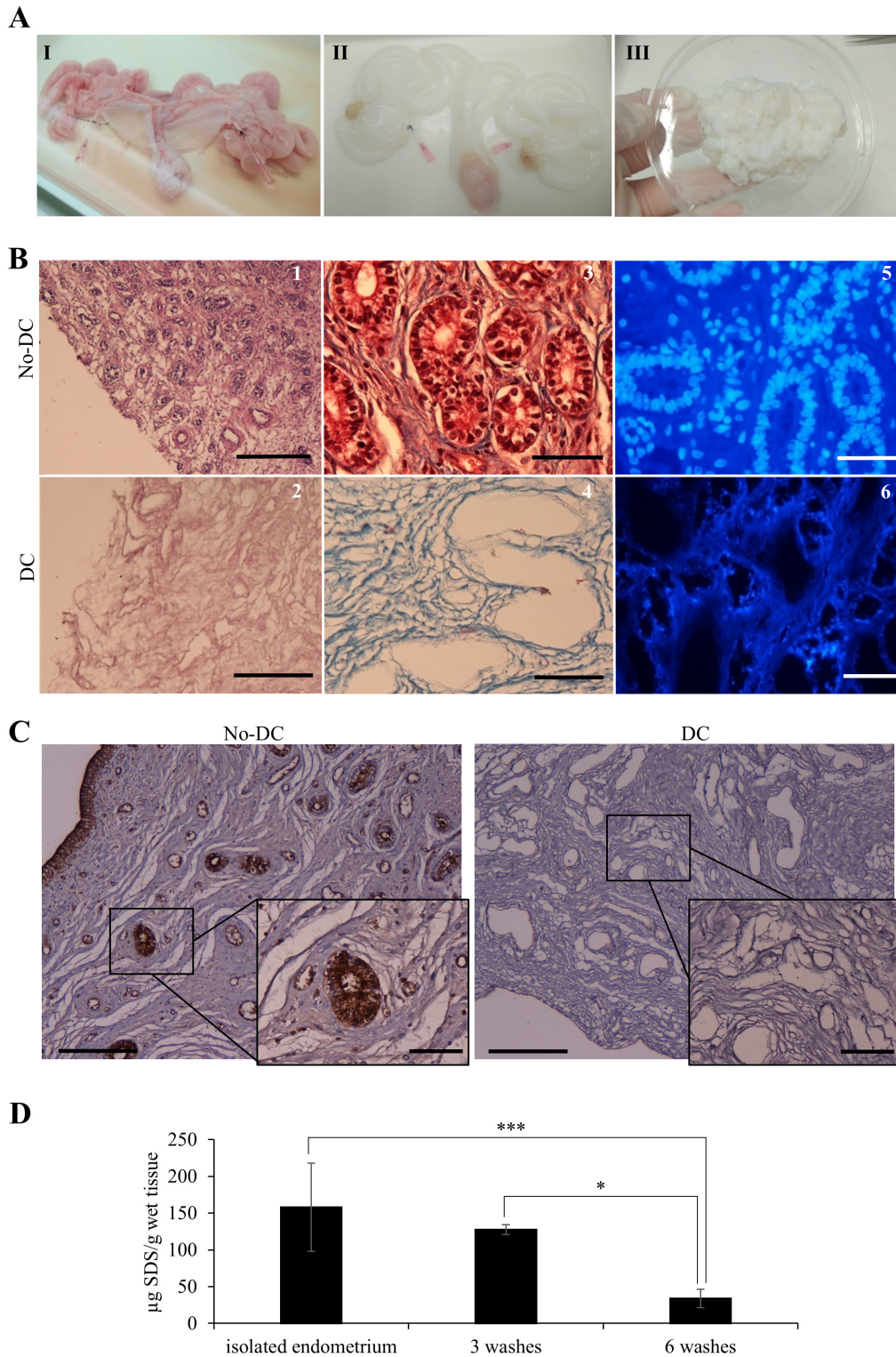
Figure 30. Porcine uterus decellularization and endometrial tissue-specific extracellular matrix purification. *A) uterus before (I) and after (II) decellularization, DC endometrial tissue stock after microdissection (III). B) No-DC endometrial (1, 3, 5) and DC endometrial tissue (2, 4, 6). H&E assessment of pure endometrium isolation (1, 2). Scale bars: 250 μm. Analysis of cellular material and collagen deposits by MT staining (3, 4) and DAPI (5, 6). Scale bars: 50 μm. C) Immunoreactive porcine α-gal residues (brown) by DAB immunolabeling in No-DC and DC endometrial tissue. Scale bars: 200 μm and 50 μm (zoom). D) SDS quantification after endometrial isolation, 3 or 6 washes of 30 min under mechanical agitation. *p<0.05, ***p<0.001.*

1.2. Endometrial extracellular matrix hydrogel and characterization

After decellularization, isolated endometrial tissue was milled and lyophilized *(Figure 31A-B)*. After ECM digestion, the resulting viscous solution was termed EndoECM, and it spontaneously formed hydrogels after incubation at 37ºC *(Figure 31C-D)*.
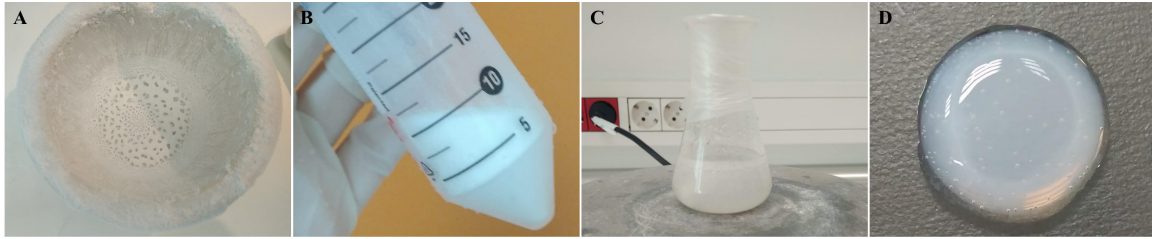
Figure 31. EndoECM hydrogel preparation. *Decellularized endometrium after A) milling, B) lyophilization, C) ECM digestion and D) the formed EndoECM hydrogel.*

Comparison of the DNA content from DC and No-DC tissues showed a significant reduction of nuclear material in DC endometrium (5.4% DNA remained in wet tissue and 7.6% DNA remained in lyophilized powder, $p < 0.001$) while electrophoretic analysis confirmed no DNA bands in DC wet tissue and lyophilized powder *(Figure 32 panel A)*.

Protein quantity and composition were analyzed for every step of the EndoECM production *(Figure 32 panel B)*. Overall, total protein content significantly decreased by 80% (19.9 and 19.2% proteins remaining in wet endometrial tissue and lyophilized endometrial powder respectively) yet collagen was significantly enriched (207% and 148% collagen present in wet endometrial tissue and lyophilized endometrial powder respectively), indicating substantial removal of the cellular protein fraction. Notably, elastin and GAGs were also preserved (25% and 18% in wet endometrial tissue and lyophilized endometrial powder respectively; $p < 0.001$). In EndoECM, the effects of pepsin were apparent by: increasing total protein content to 42%, reducing collagens to 61.3% and eliminating elastin ($p < 0.001$). In contrast, GAGs were not affected by pepsin digestion ($p < 0.001$).
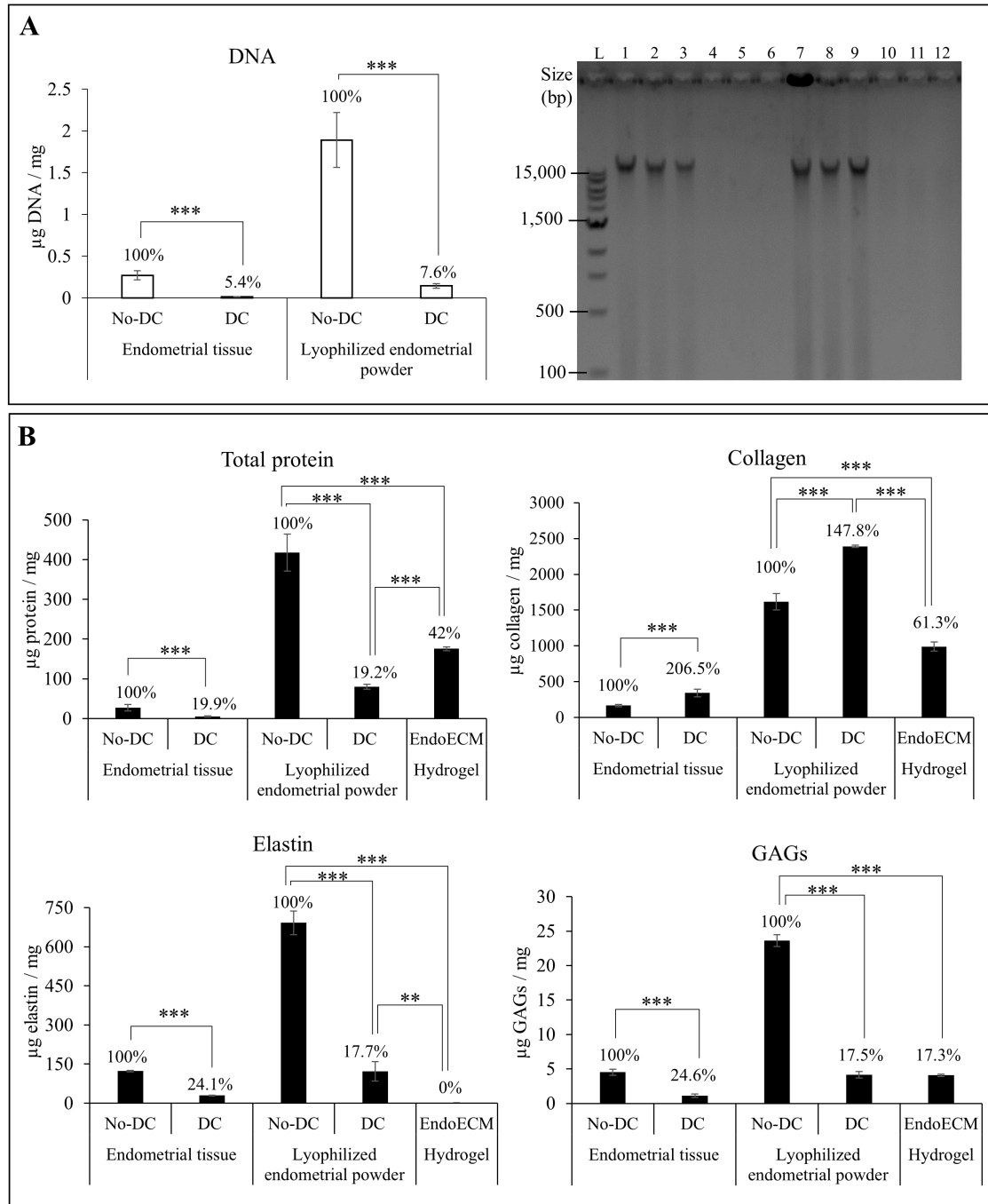
*Figure 32. DNA and protein quantification after decellularization, lyophilization, and EndoECM setup. A) DNA quantification and fragment-size analysis from endometrial DC, No-DC wet endometrial tissue and lyophilized endometrial powder. L: ladder; 1,2,3: No-DC wet endometrial tissue replicates; 4,5,6: DC wet endometrial tissue replicates; 7,8,9: No-DC lyophilized endometrial powder replicates; 10,11,12: DC lyophilized endometrial powder replicates. B) Monitoring of total protein fraction, collagen, elastin, and GAGs in DC and No-DC endometrial tissue, DC and No-DC lyophilized powder, and EndoECM hydrogel. Percentages with respect to endometrial No-DC tissue or lyophilized power. Data in µg/mg. bp: base pairs. ** p<0.01; ***p<0.001.*

1.3. Gelation kinetics, stability, and ultrastructure

The gelation kinetics of EndoECM hydrogels from different digestions were evaluated spectrophotometrically. All three digestions presented a sigmoidal curve *(Figure 33)*, with concentration-dependent increases in *S* (0.13 ± 0.03 min^{-1} in 3 mg/mL, 0.22 ± 0.05 min^{-1} in 6 mg/mL, and 0.20 ± 0.02 min^{-1} in 8 mg/mL, p<0.05) *(Table I)*.
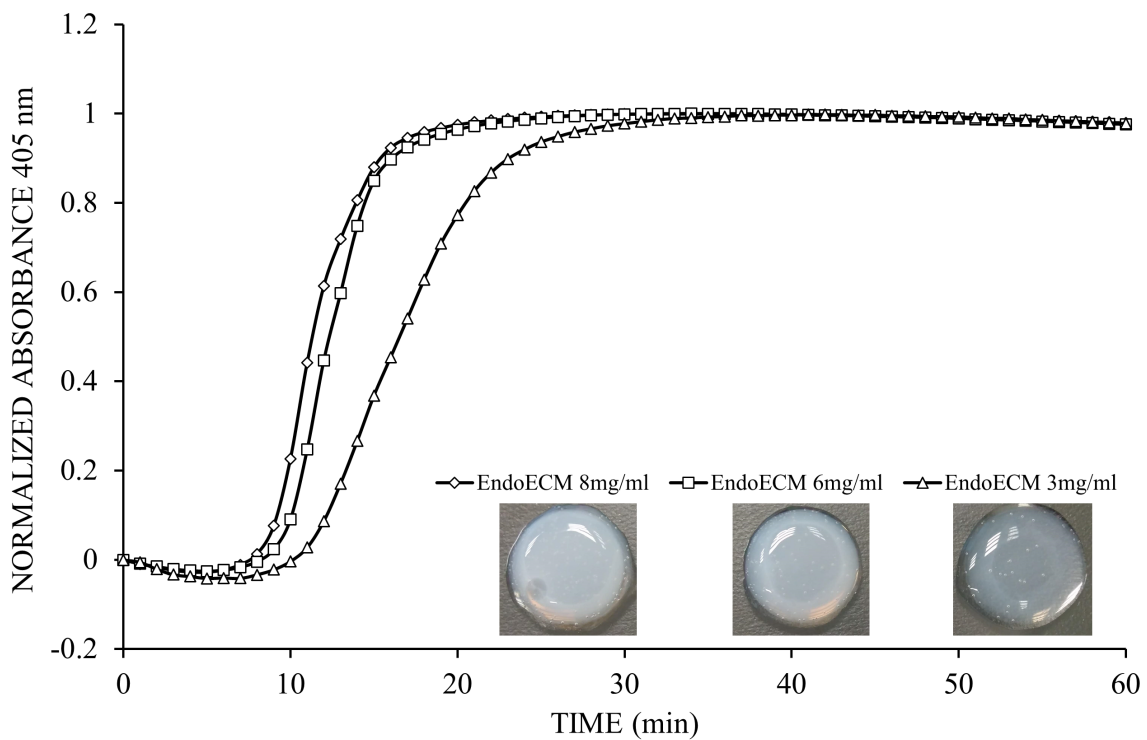
Figure 33. Turbidimetric gelation kinetics of EndoECM hydrogels. *Comparison of normalized absorbance curves; EndoECM hydrogel metrics analyzed at concentrations of 3, 6, and 8 mg/mL.*

Time to start of gelation (T_{Lag}), $T_{1/2}$, and T_1 were inversely related to hydrogel concentration (p<0.05). Hydrogels formed completely after 20 min (20.50 ± 3.81, 14.70 ± 1.12, and 14.10 ± 1.86 at 3, 6, and 8 mg/mL concentrations, respectively) *(Table VII)*. Opacity and thickness of hydrogels were proportional to ECM concentration *(Figure 33)*. EndoECM hydrogels remained intact and bacterial growth was absent during

7 days *in vitro* culture, under standard conditions, confirming long-term stability and adequate sterility.

Table VII. Comparison of turbidimetric metrics at 3, 6, and 8 mg/mL concentration.

Concentration	T_{Lag} *(min)*	$T_{1/2}$ *(min)*	T_1 *(min)*	*S (min^{-1})*
3 mg/mL	12.73±2.00	16.60±2.90	20.48±3.81	0.13±0.03
6 mg/mL	10.09±1.64	12.40±1.27*	14.72±1.12*	0.22±0.05*
8 mg /mL	9.18±1.55*	11.66±1.70*	14.14±1.86*	0.20±0.02*

T_{Lag}: Lag; $T_{1/2}$: Time to half gelation; T_1: time to complete gelation; S: gelation rate. *p<0.05.

EndoECM hydrogels presented a homogenous, randomly interlocking fibrillar ultrastructure, and no significant differences were found in fiber thickness among different concentrations *(Figure 34A-C)*. No-DC Endo also formed hydrogels, but SEM images showed residual cellular components along the fibers, altering the ultrastructure *(Figure 34A)*. Both EndoECM and MyoECM, hydrogels (made from myometrial fractions) were predominantly composed of approximately 0.10 μm thick fibers, and no significant differences were found between the two *(Figure 34A-D)*.
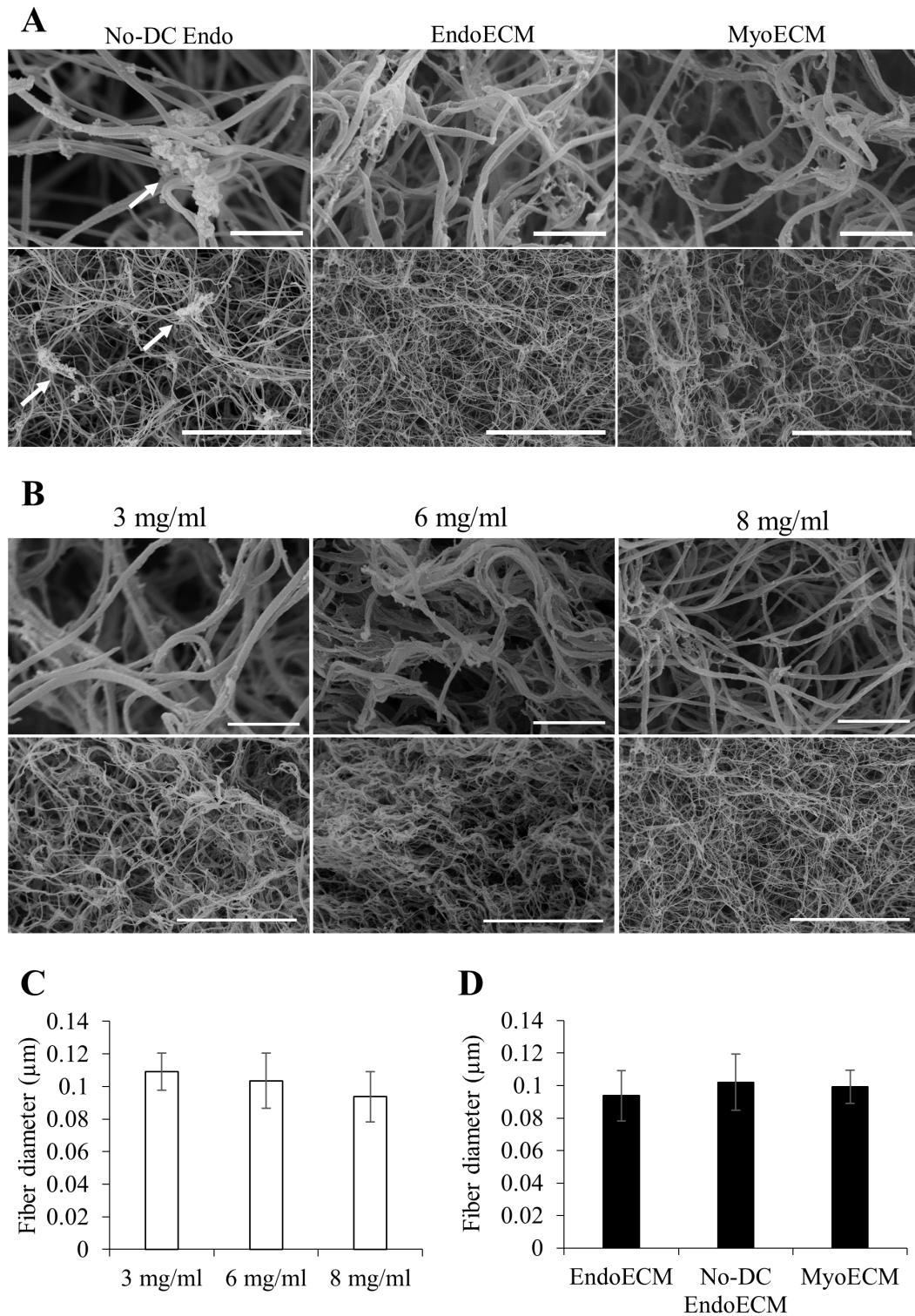
Figure 34. Analysis of extracellular matrix hydrogel ultrastructure. *A) SEM microscopy images of EndoECM hydrogels in comparison with No-DC Endo and MyoECM hydrogels. Arrows point to leftovers of cellular components in No-DC Endo. B) Micrographs of EndoECM hydrogels at 3, 6, and 8 mg/mL concentrations. C) Average fiber diameter of EndoECM hydrogels at 3, 6, and 8 mg/mL. D) Average of fiber diameter of EndoECM, No-DC EndoECM, and MyoECM hydrogels. Images at 30.0k (above) and 5.00k (below) magnifications with scale bars at 1 μm or 10 μm, respectively.*

1.4. Matrisome of endometrial extracellular matrix hydrogels

To identify the matrisome, (representing the ensemble of ECM and ECM-associated proteins), proteins were sorted according to cellular or extracellular origin, and classified into core matrisome proteins (collagens, ECM glycoproteins, and PGs) or matrisome-associated proteins (ECM regulators, ECM-affiliated proteins, and secreted factors) using the MatrisomeDB). Extracellular proteins not found in MatrisomeDB were classified as others.

Preliminary qualitative analysis showed that half of the No-DC Endo extracellular proteins were absent in EndoECM *(Figure 35A)*. There were four sub-groups of extracellular proteins in EndoECM (dermatopontin, fibrinogen, azurocidin, and extracellular kinases) which were absent in No-DC Endo *Table VIII*. The role of ECM proteins was identified using GO molecular function and refined according to those functions related to ECM *(Table VIII)*.
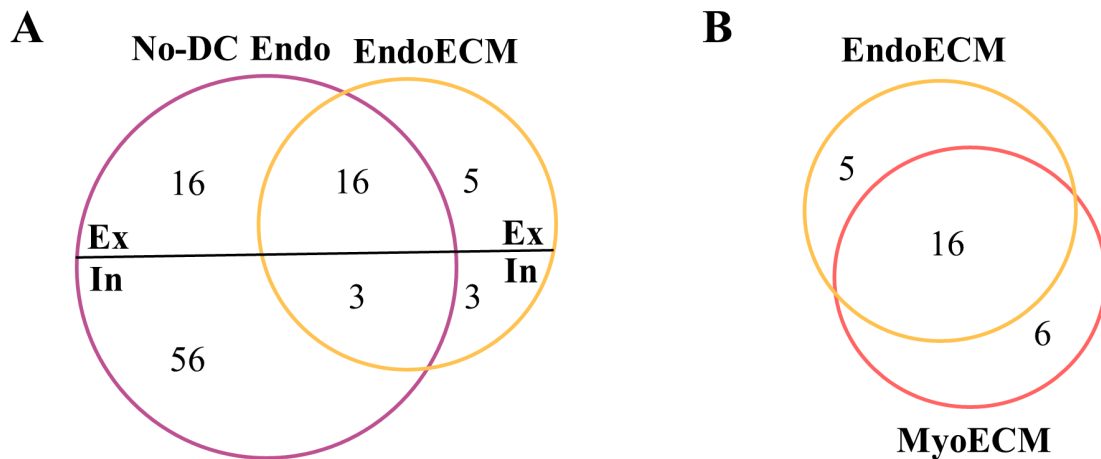
Figure 35. Relationship of the proteins in EndoECM, NO-DC Endo and MyoECM. A) The decellularization process enriched 8 proteins (5 extracellular and 3 intracellular), preserved 19 proteins (16 extracellular and 3 intracellular) and removed 72 proteins (16 extracellular and 56 intracellular). Ex: extracellular proteins, In: intracellular proteins. B) Tissue-specific and common ECM proteins in EndoECM and MyoECM. Diagrams created using BioVenn.

Table VIII. Matrisome of NO-DC Endo, EndoECM, and MyoECM. *Extracellular proteins identified by LC-MS/MS (coloured table cells) and ECM-related GO functions.*

		PROTEIN TYPE	NO-DC Endo	EndoECM	MyoECM	ECM-RELATED GO FUNCTION(S)
CORE MATRISOME	**COLLAGENS**	Collagen type I	●	●	●	ECM structural constituent; identical protein binding; PDGF binding.
		Collagen type III	●	●	●	ECM structural constituent conferring tensile strength; integrin binding; PDGF binding.
		Collagen type IV	●			ECM structural constituent conferring tensile strength; protein binding; PDGF binding.
		Collagen type V	●	●	●	ECM structural constituent conferring tensile strength; integrin binding; heparin binding; PG binding; PDGF binding.
		Collagen type VI	●	●	●	ECM structural constituent conferring tensile strength.
		Collagen type XII			●	ECM structural constituent conferring tensile strength.
	ECM GLYCOPROTEINS	Adiponectin	●			ECM structural constituent; protein binding; sialic acid binding; protein homodimerization activity.
		Apolipoprotein D	●		●	Colesterol binding.
		Dermatopontin		●	●	Collagen fibril organization; cell adhesion.
		Fibrillin-1	●	●		ECM structural constituent; integrin binding; hormone activity; heparin binding; ECM constituent conferring elasticity.
		Fibrillin-2			●	ECM structural constituent; protein binding; calcium ion binding; ECM constituent conferring elasticity.
		Fibrinogen		●		Cell adhesion molecule binding.
		Fibronectin 1	●	●	●	ECM structural constituent; integrin binding; collagen binding; heparin binding; PG binding.
		Laminin	●	●	●	ECM structural constituent; integrin binding; structural molecule activity.
		Nidogen 1	●			ECM structural constituent; collagen binding; laminin binding; proteoglycan binding.
		Von Willebrand factor	●	●		Integrin binding; collagen binding; chaperone binding.
MATRISOME-ASSOCIATED PROTEINS	**ECM REGULATORS**	α-1-antichymotrypsin 2 (Serpin Family)	●			Serine-type endopeptidase inhibitor activity.
		α-1-antitrypsin (Serpin Family)	●			Serine-type endopeptidase inhibitor activity.
		Cathepsin B	●			Collagen binding; PG binding.
		Cathepsin D	●			Aspartic-type endopeptidase activity.
		Cathepsin S	●			Fibronectin binding; collagen binding; laminin binding; PG binding.
		Cathepsin Z	●			Cysteine-type endopeptidase activity.
		Leukocyte elastase inhibitor (Serpin Family)	●	●		Serine-type endopeptidase inhibitor activity.
		Serpin family B member 6	●			Protease binding; serine-type endopeptidase inhibitor activity.
		Serpin family F member 2	●			Endopeptidase inhibitor activity; protein binding; protein homodimerization activity.
	ECM-AFFILIATED PROTEINS	Annexin	●	●	●	ECM structural constituent; phosphatidylserine binding; actin binding; S100 protein binding; cadherin binding involved in cell-cell adhesion.
		Mucin	●			ECM structural constituent.
	SECRETED FACTORS	Protein S100	●	●	●	Calcium ion binding; microtubule binding; zinc ion binding; Toll-like receptor 4 binding; arachidonic acid binding.
OTHER EXTRACELLULAR PROTEINS		Azurocidin		●	●	Heparin binding; heparan sulfate binding.
		Extracellular tyrosine-protein kinase		●		Protein kinase activity; non-membrane spanning protein tyrosine kinase activity.
		Kappa-casein			●	Protein binding.
		Serum albumin	●	●	●	Fatty acid binding; oxygen binding; metal ion binding; chaperone binding.

Quantitative analysis showed that the ECM hydrogels designed in this study consisted almost entirely of ECM (91.8% in EndoECM and 93.3% in MyoECM), compared to No-

DC Endo which consisted of only 41.4% ECM. Collagens maintained their physiological ratios and proved to be the main components enriching the ECM (83.7% in EndoECM and 82.3% in MyoECM) *(Figure 36)*. Decellularization decreased the quantity of immunoreactive molecules (41.1% cellular components and 16% immunoglobulins in No-DC Endo compared to 7.5% cellular components and 0.7% immunoglobulins in EndoECM) and eliminated MHC antigens. Furthermore, no PGs were detected either in EndoECM or No-DC Endo hydrogels.
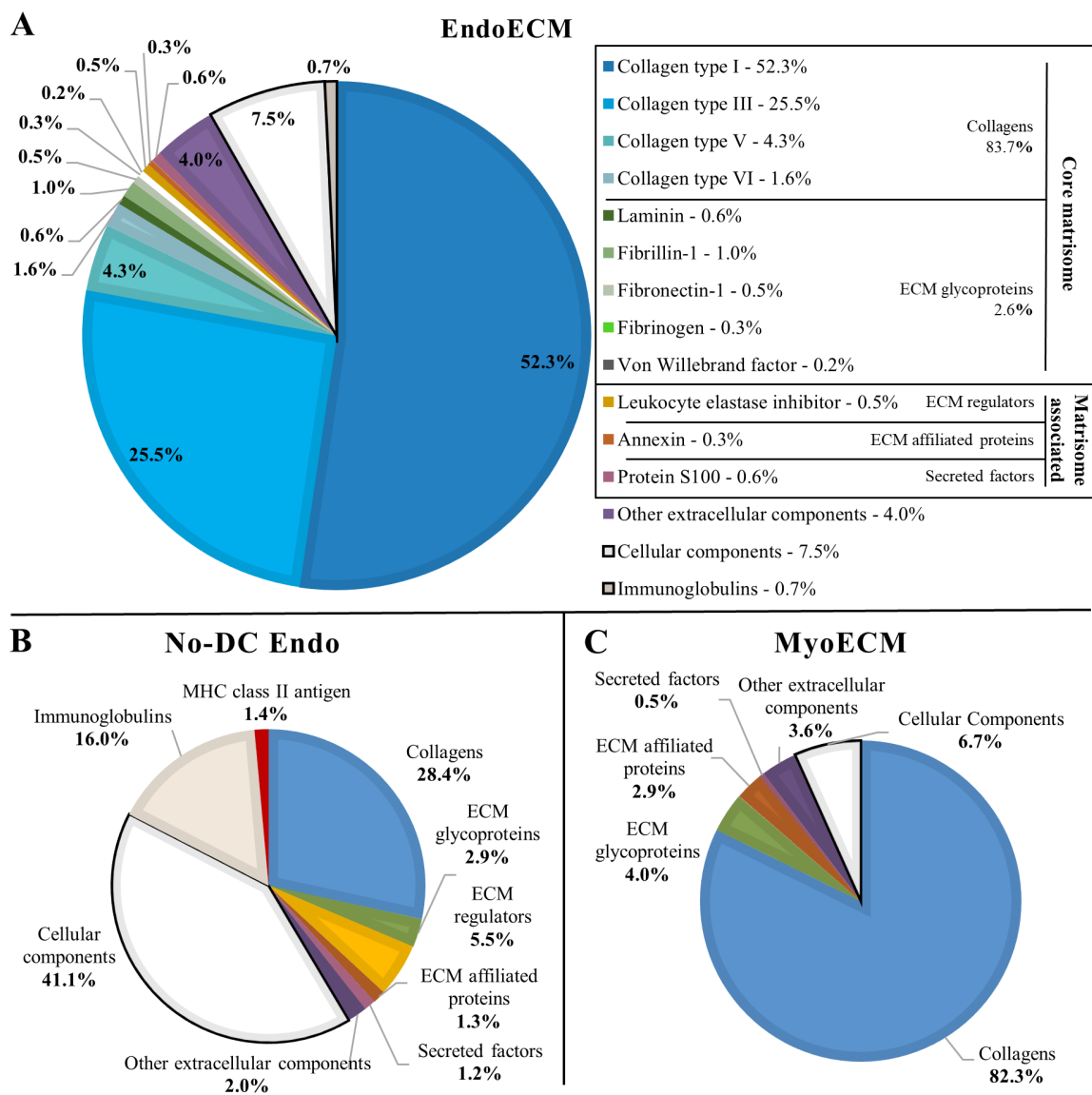
Figure 36. Quantitative proteomic analysis of EndoECM, No-DC Endo and MyoECM. *Pie charts illustrating composition of (A) EndoECM, (B) No-DC Endo and (C) MyoECM proteins identified by LC-MS/MS. The legend in (A) groups the identified proteins into their matrisome classification.*

110

Interestingly, immunoreactive components were similarly removed in the production of EndoECM and MyoECM hydrogels, but presented different compositions in both qualitative *(Figure 35B, Table VIII)* and quantitative *(Figure 36)* analysis.

2. Endometrial extracellular matrix hydrogels as a platform for three-dimensional culture *in vitro*

2.1. *In vitro* cytocompatibility of endometrial extracellular matrix hydrogels with endometrial stem and primary cells: Comparison with Collagen and Matrigel

2.1.1. *Coating culture system*

Similar cell growth was observed in non-coated wells (NoTT) and wells coated with collagen, Matrigel, EndoECM *(Figure 37A)*. Statistical analysis confirmed there were no significant differences between treatment groups.

2.1.2. *2.5D culture system*

To evaluate cytocompatibility of 2.5D culture, proliferation of different cell types placed on top of the hydrogels was evaluated *(Figure 37B)*. This assay evaluated (1) the matrix quality between 3 mg/mL collagen, Matrigel, and EndoECM, and (2) the effect of hydrogel concentration, by comparing 3, 6 and 8 mg/mL EndoECM. We observed a significant increase in proliferation of ICE6-7 endometrial stem cells in EndoECM compared to standard matrices at 3 mg/mL. In contrast, proliferation of EECs was significantly reduced in 3 mg/mL EndoECM compared to standard matrices, and Matrigel increased proliferation of ESCs. Nonetheless, we observed a significant concentration-

dependant increase in proliferation of ICE6, ICE7 and ESCs in EndoECM (up to 8 mg/mL, p<0.05).
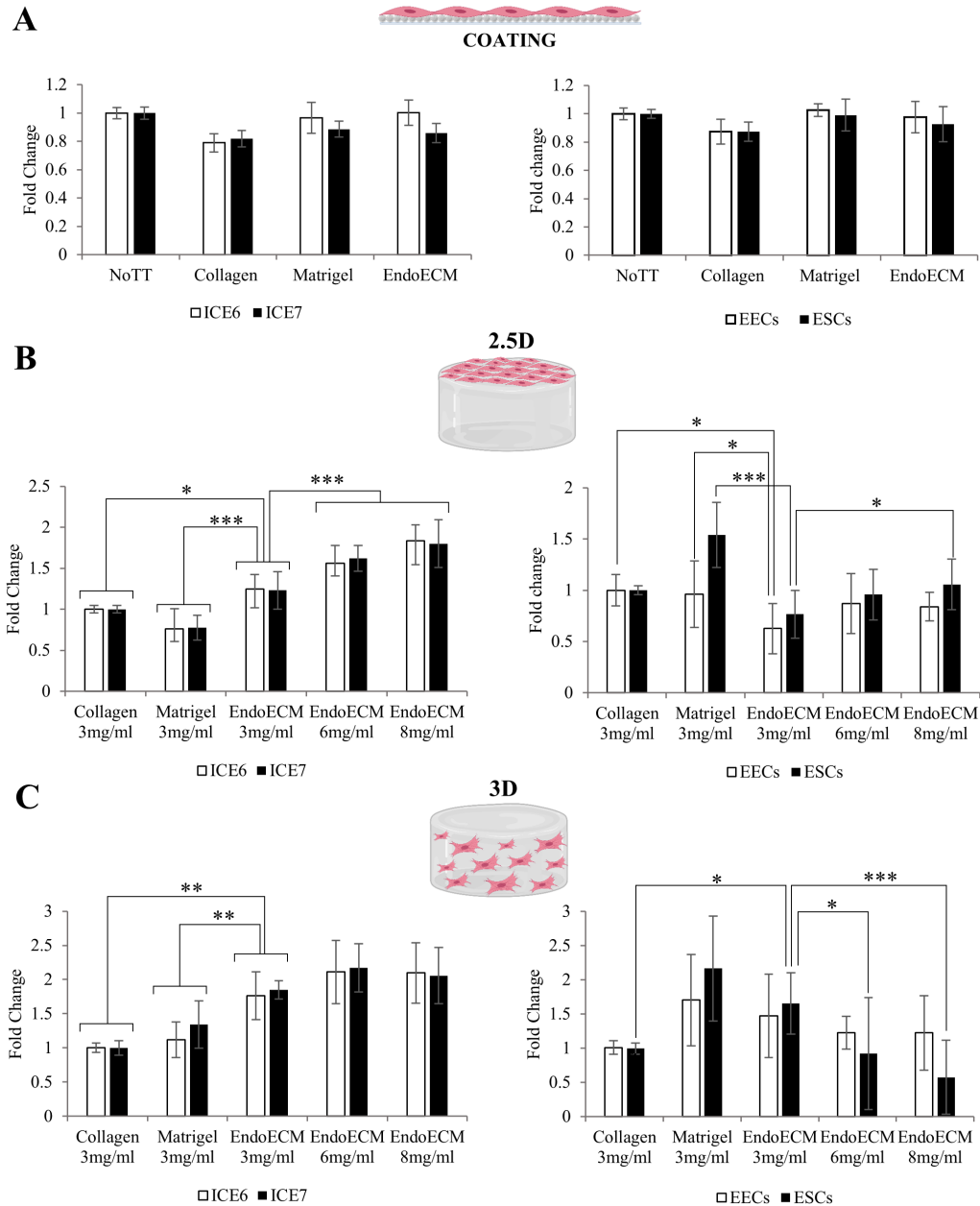
Figure 37. Tetrazolium assay of endometrial cells in two- and three-dimensional cell culture.
*A) Cell proliferation in a 2D coating system, comparing NoTT (untreated), collagen, Matrigel, or EndoECM coated conditions. B) Cell proliferation in 2.5D culture, comparing 3 mg/mL collagen, 3 mg/mL Matrigel, and 3, 6 and 8 mg/mL EndoECM hydrogels. C) Cell proliferation in 3D culture comparing 3 mg/mL collagen, 3 mg/mL Matrigel, and 3, 6 and 8 mg/mL EndoECM hydrogels. To determine fold change, data were normalized with respect to NoTT group for coating condition and the collagen group for 2.5D and 3D conditions. In all cases, statistical analysis was performed with respect to 3 mg/mL EndoECM. *p<0,05, **p<0.01, ***p<0.001.*

2.1.3. *3D culture system*

Lastly, different cell types were encapsulated in EndoECM hydrogels to form a 500-μm thick hydrogel (3D culture system*; Figure 37C)*. Encapsulation of ICE6-7 in 3 mg/mL EndoECM significantly improved their proliferation, as compared with both standard matrices, but increasing the concentration of EndoECM did not provide additional benefits for these cells. Similarly, encapsulation of ESCs in 3 mg/mL EndoECM also significantly improved their proliferation, compared to collagen, however proliferation was significantly decreased as EndoECM hydrogel concentration increased ($p<0.0001$, from 3 to 8 mg/mL). No difference in proliferative ability was noted between EECs or ESCs encapsulated in Matrigel or EndoECM at 3 mg/mL.

2.2. Long-term three-dimensional co-culture of endometrial cells

Three-dimensional co-culture systems were built using both stromal and epithelial cells from human endometrial stem cell lines (ICE6-7 constructs) or isolated human primary cells from endometrial biopsies (EECs-ESCs constructs). To slow ECM hydrogel remodeling, epithelial cells (ICE6 or EECs) were seeded on day 0 (method A) or day 3 (method B) after stromal cell encapsulation (ICE7 or ESCs). The ICE6-7 and EECs-ESCs constructs were maintained for up to 10 days.

After 5 days, all constructs underwent remarkable remodeling, forming compact spheres between days 7-10 *(Figure 38)*. Since method A constructs had a higher cell concentration to begin with, hydrogel degradation was more aggressive, and constructs acquired a disc shape.
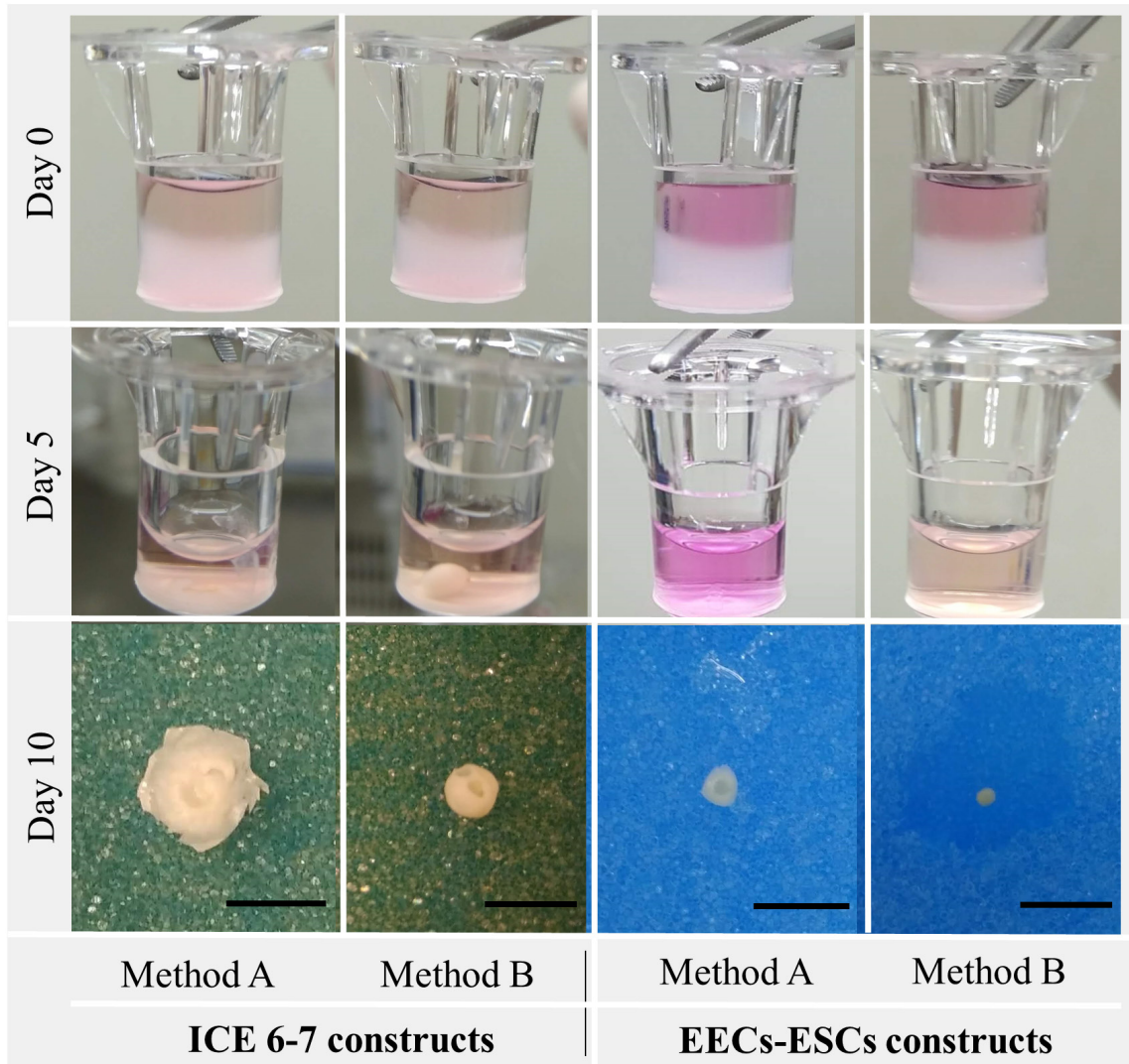
Figure 38. Macroscopic remodeling of in vitro endometrium-like culture systems. *Monitoring of ICE6-7 and EECs-ESCs constructs under 3D in vitro culture at day 0, 5 and 10 using seeding methods A-B of the epithelial fraction. On day 0 and day 5 constructs can be seen within the well insert used during the in vitro culture. Spherical or discoid constructs were recovered from the inserts on day 10. Scale bars: 50 mm.*

Viability assays showed that approximately 90% of both ICE6-7 and EECs-ESCs constructs survived up to 10 days *(Figure 39A-D)*. To analyze cellular proliferation within these constructs, Ki67 was assessed by immunohistochemistry. Approximately 33% of cells in the ICE6-7 constructs and 60% in the EECs-ESCs constructs were proliferative, no statistical difference was found between methods A and B *(Figure 39E-I)*.
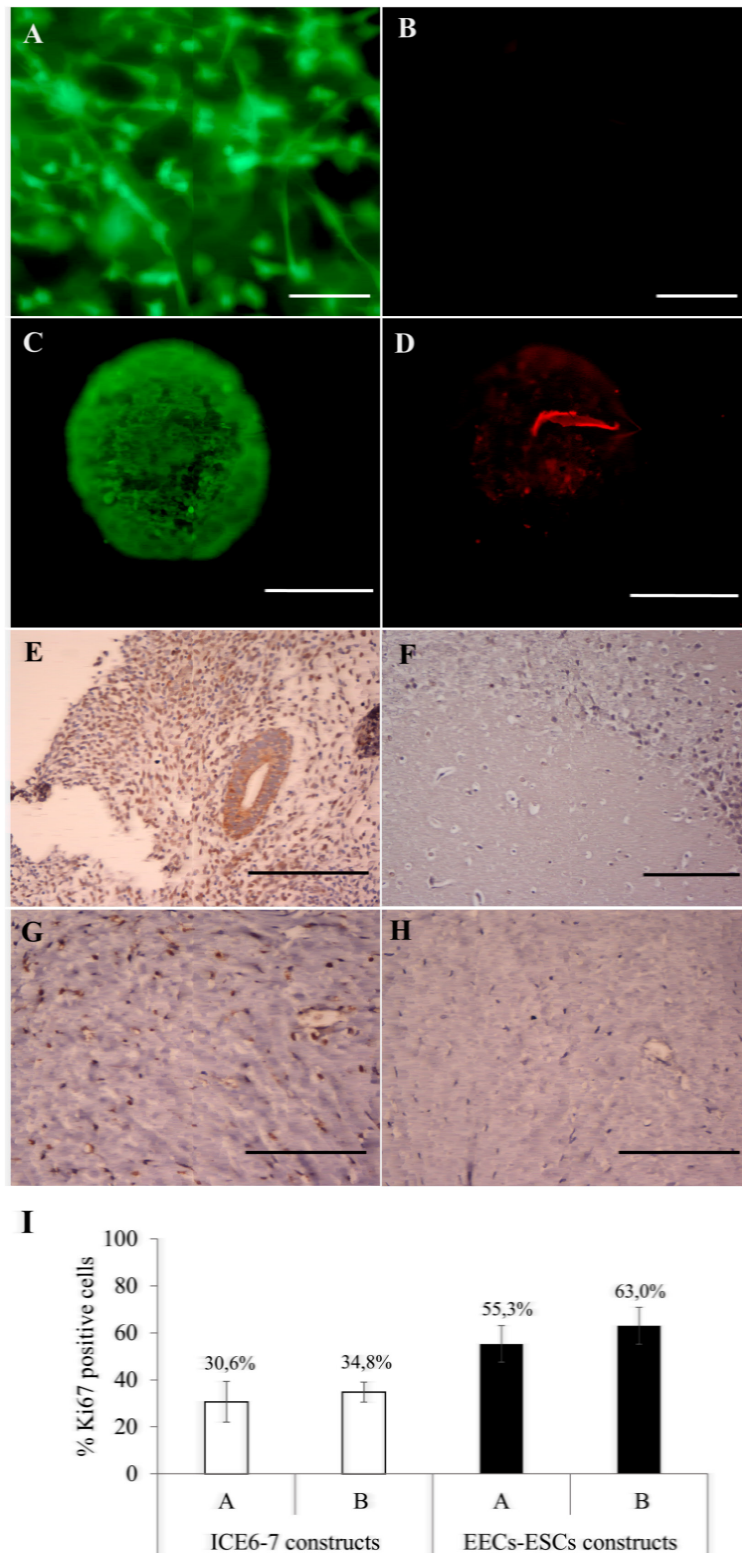
Figure 39. Cell viability and proliferation in long-term in vitro endometrium-like co-culture.
(A-D) Images taken with a ZEISS Axio Vert.A1 inverted microscope. Live (A) and dead cells (B) in an EEC-ESC construct (Method B) after 5 days 3D in vitro culture. Scale bars: 100 μm. Live (C) and dead cells (D) at day 10. Scale bars: 1 mm. Positive (human endometrium;E) and negative (mouse brain;F) control tissue stained with Ki67. Positive (G) and negative technical control (no primary antibody; H) of long-term cellular constructs stained with Ki67. Scale bars: 150 μm. I) Percentage of Ki67 positive cells at day 10, in ICE6-7 and EECs-ESCs constructs using Method A and B. *p<0.05.

Based on MT staining, the ECM of contracted constructs had a higher density of collagen than unseeded EndoECM hydrogels *(Figure 40)*. Meanwhile, the EECs-ESCs constructs produced with method B showed little to no blue staining, indicating a low fibrotic content.
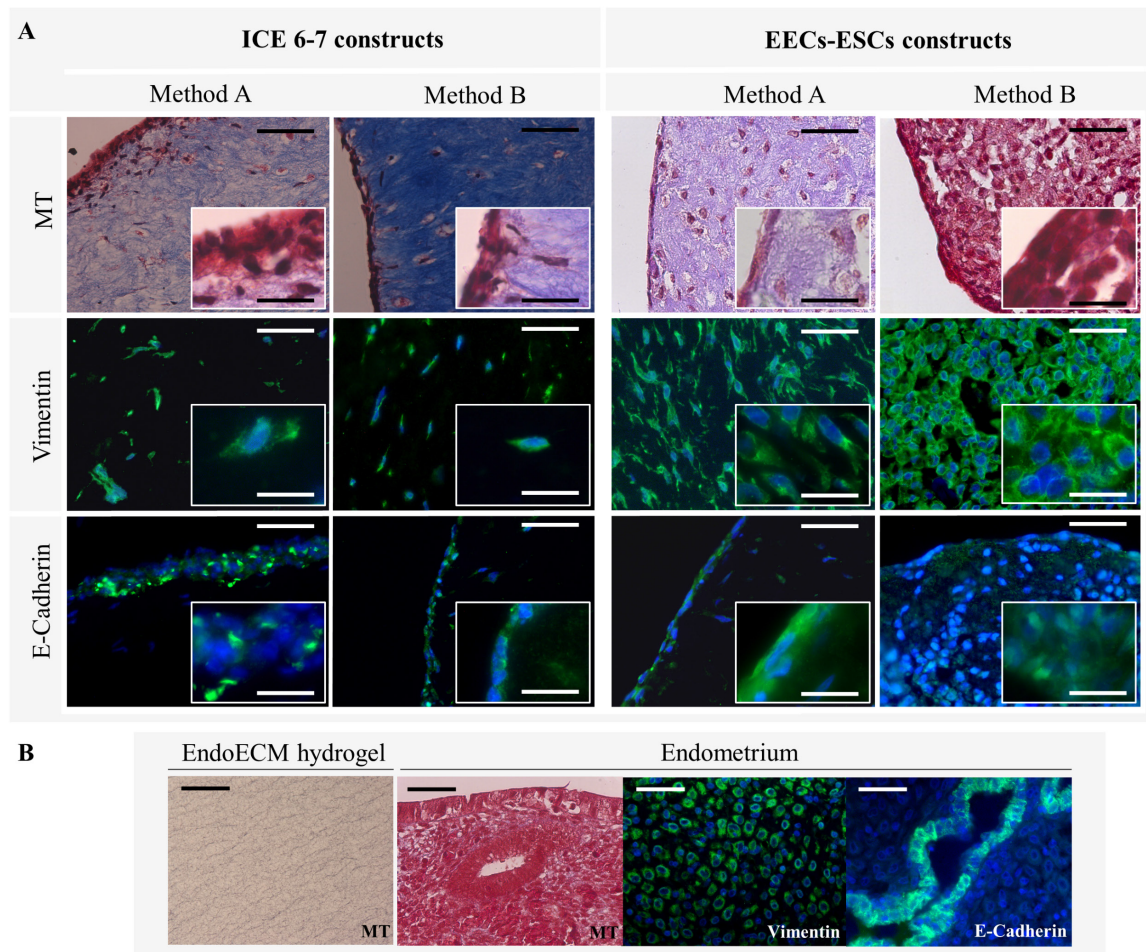
Figure 40. Microscopic remodeling of in vitro endometrium-like culture systems. A) Morphological analysis of ICE6-7 and EEC-ESC constructs at day 10, using MT staining and epithelial (E-cadherin) and stromal (vimentin) immunofluorescent markers. Scale bars at 50 μm (top row) or 5 μm (bottom row). B) Controls of morphological analysis: acellular EndoECM hydrogels and endometrium. Scale bars: 50 μm.

Both ICE6-7 and EECs-ESCs constructs had vimentin-positive stromal cells surrounded by collagen fibers in a 3D shape, and E-cadherin positive epithelial cells detected on the surface *(Figure 40 Panel A)*. However, no apico-basal polarization was observed any of

the samples. These results show that EndoECM was able to maintain viability of long-term human endometrial cells coculture in an endometrial-like configuration *in vitro*, however using this solution without supplementation (of sexual hormones, for example) was not able to reproduce all the morphological characteristics of a natural endometrium.

2.3. Endometrial extracellular matrix hydrogels and endometrial organoids development: A proof-of-concept study

2.3.1. *Establishment and characterization of a human endometrial organoid line*

In response to expansion media, free epithelial glands derived from fresh human endometrium were able to self-organize in 3D *in vitro* culture to develop endometrial organoids *(Figure 41A)*. Fragmented organoids spontaneously reassembled themselves in every passage, as well as increased in size and number throughout *in vitro* culture *(Figure 41B-C)*. The organoid line was successfully maintained up to 14 passages, with a passage frequency of 7-10 days. Organoid resistance to cryopreservation was also validated and was demonstrated by their ability to regenerate after freezing and thawing.

Cytokeratin (a marker of glandular epithelium) was heavily expressed in endometrial organoids, while vimentin (a stromal marker) was absent, confirming the epithelial origins of the organoids *(Figure 41D-E).* Notably, organoids spheres also presented a glandular epithelial polarity *(Figure 41F)*. A decrease in the growth efficiency, and a slightly change towards a more amorphous spherical morphology was observed from passage 7 organoids, suggesting senescence of this organoid line.

Remarkably, the organoid line preserved the chromosomic stability of epithelial glands, presenting a 46,XX karyotype in passage 3, without any abnormalities *(Figure 41G).* This

chromosomic stability was maintained long-term, presenting the identical genetic profile at passage 12 of the organoid line *(Figure 41G).*
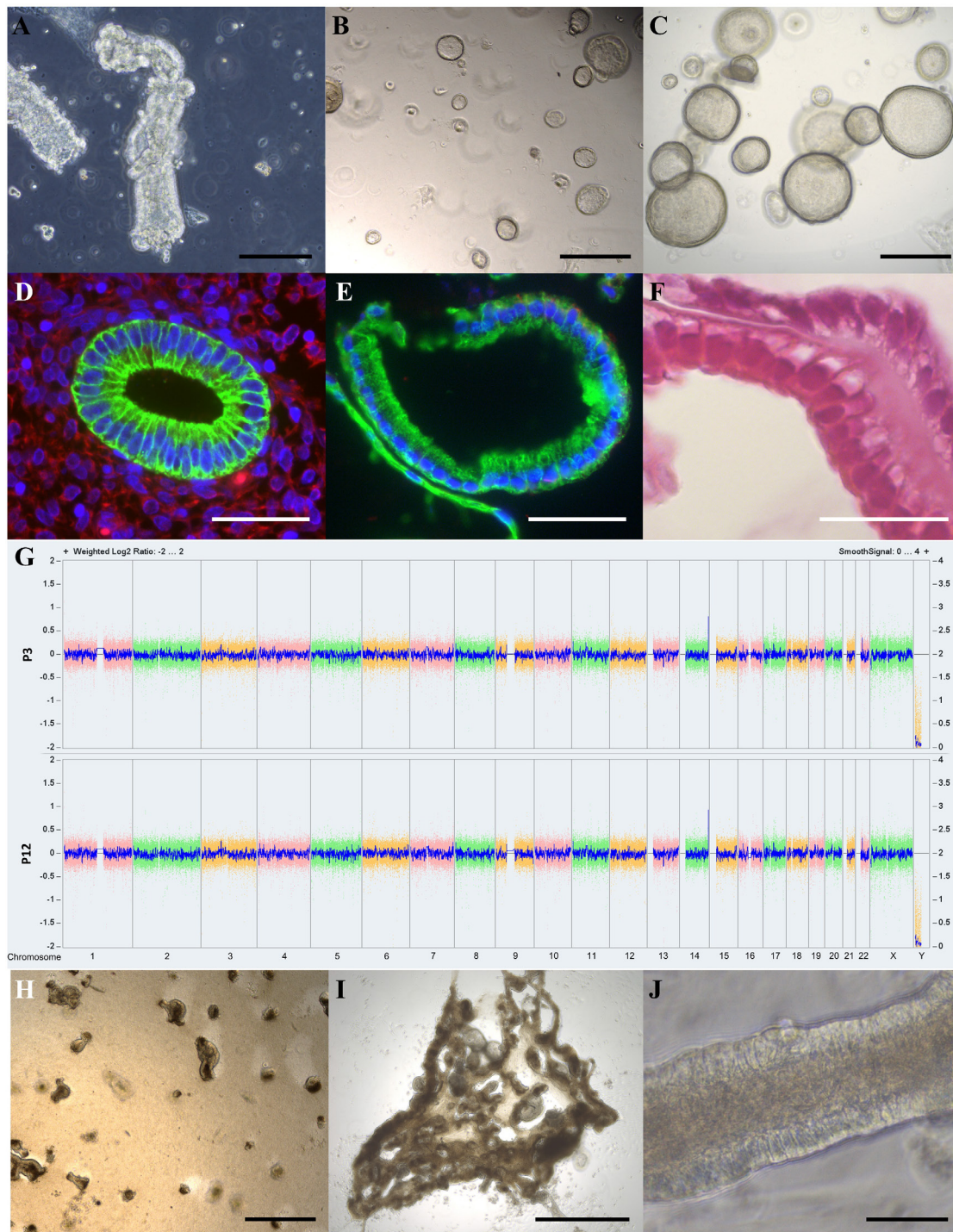
Figure 41. Endometrial extracellular matrix hydrogels and endometrial organoids development. *A) Free endometrial glands after collagenase digestion. B) Passage 5 organoids on day 2. C) Passage 5 organoids on day 5. D) Immunofluorescence staining of vimentin (red), cytokeratin (green) and DAPI (blue) in the human endometrium. E) Immunofluorescence staining of vimentin, cytokeratin and DAPI in an endometrial organoid. F) H&E staining showing polarization of the epithelia of an endometrial organoid. G) Whole Genome View of organoids from passage 3 (P3) and 12 (P12) showing the Weighted Log2 ratio from every chromosomic*

region of chromosomes 1-22, X and Y. Colors indicate the different chromosomes. The Y axis indicates the fold change in the copy number. The maintenance of the weighted Log2 ratio in a valor of 0 indicates no aberrant numbers of chromosomes and chromosomic regions. The absence of the Y chromosome confirms that the organoids are from female origin. H) Passage 5 organoids after 2 days of 3D in vitro culture in EndoECM drops. I) Passage 5 organoids after 5 days of 3D in vitro culture in EndoECM drops. J) Organoid mesh in EndoECM on day 5 at 100x magnification. Scale bars at 150 µm (A), 500 µm (B, C, H), 25 µm (D, E), 50 µm (F, J) or 1 mm (I). A-C and G-I Images were taken by ZEISS Axio Vert.A1 inverted microscope.

2.3.2. *Preliminary study of endometrial extracellular matrix as a substitute for Matrigel in endometrial organoid culture*

With the aim of achieving a more natural and endometrial-specific culture for endometrial organoid development, we evaluated the feasibility of using EndoECM hydrogels as a substitute for Matrigel. Organoids were transferred from Matrigel to EndoECM drops in different fresh passages (passage 1, 2 and 5).

After 2 days in EndoECM, inadequate expansion of the organoids was accompanied by a loss of the spherical shape typically seen in cultures with Matrigel. Organoids presented with a halo of surrounding degradation, indicating they actively break down the EndoECM *(Figure 41H)*. In fact, endometrial organoids completely degraded EndoECM drops within 5 days, consequently, interlinking with each other to form a floating mesh in the expansion media *(Figure 41I)*. Nonetheless, the columnar phenotype of epithelial cells was conserved at day 5 *(Figure 41J)*.

3. Endometrial extracellular matrix hydrogels as a regenerative treatment for reproductive pathologies *in vivo*

3.1. Preliminary *in vivo* biocompatibility of endometrial extracellular matrix hydrogels in a subcutaneous murine model

The *in vivo* biocompatibility of EndoECM hydrogels was preliminarily tested in an immunocompetent murine model. After 48 h, hydrogels appeared gelled and opaque in the subcutaneous tissue *(Figure 42A)*. Masson Trichrome staining confirmed an innate immune response in hosts, through a infiltration of rounded cells with large nuclei, (corresponding to the morphology of inflammatory cells) in both No-DC Endo and EndoECM hydrogels *(Figure 42B)*. Remarkably, there was a 4-fold increase ($p<0.0001$) in cell infiltration in No-DC Endo (6243±244 cells) compared to EndoECM (1599±402 cells) *(Figure 42C)*. Further immunological characterization revealed CD68+ early macrophage infiltration in both EndoECM and No-DC Endo hydrogels that was significantly higher in EndoECM at 48 h (72.0±15.0% and 19.2±7.77% in EndoECM and No-DC Endo respectively, $p<0.05$; *Figure 42D*). Taken together, these results proved the concept for our study.

Interestingly, the volume of both hydrogels decreased after 14 days. Although the infiltration of CD68+ cells was maintained in EndoECM (72.0±15.0% and 59.5±14.6% at 2 and 14 days, respectively), MT images of EndoECM samples showed a shift in the proportion of inflammatory-like cells toward spindle-shaped elongated fibroblast-like cells *(Figure 42E-F)*. In NO-DC Endo, encapsulation was much less evident at 14 days *(Figure 42E)*.

A

B

EndoECM   No-DC Endo

C

D

E

2 Days   7 Days   14 Days

F

2 Days   14 Days
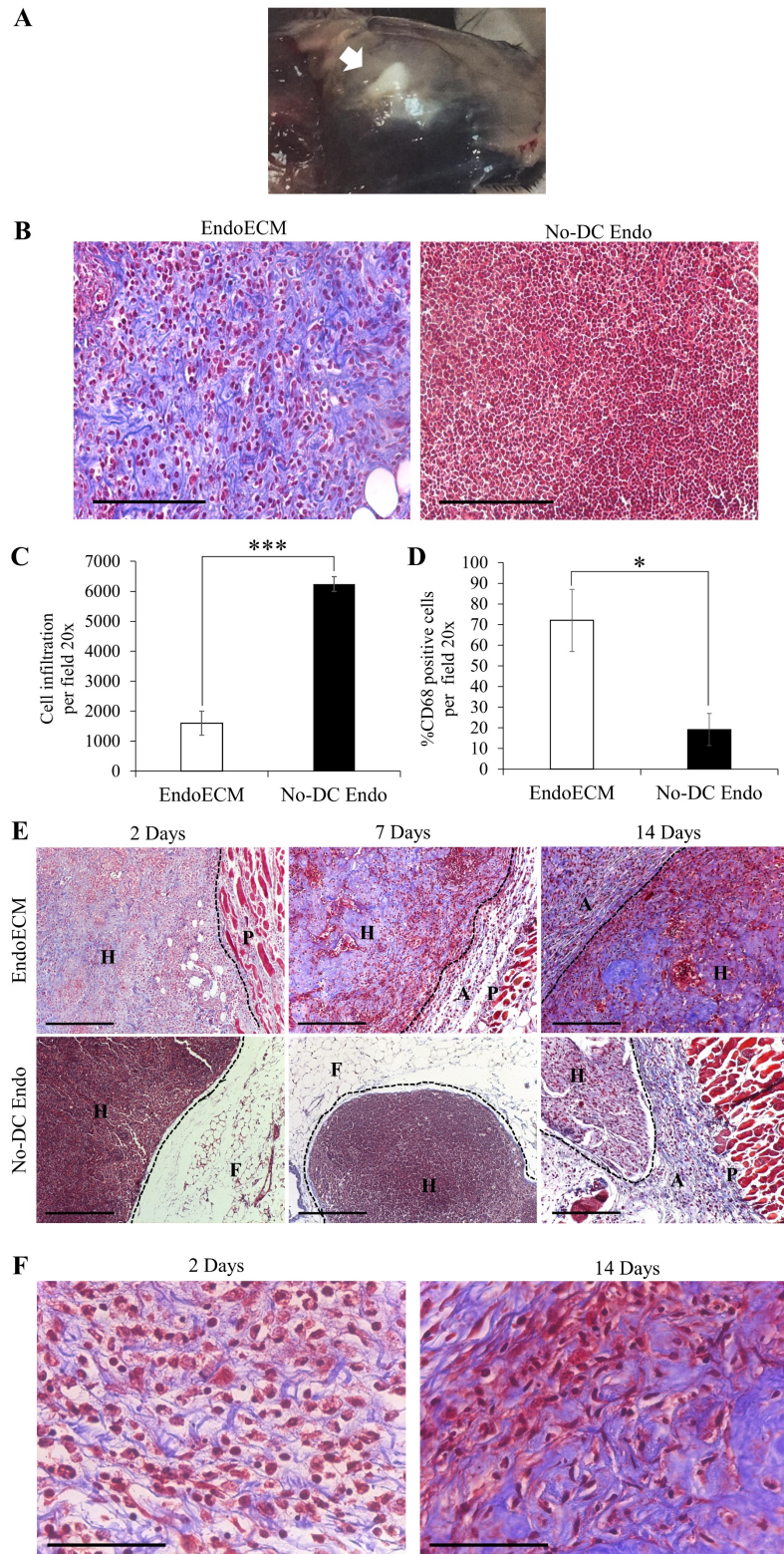
Figure 42. In vivo gelation and biocompatibility of endometrial extracellular matrix hydrogels up to 14 days. *A) EndoECM hydrogels (pointed to by arrow) 48 h after subcutaneous injection. B) Representative MT images of infiltrating round cells (cytoplasm stained in red) in EndoECM and No-DC Endo hydrogels showing the host's innate immune response that was maintained from 2 to 14 days. Scale bars: 150 µm. C) Quantification of infiltrated inflammatory cells in EndoECM and No-DC Endo hydrogels after 48 h of subcutaneous injection via MT staining.*

***p<0.001. D) Percentage of CD68+ cells in EndoECM and No-DC Endo hydrogels after 48 h. *p<0.05. E) Comparison of MT-stained day 2, 7 or 14 EndoECM and No-DC Endo sections indicating the progression of hydrogels within the subcutaneous space over the time. Dotted lines represent the edge between hydrogels and subcutaneous space. H: hydrogel; A: subcutaneous adventitia, P: panniculus carnosus. F: subcutaneous fat. Scale bars: 250 μm. F) Representative MT images demonstrating the shift from rounded mononuclear cells at 2 days towards spindle-shaped elongated cells at 14 days. Scale bars: 50 μm.

3.2. Endometrial regeneration and fertility restoration in a murine model of endometrial damage

3.2.1. *Endometrial damage, hydrogel treatments and survival rate*

To create a murine endometrial damage model, the endometrium was injured by injecting 70% ethanol directly into the uterine horn using a 25G needle according to a protocol adapted from (Kim *et al.* 2019b). The treatment with ethanol immediately produced a swelling of the uterine horn and turned them a whitish color *(Figure 43A)*. Four days later, severe damage was noticed in the endometrium, manifesting as macroscopic adhesions of the uterine horn to the surrounding fat and tissues *(Figure 43B)*.

It is important to note that the injury of the horn by ethanol did not interfere with subsequent treatment injections; hydrogel treatments were easily injected into the uterine horns using 25G needles. The only complication encountered during the second surgery was that two horns from two different mice were accidentally ruptured, and these were consequently excluded from the analysis. All mice survived both surgeries. Some mice experienced slight pain (as evidenced by squinting their eyes and diminished activity) during the 24h post-surgical recovery, however it was relieved with analgesics. Since mice exhibited normal behavior in subsequent days, we considered the procedures for inducing endometrial damage and treatment it with hydrogel as relatively safe.

Figure 43. Endometrial damage induced by ethanol. A) Endometrial damage immediately after the injection of ethanol. Uterine horn is swollen and whitish. B) Uterine horns four days after endometrial damage by ethanol (before introducing treatment).

3.2.2. *Estrous cycle profiles*

Overall, mice maintained estrous cyclicity until the end of the experiment, validating ovarian function was not disrupted by the ethanol used to induce endometrial damage *(Figure 44A)*. Since no significant differences were found between mice with unilateral or bilateral damage to the uterine horns, all the data was analyzed together. Theoretically, the duration of an estrous cycle in a normal female mouse is 4-5 days, with a proportion of 1:1:2 days for proestrus:estrus:metestrus/diestrus, indicating they can complete 3-5 cycles in 19 days. In our model, mice completed an average of 2.7±0.6 estrous cycles within 19 days (3.0±0.6, 2.5±0.8 and 2.6±0.5 cycles for saline, EndoECM and EndoECM+GF groups respectively, *Figure 44B*), which results in approximately 7 days per cycle. Furthermore, the proportion of days in each phase of the estrous cycle was altered to 1:1.5:2 (for proestrus:estrus:metestrus/diestrus; *Figure 44C*), indicating a slight increase in days in estrous. We found the maximum number of consecutive days in estrous

was on average 3.0±1.6 days (2.6±1.0, 2.6±1.3, and 3.5±2.0 days for saline, EndoECM and EndoECM+GF groups respectively, *Figure 44D*), while in metestrus/estrus was on average 3.2±1.5 days (3.0±1.6, 3.7±1.7, and 2.9±1.2 days for saline, EndoECM and EndoECM+GF groups respectively, *Figure 44E*). Notably, no significant differences were detected between the three treatments *(Figure 44)*.
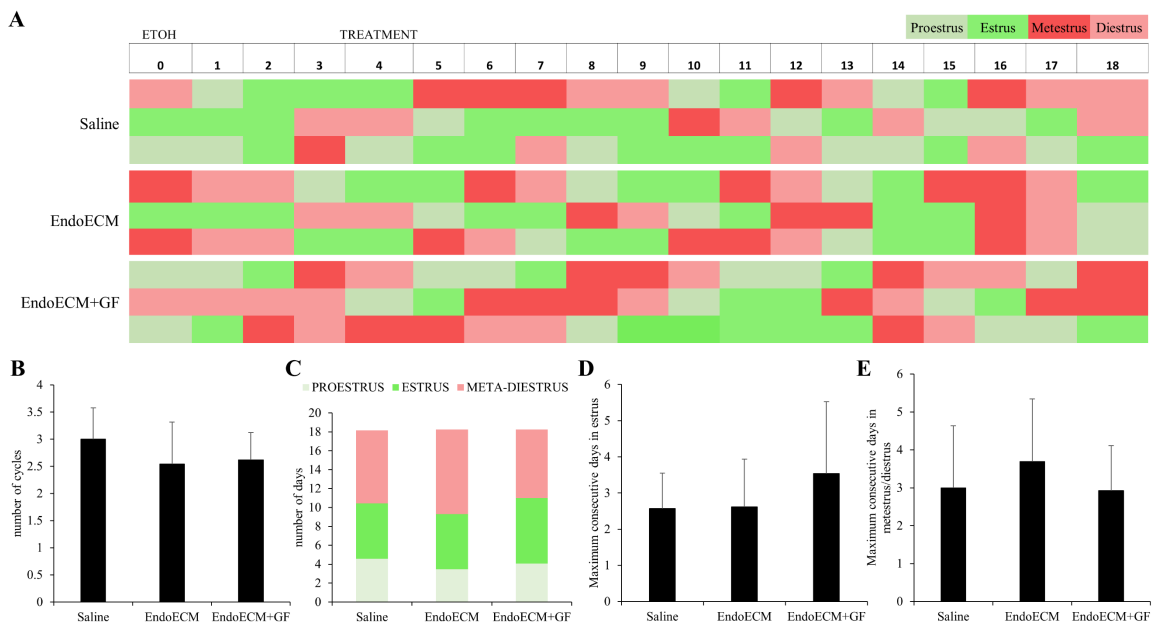
Figure 44. Monitoring of estrous cyclicity after endometrial damage with ethanol. A) Representative estrous cycle profiles from day 0 (endometrial damage by ethanol (ETOH) injection) to day 18 in three mice from each treatment group. Each row corresponds to a different mouse. Every phase of the estrous cycle is represented in a different color: proestrous in light green, estrous in bright green, metestrous in bright red and diestrous in pink. B) Total number of estrous cycles during the experiment (19-day period). C) Average number of days spent in each one of the estrous cycle phases. D) Maximum consecutive days spent in the estrus phase. E) Maximum consecutive days spent in the metestrus/diestrus phases.

3.2.3. *Evaluation of uterine regeneration*

3.2.3.1.   Localization of endometrial extracellular matrix hydrogels *in utero*

The feasibility of detecting biotin-labelled EndoECM hydrogels was successfully verified, by immunofluorescence, after injection within the uterine cavity *(Figure 45A)*.
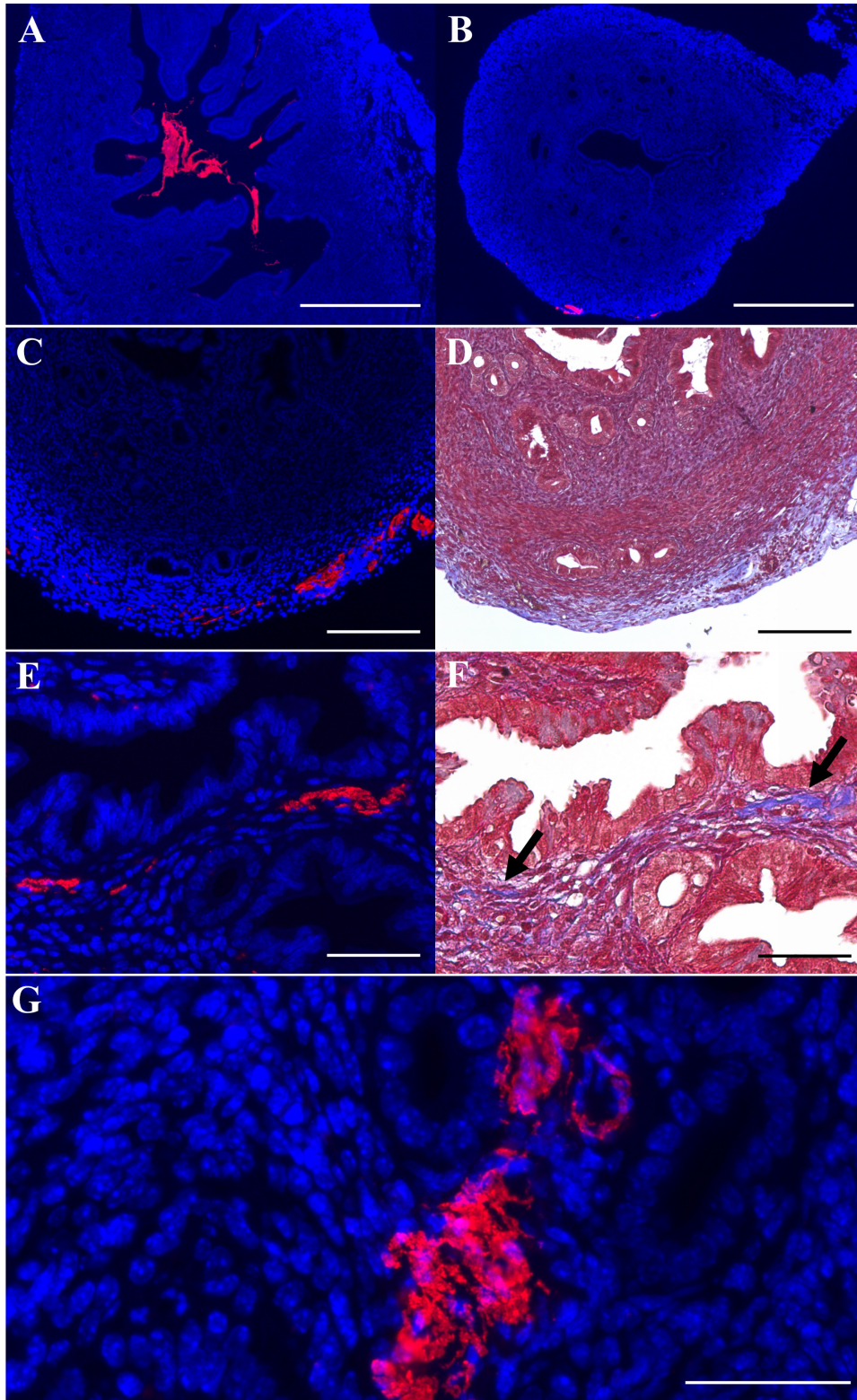
Figure 45. Biotin-labelled EndoECM hydrogels. *Immunofluorescence of biotin (red) and nuclei (DAPI, blue) in the uterine horn A) after injection of biotin-labelled hydrogels and B) 14 days later. C) Immunofluorescence and D) MT staining of biotin-labelled collagen depositions inside myometrium after 14 days. E) Immunofluorescence and F) MT staining of biotin-labelled collagen depositions inside endometrium after 14 days. G) Immunofluorescence of biotin-labelled collagen depositions inside endometrium at high magnification. Scale bars at 500 µm (A, B) or 50 µm (C-G).*

Notably, after 14 days, the EndoECM hydrogels were no longer detectable in the uterine lumen *(Figure 45B)*. Biotin was detected in 2/4 horns treated with EndoECM and 3/4 horns treated with EndoECM+GF (or 62.5% of the eight treated uterine horns), principally located within the outer myometrium *(Figure 45C-D)*. However, biotin was also immunodetected inside endometrial tissue in four out of the five positive samples *(Figure 45E-G)*, co-localizating with collagen deposits visualized by MT staining *(Figure 45E-F)*.

3.2.3.2.   Endometrial thickness, gland concentration and collagen deposition

To study endometrial regeneration after receiving treatments, endometrial thickness, gland concentration and collagen deposition were analyzed. Histological images from saline, EndoECM, or EndoECM+GF treated horns and non-damaged horns at 14 days after treatment are presented in *Figure 46A*.

Since the mice could be in different stages of the estrous cycle on the day of sacrifice, and this could influence the parameters analyzed, we took this variable into account when interpreting the results. The estrous stages for each of the eleven mice studied are summarized in *Table IX*, and demonstrate a lack of estrous synchronization among the mice in study as well as an unbalanced representation of the phases within each group. To counter estrous cycle biases and individual variability of the mice, the data obtained from each damaged/treated right horn was normalized to the respective non-damaged left horn from the same mouse. The resulting normalized ratio was compared between the different treatment groups in study (saline, EndoECM, EndoECM+GF).

Table IX. Summary of the mice belonging to the regeneration group.

Mouse number	Treatment	Damaged/treated horn	Non-damaged horn	Estrous cycle phase at end-point
1	Saline	Right	Left	Diestrus
2	Saline	Right	Left	Diestrus
3	Saline	Right	Left	Estrus
4	EndoECM	Right	Left	Estrus
5	EndoECM	Right	Left	Diestrus
6	EndoECM	Right	Left	Proestrus
7	EndoECM	Right	Left	Estrus
8	EndoECM+GF	Right	Left	Metestrus
9	EndoECM+GF	Right	Left	Metestrus
10	EndoECM+GF	Right	Left	Estrus
11	EndoECM+GF	Right	Left	Estrus

There were no statistically significant differences between treatment groups when endometrial regeneration was analyzed. The endometrial thickness was slightly improved with EndoECM and EndoECM+GF treatment (0.91±0.44, 1.05±0.43, 1.18±0.27 μm in saline, EndoECM and EndoECM+GF treated horns respectively, *Figure 46B*). Similarly, gland concentration also increased slightly (0.84±0.13, 1.18±0.20, 1.34±0.65 glands/mm^2 in saline, EndoECM and EndoECM+GF treated horns respectively; *Figure 46C*). Conversely, collagen deposition and fibrosis did not show apparent variations among the groups when analyzed by MT staining (1.03±0.08, 1.02±0.18, 0.94±0.08% collagen area in saline, EndoECM and EndoECM+GF treated horns respectively; *Figure 46D*).
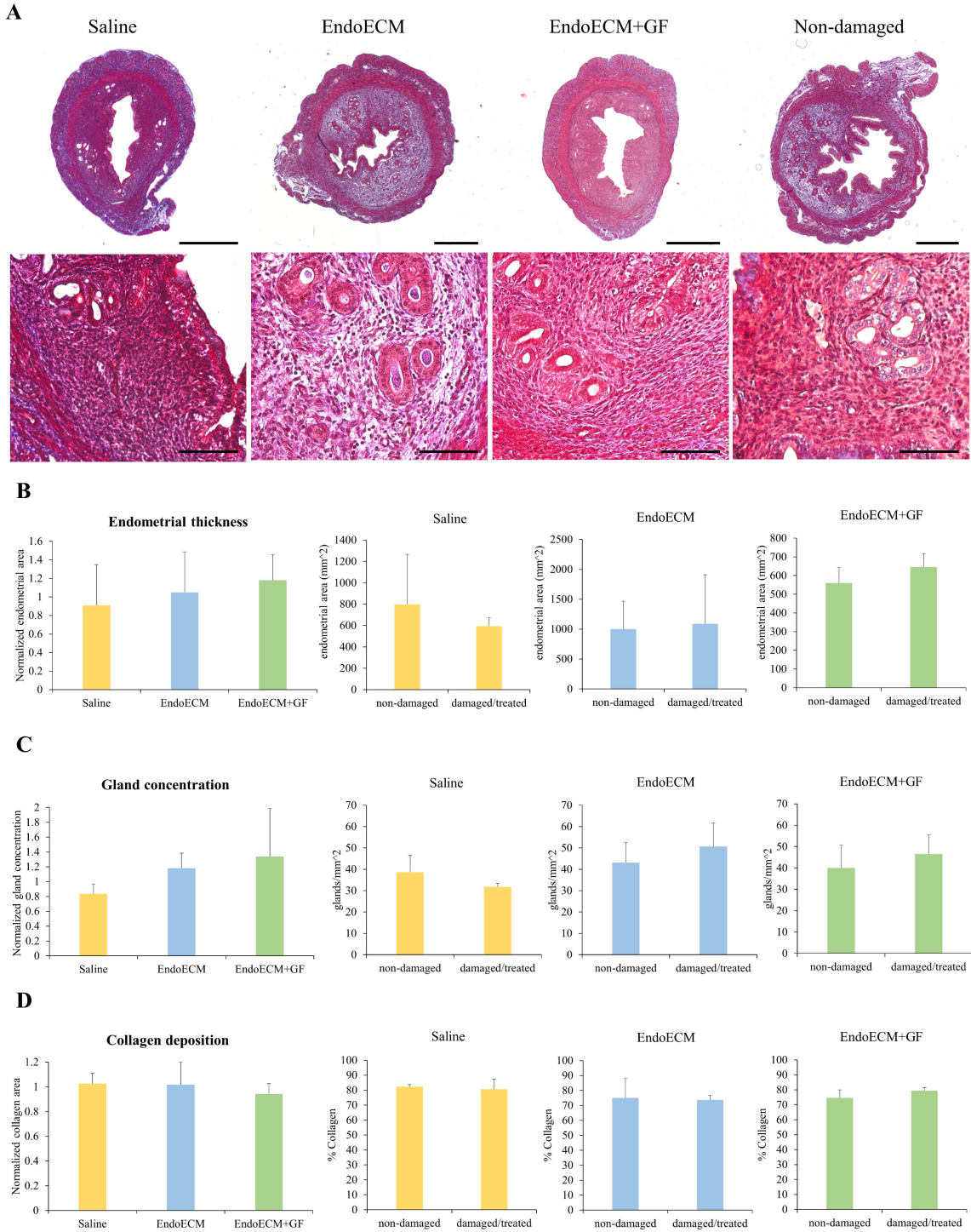
Figure 46. Histological analysis of endometrial regeneration. *A) Cross-sectional comparison of saline, EndoECM, EndoECM+GF and non-damaged uterine horns 14 days post-treatment. Sections stained with MT. Scale bars at 500 µm (top row) or 100 µm (bottom row). (B-D leftmost graphs) Normalized quantification of endometrial thickness, gland concentration and collagen deposition for each treatment group (Saline, EndoECM and EndoECM+GF). Comparison of endometrial thickness (B), gland concentration (C) and collagen deposition (D) in non-damaged and their respective damaged uterine horns treated with Saline (yellow), EndoECM (blue) or EndoECM+GF (green).*

Likewise, no statistical differences in endometrial thickness, gland concentration and collagen deposition were found between right and left horns from the same individual, regardless of the treatment group; **Figure 46B-D**). Persistence of endometrial damage (until day 14) was highlighted by the slight decrease in endometrial thickness (797.52±468.66 and 595.01±78.24 mm^2 in damaged/treated and non-damaged horns, respectively) and gland concentration (38.67±7.84 vs 31.81±1.67 glands/mm^2 in damaged/treated and non-damaged horns, respectively) found in the saline group **(Figure 46B-C)**.

3.2.3.3. Quantification of fibrotic gene expression

To further analyze the regenerative effects of the treatments (in terms of tissular fibrosis) after endometrial damaged with ethanol, we analyzed the expression of *Col1a1* gene by RT-qPCR. The *Col1a1* transcript encodes the collagen α-1 (I) chain, a component of type 1 collagen required in the assembly of mature collagen fibers in the ECM. This gene has been reported to be up-regulated in fibrotic events, and specifically, endometrial damage by AS (Jun *et al.* 2019; Gan *et al.* 2017; Ouyang *et al.* 2020).

When we analyzed *Col1a1 gene* expression between the different treatment groups (with data normalized to the respective non-damaged horns for every mouse), we found EndoECM decreased collagen expression 2-fold, and the addition of growth factors significantly reduced collagen expression 4-fold (2.74±1.26, 0.71±1.25 and -1.20±0.91 Log2 fold Change for saline, EndoECM and EndoECM+GF groups respectively, p<0.05; **Figure 47A**). Notably, no significant differences in *Col1a1 gene* expression were found between non-damaged left horns and their respective damaged right horns treated with

saline *(Figure 47B)*, EndoECM *(Figure 47C)* or EndoECM+GF *(Figure 47D)*, although

the latter presented an evident trend toward downregulation.
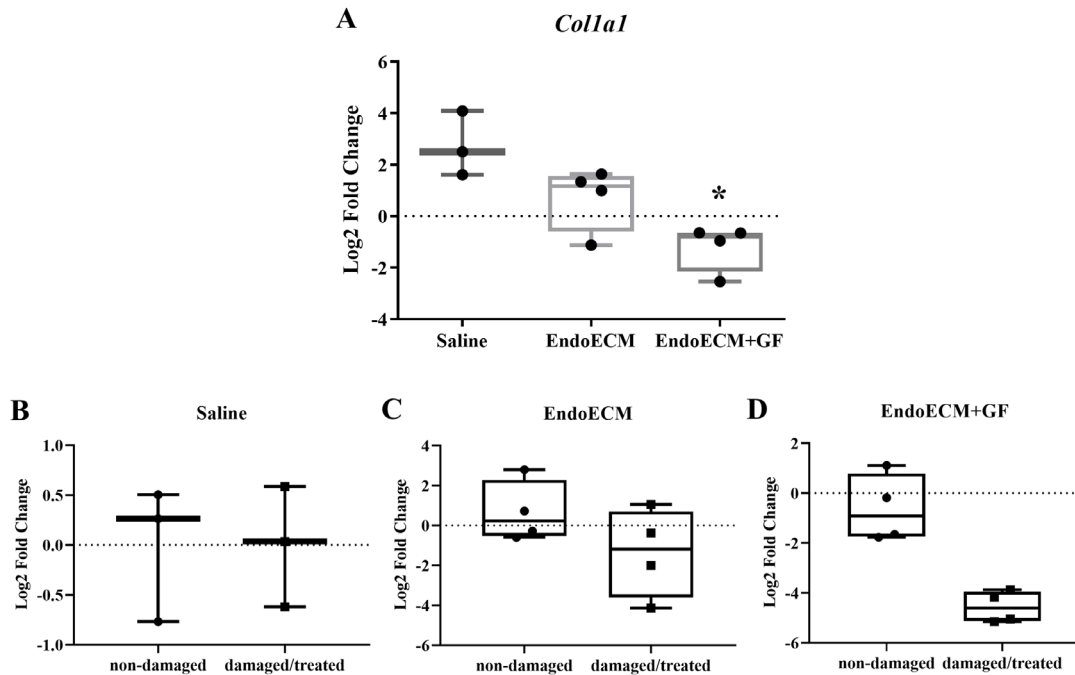
***Figure 47. Evaluation of Col1a1** gene **expression by real-time quantitative polymerase chain reaction.** A) Normalized quantitative expression of Col1a1 in saline, EndoECM and EndoECM+GF treatment groups. Comparison of Col1a1 gene expression between non-damaged and damaged uterine horns treated with Saline (B) EndoECM (C) or EndoECM+GF (D). Data presented as a mean±SD. *p<0.05.*

3.2.3.4.   Cell proliferation

One of the main features of EA and AS pathologies is the impaired endometrial growth.

To study if normal endometrial proliferation could be recovered after treatment with

EndoECM and EndoECM+GF, the expression of the Ki67 (biomarker of proliferation)

was quantified by immunohistochemistry. As endometrial cell proliferation is variable

among the different phases of the estrous cycle, the data obtained from every

damaged/treated right horn was normalized with its respective non-damaged left horn and

the resulting normalized ratio was compared between the treatment groups, following the same approach used in sections 3.2.3.2 and 3.2.3.3.

Compared to treatments with saline, EndoECM and especially EndoECM+GF amplified proliferation of endometrial cells *(Figure 48)*. Quantification of Ki67-positive cells later confirmed a 33% increase in proliferation with EndoECM and a significant doubling of proliferation with the addition of growth factors, with respect to the saline group (0.89 ± 0.32, 1.18 ± 0.35 and 1.69 ± 0.47 normalized proliferative index in saline, EndoECM and EndoECM+GF groups respectively, data normalized with the respective non-damaged horn for each mouse, $p<0.05$; *Figure 48B leftmost graph)*. No significant differences were found between damaged/treated right horns and their respective non-damaged left horns for any of the treatment groups (saline, EndoECM and EndoECM+GF; *Figure 48B*).
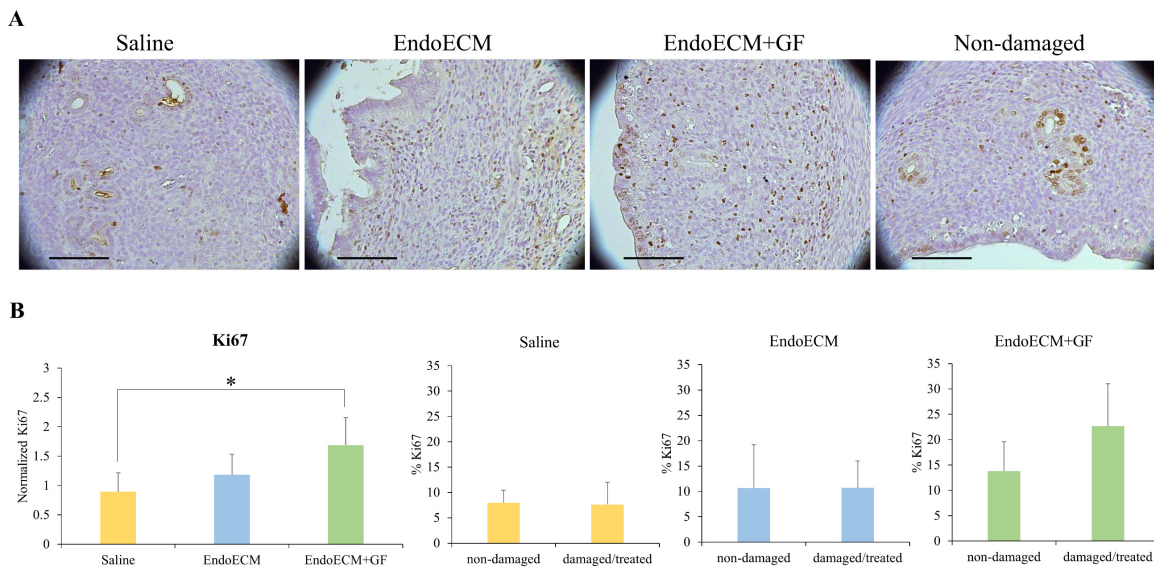
Figure 48. Endometrial cell proliferation analysis by Ki67 immunostaining. *A) Representative pictures of Ki67 immunostaining in damaged endometrial horns treated with saline, EndoECM, EndoECM compared to non-damaged horns, 14 days post-treatment. Scale bars: 100 µm. B) (leftmost graph) Quantification of endometrial cell proliferation showing the normalized Ki67 expression in Saline, EndoECM and EndoECM+GF. (right) Comparison of proliferative index in non-damaged and damaged uterine horns treated with Saline (yellow), EndoECM (blue) or EndoECM+GF (green).*

3.2.4. *Evaluation of fertility restoration*

The recovery of uterine function was evaluated two weeks post-treatment, by assessing the mice's fertility and fecundity. A total of 26 female mice with unilateral or bilaterally damaged/treated horns underwent natural mating. Sexual intercourse was confirmed by the presence of a vaginal plug, and the achievement of pregnancy as well as number of gestational sacs was assessed 10 days later. A detailed table including the treatment group, which horn(s) were damaged/treated, horn weight and number of gestational sacs found in each of the 26 mice is included in Appendix A *(Supplementary Table IV)*.

Endometrial damage by ethanol substantially disrupted fertility. A pregnancy rate of only 17% was found in the saline-treated group compared to 80% in non-damaged horns (2/12 and 12/15 pregnant horns/total uterine horns for saline-treated and non-damaged horns respectively, $p<0.01$, *Table X*). These results confirmed the suitability of ethanol to induce adequate endometrial damage in a murine model.

Table X. Evaluation of fertility restoration.

Treatment	Uterine horns	Pregnant uterine horns	Pregnancy rate	Gestational sacs	Average gestational sacs per horn
Non-damaged	15	12	80%	57	3.8±2.60
PBS	12	2*	17%	8	0.67±1.61*
EndoECM	12	1*	8%	6	0.5±1.73*
EndoECM+GF	11	5	45%	15	1.36±2.16

*$p<0.05$. Statistical analysis with respect to non-damaged group.

In terms of fecundity, a similar significant decrease in the number of gestational sacs at embryonic day 10.5 was observed in the saline-treated group compared to non-damaged group (0.67±1.61 and 3.8±2.60 gestational sacs per horn for saline and non-damaged

horns respectively, p<0.01, ***Table X*** and ***Figure 49***). Aberrant gestational sacs were excluded from the analysis and considered miscarriages (n=2 embryonic sacs in a mouse treated with saline were excluded; ***Supplementary Table IV)***.
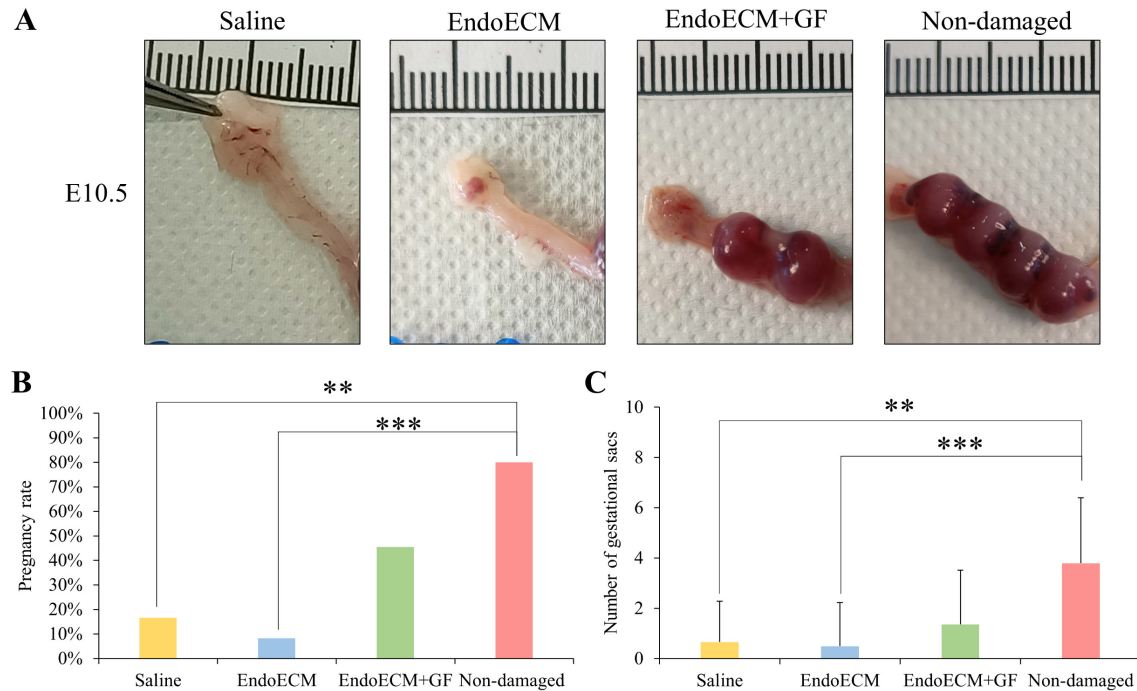
Figure 49. Evaluation of fertility restoration. *A) Representative images of uterine horns 10 days after detection of a vaginal plug (corresponding to stage E10.5 of embryo development). No gestational sacs visible in a saline-treated horn and a EndoECM horn, as well as two and four gestational sacs visible in the EndoECM+GF and non-damaged treated horns respectively. Pregnancy rate (B) and average number of evolutive gestational sacs (C) 10 days after mating confirmed by vaginal plug, in damage/treated or non-damaged groups. (**) p<0.01; (***) p<0.001.*

Surprisingly, pregnancy rates were not improved by EndoECM treatment. In fact, only one pregnancy was confirmed in 12 uterine horns (EndoECM treatment only had an 8% pregnancy rate with 0.58±1.38 gestational sacs per horn, ***Table X*** and ***Figure 49***). Furthermore, pregnancy rates and number of E10.5 gestational sacs for the EndoECM and saline groups were significantly lower than the non-damaged group (p<0.01; ***Figure 49B-C***). In contrast, EndoECM+GF restored fertility better than saline or EndoECM treatments, with a 45% pregnancy rate and 1.36±2.16 gestational sacs per horn.

Considering the aforementioned differences observed between the EndoECM and EndoECM+GF groups and similarities between the EndoECM+GF treated and non-treated horns, the addition of growth factors to the EndoECM may play a critical role in its capacity to restore fertility in this model.

VII. DISCUSSION

VII. DISCUSSION

With up to 12% of couples affected worldwide, infertility is a concerning disease of the 21st century. Many assisted reproduction techniques have been developed in recent years to mitigate infertility struggles, and huge advances have been made in the treatment of reproductive pathologies (for both men and women), mainly with the focus of producing the highest quality embryos possible. Two crucial factors are involved to acquire a successful pregnancy, a healthy embryo and a functional uterus.

The endometrium is the mucous layer lining the lumen of the uterus, responsible for receiving the embryo at implantation. This extraordinary tissue is highly regenerative, undergoing scar-free remodeling during each menstrual cycle. However, some (often iatrogenic) endometrial illnesses, like EA (characterized by an atrophic thin endometrium) and AS (which triggers endometrial destruction and formation of adhesions within the uterine cavity) can negatively affect this tissue and result in infertility. Unfortunately, both these endometrial pathologies are currently untreatable. The only options for affected women to have a genetic descendance are surrogate pregnancies and more recently, uterus transplantation. However, several ethical issues are still under debate for surrogate pregnancy, and in consequence, it is still illegal in many countries (including Spain). On the other hand, uterus transplantation, which was successfully performed by Dr. Brännström's group (Brännström *et al.* 2015), involves the general risks of an allogenic organ transplantation, such as an invasive surgery and more importantly, life-long immunosuppression for a non-life-threatening disease. For these reasons, new approaches to treat and solve these particular diseases are being investigated, including the use of tissue engineering.

The ECM is defined as a complex mixture of proteins, whose composition is unique to each tissue, including the endometrium. The ECM not only acts as a physical substrate for cell adhesion but also provides cues for tissue homeostasis and repair (Saldin *et al.* 2017; Rozario and DeSimone 2010; Theocharis *et al.* 2016; Evangelatov and Pankov 2013; Frantz, Stewart, and Weaver 2010). In the recent years, decellularization techniques have generated ECM-based hypoimmunogenic biomaterials. Among these biomaterials, ECM hydrogels have shown to retain the rich tissue-specific composition of natural tissues and to display a high potential for 3D *in vitro* culture studies and tissue regeneration treatments after specific tissular damage (Ventura *et al.* 2020; Sackett *et al.* 2018; Fercana *et al.* 2017; Link *et al.* 2017; Viswanath *et al.* 2017; Nehrenheim *et al.* 2019; Seo, Jung, and Kim 2018).

In this context, the three objectives of this thesis were to (I) develop tissue-specific ECM hydrogels derived from porcine DC endometrium, (II) use these endometrial ECM hydrogels as a platform for 3D culture systems *in vitro* and (III) apply these endometrial ECM hydrogels as a regenerative treatment for reproductive pathologies *in vivo*. To achieve these objectives, endometrial tissue was isolated from decellularized whole porcine uterus, and processed to create EndoECM hydrogels whose physicochemical properties were then studied. *In vitro* cytocompatibility of EndoECM hydrogels was analyzed with endometrial cells, in coating, 2.5D and 3D culture conditions, to assess their suitability in long-term endometrium-like co-cultures and as a support for endometrial organoid culture. Finally, EndoECM hydrogels were used *in vivo* as a potential regenerative treatment for reproductive pathologies in murine models. A preliminary biocompatibility study was conducted by subcutaneously injecting the EndoECM hydrogels into immunocompetent mice, and endometrial regeneration as well as fertility restoration were ultimately evaluated in a model for endometrial damage.

Development of endometrial extracellular matrix hydrogels from decellularized porcine uterus

Since the mammalian ECM is well conserved between species, and DC xenogeneic tissues have similar content, they are considered biocompatible (Singelyn *et al.* 2012). The main reasons behind using porcine uterus to develop our EndoECM hydrogels were the availability (pigs are bred on a large-scale) and phylogenetic similarity to humans. Due to the heterogeneity in terms of diet, age and comorbidities of human organs (or tissues) as well as the difficulty to predict when they are collected from deceased donors, pigs are considered a more reliable tissue source than human corpses (Johnson *et al.* 2014; Seif-Naraghi *et al.* 2011). Notably, porcine DC tissues are approved by The United States Food and Drug Administration and are used for a variety of clinical applications including chronic wound healing and heart valve replacement (Saldin *et al.* 2017; Crapo, Gilbert, and Badylak 2011; Traverse *et al.* 2019). Currently, application of DC porcine tissues continues to be studied in many fields of medicine (Ungerleider *et al.* 2016; Fercana *et al.* 2017; Viswanath *et al.* 2017; Saldin *et al.* 2017).

To decellularize the porcine uterus, we adapted a protocol based on SDS and Triton X-100. The guidelines established by (Crapo, Gilbert, and Badylak 2011) state that adequate decellularization is obtained when (1) no nuclei or cells are detected after H&E staining, and (2) the residual DNA is <50 ng/mg dry tissue and has a fragment length <200 base pairs visualized with gel electrophoresis. In compliance with these guidelines and corroborating results from previous studies (Fercana *et al.* 2017; Sackett *et al.* 2018; Seo, Jung, and Kim 2018; Bi, Ye, and Jin 2020), our decellularization protocol efficiently removed cells, reduced DNA content (by 92.4%), and demonstrated appropriate sized bands for DNA in gel electrophoresis (no bands detected). Although our protocol showed a retention of residual DNA (144 ng DNA/mg of lyophilized powder) which surpassed

the aforementioned guidelines almost three-fold, the role of DNA in transplant rejection is still under debate. Due to the lack of official criteria to define a good quality decellularization, further characterization of DC tissue bio- and cyto-compatibility, safety and efficacy is required prior to their clinical implementation.

To further analyze the potential adverse immune responses, we evaluated the α-gal epitope, the major cause of hyperacute rejection of porcine-derived organs xenografted in humans (Macher and Galili 2008; Pouliot *et al.* 2016). The α-gal epitope is found on the cell surface in the majority of mammals with the exception of Old World monkeys (monkeys of Asia and Africa), apes, and humans, which all produce large amounts of an anti-gal antibody that naturally destroy the cells expressing the epitope through adaptive immune responses (Macher and Galili 2008). In this thesis, we demonstrated our decellularization protocol effectively removed α-gal epitopes, encouraging biocompatibility of our endometrial-based ECM hydrogels.

Another critical factor which impacts the biocompatibility of DC biomaterials is the residual detergent content (Naahidi *et al.* 2017). To prevent cytotoxicity by SDS, we evaluated its removal during the washing of the DC endometrial tissues. Detergent concentrations that did not interfere with subsequent cellular growth were achieved after six washes, similar to previous evidence (Cebotari *et al.* 2010).

After processing the DC endometrial tissue, we developed a novel EndoECM hydrogel of porcine origin. As previously mentioned in the introductory section 5.1, the formation of ECM hydrogels is a based on a self-assembly process of polymers (mainly collagen) that is regulated by the presence of GAGs, PGs and other ECM proteins. However, the polymerization kinetics and the final structure of the hydrogel is influenced by the biochemical composition of the native tissue. While no differences in fiber thickness were found between our different EndoECM concentrations or hydrogel type, EndoECM

gelation kinetics were influenced by ECM concentration, corroborating findings using other tissue sources (Wolf *et al.* 2012).

We were interested in understanding the unique bioactive components of EndoECM hydrogels, and in consequence, we focused this study on its protein content. Likely due to the pepsin digestion during decellularization of endometrial tissues, there was a higher percentage of total protein content in EndoECM with respect to DC lyophilized powder. As described herein, enzymatic digestion by proteases can liberate cryptic ECM peptides (also known as matrikines) that have shown to exhibit bioactive properties such as chemotactic activity (Agrawal *et al.* 2011). Even though ECM digestion decreased collagen concentration and removed elastin, the concentration of GAGs was not affected. This is interesting, since GAGs have an enormous importance in the ECM and are key elements in the bioactivity of DC biomaterials (Mullen *et al.* 2010; Kowalczewski and Saul 2018). Surprisingly, PGs were not detected in porcine EndoECM or in No-DC Endo, which contrasts with previous studies of human or rabbit endometrial DC matrices developed from similar decellularization protocols (Olalekan *et al.* 2017; Campo *et al.* 2019). This feature could likely be unique to porcine endometrial tissue rather than a consequence of a harsh decellularization.

We analyzed the proteomic profile of the EndoECM and compared it to those of myometrial and non-decellularized endometrial matrices, MyoECM and No-DC Endo. The unique tissue-specific signatures found in EndoECM and MyoECM proteomic profiles validated the effectiveness of manually microdissecting the endometrium. Furthermore, comparison between EndoECM and No-DC Endo demonstrated the efficacy of decellularization as well as the ECM preservation in EndoECM hydrogels.

Focusing on the EndoECM versus No-DC Endo comparison, we observed half of the No-DC Endo extracellular proteins were removed with decellularization, and consequently

were absent in EndoECM. In contrast, we found certain ECM proteins unique to the EndoECM, probably because the decellularization procedure enriched them in EndoECM and as such, they entered the range of detection of LC-MS/MS. The enriched proteins have specific functions in wound healing, chemotaxis, immune response, and antibacterial properties, and included: dermatopontin (Kim *et al.* 2019a; Okamoto and Fujiwara 2006), azurocidin (Kasus-Jacobi *et al.* 2015; Wiesner and Vilcinskas 2010), fibrinogen (Pieters and Wolberg 2019; Halper and Kjaer 2014), and extracellular kinases (Bordoli *et al.* 2014). On the other hand, we also detected interesting bioactive ECM proteins shared by both matrisomes, including fibronectin (which supports initial attachment of endometrial cells (Cook *et al.* 2017)) and Von Willebrand factor (which binds to growth factors such as PDGFbb and promotes angiogenesis in wound healing (Ishihara *et al.* 2019)). Finally, the EndoECM matrisome also revealed an absence of immunoreactive proteins (such as immunoglobulins, MHC II) and other cellular molecules, which supports our data from earlier experiments regarding removal of cells, DNA and α-gal epitope. Taken together, these findings suggest that EndoECM not only preserves the natural ECM composition of the endometrium, but it may also diminish the probability of immune rejection and potentially function better than endometrial hydrogels obtained without decellularization.

It is important to note that the estrous cycles of pigs whose uteri were used to create the EndoECM hydrogels were not evaluated. Therefore, EndoECM hydrogels may be a heterogeneous mix of ECM molecules belonging to different phases of the pig estrous cycle, and the proteomic profile presented herein could be considered as a baseline.

Endometrial extracellular matrix hydrogels as a platform for three-dimensional culture *in vitro*

As previously stated, one of the main purposes of this thesis was to investigate the potential use of EndoECM as a platform for 3D *in vitro* culture. Our first hypothesis was that EndoECM hydrogels derived from DC porcine endometrium would be biocompatible and suitable for being used with human cells *in vitro.* Whereas our second hypothesis was that EndoECM hydrogels inherently contain endometrial-specific ECM components, which are different from those found in other uterine tissues and influence the behavior of endometrial cells, which could improve current *in vitro* culture approaches.

To test these hypotheses, we first cultured endometrial primary cells and endometrial ICE6-7 stem cell lines (Cervelló *et al.* 2010; 2011) in 2D, 2.5D and 3D *in vitro* cultures using EndoECM at different concentrations and then compared the proliferation rates in EndoECM with two standard matrices (collagen and Matrigel). Since EndoECM hydrogels are mainly composed of collagen, this provided the opportunity to compare purified natural collagen with our tissue-specific mixture. Alternatively, Matrigel was selected for being a popular non-tissue-specific basement membrane preparation rich in ECM components, growth factors and other bioactive proteins (Kleinman *et al.* 1982; 1986; Vukicevic *et al.* 1992), and comparison to the EndoECM would elucidate whether this hydrogel could equally support or improve cell growth. We detected no differences in cell proliferation when EndoECM was used as coatings, confirming cytocompatibility. Meanwhile, EndoECM significant increased proliferation in 2.5D and 3D systems, especially with endometrial stem cell lines, demonstrating the beneficial effect of EndoECM hydrogels.

The improvement of cell growth by ECM hydrogels can be attributed to their biochemical signaling, mechanical contribution or a combination of both (Stanton, Tong, and Yang

2019). In fact, several studies reported that the substrates stiffness affects stem cell differentiation and proliferation (Zhao *et al.* 2014b; Engler *et al.* 2006; Gerardo *et al.* 2019). Although the improvement of cell growth in ECM hydrogels is usually attributed to its tissue-specific properties (Fercana *et al.* 2017; Pouliot *et al.* 2016), there is a possibility that other non-tissue-specific ECM hydrogels yield similar effects and future studies are required to elucidate this. Finally, although we did not find differences in cell proliferation using the coating system, the possible influence of EndoECM in specific endometrial cell functions remains unexplored. Other studies from our group, of surfaces coated with tissue-specific ECM hydrogels from the fallopian tubes (Francés-Herrero *et al.*, 2021) and the endometrium itself (Campo *et al.*, 2019), have recently reported coating surfaces potentially enhanced the growth of rabbit embryos.

The next objective was to bioengineer the classic architecture of the human endometrium by encapsulating stromal cells within EndoECM and covering it with epithelial cells. For this experiment, we did not supplement the EndoECM or culture media (with exogenous hormones) to examine the inherent impact of the tissue-specific ECM on endometrial cell survival, growth and morphology. Our findings showed that both stem cell lines and primary endometrial constructs remained viable at long-term, and they were rapidly remodeled by endometrial cells. The compaction of EndoECM observed was the result of the degeneration and contraction of collagen-based ECM hydrogels interacting with fibroblast-like cells, a common phenomenon observed *in vitro* (Grinnell 2003). When comparing seeding strategies for co-culture of endometrial cells (result section 2.2) sequential introduction of stromal and then epithelial cells produced better results than introducing all the cells on the same day. This is probably due to the lower initial cell concentration reducing cell stress and ultimately degradation of the matrix. In contrast to previous publications (Wang *et al.* 2012), our endometrial constructs (created using

stromal and epithelial cells from stem cell lines (ICE6-7) or primary endometrial cells (EECs-ESCs)) presented low E-cadherin expression on cell membranes and no apical polarization. This could likely be due to a lack of hormonal stimulation. Future analyses with hormone-supplemented culture media could improve epithelial differentiation and polarization required to achieve a more natural endometrial epithelium organization.

In the next part of the study, we investigated the use of EndoECM hydrogels as support for endometrial organoid culture, with the aim to enhance the microenvironmental conditions currently provided by Matrigel. For this purpose, we first established an endometrial organoid line (from human endometrium) which was able to (1) self-organize in every passage, (2) display an epithelial phenotype, and (3) maintain a stable genotype until senescence. These three typical organoid features have been reported in recent publications (Turco *et al.* 2017; Boretto *et al.* 2017). Our results demonstrated that pure EndoECM could not successfully support endometrial organoid culture like Matrigel: the EndoECM was rapidly degraded, and organoids fused together, creating a centimeter-long floating mesh composed of tubular-like structures in the expansion media. Notably, a similar phenomenon was recently described in intestinal epithelial organoids, who self-organized into centimeter-long tubes in floating collagen gels, which were also degraded (Sachs *et al.* 2017). Moreover, these intestinal organoids physically aligned themselves and fused to generate macroscopic hollow structures, which were lined by a simple epithelium containing all major cell types of the small intestine (including functional stem cells). Since the structures described by Sachs *et al.* are similar to the meshes formed by our endometrial organoids in EndoECM, the potential ability of our endometrial organoids to self-organize and differentiate may be hidden by the apparent failure to support endometrial organoid development. Future studies may help elucidate this hypothesis.

Endometrial extracellular matrix hydrogels as a regenerative treatment for reproductive pathologies *in vivo*

Tissue-specific ECM hydrogels features (such as injectability, degradability, biocompatibility and bioactivity) facilitate their translatability and make hydrogel use promising for many specialties of regenerative medicine. In particular, our results showed that EndoECM minimizes the risk of immune rejection *in vivo* and support its use as biocompatible xenogeneic treatment. Additionally, EndoECM inherently contain bioactive components that could enhance endometrial tissue repair, providing a novel regenerative treatment for endometrial pathologies like EA and AS.

The *in vivo* biocompatibility of EndoECM hydrogels was tested in a proof-of-concept experiment using inbred immunocompetent C57BL/6 mice. These mice are commonly used in research, since they are genetically identical, have uniformly inherited characteristics and are free of genetic differences that could impact the response to experimental treatments. Firstly, the injectability and spontaneous *in vivo* gelation of the endometrial-derived hydrogels were verified by subcutaneously injecting the matrix solution. Secondly, as the main concern regarding the biocompatibility of DC biomaterials is the possible presence of cell debris and toxins (e.g., detergents) (Naahidi *et al.* 2017; Keane, Swinehart, and Badylak 2015; Lee *et al.* 2014; Chakraborty, Roy, and Ghosh 2020), we evaluated the overall recipient response to EndoECM hydrogels, to determine its potential short-term toxicity. EndoECM showed a first a mild infiltration of inflammatory cells accompanied by a significant increase in macrophages in comparison to No-DC Endo. Remarkably, after 14 days, cell infiltrates shifted from inflammatory-like cells toward endogenous fibroblast-like cells, demonstrating the repopulation of EndoECM hydrogels *in vivo*. Altogether these findings corroborate previous studies evaluating subcutaneous biocompatibility of DC ECM (Keane *et al.* 2013; Farnebo *et al.*

2014; Porzionato *et al.* 2015; Wua *et al.* 2015; Sackett *et al.* 2018; Zhao, Fan, and Bai 2019) where similar macrophage infiltration was also evidenced (Farnebo *et al.* 2014; Sackett *et al.* 2018; Fercana *et al.* 2017; Seo, Jung, and Kim 2018; Zhao, Fan, and Bai 2019). As previously described herein, macrophages are phagocytic cells that regulate the progression of inflammatory events in tissue repair and play a vital role in the remodeling of degradable ECM biomaterials (Badylak and Gilbert 2008; Brown *et al.* 2012; Scanameo and Ziats 2019). Interestingly, we observed the recipient's immune response degraded the EndoECM over time, and this degradation could potentially promote the reconstruction of native tissue (Wua *et al.* 2015; Naahidi *et al.* 2017; dos Santos *et al.* 2019).

Finally, we examined the potential of EndoECM to repair damaged endometrium and restore fertility, to corroborate the putative effects of tissue-specific ECM. In order to do this, we first needed to create a murine model with AS-like endometrial damage. After an extensive review of available literature, we discovered several methods or materials used to produce endometrial destruction, adherences and fibrosis: scraping (Cervelló *et al.* 2015; Ersoy *et al.* 2017; Gan *et al.* 2017; Alawadhi *et al.* 2014; Chen *et al.* 2019; Jun *et al.* 2019; Xin *et al.* 2019; Ouyang *et al.* 2020), electrocoagulation (Liu *et al.* 2019), trichloroacetic acid (Kilic *et al.* 2014), phenol mucilage (Wang *et al.* 2017), hot water (Gao *et al.* 2019) and ethanol (Jang *et al.* 2017; Domnina *et al.* 2018; Kim *et al.* 2019b; Kim *et al.* 2019c). We ultimately chose ethanol to induce damage because it produces middle-to-severe endometrial injury, and could distribute itself homogeneously along the murine uterine horn(s) (Kim *et al.* 2019b). Our results confirm that, ethanol does produce evident (macroscopic) damage to the uterine horn, and more importantly, significantly reduces fertility without interrupting ovarian function. Although estrous cyclicity was maintained until the end of the experiment, we observed an increase in the duration of

each estrous cycle (approximately 7 days per cycle) and extended estrous phases. Although the combination of longer estrous cycles and reduced fertility may seem counterintuitive, housing female mice without males is known to prolong estrous cycles duration from 4-5 days to 5-7 days. This phenomenon is known as Lee–Boot effect, and can even lead to anestrus when female mice housed together are large groups (Ma, Miao, and Novotny 1998).

To be able to track the EndoECM hydrogels *in utero*, we stained them with biotin. Biotin is a small (244Da) vitamin that irreversibly binds to streptavidin proteins (in one of the strongest natural noncovalent interactions) and can be conjugated to many proteins without altering their biological activities. The tracking of biotin-labelled tissue-specific ECM hydrogels from placenta, heart and muscle has previously been reported up to two weeks post-treatment (Francis *et al.* 2017; Singelyn *et al.* 2012; DeQuach *et al.* 2012). After two weeks *in vivo*, our hydrogels were no longer visible in the uterine lumen but biotin signals emerged within the uterus tissues, co-localized with extracellular collagen. These finding suggest the EndoECM hydrogel was possibly absorbed from uterine lumen through the endometrium, to the outer layers of the uterus, ultimately forming a new uterine ECM. Interestingly, (Francis *et al.* 2017) also reported the presence of biotin-labelled ECM in the interstitial space of injected ventricles and co-localization of collagen, 1 h after delivery in live rats.

To study endometrial regeneration after damage in our murine model, we analyzed endometrial thickness, gland concentration, collagen deposition and endometrial cell proliferation. Since the stage of the estrous cycle is known to influence these parameters, and we found lack of synchronization of the cycle among the mice being studied, the data from each mouse's damaged/treated horn was normalized to its respective non-damaged horn. We consequently found that treating damaged uterine horns with saline slightly

reduced endometrial thickness, gland concentration and cell proliferation with respect to non-damaged uterus, confirming the horns were still damaged after 14 days. It is important to note that, in this case, the absence of statistical significance between damaged and non-damaged uterus could be a consequence of the extraordinary speed of tissue regeneration in the murine uteri *per se*. In contrast, when treating the endometrial damage with EndoECM, we found a positive shift compared to saline. Regeneration was further improved when the EndoECM was supplemented with growth factors (IGF-1, bFGF and PDGFbb), which produced a significant increase in endometrial proliferation with respect to saline.

Fibrosis, or the accumulation of excess ECM (mainly collagen), is a common pathological outcome of many chronic inflammatory diseases and affects nearly every tissue in the body. Although collagen deposition is an indispensable and (typically) reversible part of wound healing, normal tissue repair can evolve into a progressively irreversible fibrotic response if the tissue injury is severe/chronic or if the wound-healing response itself becomes dysregulated (Wynn and Ramalingam 2012). In endometrial pathologies, severe endometrial damage is usually related to dysregulated fibrosis events. In these cases, the reduction of collagen deposition can be indicative of endometrial tissue repair, and is constantly used to evaluate the effectiveness of treatments (Lin *et al.* 2021; Yang *et al.* 2017; Alawadhi *et al.* 2014; Kilic *et al.* 2014; Cervelló *et al.* 2015; Gan *et al.* 2017; Jang *et al.* 2017; Ersoy *et al.* 2017; Domnina *et al.* 2018; Chen *et al.* 2019; Gao *et al.* 2019; Jun *et al.* 2019; Xin *et al.* 2019; Ouyang *et al.* 2020). Because EndoECM treatments principally consist of collagen, endometrial collagen increases must be carefully interpreted to differentiate pathological deposition of collagen from a fibrotic event (in this case, tissue repair after ethanol damage) or uterine absorption of the hydrogel. When we analyzed histological sections by immunohistochemistry, collagen deposits were

similar between saline and EndoECM treatments. However, collagen transcription was clearly reduced in EndoECM with respect to saline by RT-qPCR analysis, suggesting that treatments with EndoECM may reduce the endometrial fibrosis. Notably, fibrosis was statistically reduced when EndoECM was supplemented with growth factors.

The ultimate test to evaluate the regenerative potential of any treatment for endometrial damage is to assess fertility restoration. In our murine model of endometrial damage, injury produced by ethanol drastically diminished pregnancy rate (as demonstrated by the statistically significant difference between saline control treatment and non-damaged groups). Although our EndoECM alone was unable to counteract the substantial injury produced in the endometrium, growth factor supplemented EndoECM was able to considerably restore fertility.

As previously described herein, ECM fibers have the ability of sequester biomolecules such as growth factors, prolonging their life and controlling their action. For example, hydrogels (including our EndoECM) that contain Von Willebrand factor are able to bind to PDGFbb and act as a reservoir of this growth factor (Ishihara *et al.* 2019). Meanwhile, the supplementation of a tissue-specific ECM hydrogel with IGF-1, bFGF and PDGFbb (using the same concentrations we used in this study) can promote proliferation of adipose-derived stem cells (Farnebo *et al.* 2017).

Growth factors, such as IGF-1, bFGF and PDGFbb, are involved in tissue repair and their use is being exploited in regenerative medicine. IGF has functions related to cell proliferation, differentiation, and survival, while FGF promotes the growth of fibroblasts and endothelial cells during wound healing (Yin *et al.* 2020; Schultz and Wysocki 2009). On the other hand, PDGFbb promotes chemotaxis, mitogenesis and angiogenesis (Evrova and Buschmann 2017). Interestingly, IGF and PDGFbb are usually involved in the increase of ECM collagen (Yin *et al.* 2020; Schultz and Wysocki 2009; Evrova and

Buschmann 2017), however our results contradicted this. Furthermore, growth factors (including IGF, bFGF and PDGFbb) secreted by platelets after injury play important roles in the therapeutic effects of platelet-rich plasma (PRP) currently used to treat various traumas (Evrova and Buschmann 2017). Specifically, PRP treatment enhances cell proliferation, reduces fibrosis, and even increases implantation sites in injured endometrium (de Miguel–Gómez *et al.* 2020; Kim *et al.* 2020; Jang *et al.* 2017).

Collectively, our results suggest that supplementation with IGF-1, bFGF and PDGFbb increases the therapeutic effect of EndoECM, in terms of endometrial regeneration and restoration of fertility in a murine model with endometrial injury. EndoECM may act as a vehicle for these growth factors, enabling their sequestration and slowing their release, which ultimately increases their therapeutic potential.

Future perspectives and applications of endometrial extracellular matrix hydrogels in regenerative medicine

Even though tissue-specific ECM hydrogels have been constructed for most organ systems, their potential in reproductive medicine was largely unexplored until recently. The work presented in the herein thesis elucidates properties and functions of EndoECM use *in vitro* and *in vivo* and provides opportunities for future therapeutic applications in reproductive medicine.

The degradable nature of ECM hydrogels facilitates remodeling by endometrial cells or organoids, which could be interesting when designing some basic studies of the human endometrium. However, this feature may present some issues regarding *in vitro* applications, such as implementing EndoECM as a standard matrix for 3D *in vitro* culture of endometrial cells or organoids. Alternatively, the use of chemical cross-linking of

genipin (Výborný *et al.* 2019) or a semi-synthetic mixture with more stable compounds (Curley *et al.* 2019; Valdez *et al.* 2017) should be explored, to design matrices that are more stable and suitable for long-term culture. Moreover, due to the slow release of growth factors by the ECM fibers and/or the generation of matrikines during enzymatic digestion, EndoECM can potentially be used as a culture media supplement. In particular, it would be valuable to assess the effects of endometrial organoid expansion media supplementation with EndoECM in future experiments. Organoids are an extraordinary *ex vivo* models that mimic features of the natural tissue *in vitro*, and they have a huge potential for use in research of endometrium, as was the case with the herein thesis.

Nowadays, an important part of the efforts in regenerative medicine research are focused on applications of cell therapy. In reproductive medicine in particular, cell therapy has demonstrated its effectiveness in treating endometrial pathologies (Azizi *et al.* 2018). Nevertheless, clinical use is prevented by the possible biological risks associated with introducing living cells, such as the development of tumors (for induced pluripotent cells (iPSCs) or embryonic stem cells) and low retention in the injured area (probably due to the lack of resources in the ECM of the damaged tissue). Alternatively, the use of treatments consisting of non-living cells are an attractive substitute for cell therapy. For example, the combination of EndoECM with PRP, specific proteins or purified growth factors (such as the ones included in this study) could provide a synergic therapeutic effect and could be a suitable solution to treat endometrial pathologies such as EA and AS in the future.

VIII. CONCLUSIONS

VIII. CONCLUSIONS

The following conclusions can be drawn from this thesis:

1. Whole uterus decellularization, and the posterior processing of isolated endometrial tissue, permits the generation of endometrial extracellular matrix hydrogels with porcine origin, which maintains three-dimensional structure and displays the physicochemical features of tissue-specific extracellular matrix hydrogels.

2. Endometrial extracellular matrix hydrogels are purified mixtures of bioactive and structural components from natural endometrial extracellular matrix and contain few potentially immunoreactive molecules.

3. Porcine or non-human extracellular matrix hydrogels are biocompatible with human endometrial cells *in vitro*, support cell growth and improve the cell proliferation of endometrial stem cell lines compared to commercial collagen and Matrigel matrices in three-dimensional culture systems.

4. Endometrial cells co-cultured in three-dimensional endometrial extracellular matrix hydrogels are viable, proliferate at long-term, and able to degrade and remodel this hydrogel.

5. Subcutaneously injected endometrial extracellular matrix hydrogels minimize acute immune responses *in vivo* in a murine model, compared to non-decellularized endometrial hydrogels.

6. Although endometrial extracellular matrix hydrogels alone slightly improve tissular endometrial regeneration, they were not able to restore fertility in a murine model for endometrial damage.

7. Supplementation of endometrial extracellular matrix hydrogels with basic fibroblast growth factor, platelet-derived growth factor-BB and insulin-like growth factor-1 improves endometrial regeneration and restores fertility in a murine model of endometrial damage (not statistically significant).

REFERENCES

REFERENCES

Young, Adam D., Vaibhav Bajaj, and Karen L. Christman. 2014. "Award Winner for Outstanding Research in the PhD Category, 2014 Society for Biomaterials Annual Meeting and Exposition, Denver, Colorado, April 16-19, 2014: Decellularized Adipose Matrix Hydrogels Stimulate *in vivo* Neovascularization and Adipose Formation." *Journal of Biomedical Materials Research - Part A* 102 (6): 1641–51. https://doi.org/10.1002/jbm.a.35109.

Agrawal, Vineet, Stephen Tottey, Scott A. Johnson, John M. Freund, Bernard F. Siu, and Stephen F. Badylak. 2011. "Recruitment of Progenitor Cells by an Extracellular Matrix Cryptic Peptide in a Mouse Model of Digit Amputation." *Tissue Engineering - Part A* 17 (19–20): 2435–43. https://doi.org/10.1089/ten.tea.2011.0036.

Alawadhi, Feryal, Hongling Du, Hakan Cakmak, and Hugh S Taylor. 2014. "Bone Marrow-Derived Stem Cell (BMDSC) Transplantation Improves Fertility in a Murine Model of Asherman ' s Syndrome" 9 (5): 1–6. https://doi.org/10.1371/journal.pone.0096662.

Albamonte, Mirta S., Miguel A. Willis, María I. Albamonte, Federico Jensen, María B. Espinosa, and Alfredo D. Vitullo. 2008. "The Developing Human Ovary: Immunohistochemical Analysis of Germ-Cell-Specific VASA Protein, BCL-2/BAX Expression Balance and Apoptosis." *Human Reproduction* 23 (8): 1895–1901. https://doi.org/10.1093/humrep/den197.

Azizi, Ramyar, Leili Aghebati-Maleki, Mohammad Nouri, Faroogh Marofi, Sohrab Negargar, and Mehdi Yousefi. 2018. "Stem Cell Therapy in Asherman Syndrome and Thin Endometrium: Stem Cell- Based Therapy." *Biomedicine and Pharmacotherapy*. Elsevier Masson SAS. https://doi.org/10.1016/j.biopha.2018.03.091.

Badylak, Stephen F., and Thomas W. Gilbert. 2008. "Immune Response to Biologic Scaffold Materials." *Seminars in Immunology*. NIH Public Access. https://doi.org/10.1016/j.smim.2007.11.003.

Badylak, Stephen F., Doris Taylor, and Korkut Uygun. 2011. "Whole-Organ Tissue Engineering: Decellularization and Recellularization of Three-Dimensional Matrix Scaffolds." *Annual Review of Biomedical Engineering* 13 (1): 27–53. https://doi.org/10.1146/annurev-bioeng-071910-124743.

Bahram, Morteza, Naimeh Mohseni, and Mehdi Moghtader. 2016. "An Introduction to Hydrogels and Some Recent Applications." In *Emerging Concepts in Analysis and Applications of Hydrogels*. InTech. https://doi.org/10.5772/64301.

Bankhead, Peter, Maurice B. Loughrey, José A. Fernández, Yvonne Dombrowski, Darragh G. McArt, Philip D. Dunne, Stephen McQuaid, *et al.* 2017. "QuPath: Open Source Software for Digital Pathology Image Analysis." *Scientific Reports* 7 (1): 1–7. https://doi.org/10.1038/s41598-017-17204-5.

Bentin-Ley, Ursula, T Horn, A Sjögren, Steen Sorensen, J Falck Larsen, and L Hamberger. 2000. "Ultrastructure of Human Blastocyst-Endometrial Interactions *in vitro*." *Journal of Reproduction and Fertility* 120: 337–50. https://doi.org/10.1530/reprod/120.2.337.

REFERENCES

Bi, Huanjing, Kaiming Ye, and Sha Jin. 2020. "Proteomic Analysis of Decellularized Pancreatic Matrix Identifies Collagen V as a Critical Regulator for Islet Organogenesis from Human Pluripotent Stem Cells." *Biomaterials* 233 (March): 119673. https://doi.org/10.1016/j.biomaterials.2019.119673.

Bordoli, Mattia R., Jina Yum, Susanne B. Breitkopf, Jonathan N. Thon, Joseph E. Italiano, Junyu Xiao, Carolyn Worby, *et al.* 2014. "A Secreted Tyrosine Kinase Acts in the Extracellular Environment." *Cell* 158 (5): 1033–44. https://doi.org/10.1016/j.cell.2014.06.048.

Boretto, Matteo, Benoit Cox, Manuel Noben, Nikolai Hendriks, Amelie Fassbender, Heleen Roose, Frederic Amant, *et al.* 2017. "Development of Organoids from Mouse and Human Endometrium Showing Endometrial Epithelium Physiology and Long-Term Expandability." *Development (Cambridge)* 144 (10): 1775–86. https://doi.org/10.1242/dev.148478.

Boretto, Matteo, Nina Maenhoudt, Xinlong Luo, Aurélie Hennes, Bram Boeckx, Bich Bui, Ruben Heremans, *et al.* 2019. "Patient-Derived Organoids from Endometrial Disease Capture Clinical Heterogeneity and Are Amenable to Drug Screening." *Nature Cell Biology* 21 (8): 1041–51. https://doi.org/10.1038/s41556-019-0360-z.

Brännström, Mats, Liza Johannesson, Hans Bokström, Niclas Kvarnström, Johan Mölne, Pernilla Dahm-Kähler, Anders Enskog, *et al.* 2015. "Livebirth after Uterus Transplantation." *The Lancet* 385 (9968): 607–16. https://doi.org/10.1016/S0140-6736(14)61728-1.

Bronson, Franklin H., Charles P. Dagg, and George D. Snell. 1966. "Reproduction" in *Biology of the laboratory mouse* (Second revised edition) by the staff of The Jackson Laboratory in 2007), edited by Earl L. Bar Harbor, Baine 2007.

Brown, Bryan N., Michael J. Buckenmeyer, and Travis A. Prest. 2017. "Preparation of Decellularized Biological Scaffolds for 3D Cell Culture." In *Methods in Molecular Biology*, 1612:15–27. Humana Press Inc. https://doi.org/10.1007/978-1-4939-7021-6_2.

Brown, Bryan N., Jolene E. Valentin, Ann M. Stewart-Akers, George P. McCabe, and Stephen F. Badylak. 2009. "Macrophage Phenotype and Remodeling Outcomes in Response to Biologic Scaffolds with and without a Cellular Component." *Biomaterials* 30 (8): 1482–91. https://doi.org/10.1016/j.biomaterials.2008.11.040.

Brown, Bryan N, Ricardo Londono, Stephen Tottey, Li Zhang, Kathryn A Kukla, Matthew T Wolf, Kerry A Daly, Janet E Reing, and Stephen F Badylak. 2012. "Macrophage Phenotype as a Predictor of Constructive Remodeling Following the Implantation of Biologically Derived Surgical Mesh Materials." *Acta Biomaterialia* 8 (3): 978–87. https://doi.org/10.1016/j.actbio.2011.11.031.

Campo, Hannes, Pedro M. Baptista, Nuria López-Pérez, Amparo Faus, Irene Cervelló, and Carlos Simón. 2017. "De- and Recellularization of the Pig Uterus: A Bioengineering Pilot Study." *Biology of Reproduction* 96 (1): 34–45. https://doi.org/10.1095/biolreprod.116.143396.

Campo, Hannes, Ximo García-Domínguez, Sara López-Martínez, Amparo Faus, José S. Vicente Antón, Francisco Marco-Jiménez, and Irene Cervelló. 2019. "Tissue-Specific Decellularized Endometrial Substratum Mimicking Different Physiological Conditions Influences *in vitro* Embryo Development in a Rabbit Model." *Acta Biomaterialia* 89 (April): 126–38. https://doi.org/10.1016/j.actbio.2019.03.004.

Carrascosa, José P., José A. Horcajadas, and Juan M. Moreno-Moya. 2018. "The Molecular Signature of the Endometrial Receptivity: Research and Clinical Application." In *Reproductomics: The -Omics Revolution and Its Impact on Human Reproductive Medicine*, 279–301. Elsevier. https://doi.org/10.1016/B978-0-12-812571-7.00016-2.

Cebotari, Serghei, Igor Tudorache, Thomas Jaekel, Andres Hilfiker, Suzanne Dorfman, Waldemar Ternes, Axel Haverich, and Artur Lichtenberg. 2010. "Detergent Decellularization of Heart Valves for Tissue Engineering: Toxicological Effects of Residual Detergents on Human Endothelial Cells." *Artificial Organs* 34 (3): 206–10. https://doi.org/10.1111/j.1525-1594.2009.00796.x.

Cervelló, Irene, Claudia Gil-Sanchis, Aymara Mas, Francisco Delgado-Rosas, José Antonio Martínez-Conejero, Amparo Galán, Alicia Martínez-Romero, *et al.* 2010. "Human Endometrial Side Population Cells Exhibit Genotypic, Phenotypic and Functional Features of Somatic Stem Cells." *PLoS ONE* 5 (6). https://doi.org/10.1371/journal.pone.0010964.

Cervelló, Irene, Claudia Gil-Sanchis, Xavier Santamaría, Sergio Cabanillas, Ana Díaz, Amparo Faus, Antonio Pellicer, and Carlos Simón. 2015. "Human CD133+ Bone Marrow-Derived Stem Cells Promote Endometrial Proliferation in a Murine Model of Asherman Syndrome." *Fertility and Sterility* 104 (6): 1552-1560.e3. https://doi.org/10.1016/j.fertnstert.2015.08.032.

Cervelló, Irene, Aymara Mas, Claudia Gil-Sanchis, Laura Peris, Amparo Faus, Philippa T. K. Saunders, Hilary O. D. Critchley, and Carlos Simón. 2011. "Reconstruction of Endometrium from Human Endometrial Side Population Cell Lines." *PLoS ONE* 6 (6): e21221. https://doi.org/10.1371/journal.pone.0021221.

Chakraborty, Juhi, Subhadeep Roy, and Sourabh Ghosh. 2020. "Regulation of Decellularized Matrix Mediated Immune Response." *Biomaterials Science*. Royal Society of Chemistry. https://doi.org/10.1039/c9bm01780a.

Chaudhuri, Ovijit, Justin Cooper-White, Paul A. Janmey, David J. Mooney, and Vivek B. Shenoy. 2020. "Effects of Extracellular Matrix Viscoelasticity on Cellular Behaviour." *Nature*. Nature Research. https://doi.org/10.1038/s41586-020-2612-2.

Chen, Xing, Jingtao Sun, Xiaoyu Li, Lele Mao, Yingfang Zhou, Lei Cui, and Wenpei Bai. 2019. "Antifibrotic Effects of Decellularized and Lyophilized Human Amniotic Membrane Transplant on the Formation of Intrauterine Adhesion." *Experimental and Clinical Transplantation* 17 (2): 236–42. https://doi.org/10.6002/ect.2017.0284.

Cook, Christi D, Abby S Hill, Margaret Guo, Linda Stockdale, Julia P Papps, Keith B Isaacson, Douglas A Lauffenburger, and Linda G Griffith. 2017. "Local Remodeling of Synthetic Extracellular Matrix Microenvironments by Co-Cultured Endometrial Epithelial and Stromal Cells Enables Long-Term Dynamic Physiological Function." *Integrative Biology : Quantitative Biosciences from Nano to Macro* 9 (4): 271–89. https://doi.org/10.1039/c6ib00245e.

Crapo, Peter M., Thomas W. Gilbert, and Stephen F. Badylak. 2011. "An Overview of Tissue and Whole Organ Decellularization Processes." *Biomaterials* 32 (12): 3233–43. https://doi.org/10.1016/j.biomaterials.2011.01.057.

Crisan, Mihaela, Solomon Yap, Louis Casteilla, Chien Wen Chen, Mirko Corselli, Tea Soon Park,

REFERENCES

Gabriella Andriolo, *et al.* 2008. "A Perivascular Origin for Mesenchymal Stem Cells in Multiple Human Organs." *Cell Stem Cell* 3 (3): 301–13. https://doi.org/10.1016/j.stem.2008.07.003.

Critchley, Hilary O.D., Jacqueline A. Maybin, Gregory M. Armstrong, and Alistair R.W. Williams. 2020. "Physiology of the Endometrium and Regulation of Menstruation." *Physiological Reviews*. American Physiological Society. https://doi.org/10.1152/physrev.00031.2019.

Curley, Clive J., Eimear B. Dolan, Matthias Otten, Svenja Hinderer, Garry P. Duffy, and Bruce P. Murphy. 2019. "An Injectable Alginate/Extra Cellular Matrix (ECM) Hydrogel towards Acellular Treatment of Heart Failure." *Drug Delivery and Translational Research* 9 (1): 1–13. https://doi.org/10.1007/s13346-018-00601-2.

Daryabari, Seyedeh Sima, Abdol Mohammad Kajbafzadeh, Kiarad Fendereski, Fariba Ghorbani, Mehrshad Dehnavi, Minoo Rostami, Bahram Azizi Garajegayeh, and Seyed Mohammad Tavangar. 2019. "Development of an Efficient Perfusion-Based Protocol for Whole-Organ Decellularization of the Ovine Uterus as a Human-Sized Model and *in vivo* Application of the Bioscaffolds." *Journal of Assisted Reproduction and Genetics* 36 (6): 1211–23. https://doi.org/10.1007/s10815-019-01463-4.

De Miguel–Gómez, Lucía, Hortensia Ferrero, Sara López-Martínez, Hannes Campo, Nuria López-Pérez, Amparo Faus, David Hervás, Xavier Santamaría, Antonio Pellicer, and Irene Cervelló. 2019. "Stem Cell Paracrine Actions in Tissue Regeneration and Potential Therapeutic Effect in Human Endometrium : A Retrospective Study." *BJOG: An International Journal of Obstetrics and Gynecology*, 1–10. https://doi.org/10.1111/1471-0528.16078.

De Miguel–Gómez, Lucía, Sara López-Martínez, Hannes Campo, Emilio Francés-Herrero, Amparo Faus, Ana Díaz, Antonio Pellicer, Francisco Domínguez, and Irene Cervelló. 2020. "Comparison of Different Sources of Platelet-Rich Plasma as Treatment Option for Infertility-Causing Endometrial Pathologies." *Fertility and Sterility* 115 (2). https://doi.org/10.1016/j.fertnstert.2020.07.053.

DeQuach, Jessica A., Joy E. Lin, Cynthia Cam, Diane Hu, Michael A. Salvatore, Farah Sheikh, and Karen L. Christman. 2012. "Injectable Skeletal Muscle Matrix Hydrogel Promotes Neovascularization and Muscle Cell Infiltration in a Hindlimb Ischemia Model." *European Cells and Materials* 23: 400–412. https://doi.org/10.22203/eCM.v023a31.

Ding, Lijun, Xin'an Li, Haixiang Sun, Jing Su, Nacheng Lin, Bruno Péault, Tianran Song, Jun Yang, Jianwu Dai, and Yali Hu. 2014. "Transplantation of Bone Marrow Mesenchymal Stem Cells on Collagen Scaffolds for the Functional Regeneration of Injured Rat Uterus." *Biomaterials* 35 (18): 4888–4900. https://doi.org/10.1016/j.biomaterials.2014.02.046.

Domnina, Alisa, Polina Novikova, Julia Obidina, Irina Fridlyanskaya, Larisa Alekseenko, Irina Kozhukharova, Olga Lyublinskaya, Valeriy Zenin, and Nikolay Nikolsky. 2018. "Human Mesenchymal Stem Cells in Spheroids Improve Fertility in Model Animals with Damaged Endometrium." *Stem Cell Research and Therapy* 9 (1). https://doi.org/10.1186/s13287-018-0801-9.

Dos Santos, Bruno Paiva, Bertrand Garbay, Mathilde Fenelon, Marie Rosselin, Elisabeth Garanger, Sébastien Lecommandoux, Hugo Oliveira, and Joëlle Amédée. 2019.

"Development of a Cell-Free and Growth Factor-Free Hydrogel Capable of Inducing Angiogenesis and Innervation after Subcutaneous Implantation." *Acta Biomaterialia* 99 (November): 154–67. https://doi.org/10.1016/j.actbio.2019.08.028.

Edgar, L., T. Pu, B. Porter, J. M. Aziz, C. La Pointe, A. Asthana, and G. Orlando. 2020. "Regenerative Medicine, Organ Bioengineering and Transplantation." *British Journal of Surgery*. John Wiley and Sons Ltd. https://doi.org/10.1002/bjs.11686.

Efraim, Yael, Hadar Sarig, Noa Cohen Anavy, Udi Sarig, Elio de Berardinis, Su Yin Chaw, Muthukumar Krishnamoorthi, *et al.* 2017. "Biohybrid Cardiac ECM-Based Hydrogels Improve Long Term Cardiac Function Post Myocardial Infarction." *Acta Biomaterialia* 50 (March): 220–33. https://doi.org/10.1016/j.actbio.2016.12.015.

Emami, Asrin, Tahereh Talaei-Khozani, Saeid Tavanafar, Nehleh Zareifard, Negar Azarpira, and Zahra Vojdani. 2020. "Synergic Effects of Decellularized Bone Matrix, Hydroxyapatite, and Extracellular Vesicles on Repairing of the Rabbit Mandibular Bone Defect Model." *Journal of Translational Medicine* 18 (1): 361. https://doi.org/10.1186/s12967-020-02525-3.

Emera, Deena, Roberto Romero, and Günter Wagner. 2012. "The Evolution of Menstruation: A New Model for Genetic Assimilation: Explaining Molecular Origins of Maternal Responses to Fetal Invasiveness." *BioEssays* 34 (1): 26–35. https://doi.org/10.1002/bies.201100099.

Engler, Adam J., Shamik Sen, H. Lee Sweeney, and Dennis E. Discher. 2006. "Matrix Elasticity Directs Stem Cell Lineage Specification." *Cell* 126 (4): 677–89. https://doi.org/10.1016/j.cell.2006.06.044.

Ersoy, Gulcin Sahin, Masoumeh Majidi Zolbin, Emine Cosar, Irene Moridi, Ramanaiah Mamillapalli, and Hugh S. Taylor. 2017. "CXCL12 Promotes Stem Cell Recruitment and Uterine Repair after Injury in Asherman's Syndrome." *Molecular Therapy - Methods and Clinical Development* 4 (March): 169–77. https://doi.org/10.1016/j.omtm.2017.01.001.

Evangelatov, Aleksandar, and Roumen Pankov. 2013. "The Evolution of Three-Dimensional Cell Cultures Towards Unimpeded Regenerative Medicine and Tissue Engineering." In *Regenerative Medicine and Tissue Engineering*. https://doi.org/10.5772/55564.

Evrova, O., and J. Buschmann. 2017. "*In vitro* and *in vivo* Effects of PDGF-BB Delivery Strategies on Tendon Healing: A Review." *European Cells and Materials*. AO Research Institute Davos. https://doi.org/10.22203/eCM.v034a02.

Farnebo, Simon, Lovisa Farnebo, Maxwell Kim, Colin Woon, Hung Pham, and James Chang. 2017. "Optimized Repopulation of Tendon Hydrogel: Synergistic Effects of Growth Factor Combinations and Adipose-Derived Stem Cells." *Hand* 12 (1): 68–77. https://doi.org/10.1177/1558944715628005.

Farnebo, Simon, Colin Y.L. Woon, Taliah Schmitt, Lydia Marie Joubert, Maxwell Kim, Hung Pham, and James Chang. 2014. "Design and Characterization of an Injectable Tendon Hydrogel: A Novel Scaffold for Guided Tissue Regeneration in the Musculoskeletal System." *Tissue Engineering - Part A* 20 (9–10): 1550–61. https://doi.org/10.1089/ten.tea.2013.0207.

Fayazi, Mehri, Mojdeh Salehnia, and Saeideh Ziaei. 2017. "In-Vitro Construction of Endometrial-like Epithelium Using CD146+ Mesenchymal Cells Derived from Human Endometrium." *Reproductive BioMedicine Online* 35 (3): 241–52.

REFERENCES

https://doi.org/10.1016/j.rbmo.2017.05.020.

Fercana, George R., Saigopalakrishna Yerneni, Marie Billaud, Jennifer C. Hill, Paul VanRyzin, Tara D. Richards, Brian M. Sicari, *et al.* 2017. "Perivascular Extracellular Matrix Hydrogels Mimic Native Matrix Microarchitecture and Promote Angiogenesis via Basic Fibroblast Growth Factor." *Biomaterials* 123 (April): 142–54. https://doi.org/10.1016/j.biomaterials.2017.01.037.

Francés-Herrero, Emilio, Lucía De Miguel-Gómez, Sara López-Martínez, Hannes Campo, Ximo Garcia-Dominguez, Gianfranco Diretto, Amparo Faus, José S. Vicente, Francisco Marco-Jiménez, and Irene Cervelló. 2021. "Development of Decellularized Oviductal Hydrogels as a Support for Rabbit Embryo Culture." *Reproductive Sciences*. https://doi.org/10.1007/s43032-020-00446-6.

Francis, Michael P., Erick Breathwaite, Anna A. Bulysheva, Frency Varghese, Rudy U. Rodriguez, Sucharita Dutta, Iurii Semenov, *et al.* 2017. "Human Placenta Hydrogel Reduces Scarring in a Rat Model of Cardiac Ischemia and Enhances Cardiomyocyte and Stem Cell Cultures." *Acta Biomaterialia* 52 (April): 92–104. https://doi.org/10.1016/j.actbio.2016.12.027.

Francisco, Jairo Silva, Heleno Pinto de Moraes, and Eliane Pedra Dias. 2004. "Evaluation of the Image-Pro Plus 4.5 Software for Automatic Counting of Labeled Nuclei by PCNA Immunohistochemistry." *Pesquisa Odontológica Brasileira = Brazilian Oral Research* 18 (2): 100–104. https://doi.org/10.1590/s1806-83242004000200002.

Frantz, Christian, Kathleen M. Stewart, and Valerie M. Weaver. 2010. "The Extracellular Matrix at a Glance." *Journal of Cell Science*. The Company of Biologists Ltd. https://doi.org/10.1242/jcs.023820.

Freytes, Donald O., Jeffrey Martin, Sachin S. Velankar, Annie S. Lee, and Stephen F. Badylak. 2008. "Preparation and Rheological Characterization of a Gel Form of the Porcine Urinary Bladder Matrix." *Biomaterials* 29 (11): 1630–37. https://doi.org/10.1016/j.biomaterials.2007.12.014.

Gan, Lu, Hua Duan, Qian Xu, Yi Qun Tang, Jin Jiao Li, Fu Qing Sun, and Sha Wang. 2017. "Human Amniotic Mesenchymal Stromal Cell Transplantation Improves Endometrial Regeneration in Rodent Models of Intrauterine Adhesions." *Cytotherapy* 19 (5): 603–16. https://doi.org/10.1016/j.jcyt.2017.02.003.

Gao, Lufen, Zhongwei Huang, Haiyingjie Lin, Yuke Tian, Ping Li, and Shaoqiang Lin. 2019. "Bone Marrow Mesenchymal Stem Cells (BMSCs) Restore Functional Endometrium in the Rat Model for Severe Asherman Syndrome." *Reproductive Sciences* 26 (3): 436–44. https://doi.org/10.1177/1933719118799201.

Gargett, Caroline E., Kjiana E. Schwab, and James A. Deane. 2016. "Endometrial Stem/Progenitor Cells: The First 10 Years." *Human Reproduction Update*. Oxford University Press. https://doi.org/10.1093/humupd/dmv051.

Gerardo, Heloísa, Ana Lima, João Carvalho, João R.D. Ramos, Sofia Couceiro, Rui D.M. Travasso, Ricardo Pires das Neves, and Mário Grãos. 2019. "Soft Culture Substrates Favor Stem-like Cellular Phenotype and Facilitate Reprogramming of Human Mesenchymal Stem/Stromal Cells (HMSCs) through Mechanotransduction." *Scientific Reports* 9 (1).

https://doi.org/10.1038/s41598-019-45352-3.

Gil-Sanchis, Claudia, Irene Cervelló, Satish Khurana, Amparo Faus, Catherine Verfaillie, and Carlos Simón. 2015. "Contribution of Different Bone Marrow-Derived Cell Types in Endometrial Regeneration Using an Irradiated Murine Model." *Fertility and Sterility* 103 (6): 1596-1605.e1. https://doi.org/10.1016/j.fertnstert.2015.02.030.

Grinnell, Frederick. 2003. "Fibroblast Biology in Three-Dimensional Collagen Matrices." *Trends in Cell Biology*. Elsevier Ltd. https://doi.org/10.1016/S0962-8924(03)00057-6.

Guzmán López, Santos, Abel Guzmán López. 2014. "Anatomía Del Aparato Genital Femenino." in *Tratado de Ginecología y Obstetricia*, edited by Lluís Cabero Roura. (1): 169-76. https://uv.primo.exlibrisgroup.com/discovery/openurl?institution=34CVA_UV&vid=34C VA_UV:VU1&rft.epage=176&rft.volume=1&rfr_id=info:sid%2Fdialnet:articulos&rft.isb n=978-84-9835-268- 9&rft.btitle=Tratado%20de%20ginecolog%C3%ADa%20y%20obstetricia&rft.aufirst=Llu %C3%ADs&rft.genre=journal&rft.aulast=Cabero%20Roura&url_ver=Z39.88- 2004&rft.date=2014&rft.spage=169&%3Frft_val_fmt=info:ofi%2Ffmt:kev:mtx:journal&r ft.atitle=Anatom%C3%ADa%20del%20aparato%20genital%20femenino&rft.title=Tratad o%20de%20ginecolog%C3%ADa%20y%20obstetricia.

Haahr, Mads. 2021. "RANDOM.ORG: True Random Number Service. [ONLINE]." Randomness and Integrity Services Ltd. https://www.random.org.

Halper, Jaroslava, and Michael Kjaer. 2014. "Basic Components of Connective Tissues and Extracellular Matrix: Elastin, Fibrillin, Fibulins, Fibrinogen, Fibronectin, Laminin, Tenascins and Thrombospondins." In *Advances in Experimental Medicine and Biology*, 31–47. Springer, Dordrecht. https://doi.org/10.1007/978-94-007-7893-1_3.

Hartshorne, G.M., S. Lyrakou, H. Hamoda, E. Oloto, and F. Ghafari. 2009. "Oogenesis and Cell Death in Human Prenatal Ovaries: What Are the Criteria for Oocyte Selection?" *Molecular Human Reproduction* 15 (12): 805–19. https://doi.org/10.1093/MOLEHR/GAP055.

Hellström, M., R. R. El-Akouri, C. Sihlbom, B. M. Olsson, J. Lengqvist, H. Bäckdahl, B. R. Johansson, M. Olausson, S. Sumitran-Holgersson, and M. Brännström. 2014. "Towards the Development of a Bioengineered Uterus: Comparison of Different Protocols for Rat Uterus Decellularization." *Acta Biomaterialia* 10 (12): 5034–42. https://doi.org/10.1016/j.actbio.2014.08.018.

Hellström, Mats, Juan M Moreno-Moya, Sara Bandstein, Eva Bom, Randa R Akouri, Kaoru Miyazaki, Tetsuo Maruyama, and Mats Brännström. 2016. "Bioengineered Uterine Tissue Supports Pregnancy in a Rat Model." *Fertility and Sterility* 106 (2): 487-496.e1. https://doi.org/10.1016/j.fertnstert.2016.03.048.

Hernandez, Melissa J., Emma I. Zelus, Martin T. Spang, Rebecca L. Braden, and Karen L. Christman. 2020. "Dose Optimization of Decellularized Skeletal Muscle Extracellular Matrix Hydrogels for Improving Perfusion and Subsequent Validation in an Aged Hindlimb Ischemia Model." *Biomaterials Science* 8 (12): 3511–21. https://doi.org/10.1039/c9bm01963d.

Hiraoka, Takehiro, Yasushi Hirota, Tomoko Saito-Fujita, Mitsunori Matsuo, Mahiro Egashira, Leona Matsumoto, Hirofumi Haraguchi, *et al.* 2016. "STAT3 Accelerates Uterine Epithelial

REFERENCES

Regeneration in a Mouse Model of Decellularized Uterine Matrix Transplantation." *JCI Insight* 1 (8): 1–14. https://doi.org/10.1172/jci.insight.87591.

Hodge, Kelly, Sara Ten Have, Luke Hutton, and Angus I. Lamond. 2013. "Cleaning up the Masses: Exclusion Lists to Reduce Contamination with HPLC-MS/MS." *Journal of Proteomics* 88 (November): 92–103. https://doi.org/10.1016/j.jprot.2013.02.023.

Hoshiba, Takashi, Guoping Chen, Chiho Endo, Hiroka Maruyama, Miyuki Wakui, Eri Nemoto, Naoki Kawazoe, and Masaru Tanaka. 2016. "Decellularized Extracellular Matrix as an *in vitro* Model to Study the Comprehensive Roles of the ECM in Stem Cell Differentiation." *Stem Cells International* 2016. https://doi.org/10.1155/2016/6397820.

Huch, Meritxell, Paola Bonfanti, Sylvia F. Boj, Toshiro Sato, Cindy J.M. Loomans, Marc Van De Wetering, Mozhdeh Sojoodi, *et al.* 2013. "Unlimited *in vitro* Expansion of Adult Bi-Potent Pancreas Progenitors through the Lgr5/R-Spondin Axis." *EMBO Journal* 32 (20): 2708–21. https://doi.org/10.1038/emboj.2013.204.

Huch, Meritxell, Helmuth Gehart, Ruben van Boxtel, Karien Hamer, Francis Blokzijl, Monique M A Verstegen, Ewa Ellis, *et al.* 2015. "Long-Term Culture of Genome-Stable Bipotent Stem Cells from Adult Human Liver." *Cell* 160 (1–2): 299–312. https://doi.org/10.1016/j.cell.2014.11.050.

Hur, Christine, Jenna Rehmer, Rebecca Flyckt, and Tommaso Falcone. 2019. "Uterine Factor Infertility: A Clinical Review." *Clinical Obstetrics and Gynecology* 62 (2): 257–70. https://doi.org/10.1097/GRF.0000000000000448.

Hussein, Kamal H., Kyung Mee Park, Lina Yu, Ho Hyun Kwak, and Heung Myong Woo. 2020. "Decellularized Hepatic Extracellular Matrix Hydrogel Attenuates Hepatic Stellate Cell Activation and Liver Fibrosis." *Materials Science and Engineering C* 116 (November): 111160. https://doi.org/10.1016/j.msec.2020.111160.

Hynes, Richard O. 2012. "The Evolution of Metazoan Extracellular Matrix." *Journal of Cell Biology*. The Rockefeller University Press. https://doi.org/10.1083/jcb.201109041.

Hynes, Richard O., and Alexandra Naba. 2012. "Overview of the Matrisome-An Inventory of Extracellular Matrix Constituents and Functions." *Cold Spring Harbor Perspectives in Biology* 4 (1). https://doi.org/10.1101/cshperspect.a004903.

Ishihara, Jun, Ako Ishihara, Richard D. Starke, Claire R. Peghaire, Koval E. Smith, Thomas A.J. McKinnon, Yoji Tabata, *et al.* 2019. "The Heparin Binding Domain of von Willebrand Factor Binds to Growth Factors and Promotes Angiogenesis in Wound Healing." *Blood* 133 (24): 2559–69. https://doi.org/10.1182/blood.2019000510.

Jang, Hang Yong, Soo Min Myoung, Jeong Min Choe, Tak Kim, Yong Pil Cheon, Yong Min Kim, and Hyuntae Park. 2017. "Effects of Autologous Platelet-Rich Plasma on Regeneration of Damaged Endometrium in Female Rats." *Yonsei Medical Journal* 58 (6): 1195–1203. https://doi.org/10.3349/ymj.2017.58.6.1195.

Johnson, Todd D., Jessica A. Dequach, Roberto Gaetani, Jessica Ungerleider, Dean Elhag, Vishal Nigam, Atta Behfar, and Karen L. Christman. 2014. "Human versus Porcine Tissue Sourcing for an Injectable Myocardial Matrix Hydrogel." *Biomaterials Science* 2 (5): 735–44. https://doi.org/10.1039/c3bm60283d.

Jones, Richard E, and Kristin H Lopez. 2014. "Chapter 2 - The Female Reproductive System." In *Human Reproductive Biology* (Fourth Edition), edited by Richard E Jones and Kristin H Lopez, 23–50. San Diego: Academic Press. https://doi.org/https://doi.org/10.1016/B978-0-12-382184-3.00002-7.

Jun, Sung Min, Mira Park, Ji Yoon Lee, Sookyung Jung, Jeoung Eun Lee, Sung Han Shim, Haengseok Song, and Dong Ryul Lee. 2019. "Single Cell-Derived Clonally Expanded Mesenchymal Progenitor Cells from Somatic Cell Nuclear Transfer-Derived Pluripotent Stem Cells Ameliorate the Endometrial Function in the Uterus of a Murine Model with Asherman's Syndrome." *Cell Proliferation* 52 (3). https://doi.org/10.1111/cpr.12597.

Kaloglu, Celal, and Bilge Onarlioglu. 2010. "Extracellular Matrix Remodelling in Rat Endometrium during Early Pregnancy: The Role of Fibronectin and Laminin." *Tissue and Cell* 42 (5): 301–6. https://doi.org/10.1016/j.tice.2010.07.004.

Karthaus, Wouter R., Phillip J. Iaquinta, Jarno Drost, Ana Gracanin, Ruben Van Boxtel, John Wongvipat, Catherine M. Dowling, *et al.* 2014. "Identification of Multipotent Luminal Progenitor Cells in Human Prostate Organoid Cultures." *Cell* 159 (1): 163–75. https://doi.org/10.1016/j.cell.2014.08.017.

Kasus-Jacobi, Anne, Samaneh Noor-Mohammadi, Gina L. Griffith, Heather Hinsley, Lauren Mathias, and H. Anne Pereira. 2015. "A Multifunctional Peptide Based on the Neutrophil Immune Defense Molecule, CAP37, Has Antibacterial and Wound-Healing Properties." *Journal of Leukocyte Biology* 97 (2): 341–50. https://doi.org/10.1189/jlb.3a0214-104rr.

Keane, Timothy J., Ricardo Londono, Ryan M. Carey, Christopher A. Carruthers, Janet E. Reing, Christopher L. Dearth, Antonio D'Amore, Christopher J. Medberry, and Stephen F. Badylak. 2013. "Preparation and Characterization of a Biologic Scaffold from Esophageal Mucosa." *Biomaterials* 34 (28): 6729–37. https://doi.org/10.1016/j.biomaterials.2013.05.052.

Keane, Timothy J., Ilea T. Swinehart, and Stephen F. Badylak. 2015. "Methods of Tissue Decellularization Used for Preparation of Biologic Scaffolds and *in vivo* Relevance." *Methods*. Academic Press Inc. https://doi.org/10.1016/j.ymeth.2015.03.005.

Kessler, Mirjana, Karen Hoffmann, Volker Brinkmann, Oliver Thieck, Susan Jackisch, Benjamin Toelle, Hilmar Berger, *et al.* 2015. "The Notch and Wnt Pathways Regulate Stemness and Differentiation in Human Fallopian Tube Organoids." *Nature Communications* 6 (December). https://doi.org/10.1038/ncomms9989.

Kilic, Sevtap, Beril Yuksel, F Pinarli, and A Albayrak. 2014. "Effect of Stem Cell Application on Asherman Syndrome , an Experimental Rat Model," *Journal of Assisted Reproduction and Genetics* 31, 975–82. https://doi.org/10.1007/s10815-014-0268-2.

Kim, Ahmad, Shaikh, Jan, Seo, Lee, and Choi. 2019. "Dermatopontin in Skeletal Muscle Extracellular Matrix Regulates Myogenesis." *Cells* 8 (4): 332. https://doi.org/10.3390/cells8040332. (a)

Kim, Ji Hye, Mira Park, Jin Young Paek, Woo Sik Lee, Haengseok Song, and Sang Woo Lyu. 2020. "Intrauterine Infusion of Human Platelet-Rich Plasma Improves Endometrial Regeneration and Pregnancy Outcomes in a Murine Model of Asherman's Syndrome." *Frontiers in Physiology* 11 (February). https://doi.org/10.3389/fphys.2020.00105.

REFERENCES

Kim, Jun Sung, Ji Suk Choi, and Yong Woo Cho. 2017. "Cell-Free Hydrogel System Based on a Tissue-Specific Extracellular Matrix for *In situ* Adipose Tissue Regeneration." *ACS Applied Materials and Interfaces* 9 (10): 8581–88. https://doi.org/10.1021/acsami.6b16783.

Kim, Yoon Young, Bo Bin Choi, Ji Won Lim, Yong Jin Kim, Sung Yob Kim, and Seung Yup Ku. 2019. "Efficient Production of Murine Uterine Damage Model." *Tissue Engineering and Regenerative Medicine* 16 (2): 119–29. https://doi.org/10.1007/s13770-018-0149-3. (b)

Kim, Yoon Young, Kyu Hyung Park, Yong Jin Kim, Moon Suk Kim, Hung Ching Liu, Zev Rosenwaks, and Seung Yup Ku. 2019. "Synergistic Regenerative Effects of Functionalized Endometrial Stromal Cells with Hyaluronic Acid Hydrogel in a Murine Model of Uterine Damage." *Acta Biomaterialia* 89 (April): 139–51. https://doi.org/10.1016/j.actbio.2019.03.032. (c)

Kleinman, Hynda K., Mary L. McGarvey, John R. Hassell, Vicki L. Star, Frances B. Cannon, Gordon W. Laurie, and George R. Martin. 1986. "Basement Membrane Complexes with Biological Activity." *Biochemistry* 25 (2): 312–18. https://doi.org/10.1021/bi00350a005.

Kleinman, Hynda K., Mary L. McGarvey, Lance A. Liotta, Pamela Gehron Robey, Karl Tryggvason, and George R. Martin. 1982. "Isolation and Characterization of Type IV Procollagen, Laminin, and Heparan Sulfate Proteoglycan from the EHS Sarcoma." *Biochemistry* 21 (24): 6188–93. https://doi.org/10.1021/bi00267a025.

Kowalczewski, Christine J., and Justin M. Saul. 2018. "Biomaterials for the Delivery of Growth Factors and Other Therapeutic Agents in Tissue Engineering Approaches to Bone Regeneration." *Frontiers in Pharmacology*. Frontiers Media S.A. https://doi.org/10.3389/fphar.2018.00513.

Landgren, B M, E Johannisson, A Stavreus-Evers, L Hamberger, and H Eriksson. 1996. "A New Method to Study the Process of Implantation of a Human Blastocyst *in vitro*." *Fertility and Sterility* 65 (5): 1067–70. https://doi.org/10.1016/S0015-0282(16)58291-0.

Lebovitz, Oshrit and Raoul Orvieto. 2014. "Treating Patients with 'Thin' Endometrium-an Ongoing Challenge." *Gynecological Endocrinology* 30 (6): 409–14. https://doi.org/10.3109/09513590.2014.906571.

Lee, Jung Seung, Jisoo Shin, Hae-Min Park, Yun-Gon Kim, Byung-Gee Kim, Jong-Won Oh, and Seung-Woo Cho. 2014. "Liver Extracellular Matrix Providing Dual Functions of Two-Dimensional Substrate Coating and Three-Dimensional Injectable Hydrogel Platform for Liver Tissue Engineering." *Biomacromolecules* 15 (1): 206–18. https://doi.org/10.1021/bm4015039.

Li, Xia, Yiming Wang, Ruoyu Ma, Xin Liu, Biaobiao Song, Yongchao Duan, Jia Guo, *et al.* 2020. " Reconstruction of Functional Uterine Tissues through Recellularizing the Decellularized Rat Uterine Scaffolds by MSCs *in vivo* and *in vitro*." *Biomedical Materials*, December. https://doi.org/10.1088/1748-605x/abd116.

Lin, Jiaying, Zhen Wang, Jialyu Huang, Shengluan Tang, Qimanguli Saiding, Qianqian Zhu, and Wenguo Cui. 2021. "Microenvironment-Protected Exosome-Hydrogel for Facilitating Endometrial Regeneration, Fertility Restoration, and Live Birth of Offspring." *Small* 17 (11): 2007235. https://doi.org/10.1002/smll.202007235.

Lin, Tao, Sheng Liu, Shihao Chen, Shuai Qiu, Zilong Rao, Jianghui Liu, Shuang Zhu, *et al.* 2018.

"Hydrogel Derived from Porcine Decellularized Nerve Tissue as a Promising Biomaterial for Repairing Peripheral Nerve Defects." *Acta Biomaterialia* 73 (June): 326–38. https://doi.org/10.1016/j.actbio.2018.04.001.

Link, Patrick A., Robert A. Pouliot, Nabil S. Mikhaiel, Bethany M. Young, and Rebecca L. Heise. 2017. "Tunable Hydrogels from Pulmonary Extracellular Matrix for 3D Cell Culture." *Journal of Visualized Experiments*, no. 119: 1–9. https://doi.org/10.3791/55094.

Liu, Feiran, Shiqi Hu, Hua Yang, Zhenhua Li, Ke Huang, Teng Su, and Shaowei Wang. 2019. "Hyaluronic Acid Hydrogel Integrated with Mesenchymal Stem Cell-Secretome to Treat Endometrial Injury in a Rat Model of Asherman's Syndrome" *Advanced Healthcare Materials* 8 (14) 1900411: 1–10. https://doi.org/10.1002/adhm.201900411.

Londono, Ricardo, and Stephen F Badylak. 2015. "Biologic Scaffolds for Regenerative Medicine: Mechanisms of *in vivo* Remodeling." *Annals of Biomedical Engineering* 43 (3): 577–92. https://doi.org/10.1007/s10439-014-1103-8.

López-Martínez, Sara, Hannes Campo, Lucía de Miguel-Gómez, Amparo Faus, Alfredo T. Navarro, Ana Díaz, Antonio Pellicer, Hortensia Ferrero, and Irene Cervelló. 2021. "A Natural Xenogeneic Endometrial Extracellular Matrix Hydrogel Toward Improving Current Human *in vitro* Models and Future *in vivo* Applications." *Frontiers in Bioengineering and Biotechnology* 9 (March): 156. https://doi.org/10.3389/fbioe.2021.639688.

Lu, Pengfei, Ken Takai, Valerie M. Weaver, and Zena Werb. 2011. "Extracellular Matrix Degradation and Remodeling in Development and Disease." *Cold Spring Harbor Perspectives in Biology* 3 (12). https://doi.org/10.1101/cshperspect.a005058.

Lü, Shuang Hong, Hai Bin Wang, Hui Liu, He Ping Wang, Qiu Xia Lin, De Xue Li, Yu Xuan Song, Cui Mi Duan, Li Xin Feng, and Chang Yong Wang. 2009. "Reconstruction of Engineered Uterine Tissues Containing Smooth Muscle Layer in Collagen/Matrigel Scaffold *in vitro*." *Tissue Engineering - Part A* 15 (7): 1611–18. https://doi.org/10.1089/ten.tea.2008.0187.

Ma, Weidong, Zhongshan Miao, and Milos V. Novotny. 1998. "Role of the Adrenal Gland and Adrenal-Mediated Chemosignals in Suppression of Estrus in the House Mouse: The Lee-Boot Effect Revisited." *Biology of Reproduction* 59 (6): 1317–20. https://doi.org/10.1095/biolreprod59.6.1317.

Macher, Bruce A., and Uri Galili. 2008. "The Galα1,3Galβ1,4GlcNAc-R (α-Gal) Epitope: A Carbohydrate of Unique Evolution and Clinical Relevance." *Biochimica et Biophysica Acta - General Subjects*. NIH Public Access. https://doi.org/10.1016/j.bbagen.2007.11.003.

Masuda, Hirotaka, Siti S. Anwar, Hans Jörg Bühring, Jyothsna R. Rao, and Caroline E. Gargett. 2012. "A Novel Marker of Human Endometrial Mesenchymal Stem-like Cells." *Cell Transplantation* 21 (10): 2201–14. https://doi.org/10.3727/096368911X637362.

Mauch, Teri Jo, and Gary C Schoenwolf. 2001. "Developmental Biology. Sixth Edition. By Scott F. Gilbert." *American Journal of Medical Genetics* 99 (2): 170–71. https://doi.org/https://doi.org/10.1002/1096-8628(2000)9999:999<00::AID-AJMG1133>3.0.CO;2-G.

Medberry, Christopher J., Peter M. Crapo, Bernard F. Siu, Christopher A. Carruthers, Matthew T. Wolf, Shailesh P. Nagarkar, Vineet Agrawal, *et al.* 2013. "Hydrogels Derived from

REFERENCES

Central Nervous System Extracellular Matrix." *Biomaterials* 34 (4): 1033–40. https://doi.org/10.1016/j.biomaterials.2012.10.062.

Meng, Chun-Xia, Karin Louise Andersson, Ursula Bentin-Ley, Kristina Gemzell-Danielsson, and P G Luther Lalitkumar. 2009. "Effect of Levonorgestrel and Mifepristone on Endometrial Receptivity Markers in a Three-Dimensional Human Endometrial Cell Culture Model." *Fertility and Sterility* 91 (1): 256–64. https://doi.org/10.1016/j.fertnstert.2007.11.007.

Meyer, Michael. 2019. "Processing of Collagen Based Biomaterials and the Resulting Materials Properties." *BioMedical Engineering Online* 18 (1). https://doi.org/10.1186/s12938-019-0647-0.

Mi, Huaiyu, Anushya Muruganujan, Dustin Ebert, Xiaosong Huang, and Paul D Thomas. 2018. "PANTHER Version 14: More Genomes, a New PANTHER GO-Slim and Improvements in Enrichment Analysis Tools." *Nucleic Acids Research* 47: 419–26. https://doi.org/10.1093/nar/gky1038.

Miki, Fumie, Tetsuo Maruyama, Kaoru Miyazaki, Tomoka Takao, Yushi Yoshimasa, Satomi Katakura, Hanako Hihara, *et al.* 2019. "The Orientation of a Decellularized Uterine Scaffold Determines the Tissue Topology and Architecture of the Regenerated Uterus in Rats." *Biology of Reproduction* 100 (5): 1215–27. https://doi.org/10.1093/biolre/ioz004.

Miyazaki, Kaoru, and Tetsuo Maruyama. 2014. "Partial Regeneration and Reconstruction of the Rat Uterus through Recellularization of a Decellularized Uterine Matrix." *Biomaterials* 35 (31): 8791–8800. https://doi.org/10.1016/j.biomaterials.2014.06.052.

Miyazaki, Kaoru, Tetsuo Maruyama, Hirotaka Masuda, Akiko Yamasaki, Sayaka Uchida, Hideyuki Oda, Hiroshi Uchida, and Yasunori Yoshimura. 2012. "Stem Cell-Like Differentiation Potentials of Endometrial Side Population Cells as Revealed by a Newly Developed *In vivo* Endometrial Stem Cell Assay." *PLoS ONE* 7 (12). https://doi.org/10.1371/journal.pone.0050749.

Morelli, Sara S., Pranela Rameshwar, and Laura T. Goldsmith. 2013. "Experimental Evidence for Bone Marrow as a Source of Nonhematopoietic Endometrial Stromal and Epithelial Compartment Cells in a Murine Model1." *Biology of Reproduction* 89 (1). https://doi.org/10.1095/biolreprod.113.107987.

Mullen, Leanne M., Serena M. Best, Roger A. Brooks, Siddhartha Ghose, Jessica H. Gwynne, John Wardale, Neil Rushton, and Ruth E. Cameron. 2010. "Binding and Release Characteristics of Insulin-Like Growth Factor-1 from a Collagen–Glycosaminoglycan Scaffold." *Tissue Engineering Part C: Methods* 16 (6): 1439–48. https://doi.org/10.1089/ten.tec.2009.0806.

Naahidi, Sheva, Mousa Jafari, Megan Logan, Yujie Wang, Yongfang Yuan, Hojae Bae, Brian Dixon, and P. Chen. 2017. "Biocompatibility of Hydrogel-Based Scaffolds for Tissue Engineering Applications." *Biotechnology Advances*. Elsevier Inc. https://doi.org/10.1016/j.biotechadv.2017.05.006.

Naba, Alexandra, Karl R. Clauser, Huiming Ding, Charles A. Whittaker, Steven A. Carr, and Richard O. Hynes. 2016. "The Extracellular Matrix: Tools and Insights for the 'Omics' Era." *Matrix Biology*. Elsevier B.V. https://doi.org/10.1016/j.matbio.2015.06.003.

Naba, Alexandra, Karl R. Clauser, Sebastian Hoersch, Hui Liu, Steven A. Carr, and Richard O.

Hynes. 2012. "The Matrisome: In Silico Definition and *in vivo* Characterization by Proteomics of Normal and Tumor Extracellular Matrices." *Molecular and Cellular Proteomics* 11 (4). https://doi.org/10.1074/mcp.M111.014647.

Nehrenheim, Laura, Silja Raschke, Anja Stefanski, Mareike Barth, Jessica Isabel Selig, Andreas Barbian, Alicia Fernández-Colino, *et al.* 2019. "Native Aortic Valve Derived Extracellular Matrix Hydrogel for Three Dimensional Culture Analyses with Improved Biomimetic Properties." *Biomedical Materials* 14 (3): 035014. https://doi.org/10.1088/1748-605X/AB0791.

Nguyen, Hong P.T., Li Xiao, James A. Deane, Ker Sin Tan, Fiona L. Cousins, Hirotaka Masuda, Carl N. Sprung, Anna Rosamilia, and Caroline E. Gargett. 2017. "N-Cadherin Identifies Human Endometrial Epithelial Progenitor Cells by *in vitro* Stem Cell Assays." *Human Reproduction* 32 (11): 2254–68. https://doi.org/10.1093/humrep/dex289.

Okamoto, Osamu, and Sakuhei Fujiwara. 2006. "Dermatopontin, a Novel Player in the Biology of the Extracellular Matrix." *Connective Tissue Research*. Connect Tissue Res. https://doi.org/10.1080/03008200600846564.

Olalekan, Susan A, Joanna E Burdette, Spiro Getsios, Teresa K Woodruff, and J Julie Kim. 2017. "Development of a Novel Human Recellularized Endometrium That Responds to a 28-Day Hormone Treatment." *Biology of Reproduction* 96 (5): 971–81. https://doi.org/10.1093/biolre/iox039.

Ott, Harald C., Thomas S. Matthiesen, Saik Kia Goh, Lauren D. Black, Stefan M. Kren, Theoden I. Netoff, and Doris A. Taylor. 2008. "Perfusion-Decellularized Matrix: Using Nature's Platform to Engineer a Bioartificial Heart." *Nature Medicine* 14 (2): 213–21. https://doi.org/10.1038/nm1684.

Ouyang, Xiaolan, Shuang You, Yulin Zhang, Chanyu Zhang, Guanghui Zhang, Xiaoyan Shao, Fan He, and Lina Hu. 2020. "Transplantation of Human Amnion Epithelial Cells Improves Endometrial Regeneration in Rat Model of Intrauterine Adhesions." *Stem Cells and Development*. https://doi.org/10.1089/scd.2019.0246.

Peng, Yizhong, Xiangcheng Qing, Hui Lin, Donghua Huang, Jinye Li, Shuo Tian, Sheng Liu, *et al.* 2021. "Decellularized Disc Hydrogels for HBMSCs Tissue-Specific Differentiation and Tissue Regeneration." *Bioactive Materials* 6 (10): 3541–56. https://doi.org/10.1016/j.bioactmat.2021.03.014.

Pieters, Marlien, and Alisa S. Wolberg. 2019. "Fibrinogen and Fibrin: An Illustrated Review." *Research and Practice in Thrombosis and Haemostasis* 3 (2): 161–72. https://doi.org/10.1002/rth2.12191.

Porzionato, Andrea, Maria Martina Sfriso, Alex Pontini, Veronica Macchi, Lucia Petrelli, Piero G. Pavan, Arturo N. Natali, Franco Bassetto, Vincenzo Vindigni, and Raffaele De Caro. 2015. "Decellularized Human Skeletal Muscle as Biologic Scaffold for Reconstructive Surgery." *International Journal of Molecular Sciences* 16 (7): 14808–31. https://doi.org/10.3390/ijms160714808.

Pouliot, Robert A., Patrick A. Link, Nabil S. Mikhaiel, Matthew B. Schneck, Michael S. Valentine, Franck J. Kamga Gninzeko, Joseph A. Herbert, Masahiro Sakagami, and Rebecca L. Heise. 2016. "Development and Characterization of a Naturally Derived Lung

REFERENCES

Extracellular Matrix Hydrogel." *Journal of Biomedical Materials Research - Part A* 104 (8): 1922–35. https://doi.org/10.1002/jbm.a.35726.

Prianishnikov, V. A. 1978. "On the Concept of Stem Cell and a Model of Functional-Morphological Structure of the Endometrium." *Contraception* 18 (3): 213–23. https://doi.org/10.1016/S0010-7824(78)80015-8.

Pritchard J. A., MacDonald P. C. and Gant N.F. 1986. "Anatomía Del Aparato Reproductor Femenino." In *Williams Obstetricia* (third Edition), 7–28. Barcelona: Salvat Editores S.A.

Raya-Rivera, Atlántida M, Diego Esquiliano, Reyna Fierro-Pastrana, Esther López-Bayghen, Pedro Valencia, Ricardo Ordorica-Flores, Shay Soker, James J Yoo, and Anthony Atala. 2014. "Tissue-Engineered Autologous Vaginal Organs in Patients: A Pilot Cohort Study." *The Lancet* 384 (9940): 329–36. https://doi.org/10.1016/S0140-6736(14)60542-0.

Rozario, Tania, and Douglas W DeSimone. 2010. "The Extracellular Matrix in Development and Morphogenesis: A Dynamic View." *Developmental Biology* 341 (1): 126–40. https://doi.org/10.1016/j.ydbio.2009.10.026.

RStudio Team. 2020. "RStudio: Integrated Development Environment for R." Boston, MA: RStudio, PBC. http://www.rstudio.com/.

Rupprecht, Kevin R., Ewa Z. Lang, Svetoslava D. Gregory, Janet M. Bergsma, Tracey D. Rae, and Jeffrey R. Fishpaugh. 2015. "A Precise Spectrophotometric Method for Measuring Sodium Dodecyl Sulfate Concentration." *Analytical Biochemistry* 486 (October): 78–80. https://doi.org/10.1016/j.ab.2015.06.013.

Sachs, Norman, Yoshiyuki Tsukamoto, Pekka Kujala, Peter J. Peters, and Hans Clevers. 2017. "Intestinal Epithelial Organoids Fuse to Form Self-Organizing Tubes in Floating Collagen Gels." *Development (Cambridge)* 144 (6): 1107–12. https://doi.org/10.1242/dev.143933.

Sackett, Sara Dutton, Daniel M. Tremmel, Fengfei Ma, Austin K. Feeney, Rachel M. Maguire, Matthew E. Brown, Ying Zhou, *et al.* 2018. "Extracellular Matrix Scaffold and Hydrogel Derived from Decellularized and Delipidized Human Pancreas." *Scientific Reports* 8 (1). https://doi.org/10.1038/s41598-018-28857-1.

Saldin, Lindsey T, Madeline C Cramer, Sachin S Velankar, Lisa J White, and Stephen F Badylak. 2017. "Extracellular Matrix Hydrogels from Decellularized Tissues: Structure and Function." *Acta Biomaterialia* 49: 1–15. https://doi.org/10.1016/j.actbio.2016.11.068.

Santamaria, Xavier, Sergio Cabanillas, Irene Cervelló, Cristina Arbona, Francisco Raga, Jaime Ferro, Julio Palmero, Jose Remohí, Antonio Pellicer, and Carlos Simón. 2016. "Autologous Cell Therapy with CD133+ Bone Marrow-Derived Stem Cells for Refractory Asherman's Syndrome and Endometrial Atrophy: A Pilot Cohort Study." *Human Reproduction* 31 (5): 1087–96. https://doi.org/10.1093/humrep/dew042.

Santamaria, Xavier, Aymara Mas, Irene Cervelló, Hugh Taylor, and Carlos Simon. 2018. "Uterine Stem Cells: From Basic Research to Advanced Cell Therapies." *Human Reproduction Update*. Oxford University Press. https://doi.org/10.1093/humupd/dmy028.

Santoso, Erna G., Keita Yoshida, Yasushi Hirota, Masanori Aizawa, Osamu Yoshino, Akio Kishida, Yutaka Osuga, Shigeru Saito, Takashi Ushida, and Katsuko S. Furukawa. 2014. "Application of Detergents or High Hydrostatic Pressure as Decellularization Processes in

Uterine Tissues and Their Subsequent Effects on *in vivo* Uterine Regeneration in Murine Models." *PLoS ONE* 9 (7). https://doi.org/10.1371/journal.pone.0103201.

Sato, Toshiro, Daniel E. Stange, Marc Ferrante, Robert G.J. Vries, Johan H. Van Es, Stieneke Van Den Brink, Winan J. Van Houdt, *et al.* 2011. "Long-Term Expansion of Epithelial Organoids from Human Colon, Adenoma, Adenocarcinoma, and Barrett's Epithelium." *Gastroenterology* 141 (5): 1762–72. https://doi.org/10.1053/j.gastro.2011.07.050.

Scanameo, Alexandra, and Nicholas P. Ziats. 2019. "CHAPTER 6. Immune Responses to Decellularized Matrices." In *Decellularized Extracellular Matrix: Characterization, Fabrication and Applications*, edited by Tetsuji Yamaoka, Takashi Hoshiba. 95–115. https://doi.org/10.1039/9781788015998-00095.

Schindelin, Johannes, Ignacio Arganda-Carreras, Erwin Frise, Verena Kaynig, Mark Longair, Tobias Pietzsch, Stephan Preibisch, *et al.* 2012. "Fiji: An Open-Source Platform for Biological-Image Analysis." *Nature Methods*. Nature Publishing Group. https://doi.org/10.1038/nmeth.2019.

Schultz, Gregory S., and Annette Wysocki. 2009. "Interactions between Extracellular Matrix and Growth Factors in Wound Healing." *Wound Repair and Regeneration* 17 (2): 153-62. https://doi.org/10.1111/j.1524-475X.2009.00466.x.

Schutte, Stacey C., Christopher O. James, Neil Sidell, and Robert N. Taylor. 2015. "Tissue-Engineered Endometrial Model for the Study of Cell-Cell Interactions." *Reproductive Sciences* 22 (3): 308–15. https://doi.org/10.1177/1933719114542008.

Schwab, K. E., and C. E. Gargett. 2007. "Co-Expression of Two Perivascular Cell Markers Isolates Mesenchymal Stem-like Cells from Human Endometrium." *Human Reproduction* 22 (11): 2903–11. https://doi.org/10.1093/humrep/dem265.

Seif-Naraghi, Sonya B., Dinah Horn, Pam A. Schup-Magoffin, Michael M. Madani, and Karen L. Christman. 2011. "Patient-to-Patient Variability in Autologous Pericardial Matrix Scaffolds for Cardiac Repair." *Journal of Cardiovascular Translational Research* 4 (5): 545–56. https://doi.org/10.1007/s12265-011-9293-z.

Seo, Yoojin, Youngmee Jung, and Soo Hyun Kim. 2018. "Decellularized Heart ECM Hydrogel Using Supercritical Carbon Dioxide for Improved Angiogenesis." *Acta Biomaterialia* 67 (February): 270–81. https://doi.org/10.1016/j.actbio.2017.11.046.

Shevchenko, Andrej, Ole N. Jensen, Alexandre V. Podtelejnikov, Francis Sagliocco, Matthias Wilm, Ole Vorm, Peter Mortensen, Anna Shevchenko, Helian Boucherie, and Matthias Mann. 1996. "Linking Genome and Proteome by Mass Spectrometry: Large-Scale Identification of Yeast Proteins from Two Dimensional Gels." In *Proceedings of the National Academy of Sciences of the United States of America*, 93:14440–45. https://doi.org/10.1073/pnas.93.25.14440.

Shilov, Ignat V., Sean L. Seymourt, Alpesh A. Patel, Alex Loboda, Wilfred H. Tang, Sean P. Keating, Christie L. Hunter, Lydia M. Nuwaysir, and Daniel A. Schaeffer. 2007. "The Paragon Algorithm, a next Generation Search Engine That Uses Sequence Temperature Values Sequence Temperature Values and Feature Probabilities to Identify Peptides from Tandem Mass Spectra." *Molecular and Cellular Proteomics* 6 (9): 1638–55. https://doi.org/10.1074/mcp.T600050-MCP200.

REFERENCES

Simón, Carlos, Jose A. Horcajadas, Juan A. García-Velasco, and Antonio Pellicer. 2009. *El Endometrio Humano: Desde La Investigación a La Clínica.* (First edition). Editorial Médica Panamericana.

Simón, Carlos, Gary N. Piquette, Ana Frances, and Mary Lake Polan. 1993. "Localization of Interleukin-1 Type I Receptor and Interleukin-1 β in Human Endometrium throughout the Menstrual Cycle." *Journal of Clinical Endocrinology and Metabolism* 77 (2): 549–55. https://doi.org/10.1210/jcem.77.2.8345061.

Singelyn, Jennifer M., Priya Sundaramurthy, Todd D. Johnson, Pamela J. Schup-Magoffin, Diane P. Hu, Denver M. Faulk, Jean Wang, *et al.* 2012. "Catheter-Deliverable Hydrogel Derived from Decellularized Ventricular Extracellular Matrix Increases Endogenous Cardiomyocytes and Preserves Cardiac Function Post-Myocardial Infarction." *Journal of the American College of Cardiology* 59 (8): 751–63. https://doi.org/10.1016/j.jacc.2011.10.888.

Skardal, Aleksander, Leona Smith, Shantaram Bharadwaj, Anthony Atala, Shay Soker, and Yuanyuan Zhang. 2012. "Tissue Specific Synthetic ECM Hydrogels for 3-D *in vitro* Maintenance of Hepatocyte Function." *Biomaterials* 33 (18): 4565–75. https://doi.org/10.1016/j.biomaterials.2012.03.034.

Soto-Gutierrez, Alejandro, Li Zhang, Chris Medberry, Ken Fukumitsu, Denver Faulk, Hongbin Jiang, Janet Reing, *et al.* 2011. "A Whole-Organ Regenerative Medicine Approach for Liver Replacement." *Tissue Engineering Part C: Methods* 17 (6): 677–86. https://doi.org/10.1089/ten.tec.2010.0698.

Stanton, Alice E., Xinming Tong, and Fan Yang. 2019. "Extracellular Matrix Type Modulates Mechanotransduction of Stem Cells." *Acta Biomaterialia* 96 (September): 310–20. https://doi.org/10.1016/j.actbio.2019.06.048.

Theocharis, Achilleas D., Spyros S. Skandalis, Chrysostomi Gialeli, and Nikos K. Karamanos. 2016. "Extracellular Matrix Structure." *Advanced Drug Delivery Reviews*. Elsevier B.V. https://doi.org/10.1016/j.addr.2015.11.001.

Tiemann, T. T., A. M. Padma, E. Sehic, H. Bäckdahl, M. Oltean, M. J. Song, M. Brännström, and M. Hellström. 2020. "Towards Uterus Tissue Engineering: A Comparative Study of Sheep Uterus Decellularisation." *Molecular Human Reproduction* 26 (3): 167–78. https://doi.org/10.1093/molehr/gaaa009.

Traverse, Jay H., Timothy D. Henry, Nabil Dib, Amit N. Patel, Carl Pepine, Gary L. Schaer, Jessica A. DeQuach, Adam M. Kinsey, Paul Chamberlin, and Karen L. Christman. 2019. "First-in-Man Study of a Cardiac Extracellular Matrix Hydrogel in Early and Late Myocardial Infarction Patients." *JACC: Basic to Translational Science* 4 (6): 659–69. https://doi.org/10.1016/j.jacbts.2019.07.012.

Tsuji, Shunichiro, Momoko Yoshimoto, Kentaro Takahashi, Yoichi Noda, Tatsutoshi Nakahata, and Toshio Heike. 2008. "Side Population Cells Contribute to the Genesis of Human Endometrium." *Fertility and Sterility* 90 (4 SUPPL.): 1528–37. https://doi.org/10.1016/j.fertnstert.2007.08.005.

Turco, Margherita Y, Lucy Gardner, Jasmine Hughes, Tereza Cindrova-Davies, Maria J Gomez, Lydia Farrell, Michael Hollinshead, *et al.* 2017. "Long-Term, Hormone-Responsive

Organoid Cultures of Human Endometrium in a Chemically Defined Medium." *Nature Cell Biology* 19 (5): 568–77. https://doi.org/10.1038/ncb3516.

Uhlen, M., L. Fagerberg, B. M. Hallstrom, C. Lindskog, P. Oksvold, A. Mardinoglu, A. Sivertsson, *et al.* 2015. "Tissue-Based Map of the Human Proteome." *Science* 347 (6220): 1260419–1260419. https://doi.org/10.1126/science.1260419.

Ungerleider, Jessica L., Todd D. Johnson, Melissa J. Hernandez, Dean I. Elhag, Rebecca L. Braden, Monika Dzieciatkowska, Kent G. Osborn, Kirk C. Hansen, Ehtisham Mahmud, and Karen L. Christman. 2016. "Extracellular Matrix Hydrogel Promotes Tissue Remodeling, Arteriogenesis, and Perfusion in a Rat Hindlimb Ischemia Model." *JACC: Basic to Translational Science*. Elsevier Inc. https://doi.org/10.1016/j.jacbts.2016.01.009.

Uygun, Basak E., Alejandro Soto-Gutierrez, Hiroshi Yagi, Maria Louisa Izamis, Maria A. Guzzardi, Carley Shulman, Jack Milwid, *et al.* 2010. "Organ Reengineering through Development of a Transplantable Recellularized Liver Graft Using Decellularized Liver Matrix." *Nature Medicine* 16 (7): 814–20. https://doi.org/10.1038/nm.2170.

Valdez, Jorge, Christi D. Cook, Caroline Chopko Ahrens, Alex J. Wang, Alexander Brown, Manu Kumar, Linda Stockdale, *et al.* 2017. "On-Demand Dissolution of Modular, Synthetic Extracellular Matrix Reveals Local Epithelial-Stromal Communication Networks." *Biomaterials* 130 (June): 90–103. https://doi.org/10.1016/j.biomaterials.2017.03.030.

Valentijn, A. J., K. Palial, H. Al-Lamee, N. Tempest, J. Drury, T. Von Zglinicki, G. Saretzki, P. Murray, C. E. Gargett, and D. K. Hapangama. 2013. "SSEA-1 Isolates Human Endometrial Basal Glandular Epithelial Cells: Phenotypic and Functional Characterization and Implications in the Pathogenesis of Endometriosis." *Human Reproduction* 28 (10): 2695–2708. https://doi.org/10.1093/humrep/det285.

Vander Borght, Mélodie, and Christine Wyns. 2018. "Fertility and Infertility: Definition and Epidemiology." *Clinical Biochemistry*. Elsevier Inc. https://doi.org/10.1016/j.clinbiochem.2018.03.012.

Ventura, Reiza D, Andrew R Padalhin, Boram Kim, Myoungki Park, and Byong Taek. 2020. "Materials Science & Engineering C Evaluation of Bone Regeneration Potential of Injectable Extracellular Matrix (ECM) from Porcine Dermis Loaded with Biphasic Calcium Phosphate (BCP) Powder." *Materials Science & Engineering C* 110 (January): 110663. https://doi.org/10.1016/j.msec.2020.110663.

Hayssen, Virginia and Teri J. Orr. 2017. *Reproduction in Mammals: The Female Perspective.* Johns Hopkins University Press.

Viswanath, Aiswarya, Julie Vanacker, Loïc Germain, Julian G Leprince, Anibal Diogenes, Kevin M Shakesheff, Lisa J White, and Anne des Rieux. 2017. "Extracellular Matrix-Derived Hydrogels for Dental Stem Cell Delivery." *Journal of Biomedical Materials Research. Part A* 105 (1): 319–28. https://doi.org/10.1002/jbm.a.35901.

Vukicevic, Slobodan, Hynda K. Kleinman, Frank P. Luyten, Anita B. Roberts, Nanette S. Roche, and A. H. Reddi. 1992. "Identification of Multiple Active Growth Factors in Basement Membrane Matrigel Suggests Caution in Interpretation of Cellular Activity Related to Extracellular Matrix Components." *Experimental Cell Research* 202 (1): 1–8. https://doi.org/10.1016/0014-4827(92)90397-Q.

REFERENCES

Výborný, Karel, Jana Vallová, Zuzana Kočí, Kristýna Kekulová, Klára Jiráková, Pavla Jendelová, Jiří Hodan, and Šárka Kubinová. 2019. "Genipin and EDC Crosslinking of Extracellular Matrix Hydrogel Derived from Human Umbilical Cord for Neural Tissue Repair." *Scientific Reports* 9 (1). https://doi.org/10.1038/s41598-019-47059-x.

Wang, Fuyan, Weiyun Shi, Hua Li, Hongwei Wang, Dapeng Sun, Long Zhao, Lingling Yang, Ting Liu, Qingjun Zhou, and Lixin Xie. 2020. "Decellularized Porcine Cornea-Derived Hydrogels for the Regeneration of Epithelium and Stroma in Focal Corneal Defects." *Ocular Surface* 18 (4): 748–60. https://doi.org/10.1016/j.jtos.2020.07.020. (b)

Wang, Hai, Silvina Bocca, Sandra Anderson, Liang Yu, Bhaskara S. Rhavi, José Horcajadas, and Sergio Oehninger. 2013. "Sex Steroids Regulate Epithelial–Stromal Cell Cross Talk and Trophoblast Attachment Invasion in a Three-Dimensional Human Endometrial Culture System." *Tissue Engineering Part C: Methods* 19 (9): 676–87. https://doi.org/10.1089/ten.tec.2012.0616.

Wang, Hai, Federica Pilla, Sandra Anderson, Sebastián Martíed;nez-escribano, Isabel Herrer, Juan M. Moreno-moya, Sirisha Musti, Silvina Bocca, Sergio Oehninger, and José A. Horcajadas. 2012. "A Novel Model of Human Implantation: 3D Endometrium-like Culture System to Study Attachment of Human Trophoblast (Jar) Cell Spheroids." *Molecular Human Reproduction* 18 (1): 33–43. https://doi.org/10.1093/molehr/gar064.

Wang, Tuntun, Sitansu Sekhar Nanda, Georgia C. Papaefthymiou, and Dong Kee Yi. 2020. "Mechanophysical Cues in Extracellular Matrix Regulation of Cell Behavior." *ChemBioChem*. Wiley-VCH Verlag. https://doi.org/10.1002/cbic.201900686. (a)

Wang, Xiangzhen, Nana Ma, Qiannan Sun, Chenlingzi Huang, Yanmei Liu, and Xin Luo. 2017. "Elevated NF-KB Signaling in Asherman Syndrome Patients and Animal Models." *Oncotarget* 8 (9): 15399–406. https://doi.org/10.18632/oncotarget.14853.

Wells, J. Michael, Amit Gaggar, and J. Edwin Blalock. 2015. "MMP Generated Matrikines." *Matrix Biology*. Elsevier. https://doi.org/10.1016/j.matbio.2015.01.016.

Wells, Rebeca G. 2008. "The Role of Matrix Stiffness in Regulating Cell Behavior." *Hepatology* 47 (4): 1394–1400. https://doi.org/10.1002/hep.22193.

Wiesner, Jochen, and Andreas Vilcinskas. 2010. "Antimicrobial Peptides: The Ancient Arm of the Human Immune System." *Virulence* 1 (5): 440–64. https://doi.org/10.4161/viru.1.5.12983.

Wiwatpanit, Teerawat, Alina R. Murphy, Zhenxiao Lu, Margrit Urbanek, Joanna E. Burdette, Teresa K. Woodruff, and J. Julie Kim. 2020. "Scaffold-Free Endometrial Organoids Respond to Excess Androgens Associated With Polycystic Ovarian Syndrome." *Journal of Clinical Endocrinology and Metabolism* 105 (3). https://doi.org/10.1210/clinem/dgz100.

Wolf, Matthew T., Kerry A. Daly, Ellen P. Brennan-Pierce, Scott A. Johnson, Christopher A. Carruthers, Antonio D'Amore, Shailesh P. Nagarkar, Sachin S. Velankar, and Stephen F. Badylak. 2012. "A Hydrogel Derived from Decellularized Dermal Extracellular Matrix." *Biomaterials* 33 (29): 7028–38. https://doi.org/10.1016/j.biomaterials.2012.06.051.

Wua, Jinglei, Qing Ding, Ahana Dutta, Yezhou Wang, Yi Hui Huang, Hong Wenga, Liping Tang, and Yi Hong. 2015. "An Injectable Extracellular Matrix Derived Hydrogel for Meniscus Repair and Regeneration." *Acta Biomaterialia* 16 (1): 49–59.

https://doi.org/10.1016/j.actbio.2015.01.027.

Wynn, Thomas A., and Thirumalai R. Ramalingam. 2012. "Mechanisms of Fibrosis: Therapeutic Translation for Fibrotic Disease." *Nature Medicine*. NIH Public Access. https://doi.org/10.1038/nm.2807.

Xiao, Bang, Wenjun Yang, Dong Lei, Jinfeng Huang, Yupeng Yin, Yiqing Zhu, Zhengwei You, Fang Wang, and Shuhan Sun. 2019. "PGS Scaffolds Promote the *In vivo* Survival and Directional Differentiation of Bone Marrow Mesenchymal Stem Cells Restoring the Morphology and Function of Wounded Rat Uterus." *Advanced Healthcare Materials* 8 (5): 1801455. https://doi.org/10.1002/adhm.201801455.

Xin, Liaobing, Xiaona Lin, Yibin Pan, Xiaowen Zheng, Libing Shi, Yanling Zhang, Lie Ma, Changyou Gao, and Songying Zhang. 2019. "A Collagen Scaffold Loaded with Human Umbilical Cord-Derived Mesenchymal Stem Cells Facilitates Endometrial Regeneration and Restores Fertility." *Acta Biomaterialia* 92 (July): 160–71. https://doi.org/10.1016/j.actbio.2019.05.012.

Xing, Hao, Hudson Lee, Lijing Luo, and Themis R. Kyriakides. 2020. "Extracellular Matrix-Derived Biomaterials in Engineering Cell Function." *Biotechnology Advances*. Elsevier Inc. https://doi.org/10.1016/j.biotechadv.2019.107421.

Xu, He Lin, Jie Xu, Bi Xin Shen, Si Si Zhang, Bing Hui Jin, Qun Yan Zhu, De Li ZhuGe, Xue Qing Wu, Jian Xiao, and Ying Zheng Zhao. 2017. "Dual Regulations of Thermosensitive Heparin-Poloxamer Hydrogel Using ϵ-Polylysine: Bioadhesivity and Controlled KGF Release for Enhancing Wound Healing of Endometrial Injury." *ACS Applied Materials and Interfaces* 9 (35): 29580–94. https://doi.org/10.1021/acsami.7b10211.

Yang, Huan, Su Wu, Ran Feng, Junjiu Huang, Lixiang Liu, Feng Liu, and Yuqing Chen. 2017. "Vitamin C plus Hydrogel Facilitates Bone Marrow Stromal Cell-Mediated Endometrium Regeneration in Rats." *Stem Cell Research and Therapy* 8 (1). https://doi.org/10.1186/s13287-017-0718-8.

Yao, Qing, Ya Wen Zheng, Hui Long Lin, Qing Hua Lan, Zhi Wei Huang, Li Fen Wang, Rui Chen, *et al.* 2020. "Exploiting Crosslinked Decellularized Matrix to Achieve Uterus Regeneration and Construction." *Artificial Cells, Nanomedicine and Biotechnology* 48 (1): 218–29. https://doi.org/10.1080/21691401.2019.1699828.

Yin, Yitong, Ying Han, Chang Shi, and Zhijun Xia. 2020. "IGF-1 Regulates the Growth of Fibroblasts and Extracellular Matrix Deposition in Pelvic Organ Prolapse." *Open Medicine (Poland)* 15 (1): 833–40. https://doi.org/10.1515/med-2020-0216.

Young, Roger C., and Gabriela Goloman. 2013. "Allo- and Xeno-Reassembly of Human and Rat Myometrium from Cells and Scaffolds." *Tissue Engineering Part A* 19 (19–20): 2112–19. https://doi.org/10.1089/ten.tea.2012.0549.

Yuan, Xiaoning, Yiyong Wei, Aránzazu Villasante, Johnathan J.D. Ng, Derya E. Arkonac, Pen hsiu Grace Chao, and Gordana Vunjak-Novakovic. 2017. "Stem Cell Delivery in Tissue-Specific Hydrogel Enabled Meniscal Repair in an Orthotopic Rat Model." *Biomaterials* 132 (July): 59–71. https://doi.org/10.1016/j.biomaterials.2017.04.004.

Zegers-Hochschild, F., G. D. Adamson, J. de Mouzon, O. Ishihara, R. Mansour, K. Nygren, E. Sullivan, and S. Vanderpoel. 2009. "International Committee for Monitoring Assisted

REFERENCES

Reproductive Technology (ICMART) and the World Health Organization (WHO) Revised Glossary of ART Terminology, 2009*.” *Fertility and Sterility* 92 (5): 1520–24. https://doi.org/10.1016/j.fertnstert.2009.09.009.

Zhang, Si Si, Xin Xin Xu, Wei Wei Xiang, Hui Heng Zhang, Hui Long Lin, Lai En Shen, Qi Lin, Feng Lin, and Zhi Yang Zhou. 2020. “Using 17β-Estradiol Heparin-Poloxamer Thermosensitive Hydrogel to Enhance the Endometrial Regeneration and Functional Recovery of Intrauterine Adhesions in a Rat Model.” *FASEB Journal* 34 (1): 446–57. https://doi.org/10.1096/fj.201901603RR.

Zhang, Yanling, Xiaona Lin, Yongdong Dai, Xiaoxiao Hu, Haiyan Zhu, Yinshen Jiang, and Songying Zhang. 2016. “Endometrial Stem Cells Repair Injured Endometrium and Induce Angiogenesis via AKT and ERK Pathways.” *Reproduction* 152 (5): 389–402. https://doi.org/10.1530/REP-16-0286.

Zhao, Jing, Qiong Zhang, Yonggang Wang, and Yanping Li. 2015. “Uterine Infusion with Bone Marrow Mesenchymal Stem Cells Improves Endometrium Thickness in a Rat Model of Thin Endometrium.” *Reproductive Sciences* 22 (2): 181–88. https://doi.org/10.1177/1933719114537715.

Zhao, Jing, Zhang Qiong, Wang Yonggang, and Li Yanping. 2014. “Rat Bone Marrow Mesenchymal Stem Cells Improve Regeneration of Thin Endometrium in Rat.” *Fertility and Sterility* 101 (2). https://doi.org/10.1016/j.fertnstert.2013.10.053. (a)

Zhao, Wen, Xiaowei Li, Xiaoyan Liu, Ning Zhang, and Xuejun Wen. 2014. “Effects of Substrate Stiffness on Adipogenic and Osteogenic Differentiation of Human Mesenchymal Stem Cells.” *Materials Science and Engineering C* 40 (July): 316–23. https://doi.org/10.1016/j.msec.2014.03.048.   (b)

Zhao, Yu, Jun Fan, and Shuling Bai. 2019. “Biocompatibility of Injectable Hydrogel from Decellularized Human Adipose Tissue *in vitro* and *in vivo*.” *Journal of Biomedical Materials Research - Part B Applied Biomaterials* 107 (5): 1684–94. https://doi.org/10.1002/jbm.b.34261.

Zhao, Zhitong, Catarina Vizetto-Duarte, Zi Kuang Moay, Magdiel Inggrid Setyawati, Moumita Rakshit, Mustafa Hussain Kathawala, and Kee Woei Ng. 2020. “Composite Hydrogels in Three-Dimensional *in vitro* Models.” *Frontiers in Bioengineering and Biotechnology*. Frontiers Media S.A. https://doi.org/10.3389/fbioe.2020.00611.

Zhong, Gang, Jun Yao, Xing Huang, Yixuan Luo, Meng Wang, Jinyu Han, Fei Chen, and Yin Yu. 2020. “Injectable ECM Hydrogel for Delivery of BMSCs Enabled Full-Thickness Meniscus Repair in an Orthotopic Rat Model.” *Bioactive Materials* 5 (4): 871–79. https://doi.org/10.1016/j.bioactmat.2020.06.008.

APPENDIX

APPENDIX A. Supplementary Tables

Supplementary Table I. List of peptides found in proteomic analysis of endometrial extracellular matrix hydrogels.

General protein classification	Protein classification	Peptide name	% Cov (Coverage)	Accession
Collagen	Collagen type I	Collagen alpha-1(I) chain (Fragments) OS=Cyclopes didactylus OX=84074 GN=COL1A1 PE=1 SV=1	94.9199975	sp|C0HJP1|CO1A1_CYCDI
Collagen	Collagen type I	Collagen alpha-1(I) chain (Fragments) OS=Toxodon sp. OX=1563122 GN=COL1A1 PE=1 SV=1	88.1900012	sp|C0HJP7|CO1A1_TOXSP
Collagen	Collagen type I	Collagen alpha-1(I) chain OS=Dipodomys ordii OX=10020 GN=Col1a1 PE=4 SV=1	64.9100006	tr|A0A1S3GXN3|A0A1S3GXN3_DIPOR
Collagen	Collagen type I	Collagen alpha-1(I) chain OS=Erinaceus europaeus OX=9365 GN=COL1A1 PE=4 SV=1	64.7700012	tr|A0A1S2ZWH5|A0A1S2ZWH5_ERIEU
Collagen	Collagen type I	Collagen alpha-1(I) chain OS=Tarsius syrichta OX=1868482 GN=COL1A1 PE=4 SV=1	54.7200024	tr|A0A1U7U3X6|A0A1U7U3X6_TARSY
Collagen	Collagen type I	Collagen type I alpha 1 chain OS=Myotis lucifugus OX=59463 GN=COL1A1 PE=4 SV=1	65.6400025	tr|G1QDY4|G1QDY4_MYOLU
Collagen	Collagen type I	Collagen type I alpha 1 chain OS=Otolemur garnettii OX=30611 GN=COL1A1 PE=4 SV=1	63.5699987	tr|H0XLS8|H0XLS8_OTOGA
Collagen	Collagen type I	Collagen type I alpha 1 chain OS=Sus scrofa OX=9823 GN=COL1A1 PE=1 SV=1	68.0100024	tr|A0A287A1S6|A0A287A1S6_PIG
Collagen	Collagen type I	Collagen alpha-2(I) chain (Fragments) OS=Orycteropus afer OX=9818 GN=COL1A2 PE=1 SV=1	57.9699993	sp|C0HJN4|CO1A2_ORYAF
Collagen	Collagen type I	Collagen alpha-2(I) chain OS=Bos taurus OX=9913 GN=COL1A2 PE=1 SV=2	61.0000014	sp|P02465|CO1A2_BOVIN
Collagen	Collagen type I	Collagen alpha-2(I) chain OS=Mammut americanum OX=39053 PE=1 SV=3	66.2500024	sp|P85154|CO1A2_MAMAE
Collagen	Collagen type I	Collagen alpha-2(I) chain OS=Pteropus alecto OX=9402 GN=PAL_GLEAN10021742 PE=4 SV=1	43.75	tr|L5KNP2|L5KNP2_PTEAL
Collagen	Collagen type I	Collagen alpha-2(I) chain OS=Rattus norvegicus OX=10116 GN=Col1a2 PE=1 SV=3	49.7099996	tr|F1LS40|F1LS40_RAT
Collagen	Collagen type I	Collagen type I alpha 2 chain OS=Mustela putorius furo OX=9669 GN=COL1A2 PE=4 SV=1	60.2800012	tr|M3XR96|M3XR96_MUSPF
Collagen	Collagen type I	Collagen type I alpha 2 chain OS=Otolemur garnettii OX=30611 GN=COL1A2 PE=4 SV=1	53.0099988	tr|H0WT85|H0WT85_OTOGA
Collagen	Collagen type III	Collagen alpha-1(III) chain OS=Mesocricetus auratus OX=10036 GN=Col3a1 PE=4 SV=1	45.5300003	tr|A0A1U7QZS1|A0A1U7QZS1_MESAU
Collagen	Collagen type III	Collagen type III alpha 1 chain OS=Cavia porcellus OX=10141 GN=COL3A1 PE=4 SV=2	49.5200008	tr|H0V8P9|H0V8P9_CAVPO
Collagen	Collagen type III	Collagen type III alpha 1 chain OS=Felis catus OX=9685 GN=COL3A1 PE=4 SV=2	52.2199988	tr|M3WL90|M3WL90_FELCA
Collagen	Collagen type III	Collagen type III alpha 1 chain OS=Ictidomys tridecemlineatus OX=43179 GN=COL3A1 PE=4 SV=1	44.3199992	tr|A0A287DCB4|A0A287DCB4_ICTTR
Collagen	Collagen type III	Collagen type III alpha 1 chain OS=Loxodonta africana OX=9785 GN=COL3A1 PE=4 SV=1	38.1000012	tr|G3TH25|G3TH25_LOXAF
Collagen	Collagen type III	Collagen type III alpha 1 chain OS=Myotis lucifugus OX=59463 GN=COL3A1 PE=4 SV=1	41.2800014	tr|G1PR85|G1PR85_MYOLU
Collagen	Collagen type III	Collagen type III alpha 1 chain OS=Oryctolagus cuniculus OX=9986 GN=COL3A1 PE=4 SV=1	50.1999974	tr|G1T8J0|G1T8J0_RABIT
Collagen	Collagen type III	Collagen type III alpha 1 chain OS=Ovis aries OX=9940 GN=COL3A1 PE=4 SV=1	50.7200003	tr|W5Q4S0|W5Q4S0_SHEEP
Collagen	Collagen type III	Collagen, type III, alpha 1 OS=Bos taurus OX=9913 GN=COL3A1 PE=2 SV=1	49.9300003	tr|Q08E14|Q08E14_BOVIN
Collagen	Collagen type III	REVERSED Collagen type III alpha 1 chain OS=Ailuropoda melanoleuca OX=9646 GN=COL3A1 PE=4 SV=1	44.9499995	RRRRRtr|G1LYT1|G1LYT1_AILME
Collagen	Collagen type V	ProCollagen alpha 1(V) OS=Sus scrofa OX=9823 GN=COL5A1 PE=2 SV=1	13.0400002	tr|Q59IP3|Q59IP3_PIG
Collagen	Collagen type V	ProCollagen alpha 2(V) OS=Sus scrofa OX=9823 GN=COL5A2 PE=2 SV=1	38.1599993	tr|Q59IP2|Q59IP2_PIG
Collagen	Collagen type V	Collagen type V alpha 2 chain OS=Sarcophilus harrisii OX=9305 GN=COL5A2 PE=4 SV=1	26.5300006	tr|G3VWK0|G3VWK0_SARHA
Collagen	Collagen type VI	Collagen alpha-2(VI) chain OS=Fukomys damarensis OX=885580 GN=H920_10447 PE=4 SV=1	12.7399996	tr|A0A091DC51|A0A091DC51_FUKDA
Collagen	Collagen type VI	Collagen type VI alpha 3 chain OS=Otolemur garnettii OX=30611 GN=COL6A3 PE=4 SV=1	3.02799996	tr|H0XEJ5|H0XEJ5_OTOGA
Collagen	Collagen type VI	Collagen type VI alpha 3 chain OS=Sus scrofa OX=9823 GN=COL6A3 PE=1 SV=1	7.11300001	tr|A0A287BLM4|A0A287BLM4_PIG
Collagen	Collagen type VI	Collagen, type VI, alpha 3 OS=Mus musculus OX=10090 GN=Col6a3 PE=1 SV=2	5.54200001	tr|E9PWQ3|E9PWQ3_MOUSE
ECM glycoproteins	Laminin	Laminin subunit beta 2 OS=Felis catus OX=9685 GN=LAMB2 PE=4 SV=2	7.10299984	tr|M3WC88|M3WC88_FELCA
ECM glycoproteins	Laminin	Laminin subunit alpha 5 OS=Sus scrofa OX=9823 GN=LAMA5 PE=4 SV=1	1.822	tr|A0A287AEH1|A0A287AEH1_PIG
ECM glycoproteins	Laminin	Laminin, alpha 5 OS=Pan troglodytes OX=9598 GN=LAMA5 PE=2 SV=1	1.75899994	tr|K7D2I3|K7D2I3_PANTR
ECM glycoproteins	Fibrillin	Fibrillin-1 OS=Sus scrofa OX=9823 GN=FBN1 PE=1 SV=3	18.8800007	tr|F1SN67|F1SN67_PIG
ECM glycoproteins	Fibronectin 1	Fibronectin 1 OS=Sus scrofa OX=9823 GN=FN1 PE=1 SV=1	9.16000009	tr|A0A286ZY95|A0A286ZY95_PIG

APPENDIX A

ECM glycoproteins	Fibrinogen	Fibrinogen beta chain OS=Sus scrofa OX=9823 GN=FGB PE=1 SV=2	4.62599993	tr|I3L651|I3L651_PIG
ECM glycoproteins	von Willebrand factor	von Willebrand factor OS=Sus scrofa OX=9823 GN=VWF PE=1 SV=2	2.77900007	tr|K7GNN0|K7GNN0_PIG
ECM regulators	Leukocyte elastase inhibitor	Leukocyte elastase inhibitor OS=Sus scrofa OX=9823 GN=SERPINB1 PE=1 SV=1	10.0500003	tr|F2Z5B1|F2Z5B1_PIG
ECM-affiliated proteins	Annexin	Annexin OS=Pteropus alecto OX=9402 GN=PAL_GLEAN10023415 PE=3 SV=1	6.15300015	tr|L5K0Z3|L5K0Z3_PTEAL
Secreted factors	Protein S100	Protein S100 OS=Pan troglodytes OX=9598 GN=S100A8 PE=3 SV=1	11.8299998	tr|H2Q028|H2Q028_PANTR
Others extracellular components	Azurocidin	Azurocidin OS=Sus scrofa OX=9823 GN=AZU1 PE=1 SV=2	51.6300023	sp|P80015|CAP7_PIG
Others extracellular components	Dermatopontin	Dermatopontin OS=Ovis aries OX=9940 GN=DPT PE=4 SV=1	11.9400002	tr|W5PHI8|W5PHI8_SHEEP
Others extracellular components	extracellular tyrosine-protein kinase	xtracellular tyrosine-protein kinase PKDCC OS=Dipodomys ordii OX=10020 GN=Pkdcc PE=4 SV=1	2.67399997	tr|A0A1S3F9Z3|A0A1S3F9Z3_DIPOR
Others extracellular components	Serum albumin	Serum albumin OS=Homo sapiens OX=9606 PE=2 SV=1	7.38900006	tr|Q56G89|Q56G89_HUMAN
Cellular components	Beta actin	Beta actin OS=Cricetidae sp. OX=36483 PE=2 SV=1	22.6699993	tr|O35247|O35247_CRISP
Cellular components	Caveolin	Caveolin OS=Myotis davidii OX=225400 GN=MDA_GLEAN10003317 PE=3 SV=1	14.61	tr|L5LJI4|L5LJI4_MYODS
Cellular components	Caveolin	Caveolin OS=Sus scrofa OX=9823 GN=CAV2 PE=2 SV=1	17.2800004	tr|G8GCE6|G8GCE6_PIG
Cellular components	cellular enzymes	Glyceraldehyde-3-phosphate dehydrogenase OS=Gammaproteobacteria bacterium OX=1913989 GN=gap PE=3 SV=1	6.45200014	|A0A2G6KYX1|A0A2G6KYX1_9GAMM
Cellular components	cellular enzymes	Glyceraldehyde-3-phosphate dehydrogenase OS=Homo sapiens OX=9606 GN=HEL-S-162eP PE=2 SV=1	10.4500003	tr|V9HVZ4|V9HVZ4_HUMAN
Cellular components	cellular enzymes	GMP synthase [glutamine-hydrolyzing] OS=Deltaproteobacteria bacterium OX=2026735 GN=guaA PE=3 SV=1	3.92899998	tr|A0A2G6NF56|A0A2G6NF56_9DELT
Cellular components	Junction plakoglobin	Junction plakoglobin OS=Ailuropoda melanoleuca OX=9646 GN=JUP PE=4 SV=1	26.96	tr|G1LGG3|G1LGG3_AILME
Cellular components	Heat shock protein	Epididymis secretory protein Li 102 OS=Homo sapiens OX=9606 GN=HEL-S-102 PE=2 SV=1	34.6300006	tr|V9HW43|V9HW43_HUMAN
Ig	IgG	IgG heavy chain OS=Sus scrofa OX=9823 GN=IGHG PE=2 SV=1	13.6500001	tr|L8B0U3|L8B0U3_PIG

Supplementary Table II. List of peptides found in proteomic analysis of MyoECM.

General protein classification	Protein classification	Peptide name	% Cov (Coverage)	Accession
Collagen	Collagen type I	Collagen alpha-1(I) chain (Fragments) OS=Cyclopes didactylus OX=84074 GN=COL1A1 PE=1 SV=1	91.50000215	sp|C0HJP1|CO1A1_CYCDI
Collagen	Collagen type I	Collagen alpha-1(I) chain (Fragments) OS=Equus sp. OX=46122 GN=COL1A1 PE=1 SV=1	78.21000218	sp|C0HJN9|CO1A1_EQUSP
Collagen	Collagen type I	Collagen alpha-1(I) chain OS=Castor canadensis OX=51338 GN=COL1A1 PE=4 SV=1	59.85999703	tr|A0A250Y7T0|A0A250Y7T0_CASCN
Collagen	Collagen type I	Collagen alpha-1(I) chain OS=Dipodomys ordii OX=10020 GN=Col1a1 PE=4 SV=1	63.8899982	tr|A0A1S3GXN3|A0A1S3GXN3_DIPOR
Collagen	Collagen type I	Collagen alpha-1(I) chain OS=Fukomys damarensis OX=885580 GN=H920_03660 PE=4 SV=1	41.76999927	tr|A0A091DWW2|A0A091DWW2_FUKDA
Collagen	Collagen type I	Collagen type I alpha 1 chain OS=Chlorocebus sabaeus OX=60711 GN=COL1A1 PE=4 SV=1	64.55000043	tr|A0A0D9QYW4|A0A0D9QYW4_CHLSB
Collagen	Collagen type I	Collagen type I alpha 1 chain OS=Felis catus OX=9685 GN=COL1A1 PE=4 SV=2	63.05999756	tr|M3W2F5|M3W2F5_FELCA
Collagen	Collagen type I	Collagen type I alpha 1 chain OS=Gorilla gorilla gorilla OX=9595 GN=COL1A1 PE=4 SV=1	65.03000259	tr|G3RBN8|G3RBN8_GORGO
Collagen	Collagen type I	Collagen type I alpha 1 chain OS=Monodelphis domestica OX=13616 GN=COL1A1 PE=4 SV=2	60.40999889	tr|F7CV32|F7CV32_MONDO
Collagen	Collagen type I	Collagen type I alpha 1 chain OS=Myotis lucifugus OX=59463 GN=COL1A1 PE=4 SV=1	63.92999887	tr|G1QDY4|G1QDY4_MYOLU
Collagen	Collagen type I	Collagen type I alpha 1 chain OS=Ornithorhynchus anatinus OX=9258 GN=COL1A1 PE=4 SV=1	43.88999939	tr|F7ESN3|F7ESN3_ORNAN
Collagen	Collagen type I	Collagen type I alpha 1 chain OS=Ovis aries OX=9940 GN=COL1A1 PE=4 SV=1	61.73999906	tr|W5P481|W5P481_SHEEP
Collagen	Collagen type I	Collagen type I alpha 1 chain OS=Sus scrofa OX=9823 GN=COL1A1 PE=1 SV=1	70.87000012	tr|A0A287A1S6|A0A287A1S6_PIG
Collagen	Collagen type I	Collagen type I alpha 2 OS=Felis catus OX=9685 GN=COL1A2 PE=4 SV=2	63.59000206	tr|M3WVN3|M3WVN3_FELCA
Collagen	Collagen type I	Collagen type I alpha 2 chain OS=Loxodonta africana OX=9785 GN=COL1A2 PE=4 SV=1	49.48999882	tr|G3TIC0|G3TIC0_LOXAF
Collagen	Collagen type I	Collagen type I alpha 2 chain OS=Mustela putorius furo OX=9669 GN=COL1A2 PE=4 SV=1	58.74000192	tr|M3XR96|M3XR96_MUSPF
Collagen	Collagen type I	Collagen type I alpha 2 chain OS=Otolemur garnettii OX=30611 GN=COL1A2 PE=4 SV=1	49.77999926	tr|H0WT85|H0WT85_OTOGA
Collagen	Collagen type I	Collagen alpha-2(I) chain (Fragments) OS=Equus sp. OX=46122 GN=COL1A2 PE=1 SV=1	79.71000075	sp|C0HJP0|CO1A2_EQUSP
Collagen	Collagen type I	Collagen alpha-2(I) chain (Fragments) OS=Orycteropus afer OX=9818 GN=COL1A2 PE=1 SV=1	69.42999959	sp|C0HJN4|CO1A2_ORYAF
Collagen	Collagen type I	Collagen alpha-2(I) chain (Fragments) OS=Toxodon sp. OX=1563122 GN=COL1A2 PE=1 SV=1	81.83000088	sp|C0HJP8|CO1A2_TOXSP
Collagen	Collagen type I	Collagen alpha-2(I) chain OS=Bos taurus OX=9913 GN=COL1A2 PE=1 SV=2	59.68000293	sp|P02465|CO1A2_BOVIN
Collagen	Collagen type I	Collagen alpha-2(I) chain OS=Canis lupus familiaris OX=9615 GN=COL1A2 PE=4 SV=1	58.49000216	tr|F1PHY1|F1PHY1_CANLF
Collagen	Collagen type I	Collagen alpha-2(I) chain OS=Oryctolagus cuniculus OX=9986 GN=COL1A2 PE=4 SV=1	47.06999958	tr|G1T2Z5|G1T2Z5_RABIT
Collagen	Collagen type I	Collagen alpha-2(I) chain OS=Pteropus alecto OX=9402 GN=PAL_GLEAN10021742 PE=4 SV=1	43.45999956	tr|L5KNP2|L5KNP2_PTEAL
Collagen	Collagen type I	Collagen alpha-2(I) chain OS=Rattus norvegicus OX=10116 GN=Col1a2 PE=1 SV=3	45.91999948	tr|F1LS40|F1LS40_RAT
Collagen	Collagen type III	Collagen type III alpha 1 chain OS=Ailuropoda melanoleuca OX=9646 GN=COL3A1 PE=4 SV=1	43.09999943	tr|G1LYT1|G1LYT1_AILME
Collagen	Collagen type III	Collagen type III alpha 1 chain OS=Equus caballus OX=9796 GN=COL3A1 PE=4 SV=1	39.75999951	tr|F6R528|F6R528_HORSE
Collagen	Collagen type III	Collagen type III alpha 1 chain OS=Felis catus OX=9685 GN=COL3A1 PE=4 SV=2	53.04999948	tr|M3WL90|M3WL90_FELCA
Collagen	Collagen type III	Collagen type III alpha 1 chain OS=Ictidomys tridecemlineatus OX=43179 GN=COL3A1 PE=4 SV=1	40.63000083	tr|A0A287DCB4|A0A287DCB4_ICTTR
Collagen	Collagen type III	Collagen type III alpha 1 chain OS=Myotis lucifugus OX=59463 GN=COL3A1 PE=4 SV=1	39.84999955	tr|G1PR85|G1PR85_MYOLU
Collagen	Collagen type V	ProCollagen alpha 2(V) OS=Sus scrofa OX=9823 GN=COL5A2 PE=2 SV=1	19.81000006	tr|Q59IP2|Q59IP2_PIG
Collagen	Collagen type V	Collagen type V alpha 1 chain OS=Ailuropoda melanoleuca OX=9646 GN=COL5A1 PE=4 SV=1	30.82999885	tr|G1LX86|G1LX86_AILME
Collagen	Collagen type V	Collagen type V alpha 2 chain OS=Sarcophilus harrisii OX=9305 GN=COL5A2 PE=4 SV=1	23.92999977	tr|G3VWK0|G3VWK0_SARHA
Collagen	Collagen type VI	Collagen type VI alpha 1 chain OS=Mustela putorius furo OX=9669 GN=COL6A1 PE=4 SV=1	10.32999977	tr|M3XRA5|M3XRA5_MUSPF
Collagen	Collagen type VI	Collagen type VI alpha 2 chain OS=Ailuropoda melanoleuca OX=9646 GN=COL6A2 PE=4 SV=1	18.73999983	tr|G1L445|G1L445_AILME
Collagen	Collagen type VI	Collagen alpha-2(VI) chain OS=Bos mutus OX=72004 GN=M91_02728 PE=4 SV=1	25.29000044	tr|L8I5Z3|L8I5Z3_9CETA
Collagen	Collagen type VI	Collagen type VI alpha 3 chain OS=Gorilla gorilla gorilla OX=9595 GN=COL6A3 PE=4 SV=2	8.90500024	tr|G3S5Z6|G3S5Z6_GORGO

APPENDIX A

Collagen	Collagen type VI	Collagen type VI alpha 3 chain OS=Otolemur garnettii OX=30611 GN=COL6A3 PE=4 SV=1	6.593000144	tr|H0XEJ5|H0XEJ5_OTOGA
Collagen	Collagen type VI	Collagen type VI alpha 3 chain OS=Ovis aries OX=9940 GN=COL6A3 PE=4 SV=1	8.370000124	tr|W5QCP9|W5QCP9_SHEEP
Collagen	Collagen type VI	Collagen type VI alpha 3 chain OS=Sus scrofa OX=9823 GN=COL6A3 PE=1 SV=1	13.33000064	tr|A0A287BLM4|A0A287BLM4_PIG
Collagen	Collagen type XII	Collagen type XII alpha 1 chain OS=Ovis aries OX=9940 GN=COL12A1 PE=4 SV=1	3.392000124	tr|W5P8W6|W5P8W6_SHEEP
ECM glycoproteins	Laminin	Laminin subunit alpha 5 OS=Sus scrofa OX=9823 GN=LAMA5 PE=4 SV=1	3.616999835	tr|A0A287AEH1|A0A287AEH1_PIG
ECM glycoproteins	Laminin	Laminin, alpha 5 OS=Pan troglodytes OX=9598 GN=LAMA5 PE=2 SV=1	2.490000054	tr|K7D2I3|K7D2I3_PANTR
ECM glycoproteins	Laminin	Laminin subunit beta 2 OS=Sus scrofa OX=9823 GN=LAMB2 PE=1 SV=3	12.98999935	tr|F1SPT5|F1SPT5_PIG
ECM glycoproteins	Fibrillin	Fibrillin-1 OS=Sus scrofa OX=9823 GN=FBN1 PE=1 SV=3	20.64999938	tr|F1SN67|F1SN67_PIG
ECM glycoproteins	Fibrillin	fibrillin-2 OS=Erinaceus europaeus OX=9365 GN=FBN2 PE=4 SV=1	7.417999953	tr|A0A1S3A1M5|A0A1S3A1M5_ERIEU
ECM glycoproteins	Fibronectin 1	Fibronectin 1 OS=Sus scrofa OX=9823 GN=FN1 PE=1 SV=1	8.109000325	tr|A0A286ZY95|A0A286ZY95_PIG
ECM glycoproteins	Apolipoprotein D	Apolipoprotein D OS=Homo sapiens OX=9606 GN=APOD PE=1 SV=1	38.10000122	sp|P05090|APOD_HUMAN
ECM-affiliated proteins	Annexin	Annexin OS=Equus caballus OX=9796 GN=ANXA2 PE=2 SV=1	37.45999932	tr|F6ZI51|F6ZI51_HORSE
ECM-affiliated proteins	Annexin	Annexin OS=Sus scrofa OX=9823 GN=ANXA6 PE=2 SV=1	17.38000065	tr|M3VH45|M3VH45_PIG
ECM-affiliated proteins	Dermatopontin	Dermatopontin OS=Ovis aries OX=9940 GN=DPT PE=4 SV=1	11.94000021	tr|W5PHI8|W5PHI8_SHEEP
Secreted factors	Protein S100	Protein S100 OS=Pan troglodytes OX=9598 GN=S100A8 PE=3 SV=1	11.82999983	tr|H2Q028|H2Q028_PANTR
Others extracellular components	Azurocidin	Azurocidin OS=Sus scrofa OX=9823 GN=AZU1 PE=1 SV=2	52.85000205	sp|P80015|CAP7_PIG
Others extracellular components	Kappa-casein	Kappa-casein (Fragment) OS=Bos indicus x Bos taurus OX=30522 GN=CSN3 PE=4 SV=1	17.4999997	tr|Q9N273|Q9N273_BOBOX
Others extracellular components	Serum albumin	Serum albumin OS=Homo sapiens OX=9606 PE=2 SV=1	14.77999985	tr|Q56G89|Q56G89_HUMAN
Cellular Components	Caveolin	Caveolin OS=Castor canadensis OX=51338 GN=CAV1 PE=3 SV=1	19.09999996	tr|A0A250XVR7|A0A250XVR7_CASCN
Cellular Components	Caveolin	Caveolin OS=Sus scrofa OX=9823 GN=CAV2 PE=2 SV=1	17.28000045	tr|G8GCE6|G8GCE6_PIG
Cellular Components	cellular enzymes	Histone acetyltransferase (Fragment) OS=Tupaia chinensis OX=246437 GN=TREES_T100014382 PE=3 SV=1	0.775900017	tr|L9JAG0|L9JAG0_TUPCH
Cellular Components	cellular enzymes	Glyceraldehyde-3-phosphate dehydrogenase OS=Homo sapiens OX=9606 GN=HEL-S-162eP PE=2 SV=1	15.21999985	tr|V9HVZ4|V9HVZ4_HUMAN
Cellular Components	cellular enzymes	Phosphoinositide 3-kinase adapter protein 1 (Fragment) OS=Heterocephalus glaber OX=10181 GN=GW7_11923 PE=4 SV=1	2.553999983	tr|G5BEU1|G5BEU1_HETGA
Cellular Components	myosin 11	REVERSED MKIAA0866 protein (Fragment) OS=Mus musculus OX=10090 GN=Myh11 PE=2 SV=1	0.453600008	RRRRRtr|Q69ZX3|Q69ZX3_MOUSE
Cellular Components	Actin	Actin, aortic smooth muscle OS=Cricetulus griseus OX=10029 GN=H671_3g9856 PE=3 SV=1	24.60000068	tr|G3HQY2|G3HQY2_CRIGR
Cellular Components	Ribosomal proteins	OS=Camelus ferus OX=419612 GN=CB1_000878024 PE=4 SV=1	30.98999858	tr|S9Y7C3|S9Y7C3_CAMFR
Cellular Components	Beta-1-syntrophin	Beta-1-syntrophin OS=Fukomys damarensis OX=885580 GN=H920_03321 PE=4 SV=1	3.694999963	tr|A0A091EIA7|A0A091EIA7_FUKDA
Cellular Components	Myeloid-associated differentiation marker	Myeloid-associated differentiation marker tv2 OS=Sus scrofa OX=9823 GN=MYADM PE=2 SV=1	18.32000017	tr|M3UZ75|M3UZ75_PIG
Cellular Components	Junction plakoglobin	Junction plakoglobin OS=Myotis brandtii OX=109478 GN=D623_10015352 PE=4 SV=1	22.82000035	tr|S7NBB7|S7NBB7_MYOBR

Supplementary Table III. List of peptides found in proteomic analysis of No-DC Endo.

General protein classification	Protein classification	Peptide name	% Cov (Coverage)	Accession
Collagen	Collagen type I	Collagen alpha-1(I) chain (Fragments) OS=Cyclopes didactylus OX=84074 GN=COL1A1 PE=1 SV=1	90.200001	sp|C0HJP1|CO1A1_CYCDI
Collagen	Collagen type I	Collagen alpha-1(I) chain (Fragments) OS=Toxodon sp. OX=1563122 GN=COL1A1 PE=1 SV=1	88.09000254	sp|C0HJP7|CO1A1_TOXSP
Collagen	Collagen type I	Collagen alpha-1(I) chain OS=Castor canadensis OX=51338 GN=COL1A1 PE=4 SV=1	63.22000027	tr|A0A250Y7T0|A0A250Y7T0_CASCN
Collagen	Collagen type I	Collagen alpha-1(I) chain OS=Dipodomys ordii OX=10020 GN=Col1a1 PE=4 SV=1	59.43999887	tr|A0A1S3GXN3|A0A1S3GXN3_DIPOR
Collagen	Collagen type I	Collagen type I alpha 1 chain OS=Felis catus OX=9685 GN=COL1A1 PE=4 SV=2	66.53000116	tr|M3W2F5|M3W2F5_FELCA
Collagen	Collagen type I	Collagen type I alpha 1 chain OS=Sus scrofa OX=9823 GN=COL1A1 PE=1 SV=1	70.05000114	tr|A0A287A1S6|A0A287A1S6_PIG
Collagen	Collagen type I	Collagen type I alpha 2 chain OS=Otolemur garnettii OX=30611 GN=COL1A2 PE=4 SV=1	42.44999886	tr|H0WT85|H0WT85_OTOGA
Collagen	Collagen type I	Collagen alpha-2(I) chain OS=Mammut americanum OX=39053 PE=1 SV=3	57.49999881	sp|P85154|CO1A2_MAMAE
Collagen	Collagen type I	Collagen alpha-2(I) chain OS=Rattus norvegicus OX=10116 GN=Col1a2 PE=1 SV=3	45.26000023	tr|F1LS40|F1LS40_RAT
Collagen	Collagen type III	Collagen alpha-1(III) chain OS=Bos taurus OX=9913 GN=COL3A1 PE=1 SV=1	69.20999885	sp|P04258|CO3A1_BOVIN
Collagen	Collagen type III	Collagen type III alpha 1 chain OS=Equus caballus OX=9796 GN=COL3A1 PE=4 SV=1	37.94000149	tr|F6R528|F6R528_HORSE
Collagen	Collagen type III	Collagen type III alpha 1 chain OS=Mustela putorius furo OX=9669 GN=COL3A1 PE=4 SV=1	41.53999984	tr|M3YLM6|M3YLM6_MUSPF
Collagen	Collagen type III	Collagen type III alpha 1 chain OS=Myotis lucifugus OX=59463 GN=COL3A1 PE=4 SV=1	42.10000038	tr|G1PR85|G1PR85_MYOLU
Collagen	Collagen type IV	Collagen type IV alpha 1 chain OS=Mustela putorius furo OX=9669 GN=COL4A1 PE=3 SV=1	16.36999995	tr|M3YI93|M3YI93_MUSPF
Collagen	Collagen type IV	Collagen type IV alpha 2 chain OS=Sus scrofa OX=9823 GN=COL4A2 PE=1 SV=3	12.72999942	tr|F1RLL9|F1RLL9_PIG
Collagen	Collagen type V	ProCollagen alpha 1(V) OS=Sus scrofa OX=9823 GN=COL5A1 PE=2 SV=1	19.23999935	tr|Q59IP3|Q59IP3_PIG
Collagen	Collagen type V	ProCollagen alpha 2(V) OS=Sus scrofa OX=9823 GN=COL5A2 PE=2 SV=1	27.27999985	tr|Q59IP2|Q59IP2_PIG
Collagen	Collagen type VI	Collagen type VI alpha 1 chain OS=Otolemur garnettii OX=30611 GN=COL6A1 PE=4 SV=1	10.27000025	tr|H0Y0P4|H0Y0P4_OTOGA
Collagen	Collagen type VI	Collagen type VI alpha 2 chain OS=Bos taurus OX=9913 GN=COL6A2 PE=1 SV=1	14.8300007	tr|Q1JQB0|Q1JQB0_BOVIN
Collagen	Collagen type VI	Collagen type VI alpha 3 chain OS=Otolemur garnettii OX=30611 GN=COL6A3 PE=4 SV=1	4.416000098	tr|H0XEJ5|H0XEJ5_OTOGA
Collagen	Collagen type VI	Collagen type VI alpha 3 chain OS=Ovis aries OX=9940 GN=COL6A3 PE=4 SV=1	5.040999874	tr|W5QCP9|W5QCP9_SHEEP
Collagen	Collagen type VI	Collagen type VI alpha 3 chain OS=Sus scrofa OX=9823 GN=COL6A3 PE=1 SV=1	10.22000015	tr|A0A287BLM4|A0A287BLM4_PIG
Collagen	Collagen type VI	Collagen type VI alpha 3 chain OS=Sus scrofa OX=9823 GN=COL6A3 PE=1 SV=2	4.397	tr|I3LUR7|I3LUR7_PIG
ECM glycoproteins	Laminin	Laminin subunit alpha 5 OS=Sus scrofa OX=9823 GN=LAMA5 PE=4 SV=1	2.474999987	tr|A0A287AEH1|A0A287AEH1_PIG
ECM glycoproteins	Laminin	Laminin, alpha 5 OS=Pan troglodytes OX=9598 GN=LAMA5 PE=2 SV=1	1.813000068	tr|K7D2I3|K7D2I3_PANTR
ECM glycoproteins	Laminin	Laminin subunit beta 1 OS=Sus scrofa OX=9823 GN=LAMB1 PE=1 SV=3	2.50599999	tr|F1SAE9|F1SAE9_PIG
ECM glycoproteins	Laminin	Laminin subunit beta 2 OS=Sus scrofa OX=9823 GN=LAMB2 PE=1 SV=3	7.274000347	tr|F1SPT5|F1SPT5_PIG
ECM glycoproteins	Fibrillin	Fibrillin-1 OS=Sus scrofa OX=9823 GN=FBN1 PE=1 SV=3	17.82999933	tr|F1SN67|F1SN67_PIG
ECM glycoproteins	Fibronectin 1	Fibronectin 1 OS=Sus scrofa OX=9823 GN=FN1 PE=1 SV=1	12.26999983	tr|A0A286ZY95|A0A286ZY95_PIG
ECM glycoproteins	Nidogen 1	Nidogen 1 OS=Sus scrofa OX=9823 GN=NID1 PE=1 SV=3	6.768999994	tr|F1RGY5|F1RGY5_PIG
ECM glycoproteins	von Willebrand factor	von Willebrand factor OS=Sus scrofa OX=9823 GN=VWF PE=1 SV=2	4.417999834	tr|K7GNN0|K7GNN0_PIG
ECM glycoproteins	Apolipoprotein D	Apolipoprotein D OS=Ovis aries OX=9940 GN=APOD PE=3 SV=1	13.15000057	tr|W5QGP4|W5QGP4_SHEEP
ECM glycoproteins	Adiponectin	30 kDa adipocyte complement-related protein OS=Rattus norvegicus OX=10116 GN=Adipoq PE=1 SV=1	24.17999953	tr|Q8K3R4|Q8K3R4_RAT
ECM regulators	Serpin Family	Leukocyte elastase inhibitor OS=Sus scrofa OX=9823 GN=SERPINB1 PE=1 SV=1	47.62000144	tr|F2Z5B1|F2Z5B1_PIG
ECM regulators	Serpin Family	Serpin family B member 6 OS=Sus scrofa OX=9823 GN=SERPINB6 PE=1 SV=2	25.40000081	tr|I3LCP8|I3LCP8_PIG
ECM regulators	Serpin Family	Serpin family F member 2 OS=Sus scrofa OX=9823 GN=SERPINF2 PE=1 SV=1	10.30000001	tr|A0A287B9B3|A0A287B9B3_PIG
ECM regulators	Serpin Family	Alpha-1-antichymotrypsin 2 OS=Sus scrofa OX=9823 GN=SERPINA3-2 PE=3 SV=1	12.04999983	tr|Q9GMA6|Q9GMA6_PIG
ECM regulators	Serpin Family	Alpha-1-antitrypsin OS=Sus scrofa OX=9823 GN=SERPINA1 PE=3 SV=2	15.0000006	tr|F1SCF0|F1SCF0_PIG
ECM regulators	Cathepsin	Cathepsin B OS=Sus scrofa OX=9823 GN=CTSB PE=1 SV=1	21.2500006	tr|A0A287BF94|A0A287BF94_PIG

ECM regulators	Cathepsin	Cathepsin D protein (Fragment) OS=Sus scrofa OX=9823 PE=2 SV=1	23.0399996	tr|Q5MJE5|Q5MJE5_PIG
ECM regulators	Cathepsin	Cathepsin K OS=Sus scrofa OX=9823 GN=CTSS PE=1 SV=2	9.063000232	tr|F1SS93|F1SS93_PIG
ECM regulators	Cathepsin	Cathepsin Z OS=Sus scrofa OX=9823 GN=CTSZ PE=1 SV=1	11.18000001	tr|A5GFX7|A5GFX7_PIG
ECM-affiliated proteins	Annexin	Annexin OS=Sus scrofa OX=9823 GN=ANXA1 PE=1 SV=2	22.22000062	tr|K7GLE1|K7GLE1_PIG
ECM-affiliated proteins	Annexin	Annexin OS=Sus scrofa OX=9823 GN=ANXA2 PE=1 SV=1	18.84000003	tr|A0A286ZJV6|A0A286ZJV6_PIG
ECM-affiliated proteins	Mucin	Mucin 5AC, oligomeric mucus/gel-forming OS=Sus scrofa OX=9823 GN=MUC5AC PE=1 SV=1	1.121000014	tr|A0A287ANG4|A0A287ANG4_PIG
Secreted factors	Protein S100	Protein S100 OS=Pan troglodytes OX=9598 GN=S100A8 PE=3 SV=1	37.63000071	tr|H2Q028|H2Q028_PANTR
Others extracellular components	Serum albumin	Serum albumin (Fragment) OS=Homo sapiens OX=9606 GN=ALB PE=1 SV=1	19.59999949	tr|H0YA55|H0YA55_HUMAN
Others extracellular components	Serum albumin	Serum albumin OS=Sus scrofa OX=9823 GN=ALB PE=1 SV=1	44.47999895	tr|F1RUN2|F1RUN2_PIG
Cellular components	cellular enzymes	Glyceraldehyde-3-phosphate dehydrogenase OS=Homo sapiens OX=9606 GN=HEL-S-162eP PE=2 SV=1	27.1600008	tr|V9HVZ4|V9HVZ4_HUMAN
Cellular components	cellular enzymes	Cytidine deaminase OS=Bos mutus OX=72004 GN=M91_09666 PE=3 SV=1	23.97000045	tr|L8I1I7|L8I1I7_9CETA
Cellular components	cellular enzymes	D-aminoacyl-tRNA deacylase OS=Sus scrofa OX=9823 GN=DTD1 PE=1 SV=2	16.26999974	tr|F1SBH1|F1SBH1_PIG
Cellular components	cellular enzymes	Dicarbonyl and L-xylulose reductase OS=Sus scrofa OX=9823 GN=DCXR PE=4 SV=1	23.77000004	tr|A0A286ZQ44|A0A286ZQ44_PIG
Cellular components	cellular enzymes	Glucosidase alpha, acid OS=Sus scrofa OX=9823 GN=GAA PE=1 SV=2	7.427000254	tr|I3LQL8|I3LQL8_PIG
Cellular components	cellular enzymes	Glutathione peroxidase OS=Sus scrofa OX=9823 GN=GPX3 PE=1 SV=1	23.99999946	tr|A0A287AIJ3|A0A287AIJ3_PIG
Cellular components	cellular enzymes	GMP reductase OS=Ovis aries OX=9940 GN=GMPR2 PE=3 SV=1	24.78999943	tr|W5QCY6|W5QCY6_SHEEP
Cellular components	cellular enzymes	GMP synthase [glutamine-hydrolyzing] OS=Cricetulus griseus OX=10029 GN=I79_004230 PE=4 SV=1	4.055000097	tr|G3H229|G3H229_CRIGR
Cellular components	cellular enzymes	Thioredoxin-dependent peroxide reductase, mitochondrial OS=Bos mutus OX=72004 GN=M91_10467 PE=4 SV=1	16.73000008	tr|L8I536|L8I536_9CETA
Cellular components	cellular enzymes	Maltase-glucoamylase OS=Sus scrofa OX=9823 GN=MGAM PE=1 SV=1	12.48999983	tr|A0A287A042|A0A287A042_PIG
Cellular components	cellular enzymes	N-acetylglucosamine-6-sulfatase OS=Sus scrofa OX=9823 GN=GNS PE=1 SV=1	8.696000278	tr|K9IVU5|K9IVU5_PIG
Cellular components	cellular enzymes	N-acylethanolamine acid amidase OS=Sus scrofa OX=9823 GN=NAAA PE=1 SV=2	16.57000035	tr|F1RYU7|F1RYU7_PIG
Cellular components	cellular enzymes	N-acylsphingosine amidohydrolase 1 OS=Sus scrofa OX=9823 GN=ASAH1 PE=1 SV=3	24.05000031	tr|F1SES5|F1SES5_PIG
Cellular components	cellular enzymes	Palmitoyl-protein thioesterase 1 OS=Ovis aries OX=9940 GN=PPT1 PE=4 SV=1	19.86999959	tr|W5QG24|W5QG24_SHEEP
Cellular components	cellular enzymes	Peptidyl-prolyl cis-trans isomerase OS=Cricetulus griseus OX=10029 GN=I79_005402 PE=3 SV=1	9.72200036	tr|G3H533|G3H533_CRIGR
Cellular components	cellular enzymes	Phospholipase B-like OS=Sus scrofa OX=9823 GN=PLBD2 PE=1 SV=3	4.244000092	tr|F1RKC7|F1RKC7_PIG
Cellular components	cellular enzymes	Phospholipase D3 isoform 7-like protein OS=Camelus ferus OX=419612 GN=CB1_000338009 PE=4 SV=1	6.395000219	tr|S9YPW0|S9YPW0_CAMFR
Cellular components	cellular enzymes	Prostaglandin D synthase (Fragment) OS=Sus scrofa OX=9823 GN=pgds PE=2 SV=1	30.93000054	tr|Q765P8|Q765P8_PIG
Cellular components	cellular enzymes	Superoxide dismutase [Cu-Zn] OS=Sus scrofa OX=9823 GN=SOD1 PE=2 SV=1	39.21999931	tr|D9D839|D9D839_PIG
Cellular components	cellular enzymes	Transaldolase OS=Sus scrofa OX=9823 GN=TALDO1 PE=1 SV=3	10.98000035	tr|F1RYY6|F1RYY6_PIG
Cellular components	cellular enzymes	3-hydroxybutyrate dehydrogenase type 2 OS=Fukomys damarensis OX=885580 GN=H920_12791 PE=3 SV=1	10.98000035	tr|A0A091D5V5|A0A091D5V5_FUKDA
Cellular components	cellular enzymes	Histone acetyltransferase (Fragment) OS=Tupaia chinensis OX=246437 GN=TREES_T100014382 PE=3 SV=1	4.518000036	tr|L9JAG0|L9JAG0_TUPCH
Cellular components	cellular enzymes	Ribonuclease 4 OS=Sus scrofa OX=9823 GN=RNASE4 PE=1 SV=3	35.3700012	sp|P15468|RNAS4_PIG
Cellular components	Caveolin	Caveolin OS=Sus scrofa OX=9823 GN=CAV2 PE=2 SV=1	17.28000045	tr|G8GCE6|G8GCE6_PIG
Cellular components	Myosin	Myosin heavy chain 9 OS=Felis catus OX=9685 GN=MYH9 PE=3 SV=2	8.27300027	tr|M3VW11|M3VW11_FELCA
Cellular components	Myosin	Myosin-10 isoform 2 OS=Callithrix jacchus OX=9483 GN=MYH10 PE=2 SV=1	6.123000011	tr|U3F1R2|U3F1R2_CALJA
Cellular components	Myosin	Myosin-11 OS=Pteropus alecto OX=9402 GN=PAL_GLEAN10009738 PE=3 SV=1	9.788999707	tr|L5KQB6|L5KQB6_PTEAL
Cellular components	Tropomiosin	Tropomyosin 1 (Alpha), isoform CRA_f OS=Homo sapiens OX=9606 GN=TPM1 PE=1 SV=1	52.14999914	tr|Q6ZN40|Q6ZN40_HUMAN
Cellular components	Tropomiosin	Tropomyosin alpha-1 chain isoform 3 OS=Callithrix jacchus OX=9483 GN=TPM1 PE=2 SV=1	60.21000147	tr|L5K201|L5K201_PTEAL
Cellular components	Tropomiosin	Tropomyosin alpha-3 chain isoform 2 OS=Macaca mulatta OX=9544 GN=TPM3 PE=2 SV=1	68.54000092	tr|U3E2P5|U3E2P5_CALJA

Cellular components	Tropomiosin	Tropomyosin alpha-3 chain OS=Pteropus alecto OX=9402 GN=PAL_GLEAN10023407 PE=3 SV=1	48.51999879	tr|H9YZ58|H9YZ58_MACMU
Cellular components	Tropomiosin	Tropomyosin 2 OS=Ovis aries OX=9940 GN=TPM2 PE=3 SV=1	57.74999857	tr|W5PQL4|W5PQL4_SHEEP
Cellular components	Tropomiosin	Epididymis secretory protein Li 108 OS=Homo sapiens OX=9606 GN=HEL-S-108 PE=2 SV=1	74.59999919	tr|V9HW56|V9HW56_HUMAN
Cellular components	Histones	Heterogeneous nuclear ribonucleoprotein U OS=Ovis aries OX=9940 GN=HNRNPU PE=4 SV=1	6.612999737	tr|W5P4I9|W5P4I9_SHEEP
Cellular components	Histones	Heterogeneous nuclear ribonucleoprotein H3 OS=Loxodonta africana OX=9785 GN=HNRNPH3 PE=4 SV=1	16.14000052	tr|G3TAE6|G3TAE6_LOXAF
Cellular components	Histones	Core histone macro-H2A OS=Sarcophilus harrisii OX=9305 GN=H2AFY PE=4 SV=1	11.02000028	tr|G3W5X9|G3W5X9_SARHA
Cellular components	Others	Proliferating cell nuclear antigen OS=Ovis aries OX=9940 GN=PCNA PE=3 SV=1	13.1099999	tr|W5Q6P4|W5Q6P4_SHEEP
Cellular components	Others	SEC22 homolog B, vesicle trafficking protein (gene/pseudogene) OS=Ovis aries OX=9940 GN=SEC22B PE=3 SV=1	6.421999633	tr|W5QGX9|W5QGX9_SHEEP
Cellular components	Others	Selenium binding protein 1 OS=Sus scrofa OX=9823 GN=SELENBP1 PE=1 SV=2	17.03000069	tr|F1ST01|F1ST01_PIG
Cellular components	Others	Solute carrier family 44 member 1 OS=Ovis aries OX=9940 GN=SLC44A1 PE=3 SV=1	4.715000093	tr|W5PBL5|W5PBL5_SHEEP
Cellular components	Others	Spectrin beta chain OS=Ovis aries OX=9940 GN=SPTBN1 PE=3 SV=1	3.088999912	tr|W5NZX9|W5NZX9_SHEEP
Cellular components	Others	transcriptional activator protein Pur-alpha OS=Dipodomys ordii OX=10020 GN=Pura PE=4 SV=1	13.84000033	tr|A0A1S3FI87|A0A1S3FI87_DIPOR
Cellular components	Others	Caveolae associated protein 1 OS=Chlorocebus sabaeus OX=60711 GN=CAVIN1 PE=4 SV=1	18.62999946	tr|A0A0D9S1T8|A0A0D9S1T8_CHLSB
Cellular components	Others	CDGSH iron sulfur domain 2 OS=Ovis aries OX=9940 GN=CISD2 PE=4 SV=1	13.72999996	tr|W5PRB3|W5PRB3_SHEEP
Cellular components	Others	Filamin A OS=Sus scrofa OX=9823 GN=FLNA PE=4 SV=1	2.410000004	tr|A0A287B242|A0A287B242_PIG
Cellular components	Others	Filamin C OS=Ovis aries OX=9940 GN=FLNC PE=4 SV=1	6.216000021	tr|W5NZK9|W5NZK9_SHEEP
Cellular components	Others	Ferritin OS=Camelus ferus OX=419612 GN=CB1_000743158 PE=3 SV=1	13.24999928	tr|S9WS69|S9WS69_CAMFR
Cellular components	Others	Hemoglobin subunit beta OS=Sus scrofa OX=9823 GN=HBB PE=3 SV=1	45.57999969	tr|F1RII7|F1RII7_PIG
Cellular components	Others	Voltage-dependent anion channel 1 OS=Ictidomys tridecemlineatus OX=43179 GN=VDAC1 PE=4 SV=2	31.85000122	tr|I3MAD1|I3MAD1_ICTTR
Cellular components	Others	voltage-dependent anion-selective channel protein 3 OS=Dipodomys ordii OX=10020 GN=Vdac3 PE=4 SV=1	29.67999876	tr|A0A1S3G0R9|A0A1S3G0R9_DIPOR
Cellular components	Others	Polyubiquitin-C OS=Macaca fascicularis OX=9541 GN=EGM_07462 PE=4 SV=1	31.36999905	tr|G7PTR1|G7PTR1_MACFA
Cellular components	Others	Prelamin-A/C OS=Sus scrofa OX=9823 GN=LMNA PE=1 SV=1	12.5	tr|F1RLQ2|F1RLQ2_PIG
Cellular components	Ribosomal proteins	Ribosomal protein S3 OS=Ovis aries OX=9940 GN=RPS3 PE=3 SV=1	17.08000004	tr|W5PPH6|W5PPH6_SHEEP
Cellular components	Ribosomal proteins	40S ribosomal protein S3a OS=Ovis aries OX=9940 GN=RPS3A PE=3 SV=1	24.24000055	tr|W5QG75|W5QG75_SHEEP
Cellular components	Ribosomal proteins	40S ribosomal protein SA OS=Myotis brandtii OX=109478 GN=RPSA PE=3 SV=1	29.19000089	tr|S7P8J3|S7P8J3_MYOBR
Cellular components	Ribosomal proteins	60S ribosomal protein L18 OS=Camelus ferus OX=419612 GN=CB1_007371005 PE=4 SV=1	19.14999932	tr|S9W5U7|S9W5U7_CAMFR
Cellular components	Ribosomal proteins	60S ribosomal protein L22 OS=Pteropus alecto OX=9402 GN=PAL_GLEAN10013085 PE=4 SV=1	11.21999994	tr|L5KGY7|L5KGY7_PTEAL
Cellular components	Inter-alpha-trypsin inhibitor	Inter-alpha-trypsin inhibitor heavy chain H1 OS=Sus scrofa OX=9823 GN=ITIH1 PE=1 SV=3	10.09000018	tr|F1SH96|F1SH96_PIG
Cellular components	Junction plakoglobin	Junction plakoglobin OS=Myotis brandtii OX=109478 GN=D623_10015352 PE=4 SV=1	22.14999944	tr|S7NBB7|S7NBB7_MYOBR
Cellular components	Legumain	Legumain OS=Sus scrofa OX=9823 GN=LGMN PE=1 SV=2	2.740000002	tr|I3LKM9|I3LKM9_PIG
Cellular components	Thioredoxin	Thioredoxin OS=Sus scrofa OX=9823 GN=TRX1 PE=2 SV=1	46.66999876	tr|H6TBN0|H6TBN0_PIG
Cellular components	peroxiredoxin	Epididymis secretory sperm binding protein Li 97n OS=Homo sapiens OX=9606 GN=HEL-S-97n PE=2 SV=1	15.12999982	tr|V9HW63|V9HW63_HUMAN
Ig	IgA	IgA heavy chian constant region (Fragment) OS=Sus scrofa OX=9823 GN=IGHA PE=4 SV=1	17.2999993	tr|K7ZRK0|K7ZRK0_PIG
Ig	IgG	IgG H chain OS=Homo sapiens OX=9606 PE=2 SV=1	20.09000033	tr|S6BAP0|S6BAP0_HUMAN
Ig	IgG	IgG heavy chain OS=Sus scrofa OX=9823 GN=IGHG PE=2 SV=1	49.88999963	tr|L8B0R9|L8B0R9_PIG
Ig	IgG	IgG heavy chain OS=Sus scrofa OX=9823 GN=IGHG PE=2 SV=1	55.22000194	tr|L8B0W0|L8B0W0_PIG
Ig	IgG	IgG heavy chain OS=Sus scrofa OX=9823 GN=IGHG PE=2 SV=1	45.35999894	tr|L8B0V6|L8B0V6_PIG
Ig	IgG	IgG heavy chain OS=Sus scrofa OX=9823 GN=IGHG PE=2 SV=1	38.49000037	tr|L8B139|L8B139_PIG
Ig	IgG	IgG heavy chain OS=Sus scrofa OX=9823 GN=IGHG PE=2 SV=1	38.17000091	tr|L8B0S2|L8B0S2_PIG

APPENDIX A

Ig	IgG	IgG heavy chain OS=Sus scrofa OX=9823 GN=IGHG PE=2 SV=1	45.9100008	tr|L8B180|L8B180_PIG
Ig	IgG	IgG heavy chain OS=Sus scrofa OX=9823 GN=IGHG PE=2 SV=1	39.48000073	tr|L8AXL3|L8AXL3_PIG
Ig	IgG	IgG heavy chain OS=Sus scrofa OX=9823 GN=IGHG PE=2 SV=1	40.43000042	tr|L8B0U8|L8B0U8_PIG
Ig	IgG	IgG heavy chain OS=Sus scrofa OX=9823 GN=IGHG PE=2 SV=1	27.75000036	tr|L8AXL9|L8AXL9_PIG
Ig	IgG	IgG heavy chain OS=Sus scrofa OX=9823 GN=IGHG PE=2 SV=1	49.03999865	tr|L8B173|L8B173_PIG
Ig	IgG	IgG heavy chian constant region (Fragment) OS=Sus scrofa OX=9823 GN=IGHG5-1 PE=4 SV=1	31.58000112	tr|K7ZPU8|K7ZPU8_PIG
Ig	IgG	IgG L chain OS=Homo sapiens OX=9606 PE=2 SV=1	8.64899978	tr|S6B294|S6B294_HUMAN
MHC class II antigen	MHC class II antigen	MHC class II antigen OS=Sus scrofa OX=9823 GN=SLA-DQB PE=2 SV=1	20.69000006	tr|Q8SPA1|Q8SPA1_PIG
MHC class II antigen	MHC class II antigen	MHC class II antigen OS=Sus scrofa OX=9823 GN=SLA-DRA PE=2 SV=1	6.746000051	tr|Q860P1|Q860P1_PIG
MHC class II antigen	MHC class II antigen	MHC class II antigen OS=Sus scrofa OX=9823 GN=SLA-DRB1 PE=2 SV=1	16.92000031	tr|B1A9N6|B1A9N6_PIG

Supplementary Table IV. Fertility restoration database.

GROUP	MOUSE	RIGHT HORN			LEFT HORN			OBSERVATIONS
		TREATMENT	HORN WEIGHT (g)*	GESTATIONAL SACS	TREATMENT	HORN WEIGHT (g)*	GESTATIONAL SACS	
Saline	#1	damaged/treated	no data	0	non-damaged	0.9888	7	
	#2	damaged/treated	no data	0	non-damaged	1.2168	5	
	#3	damaged/treated	no data	0	non-damaged	no data	0	
	#4	damaged/treated	no data	0	non-damaged	0.9031	9	
	#5	damaged/treated	no data	0	damaged/treated	no data	0	
	#6	damaged/treated	0.4654	5	damaged/treated	no data	0	Right and left horns both had one very small gestational sac with an aberrant coloration. Both were catalogued as miscarries and excluded from the analysis.
	#7	damaged/treated	no data	0	damaged/treated	0.3762	3	
	#8	damaged/treated	no data	0	damaged/treated	no data	0	
EndoECM	#9	damaged/treated	no data	0	non-damaged	0.5055	3	
	#10	damaged/treated	no data	0	non-damaged	0.609	5	
	#11	damaged/treated	0.693	6	non-damaged	0.4554	3	
	#12	damaged/treated	no data	0	non-damaged	0.033	0	
	#13	damaged/treated	no data	0	non-damaged	0.5004	4	
	#14	damaged/treated	no data	0	non-damaged	no data	0	
	#15	damaged/treated	no data	0	damaged/treated	no data	0	
	#16	damaged/treated	no data	0	damaged/treated	no data	0	
	#17	damaged/treated	no data	0	damaged/treated	no data	0	
EndoECM+GF	#18	damaged/treated	no data	no data	damaged/treated	no data	0	Right horn ruptured during surgery. Excluded from the analysis.
	#19	damaged/treated	0.4865	5	non-damaged	0.2942	2	
	#20	damaged/treated	0.5864	6	non-damaged	0.5051	4	
	#21	damaged/treated	no data	0	non-damaged	no data	6	Fetuses collected seemed to be in E12.5. Fetuses were subsequently sacrificed without weighing.
	#22	damaged/treated	no data	0	non-damaged	0.8948	5	
	#23	damaged/treated	0.0864	1	non-damaged	0.129	4	
	#24	damaged/treated	0.279	2	damaged/treated	0.1329	1	
	#25	damaged/treated	no data	0	damaged/treated	no data	no data	Left horn ruptured during surgery. Excluded from the analysis.
	#26	damaged/treated	no data	0	damaged/treated	no data	0	

*Only uterine horns with gestational sacs were weighed.

APPENDIX B. Scientific production PhD student

1. International scientific publications

Publications directly related to this doctoral thesis

- Campo, Hannes, Ximo García-Domínguez, **Sara López-Martínez**, Amparo Faus, José S. Vicente Antón, Francisco Marco-Jiménez, and Irene Cervelló. **2019**. "Tissue-Specific Decellularized Endometrial Substratum Mimicking Different Physiological Conditions Influences *in vitro* Embryo Development in a Rabbit Model." *Acta Biomaterialia* 89 (April): 126–38. https://doi.org/10.1016/j.actbio.2019.03.004.

- **López-Martínez, Sara**†, Hannes Campo†, Lucía de Miguel-Gómez, Amparo Faus, Alfredo T. Navarro, Ana Díaz, Antonio Pellicer, Hortensia Ferrero, and Irene Cervelló. **2021**. "A Natural Xenogeneic Endometrial Extracellular Matrix Hydrogel Toward Improving Current Human *in vitro* Models and Future *in vivo* Applications." *Frontiers in Bioengineering and Biotechnology* 9 (March): 156. https://doi.org/10.3389/fbioe.2021.639688.

- Francés-Herrero, Emilio†, Elena Juárez-Barber†, Hannes Campo, **Sara López-Martínez**, Lucía de Miguel-Gómez, Amparo Faus, Antonio Pellicer, Hortensia Ferrero, Irene Cervelló. **2021**. "Improved models of human endometrial organoids based on hydrogels from decellularized endometrium". *Journal of Personalized Medicine*. 11, no. 6: 504. https://doi.org/10.3390/jpm11060504.

- **López-Martínez, Sara**†, Adolfo Rodríguez-Eguren†, Lucía de Miguel-Gómez, Emilio Francés-Herrero, Amparo Faus, Ana Díaz, Antonio Pellicer, Hortensia Ferrero, Irene Cervelló. **2021**. "Bioengineered Endometrial Hydrogels with Growth Factors Promote Tissue Regeneration and Restore Fertility in Murine Models." *Acta Biomaterialia.* Manuscript status: Accepted and under preproduction.

Publications not directly related to this doctoral thesis

- De Miguel–Gómez†, Lucía, Hortensia Ferrero†, **Sara López-Martínez**, Hannes Campo, Nuria López-Pérez, Amparo Faus, David Hervás, Xavier Santamaría, Antonio Pellicer, and Irene Cervelló. **2019**. "Stem Cell Paracrine Actions in Tissue Regeneration and Potential Therapeutic Effect in Human Endometrium : A Retrospective Study." *BJOG: An International Journal of Obstetrics and Gynecology*, 1–10. https://doi.org/10.1111/1471-0528.16078.

- De Miguel–Gómez, Lucía, **Sara López-Martínez**, Hannes Campo, Emilio Francés-Herrero, Amparo Faus, Ana Díaz, Antonio Pellicer, Francisco Domínguez, and Irene Cervelló. **2020**. "Comparison of Different Sources of Platelet-Rich Plasma as Treatment Option for Infertility-Causing Endometrial Pathologies." *Fertility and Sterility* 115 (2). https://doi.org/10.1016/j.fertnstert.2020.07.05.

- Francés-Herrero, Emilio, Lucía De Miguel-Gómez, **Sara López-Martínez**, Hannes Campo, Ximo Garcia-Dominguez, Gianfranco Diretto, Amparo Faus, José S. Vicente, Francisco Marco-Jiménez, and Irene Cervelló. **2021**. "Development of Decellularized Oviductal Hydrogels as a Support for Rabbit Embryo Culture." *Reproductive Sciences*. https://doi.org/10.1007/s43032-020-00446-6.

- Lucía de Miguel-Gómez†, **Sara López-Martínez**†, Emilio Francés-Herrero†, Adolfo Rodríguez-Eguren, Antonio Pellicer, and Irene Cervelló. **2021**. "Stem Cells and the Endometrium: From the Discovery of Adult Stem Cells to Pre-Clinical Models." Cells 10 (3): 595. https://doi.org/10.3390/cells10030595.

† These authors have contributed equally to this work and share first authorship.

2. Book chapters

- Campo, Hannes, **Sara López-Martínez** and Irene Cervelló. "Section 14: Female Reproductive System; Chapter 1: Uterus". Decellularization Methods of Tissue and Whole Organ in Tissue Engineering. *Advances in Experimental Medicine and Biology* (AMEB) series. Springer. Manuscript status: Accepted and under preproduction.

- Campo, Hannes, **Sara López-Martínez** and Irene Cervelló. "Section 14: Female Reproductive System; Chapter 2: Ovary." Decellularization Methods of Tissue and Whole Organ in Tissue Engineering. *Advances in Experimental Medicine and Biology* (AMEB) series. Springer. Manuscript status: Accepted and under preproduction.

- **López-Martínez, Sara**, Hannes Campo and Irene Cervelló. "Section 14: Female Reproductive System; Chapter 3: Vagina and Cervix". Decellularization Methods of Tissue and Whole Organ in Tissue Engineering. *Advances in Experimental Medicine and Biology* (AMEB) series. Springer. Manuscript status: Accepted and under preproduction.

3. Works submitted to national or international conferences

Oral presentation

- **López-Martínez Sara**, Hannes Campo, Lucía de Miguel Gómez, Amparo Faus Esteve, Hortensia Ferrero Chafer and Irene Cervelló Alcaraz. "Improving three-dimensional *in vitro* culture methods of human endometrial stem cells: bioengineering tissue-specific hydrogels." Conference: European Society of Human Reproduction and Embryology - 35th annual meeting. City of event: Vienna, Austria. Date of event: 23/06/2019 End date: 26/09/2019 Organizing entity: the European Society of Human Reproduction and Embryology (ESRHE).

- Francés-Herrero, Emilio, Elena Juárez-Barber, Hannes Campo, **Sara López-Martínez**, Lucía de Miguel-Gomez, Amparo Faus, Antonio Pellicer, Hortensia Ferrero and Irene Cervelló. "Next Generation of Human Endometrial Organoids: Bioengineering-Based Strategies for Preserving Tissue-Specific Extracellular Environment.". Conference: Society for Reproductive Investigation - 68th annual scientific meeting. City of event: Boston, USA. Date of event: 06/07/2021 End date: 09/07/2021. Organizing entity: Society for Reproductive Investigation (SRI).

Posters

- Francisco Marco-Jiménez, Hannes Campo, Ximo García-Domínguez, **Sara López-Martínez**, Jose Salvador, Vicente Antón and Irene Cervelló. "Biomimetic Coatings from Decellularized Rabbit Endometrium Influence the *In vitro* Development of Pre-Implantation Embryos." Conference: Society for Reproductive Investigation -66th Annual Scientific Meeting. City of event: Paris, France. Date of event: 12/03/2019 End date: 16/03/2019. Organizing entity: Society for Reproductive Investigation (SRI).

- Lucía de Miguel-Gómez, Amparo Faus, **Sara López-Martínez**, Nuria López-Pérez, Gemma Castillón-Cortés, Antonio Pellicer and Irene Cervelló. "Human Platelet-Rich Plasma from Patients with Uterine Pathologies Contributes to Endometrial Regeneration: A Current Therapeutic Approach?" Conference: Society for Reproductive Investigation -66th Annual Scientific Meeting. City of event: Paris, France. Date of event: 12/03/2019. End date: 16/03/2019. Organizing entity: Society for Reproductive Investigation (SRI).

- **Sara López-Martínez***†*, Hannes Campo*†*, Lucía de Miguel-Gómez, Amparo Faus, Hortensia Ferrero and Irene Cervelló. "Bioengineering Endometrial Extracellular Matrix Hydrogels: A New Option to Improve Human Three-dimensional Endometrial Cell Culture and Organoid Development." Conference: Society for Reproductive Investigation - 67th annual scientific meeting. City of event: Vancouver, Canada. Date of event: 10/03/2020 End date: 14/03/2020. (Cancelled due to COVID-19) Organizing entity: Society for Reproductive Investigation (SRI).

- Lucía de Miguel-Gomez, Hortensia Ferrero, **Sara López-Martínez**, Amparo Faus, David Hervás-Marín and Irene Cervelló. "Stem Cell therapy induces a shift from an inflammatory environment towards an immune tolerant scenario promoting endometrial tissue regeneration." Conference: Society for Reproductive Investigation - 67th annual scientific meeting. City of event: Vancouver, Canada. Date of event: 10/03/2020 End date: 14/03/2020. (Cancelled due to COVID-19) Organizing entity: Society for Reproductive Investigation (SRI).

- Lucía de Miguel-Gómez, Amparo Faus, **Sara López-Martínez**, Hannes Campo, Guillermo Mollá-Robles, Antonio Pellicer, Francisco Domínguez and Irene Cervelló. "Human Platelet-Rich Plasma from Adult Peripheral and Umbilical Cord Blood: Endometrial Regeneration and Proteomic Profiles in a Murine Model of Asherman Syndrome." Conference: Society for Reproductive Investigation - 67th annual scientific meeting. City of event: Vancouver, Canada. Date of event: 10/03/2020 End date: 14/03/2020. (Cancelled due to COVID-19) Organizing entity: Society for Reproductive Investigation (SRI).

- Hannes Campo, Emilio Francés-Herrero, **Sara López-Martínez**, Amparo Faus, Antonio Pellicer and Irene Cervelló. "In Pursuit of the Optimal Hydrogel for Follicle Culture: An In-depth Comparison of Ovarian Decellularization Protocols." Conference: Society for Reproductive Investigation - 67th annual scientific meeting. City of event: Vancouver, Canada. Date of event: 10/03/2020 End date: 14/03/2020. (Cancelled due to COVID-19) Organizing entity: Society for Reproductive Investigation (SRI).

- Hannes Campo†, Emilio Francés-Herrero†, **Sara López-Martinez**, Amparo Faus, Antonio Pellicer, Irene Cervelló. "Towards the Development of the Bioengineered Ovary: Comparative Proteomic Analysis of Different Extracellular Matrix Hydrogels." Conference: Society for Reproductive Investigation - 68th annual scientific meeting. City of event: Boston, USA. Date of event: 06/07/2021 End date: 09/07/2021. Organizing entity: Society for Reproductive Investigation (SRI).

- **Sara López-Martínez**, Adolfo Rodríguez-Eguren, Lucía de Miguel-Gómez, Amparo Faus, Emilio Francés-Herrero, Antonio Pellicer, Hortensia Ferrero and Irene Cervelló. "Extracellular Matrix Hydrogels from Decellularized Endometrium Promote Tissue Regeneration and Fertility Restoration in a Murine Model of Endometrial Damage." Conference: Society for Reproductive Investigation - 68th annual scientific meeting. City of event: Boston, USA. Date of event: 06/07/2021 End date: 09/07/2021. Organizing entity: Society for Reproductive Investigation (SRI).

† These authors have contributed equally to this work and share first authorship.